List of Publication 20222-23

Prof. (Dr.) A. Mishra Publication

1. Synthesis and characterization of Cr substituted Mn–Zn nanoferrites with improved dielectric, electrical conductivity and impedance properties for electronic device applications. K. Patil, S. Phadke, M. Das and **A. Mishra**, Journal of the Korean Ceramic Society **volume 59**, pages427–435 (2022).

2. Structure and ac conductivity of (Cu/Co) Fe_2O_4 spinel materials. Kaliram Patil, S. Phadke, **A. Mishra,** Materials Today: Proceedings,https://doi.org/10.1016/j.matpr. 2022.05.496.journal homepage: www.elsevier.com/locate/matpr (2022).

3. SYNTHESIS AND XRD CHARACTERIZATION OF COPPER (II) CONTAINING METAL COMPLEXES. Nitin Upadhyay, Dr. B. D. Shrivastava, **Dr. Ashutosh Mishra,** Journal of emerging technologies and innovative research, (JETIR) September 2022, Volume 9, Issue 9, pp a641-a643, www.jetir.org (ISSN-2349-5162)

4. SEM & EDX INVESTIGATION OF COPPER (II) CONTAINING METAL COMPLEXES. Mr. Nitin Upadhyay, Dr. B. D. Shrivastava, **Dr. Ashutosh Mishra,** Mr. Vinod Kumar Sahu, Journal of emerging technologies and innovative research, (JETIR) September 2022, Volume 9, Issue 9, pp e537-e540, www.jetir.org (ISSN-2349-5162).

5. Structural, electrical and magnetic properties of (Cu/Co)Fe_2O_4 spinel ferrite materials. Kaliram Patil, M. Saleem, S. Phadke, **A. Mishra,** Applied Physics A (2022) 128:988. Material Science & processing https://doi.org/10.1007/s00339-022-06149-w.

6. Evaluation of structural and multifunctional properties of $BaTiO_3$–$NiFe_{2-x}Sm_xO_4$ ceramic composites. Mehjabeen Khan, Jyoti Shukla, Pallavi Saxena, **Ashutosh Mishra**, Pradeep Sharma, Applied Physics A (2022) 128:1120 https://doi.org/10.1007/s00339-022-06233-1.

7. Structural and Optical Properties of CoO Nanoparticles Doped PMMA Films. Shailendra S. Rajput, **A. Mishra,** A. Sharma, J. Singh, G. S. Chandrawat and J. Tripathi, Nano World Journal Review Article Open Access, Nano World Journal S45- S48, Volume 8,Supplement 1, 2022, https://doi.org/10.17756/nwj.2022-s1-009.

8. Impact of Mn and Cd ion doping on the structural and dielectric properties of ternary Zn0.94Tm0.01Cu0.05O (Tm = Mn, Cd) metal oxide. Pallavi Saxena, Bhargav Pathak, Prachi Joshi, Anand Yadav, and **Ashutosh Mishra,** J Mater Sci: Mater Electron (2023) 34:611, https://doi.org/10.1007/s10854-023-10025-5.

9. Influence of B-site zr ion substitution on the structural, dielectric and ferroelectric properties in $Bi_{0.5}Na_{0.5}TiO_3$- based lead-free ceramics. Susheel Patel, Jyoti Shukla, Virendra Nath Rai and **Ashutosh**

Mishra, J Mater Sci: Mater Electron (2023) 34:889, https://doi.org/10.1007/s10854-023-10308-x. Published online: 04 April 2023.

10. Electrical transport mechanism and magnetoresistive behavior of trilayer $La_{0.7}Sr_{0.3}MnO_3/\gamma$ $Fe_2O_3/La_{0.7}Sr_{0.3}MnO_3$ (FM/FIM/FM) manganites. Pooja Narwat, R J Choudhary and **A Mishra,** Phys. Scr. 98 (2023) 055934, https://doi.org/10.1088/1402-4896/acc5b9, 2023 IOP Publishing Ltd.

11. XANES and EXAFS studies of Aceto 5,5dimethyl-2-(2-(4-methoxyphenyl) hydrazono) cyclohexane-1,3-dione cobalt (II) hydrate schiff base complex. Pankaj Agrawal, Pradeep Sharma and **Ashutosh Mishra,** Asian journal of chemical and environment research, vol 15, (1-4), 54-58 (2022).

12. X-Ray absorption fine structure study of schiff base cobalt (II) complexes of 5,5- dimethyl-2-(4-arylhydrazono) cyclohexane1,3-dione. Pankaj Agrawal, Pradeep Sharma and **Ashutosh Mishra,** Journal of Physics: Conference Series 2484 (2023) 012011 IOP Publishing doi:10.1088/1742-6596/2484/1/012011, ICMMT-22, IOP Publishing.

13. Investigating magnetic and magneto-transport properties of ferromagnetic (FM) structure and antiferromagnetic/ferromagnetic (AFM/ FM) heterostructures. Pooja Narwat, R.J. Choudhary, **A. Mishra**, Physica B 665 (2023) 415048, Physica B: Condensed Matter, https://doi.org/10.1016/j.physb.2023.415048.

14. Investigation of temperature-dependent dielectric and transport characteristics of Y0.95Ba0.05Mn0.95Zr0.05O3 manganite ceramic. Jyoti Shukla, Pallavi Saxena, Virendra Nath Rai, and **Ashutosh Mishra,** J Mater Sci: Mater Electron (2023) 34:1776, https://doi.org/10.1007/s10854-023-11203-1.

Prof. (Dr.) Shashank N. Kane Publication between 2022 till June 2023 :

01. "In-field ^{57}Fe Mössbauer study of $Mg_xZn_{1-x}Fe_2O_4$ prepared by green synthesis method", P. Tiwari, R.Verma, S. S. Modak, V. R. Reddy, **_S. N. Kane_**, Hyperfine Interactions 243 (2022) 7-1−7-15 ,https://doi.org/10.1007/s10751-022-01794-2

02. "Si^{9+} Ion-Irradiation Induced Modification of Structural and Magnetic Properties of Zn-Nanoferrite" C. Parmar, R. Verma, S. S. Modak, F. Mazaleyrat, **_S. N. Kane_**, ECS J. of Solid State Sci. and Tech. 11 (2022) 053015-1 - 053015-9, https://doi.org/10.1149/2162-8777/ac6f1b

03. "Synthesis and characterization of thermally treated $Co_{1-x}Fe_{2+x}O_4$ (x = 0.0−0.8) spinel nano ferrite", C Parmar, R Verma, S S Modak, F Mazaleyrat and **_S N. Kane_**, IOP Conf. Series: Materials Science and Engineering 1258 (2022) 012009-1 □ 012009-9, https://doi:10.1088/1757-899X/1258/1/012009

04."Structural, Mössbauer and magnetic study of $Co_{1-x}Zn_xFe_2O_4$ (x = 0.0 − 0.56) nano ferrites, **_S. N. Kane,_** R. Verma, S. S. Modak, V. R. Reddy, F. Mazaleyrat, Hyperfine Interactions 244 (2023) 3-1−3-15, https://doi.org/10.1007/s10751-022-01814-1

List of Publication of Y Choyal Sir

ASIAN JOURNAL OF PHYSICS

1. **Analysis and Characterization of Kr/Cl based 222 nm Far UV-C Excimer source**
Surbhi Bidawat, Navin Kumar Sharma, R P Lamba, Mahendra Singh, Alok Mishra, Y Choyal and U N Pal

2. **Development of Cold Atmospheric Pressure Plasma Jet Sources for Biomedical Application**
Navin K Sharma, Priti Pal, Mahendra Singh, Vishali Singh, R Kumar, Alok Mishra, R P Lamba, Y Choyal and Udit Narayan Pal

3. Simulation of High Frequency Short Pulse Excitation of Co-axial Xenon Excimer Source for Generation of 172 nm radiation
Navin K Sharma, Y Choyal Udit Narayan Pal and Ram Prakash Lamba

4. Theoretical Investigation on Impact Ionization of Argon Gas-filled Cavities
Navin Kumar Sharma, Ram Prakash Lamba Udit Narayan Pal and Y Choyal

5. **S. Bidawat** *et al.*, **"Experimental and Numerical Characterization of Dielectric Barrier Discharge-Based Coaxial Kr/Cl2 Excilamp," in** *IEEE Transactions on Plasma Science*, **vol. 51, no. 12, pp. 3531-3537, Dec. 2023, doi: 10.1109/TPS.2023.3337631.**

In Press, Corrected Proof   ? What's this? ↗

Proposed approximate hybrid memory architecture for handheld multimedia devices

Priyanka Sharma 👤 ✉ , Vaibhav Neema ✉ , Ashish Panchal ✉

Show more ⌄

ⓒ Share   " Cite

Abstract

Nowadays Handheld multimedia devices demand is growing rapidly, as the demand for mobility in work and lifestyle increases. Power consumption has become the paramount concern in the design of Handheld multimedia battery-operated devices. Approximate computing promises energy efficiency computing paradigms when small quality degradation is permissible. Most multimedia processing is image or video processing, where the end user is a human. The imperceptibility of the human visual system is to allow the output of this processing to be approximate rather than accurate. This research paper proposed an energy-efficient Moving Picture Experts Group 4 (MPEG-4) video decoder architecture with a circuit-level approximate method for Handhandle multimedia devices. Hence, in this research work instead of using conventional 6T memory cells during video decoding processing, an approximate Hybrid 6T/8T memory architecture is proposed, where the 8-bit Luminance pixels are stored favourably in consonance with their effect on the output quality. The higher order luminance bits (MSBs) require high stability and thus these bits are stored in the 8T bit cells and the remaining bits (LSBs) are stored in the conventional 6T bit cells for more optimal configurations compared with previous work. The failure probability of 6T cells is significantly large 0.0988 at 600mV supply voltage (as compared to $0.28*10^{-2}$ at 800mV supply voltage), leading to a decrease in the output quality of the decoded video. The hybrid memory matrix formulation calculates that storing higher-order MSB bits in highly stable memory cells will provide high-quality video processing compared to the conventional technique because the human eye is more susceptible to higher-order luminance bits. The proposed approximate 6T/8T hybrid memory units, and evaluate them to demonstrate the efficacy of our approach. Simulations result indicate power savings of up to 50% with an insignificant loss in output quality (3.6dB) when compared to the conventional memory unit. Compared to the hybrid and conventional 6T memory array at 600mV supply voltage, the worst minimum PSNR is 15.04dB improved.

Methods for noise margin analysis of conventional 6T and 8T SRAM cell

Aastha Gupta ✉ , Ravi Sindal ✉ , Priyanka Sharma ✉ , Ashish Panchal ✉ , Vaibhav Neema ✉

Show more ⌄

ⵦ Share 🟃 Cite

Abstract

SRAM is one of the essential components for portable devices which contributes significantly and determines the overall device performance. This paper analyzes the methods for calculating noise margin of conventional 6 transistor (6T) and 8 transistor (8T) SRAM cell. For calculation of noise margins in memory cell, this paper considered butterfly analysis and noise-curve methods. From the simulation results obtained from the above-mentioned method, the findings shows that 8 transistor SRAM cell provides higher read noise margin than 6 transistor SRAM cell. The aim of this paper is to verify and validate butterfly analysis and noise-curve methods for calculation of noise margins in memory cells. From the simulation data it is observed that major limitation of using butterfly analysis to measure SNM is the inability of measuring SNM using inline techniques and it's time consuming and complex process. It may sometimes give inaccurate/misleading results due to computational error. Whereas, N-curve method for SRAM cell analysis is used for inline testing and also provides additional information regarding current and voltage stability. Additionally, the N-curve can be utilized to perform an analysis of the power dissipation by the SRAM cell while it is undergoing read or write operation. Using 90 nm technology file, cadence virtuoso EDA tools simulate both 6 transistor and 8 transistor SRAM cells.

Introduction

Static Random Access Memory (SRAM) is the type of memory technology that is used primarily as an on-chip memory in various processors. Now-a-days multilevel cache are also being used for reducing delay of executing instruction in the applications such as internetworking, signal processing etc. [1]. The SRAM cell occupies large chip area due to which the overall power consumption increases [2]. So, the progressive

Design of leakage current sensing technique based continues NBTI monitoring sensor using only NMOS

Natwar Bhootda 👤 ✉ , Ankit Yadav, Vaibhav Neema

Show more ⌄

∝° Share 🗩 Cite

Referred to by   **5 NANO 2021 – EXPRESSION OF CONCERN – PART 1**
Materials Today: Proceedings, Volume 80, Part 3, 2023, Pages 1701

📄 View PDF

Abstract

As the technology is scaled-down and with a decrease in oxide thickness, the effect of NBTI is a major reliability issue in semiconductor industries. NBTI is an aging phenomenon in which the PMOS transistor degraded over time. Deviation in the threshold voltage of PMOS transistor results from NBTI with stress time which affects various parameter of SRAM memory such as degradation in drain current, RSNM, HSNM and access time. NBTI induced aging effect on 6T and 8T SRAM cell have been analyzed in this paper for the stress time of 10years. The reliability parameters of 6T SRAM cell obtained from simulation result shows there is 6.53%, 23.86%, 3.36% and 13.42% change in Hold SNM (HSNM), Read SNM (RSNM), Write margin and standby leakage current respectively after 10years. Similarly in 8T SRAM cell HSNM, RSNM, Write margin and leakage current changes by 5.81%, 5.01%, 3.11%, and 13.24% respectively. This paper also presents the leakage current sensing technique based NBTI monitoring sensor using NMOS transistors only. The sensitivity of the sensor is 40μV/nA and the linearity of the sensor is upto the practical leakage current range of SRAM cell. Thus we can conclude that the proposed sensor works fine with greater linearity and sensitivity.

Introduction

Metal Oxide Semiconductor Field Effect Transistors (MOSFETs) is a key element for any high performance and energy-efficient system. With the shrinkage of device dimensions, integration of transistors per chip

Microsoft Excel powered virtual electron diffraction tube experiment as an enhanced educational tool

Vijay Bhat[1,*] and Uma Rathore Bhatt[2]

[1] Institute of Advance Computing SAGE University, Indore, India
[2] Institute of Engineering & Technology, Devi Ahilya University, Indore, India

E-mail: bhatvijaybhat@gmail.com

Abstract

This paper presents a novel Microsoft Excel based virtual electron diffraction experiment, which replicates all functionality of an electron diffraction tube which is an important tool for the verification of the concept of matter waves. Unlike most of virtual labs where accessibility is mostly online; presented simulator is simply a downloadable excel file and can be used offline as a learning resource. Impact of the presented simulator on the learning was analysed by the test conducted for the control and the experimental group of students. Results of the test show the enhanced performance by the experimental group of students, indicating the positive impact of using the simulator along with conventional classroom teaching. This simulator intends to simplify the abstract quantum mechanical concept of matter waves by bringing the laboratory sort of experience in classroom.

Keywords: virtual experiment, electron diffraction, matter waves

1. Introduction

In the field of science teaching/learning of the quantum mechanics (QM) is considered as an extreme difficult subject. Conceptualization of the abstract quantum mechanical ideas has always been a challenge for the students and as well as for the educators [1, 2], presents an extensive review of the student difficulties in learning of QM. The review work highlights the misconceptions between the mathematical skills and the actual understanding of the subject. In order to assess and address the difficulty associated with the teaching/learning of the QM; researchers have explored various approaches, some of which has been summarized in the table 1.

In this work we report an excel powered electron diffraction tube simulator and assess its

* Author to whom any correspondence should be addressed.

Online Strainer Based Scheduling (OSBS) for Improving Energy Efficiency in FiWi Access Networks

Vijendra Mishra[1] · Raksha Upadhyay[1] · Uma Rathore Bhatt[1] · Abhay Kumar[2]

Abstract

Integration of wireless frontend with optical backend leads to the fiber wireless access network, which provides high bandwidth and flexibility. Energy efficiency in such networks is very crucial and can be achieved by implementing multiplexing, scheduling and optimized components placement. Our prime objective is to improve energy efficiency. Architecture has wavelength agile and radio agile multiplexing at backend and frontend respectively. Firstly, we optimize optical network units using whale optimization and secondly, a novel online scheduling is implemented to obtain better energy efficiency with controlled delay. Proposed methodology shows better energy efficiency and delay performance compare to existing approaches.

Keywords Whale optimization algorithm · Online scheduling · Fiber wireless access networks (FiWi) · Energy efficiency · Wavelength agile

1 Introduction

In today's scenario of high bandwidth applications where each user at distinct locations needs internet access at high data rate, it becomes crucial to develop and update access networks which can support high bandwidth. Conventional digital scribe line (DSL) were not capable of providing high bandwidth to handle applications like live video streaming, multiplayer gaming etc., therefore optical access as a closest solution, have been in use in present decade. Optical fibers are capable of providing high bandwidth but it is not cost

✉ Vijendra Mishra
  vijendramishra88@gmail.com

  Raksha Upadhyay
  rupadhyay@ietdavv.edu.in

  Uma Rathore Bhatt
  umarathore@rediffmail.com

  Abhay Kumar
  dr.abhaykumar@gmail.com

[1] Department of Electronics and Telecommunication, Institute of Engineering and Technology, Devi Ahilya University, Khandwa Road, Indore, India

[2] School of Electronics, Devi Ahilya University, Takshila Parisar, Khandwa Road, Indore, India

FiWi network planning for WiFi enabled gram panchayats of India: A frame work using component placement optimization

Nitin Chouhan [a], Uma Rathore Bhatt [a,*], Raksha Upadhyay [a], Vijay Bhat [b]

[a] Department of Electronics & Telecommunication Engineering, Institute of Engineering & Technology, Devi Ahilya University, Indore 452001, India
[b] Institute of Advance Computing, SAGE University, Indore, India

ABSTRACT

Fiber Wireless (FiWi) access network consists of high speed passive optical network (PON) at back end and wireless mesh network at front end. It is emerging as the most prominent access network due to its inherent feature. It may provide fast Internet services at minimum possible cost. Many of the villages of the India are still not connected with high speed network hence the present paper provides FiWi network planning for creating the Wireless Fidelity (WIFI) enabled villages (Gram Panchayats) of India. The main aim of the paper is to deploy the cost effective FiWi network to provide the faster Internet services at reasonable prices to the users of the gram panchayat (GP) in India. The area of the GP and the user's location in particular GP is taken as input for network planning. The proposed planning provides the optimized position of wireless routers and Optical Network Units (ONUs) in terms of latitude and longitude. For optimizing position of wireless router and ONUs, we propose to use customized Slime Mould algorithm (SMA). We considered four gram panchayats of Indore region of India to make them WiFi enabled using FiWi access network. The customized SMA algorithm provides the best possible position and number of wireless routers and ONUs to connect all the users of gram panchayat. Beside, the total fiber length from the Optical Line Terminal (OLT) to all the ONUs and total cost estimation is also given to create the complete network.

1. Introduction

With the ever increasing demand of bandwidth intensive applications and its related services, the proper network designing and planning is very important to deploy any type of communication network. Good network planning facilitates to design a scalable network to serve users Internet services with good quality of services [1]. Also, it helps to design a network to serve users with future Internet demand. In general, network planning includes Internet demand forecast, infrastructure of the network area and network installation [2]. Internet demand forecast involves the current and future need of internet services produced by the users. Infrastructure of the network area involves the number of users, layouts of the area and the population distribution. Network installation involves the installation of the network equipment and cables among these equipments. The goal of network planning is to place and interconnect network components efficiently in order to share resources among several users. Good network planning exhibit high level performance, efficient placement of components, provides better scalability and reliability, and minimizes the network cost.

This paper focuses on network planning for communication networks. Communication networks create challenges to the researchers to design a new future access network which can handle services at high capacity with lower cost. Optical access network and wireless access network are the two significant existing technologies which provide services to users. Passive Optical Network (PON) [3–4] is one of the leading technologies due to its high capacity, better stability with longer distance communication and reduces transmission losses. However, PON technology is costly for the users because of usage of optical devices and also it is not practically possible to deploy fiber everywhere. Alternately, wireless access network [5–7] such as WiFi, WiMAX etc. provide better flexibility, easy deployment and services to the users at lower cost with mobility. However, wireless technologies are bandwidth limited due to limited spectrum. To meet up the demand of increasing bandwidth, researchers evolved a new future access network called as Wireless Optical Broadband Access Network (WOBAN) or Fiber Wireless access network (FiWi) [8–13]. This newly network is the integration of optical network and wireless network and it is a prominent solution to provide high bandwidth services to the users at minimal cost. Fig. 1

RESEARCH ARTICLE

Fiber Wireless (FiWi) Access Network Planning & Deployment using Reptile Search Algorithm

Nitin Chouhan[1], Uma Rathore Bhatt[1,*] and Vijay Bhat[2]

[1]Department of Electronics and Telecommunication, Institute of Engineering and Technology, Devi Ahilya University, Indore, India; [2]Department of Advance Computing, Institute of Advance Computing, SAGE University, Indore, India

Abstract: *Aim:* The aim of this study is the deployment of components in an efficient manner to make a cost-effective FiWi network.

Background: Fiber Wireless access network is the boost to broadband access technology for providing network services to Internet users at a lower cost. Deployment of components in FiWi access network is very crucial since it affects the deployment cost and network performance.

Objective: We investigate the planning process for efficient placement of components in FiWi access networks. For optimizing the position of components (wireless routers and ONUs) in the network, a novel nature inspired Reptile Search Algorithm (RSA) is proposed in the paper.

Methods: Extensive simulation is carried out to implement proposed work. A simulation model and code is developed in MATLAB to get the optimized position of components for existing and proposed algorithms.

Results: We compare the performance of proposed algorithm with existing algorithm. The obtained results show that the proposed algorithm has superior performance than the existing algorithm.

Conclusion: The present work optimizes the position of components using RSA algorithm. RSA returns the lower number of required wireless routers/ONUs, lesser TCD, increased AONUC, fast convergence rate, lesser execution run time than WSSA algorithm. The outcome of the paper highlights the importance of the proposed work in network planning and component deployment in FiWi access network.

Keywords: Network planning, Fiber Wireless (FiWi) access network, component placement, optimization algorithms, Optical Network Units (ONUs), wireless routers, Reptile Search Algorithm (RSA).

1. INTRODUCTION

The demand of bandwidth intensive applications and its related services has been significantly increasing day by day. The previous broadband access networks, such as optical networks and wireless networks, are not sufficient to provide high bandwidth requirements at a lower cost. Passive optical network (PON) is one of the leading technologies due to its high capacity, longer distance communication, but it is costly for the users due to the usage of optical devices. Alternately, wireless access network provides better flexibility, easy deployment, and lower cost with mobility, but its bandwidth is limited due to limited spectrum. To meet up the demand for increasing bandwidth, researchers evolved a new

future access network called a Wireless Optical Broadband Access Network or Fiber Wireless access network (FiWi) [1-3]. This new network is the integration of optical network and wireless network, and it is a prominent solution to provide high bandwidth services to the users at minimal cost.

Fig. (1) shows the schematic of FiWi access network with two segments that consist of an optical network at back-end and wireless network at front-end, respectively. At back-end of FiWi network, single Optical Line Terminal (OLT) connects several Optical Network Units (ONUs) via feeder fiber, optical splitter and distribution fiber in each segment. In front-end, users and wireless routers are scattered all over the area. Each ONU in FiWi network is connected to a wireless gateway through which an interface is possible between both ends.

FiWi access network comes up with several challenging issues such as Component Placement, Survivability, Energy

*Address correspondence to this author at the Department of Electronics and Telecommunication, Institute of Engineering and Technology, Devi Ahilya University, Indore, India; Tel: +91-942-533-3837; E-mail: urrathore@gmail.com

PCA Based Components Selection Criteria for Computationally Efficient Physical Layer Key Generation (PLKG) System

Tapesh Sarsodia, Uma Rathore Bhatt, Raksha Upadhyay, and Vijay Bhat

Abstract—Data security is one of the prime concerns in wireless networks. PLKG has been emerging as an attractive alternative to traditional cryptographic techniques. PLKG is more computationally efficient than cryptography. Moreover, PLKG using Principal component analysis (PCA) as pre-processing may further save computations. This paper proposes three mechanisms to select components of PCA which are based on Information content, Mean and Histfit. Bit Disagreement Rate (BDR) is compared for each mechanism. Histfit based method is found to be best. Since only two components are supposed to be processed for key generation, it is computationally efficient/ power efficient too.

Keywords—wireless networks; received signal strength; Principal component analysis; physical layer key generation; Mean; Histfit

I. INTRODUCTION

MODERN world inching more towards low powered wireless application networks. IoT networks are such long range, low powered wireless networks which are getting more attraction due to recent developments in automation based applications. IoT networks have numerous advantages like smart operation of the devices, easy data collection, good for personal safety and security etc. Due to all these features, IoT networks are able to support various application areas like Alexa models, home automation, smart city monitoring, operating electrical or electronic devices remotely etc.[1-3]. Apart from all these features, IoT networks still facing data security problems over the channel, because of various types of wireless attacks and they are open to intruders/ attackers which can hack data easily[4], predict their locations, or extract confidential information etc. This security problem leads researchers to design IoT networks to be highly reliable and secure. They are trying to design modern IoT networks in such a way that they have proper authentication between users, confidentiality of the data should be maintained, easy and global access controls to the network, more prone to network attacks, software attacks, encryption attacks etc.[5].

Classical cryptography techniques serve the purpose of making IoT networks more secure as far as data security is concern [6]. Typical cryptographic techniques include public key infrastructure, symmetric and asymmetric cryptography etc.

These techniques are implemented over upper layers of network architectures and are complex in nature. They require fix and complex key infrastructures for sharing secret keys over the channel, which are not compatible with future generation smart energy aware nodes. So, alternate to these researcher's move towards security at the physical layer and designed PLKG systems for modern IoT-like power-constrained networks. This PLKG technique doesn't share keys over the channel. So, PLKG-based key generation is a reliable solution for future-generation secured networks. Physical layer security techniques utilize channel characteristics to generate keys between legitimate users using RSSI, CSI, Angle of arrival (AoA) etc.[7]. RSSI is the channel parameter which is being shared between two nodes before actual data transmission takes place. By refining the raw RSSI data, network parameters can be improved and it can be achieved by applying various preprocessing technique on raw RSSI. These preprocessing techniques improves system parameters by removing different redundancies from raw data like noise, data dimension etc. Various application areas based on RSSI preprocessing are Human activity recognition (HAR), wireless node identification, channel identification, energy-aware wireless networks, PLKG systems etc. Different techniques available to pre-process RSSI are dimensionality reduction techniques like PCA, Individual component analysis (ICA), decision tree, Linear discriminant analysis (LDA), etc. which help to reduce data dimension which further reduces computational complexities of the network. We can also use filtering techniques like mean filter, gaussian-Kalman filtering, etc. to reduce redundancies in the raw RSSI signal, which results in improved network parameters, transformation techniques like Discrete wavelet transform (DWT), Discrete cosine transform (DCT), etc. also plays crucial role in preprocessing of RSSI, which is reported in various works so far.

So, in a PLKG system RSSI collection and preprocessing of it plays a vital role in designing future generation wireless applications. Now, let us discuss the PLKG system in detail. PLKG system has five main stages[8]: RSS acquisition, preprocessing, quantization and encoding, information reconciliation, and privacy, amplification, as shown in Fig. 1.

T. Sarsodia, U. R. Bhatt, R. Upadhyay are with Institute of Engineering and Technology, Devi Ahilya University, Indore, India (e-mail: tapeshi162@gmail.com, urrathore@gmail.com, rupadhyay@ietdavv.edu.in).

V. Bhat is with Sage University, Indore, Madhya Pradesh, India (e-mail: bhatvijaybhat@gmail.com).

Design, implementation and performance evaluation of different digital control techniques for current controlled DC-DC Buck converter

Dipen M. Vachhani* and Rajesh Arya

Laser Electronics Division,
Raja Ramanna Centre for Advanced Technology,
Indore – 452013, India
Email: dipen@rrcat.gov.in
Email: rajarya@rrcat.gov.in
*Corresponding author

Uma Rathore Bhatt

Department of Electronics and Telecommunication,
Institute of Engineering and Technology,
Devi Ahilya University,
Khandawa Road, Indore – 452017, India
Email: umabhatt@ietdavv.edu.in

Abstract: The paper presents modelling, control architecture, analysis and design of digital compensators for single feedback-loop voltage mode control as well as two feedback-loop average current mode control and peak current mode control of current controlled DC-DC Buck converter operating in continuous conduction mode with output current as control variable. The compensators are derived using digital redesign approach, simulated on MATLAB, implemented as control algorithms on Texas Instruments' 32-bit TMS320F28069M microcontroller platform, and experimentally validated by testing with a laboratory prototype of current controlled Buck converter. Simulation and experimental results are discussed, compared and evaluated for converter output current performance in tracking reference current signal as well as in regulation against input voltage and load disturbances. Salient features of each control technique are identified and described to determine its suitability in applications of DC-DC converters requiring controlled output current.

Keywords: digital control techniques; digital voltage mode control; digital average current mode control; digital peak current mode control; current controlled DC-DC Buck converter; continuous conduction mode; digital redesign; digital compensators; type-2 compensator; 2p2z compensator.

Reliable Friend-Assisted Algorithm in Wireless Optical Broadband Access Network

Sangita Solanki[1], Raksha Upadhyay[2], Uma Rathore Bhatt[3]

[1,2,3]Electronics and Telecommunication Department, Institute of Engineering & Technology, Indore

Email: [1]ssolanki@ietdavv.edu.in, [2]rupadhyay@ietdavv.edu.in, [3]urvrathore@gmail.com

Abstract:

The capability to access the network in the presence of component/path failures is a fundamental need. So, maintaining survivability is essential for WOBAN also. In this paper, we propose a reliable friend-assisted algorithm (RFAA) in front-end WOBAN for finding the reliable path or route. This paper aims to optimize the wireless route based on communication range. The simulation results show that the proposed algorithm achieves better end-to-end delay performance as compared existing maximum protection minimum link cost (MPMLC) algorithm with multiple link failure.

Keywords: WOBAN, survivability, RFAA, (Received signal strength indicator) RSSI.

1. INTRODUCTION

In recent times, the growth of users for internet access using mobile devices and multimedia applications requires high capacity, high flexibility, and low-cost broadband access [1-2]. WOBAN is one of the most suggested access networks. In a typical WOBAN, a high-capacity passive optical network (PON) consists of an OLT, Splitter, and ONU. While a flexible WMN consists of a wireless router and gateway as shown in figure 1., which shows an architecture of WOBAN that provides wide-area connectivity to users [3-4]. The process of sending packets from the wireless router to the internet backbone is as follows. A user sends a packet to its nearby wireless router, using a multi-hop wireless path. Then router send directs to ONU. Then, the packet is received at the OLT via fiber cable and finally, the packet is injected into the internet backbone. For downstream communication, the whole process is repeated in a reverse manner. During sending packets from the router to OLT, any failure occurs such as link or distribution fiber. a lot of traffic losses arise in the network. Such types of failure affect services for users. In WOBAN, Survivability is an important issue.

For reliable data transmission, we proposed a reliable friend-assisted routing algorithm. Which provides a reliable path in the network based on the communication range between two nodes. In this paper include, link failure detection based on RSSI. Based on various network factors, such as latency and end-to-end delay, we compare the performance of suggested algorithms with that of the existing algorithm MPMLC.

The remainder of the paper is structured as follows. The literature review for the WOBAN survivability problem is discussed in Section 2. The problem statement and the system model are described in Section 3. Section 4 provides a description of the suggested optimization algorithm. Simulator output is displayed in Section 5. Finally, Section 6 brings the paper to a

Send Orders for Reprints to reprints@benthamscience.net

Int. J. Sens. Wirel. Commun. Control, xxxx, xx, 00-00   **1**

RESEARCH ARTICLE

Front-End Survivability in Wireless Optical Broadband Access Network

Sangita Solanki[1,*], Raksha Upadhyay[1] and Uma Rathore Bhatt[1]

[1]*Department of Electronics & Telecommunication Engineering, Institute of Engineering & Technology, DAVV, Indore, India*

Abstract: ***Background***: Survivability is one of the key issues of wireless optical broadband (WOBAN) access networks. Survivability means providing continuous services to users if a device/link failure occurs in the network. The component /link failure can occur in the network due to any reason. In this condition, huge data loss will occur in the network.

Methods: In this paper, we consider the front-end survivability in WOBAN. We propose a novel maximum protection minimum link cost routing algorithm (MPMLC) that provides path protection with a minimum link cost to the front-end of the WOBAN. The proposed MPMLC algorithm assigns weight/cost to a wireless link using link-state prediction (LSP). The path with minimum cost is selected to route the traffic (actual/affected due to failure) of the front-end network.

Results: The proposed algorithm outperforms in terms of reduced network delay and wireless link cost. It is also observed from simulation results that when multiple link failures occur in the network, the proposed MPMLC algorithm exhibit better results in reduced wireless link cost than the existing algorithm.

Conclusion: The proposed MPMLC offers better candidature than the existing algorithm for the front-end survivability of the WOBAN.

Keywords: Wireless network, optical network, MPMCL, MHRA, LSP & survivability, broadband access network.

1. INTRODUCTION

A WOBAN network is a concatenation of two networks that confer the benefits of both an optical network [1, 2] and a wireless network. In an optical network, the passive optical network provides high speed for the back-end and is combined with the WMN, which is a resilient access network. Fig. (**1**) represents the architecture of a WOBAN. A PON is a credible low-cost optical network, and it includes optical line terminal (OLT), splitter, and optical network units (ONU).

In a PON, the downstream data is sent from OLT towards ONUs which divide at a splitter and propagate to each of ONUs. In upstream transmissions from ONUs to the OLT, polling is employed as a TDMA multiple access technology to allow the ONUs to share a similar optical line. ONUs are assigned time slots, and they are allowed to transmit data only during the assigned time slots. Another part, WMN, consists of mesh routers and ONUs where mesh routers are located in a multi-hop manner and maintain the router to router connectivity in the network [3, 4].

In recent years, the advantages of both wireless networks and optical networks have been pondered to get more efficient access solutions in the future [5, 6]. It also provides a cost-efficient infrastructure to support a wide range of emerging 5G applications [7-9]. Several issues such as placement of ONUs, routing, energy efficiency, and survivability are present in the WOBAN network. The issue of ONU placement arises in network planning when considering how to properly place ONU in the network so that the network may cover the whole network area efficiently. This issue impresses the cost performance of the network. Usually, by putting low-loaded devices into sleep mode, energy can be saved [10] The issue of survivability is also more crucial in WOBAN [11-13]. Survivability means to supply sustained services to users if a component failure occurs in the network. A large amount of traffic could be affected if the network were to fail. Huge losses may occur as a result of this.

WOBAN consists of a front-end network and back-end network, in which wireless link failure occurs in the front end and ONU failure & OLT failures occur in the back-end. Repairing in failed WOBAN may result from front-end survivability or back-end survivability [14]. Most of the research works are related to back-end survivability but we consider front-end survivability because it also affects the overall per-

*Address correspondence to this author at the Department of Electronics & Telecommunication Engineering, Institute of Engineering & Technology., DAVV, Indore, P.O. Box: 452017, Indore, India;
E-mail: ssolanki@ietdavv.edu.in

A Novel Software Quality Characteristic Recommendation Model to Handle the Dynamic Requirements of Software Projects that Improves Service Quality and Cost

Kamal Borana[1], Meena Sharma[2], Deepak Abhyankar[3]

Research Scholar, Computer Engineering Department-Institute of Engineering and Technology,
Devi Ahilya Vishwavidyalaya, Indore, India[1]

Professor, Computer Engineering Department-Institute of Engineering and Technology,
Devi Ahilya Vishwavidyalaya, Indore, India[2]

Software Engineer, School of Computer Science & IT, Devi Ahilya Vishwavidyalaya, Indore, India[3]

Abstract—The software is created and constructed to address particular issues in the applied field. In this context, there is a need to be aware of the crucial characteristics to assess the quality of software. But not all software requires checking all the quality-of-service parameters, resulting in effort loss and time consumption. Therefore, it is required to develop software quality characteristics recommendation model to address and resolve the issue. The proposed work involved in this paper can be subdivided into three main parts (1) a review of popular software quality models and their comparison to create a complete set of predictable, and (2) the design of an ML-based recommendation model for recommending the software quality model and software quality characteristics (3) performance analysis. The proposed recommendation system utilizes the different software quality of service attributes as well as the software attributes where these models are suitably applied to satisfy the demands. Profiling of applications and their essential requirements have been performed Based on the different quality of service parameters and the requirements of applications. These profiles are learned by machine learning algorithms for distinguishing the application-based requirement and recommending the essential attributes. The implementation of the proposed technique has been done using Python technology. The simulation aims to demonstrate how to minimize the cost of software testing and improve time and accuracy by utilizing the appropriate quality matrix. Finally, a conclusion has been drawn and the future extension of the proposed model has been reported.

Keywords—Recommendation system; software quality model; ML (Machine Learning); quality matrix; software quality characteristics

I. INTRODUCTION

Machine learning provides ease in several real-world applications; in addition, improves the capacity and capability of existing research and methodologies.ML techniques are also used to improve and optimize different process models for improving the cost of employment and productivity[1][2].In this context, software quality evaluation is one of the essential steps. There are several different software quality measuring models currently utilized. These models include several different quality measuring characteristics.

Software quality is an emerging research area in the field of software engineering. The work presented here is relevant to the research around software quality models which gives a better understanding and knowledge of software quality attributes in Software quality models. Achieving software quality assurance requires the use of software quality models [3]. These quality attributes might be used to describe the software's quality. It might be difficult to decide which of the excellent models to utilize [4]. In Addition, software quality models are used for the global assessment of the software product. Therefore, the proposed issue of applying and selecting the appropriate quality matrix is defined here as the recommendation problem. The recommendation engines are the machine learning technique for evaluating the problem's current scenario and suggesting the most suitable solutions for the given set of problems [5].

There are different kinds of recommendation systems available, which will also work as the information filter to reduce the less relevant data and optimize the ranking of the desired set of information [6][7]. The proposed software quality characteristics recommendation model includes the technique of machine learning to learn when, where, and which software characteristic is appropriate for evaluation based on profiling of the software quality of service requirements. In this context, the proposed work is subdivided into the following essential task:

- Examination of different software quality characteristics and models.

- Implement and design a content-based recommendation model to suggest the appropriate quality matrix.

- Study the impact of the software quality characteristic recommendation model over the existing models.

A Review on forecasting the photovoltaic power Using Machine Learning

Amit Kumar Mittal[1, 4], Dr. Kirti Mathur[2], Shivangi Mittal[3]

[1] Assistant Professor Computer Engineering IET DAVV, Indore, Madhya Pradesh, India
[2] Associate Professor IIPS DAVV, Indore, Madhya Pradesh, India
3 Lecturer Electrical Engineering Govt. Polytechnic College Dewas Madhya Pradesh, India

[4]Email: amittal@ietdavv.edu.in

Abstract. In this review paper on different forecasting method of the solar power output for effective generation of the power grid and proper management of transfer rate of energy per unit area occurred into the solar PV system. Essential part in focusing the prediction of solar power is irradiance and temperature. The irradiance can be forecasted by many algorithm and method is applied in prediction of generation of Short-term photovoltaic power and long term solar power forecasting. And many papers describes on numerical weather forecasting and some algorithm like neural networks or support vector regression for two step approach for predicting the PV power. In this review shown that methods like Bagging Model , deep learning, genetic algorithm, random forest, gradient boosting and artificial neural network. We found that for enhancing the performance of predicting PV power many authors proposed the ensemble method that is the hybrid models of different algorithm. And I found that on this review process ensemble methods show that good results and improve the forecasting solar PV power.

Keyword
Photovoltaic Power, Irradiance, Machine learning, LSTM, Performance, forecasting, deep learning,.

1. Introduction

In the era of renewable energy, we have focused on energy produced by solar cell and with the large drop in prices of photovoltaic (PV) cell the use of solar energy has increased [1]. Today one of the renewable energy Source is PV power and in the future electricity generation it plays important role. A great part of net electricity capacity of the globe growth occur in year 2017. Between years 2019 to 2024 the net renewable energy is expected to grow 50 percent globally. The proportion of solar power in renewable energy is 60 percent [4].

The solar power forecasting has some benefit like efficient operation in the power grid, optimization of energy into the PV power system, power plant Schedule, Congestion management, Trade the produce energy in the energy market, Price reduction for power generation.

A Software Quality Characteristics Optimization Model to Reduce Evaluation Overhead

Kamal Borana[1]([✉]), Meena Sharma[1], and Deepak Abhyankar[2]

[1] IET, DAVV, Indore, India
kamalborana2006@gmail.com
[2] SCSIT, DAVV, Indore, India

Abstract. Software quality evaluation is one of the critical processes for delivering good quality software products. The software quality evaluation has a significant effect on the entire project. However, for software quality evaluation a number of techniques are available. Most of the models are based on the characteristics of software and relevant scores. But consideration and evaluation of software on all the quality characteristics are time is taken and complex, which is not suitable for all kinds of projects. Therefore, in order to reduce the software quality assessment effort, this paper proposes a categorization of essential quality characteristics based on software project needs. Additionally, a Particle Swarm Optimization Process is proposed for recommending the suitable software quality evaluation attributes. The simulation of the model has been carried out and their performance analysis has been done. Based on the experimental analysis the results are presented and the future scope of the proposed work is explained.

Keywords: Software Quality Models · Recommendation System · Machine Learning · Testing Cost · Model Selection

1 Introduction

Software quality is essential for an efficient and reliable software product development [1]. Therefore, evaluation of software is an essential step of software development. The software quality is depends on different processes and activities involved in software development life cycle (SDLC) [2]. However, there are a number of software quality measuring models available based on different attributes and scoring techniques. These quality measuring characteristics used to express the quality of the software product. Additionally, different software quality evaluation models are recommending different characteristics for product evaluation. Therefore, selection of suitable software quality evaluation models is a challenging task [3].

Therefore, the proposed work is keenly interested to explore the possibility for applying and selecting the appropriate quality measuring characteristics. The proposed technique is evaluating of the software attributes as well as the different quality measuring attributes for suggesting appropriate quality evaluation attributes. The proposed model

ORIGINAL CONTRIBUTION

A Finite Element Model-Based Approach for Rotor Unbalance Detection and Balancing

Dinesh Kumar Pasi[1] · Manoj Chouksey[1] ·
Ashesh Tiwari[2]

Abstract An unbalance identification and balancing technique have been presented using a finite element model of the rotor system. Unlike conventional methods of balancing, the proposed approach of balancing computes influence coefficients using the system's finite element (FE) model. Identification of unbalance in a single disc rotor system has served as a demonstration of the method's applicability. The traditional method of balancing involves the laborious addition of trial weights and vibration measurement during the process of calculating influence coefficients. As the necessary information is derived from the FE model of the rotor system, the suggested method of balancing does not require the addition of trial weights. It is suggested to use an updated FE model of the rotor system in order to compute the vibration data necessary in the calculation of influence coefficients. The finite element model of the rotor system has been updated using the Inverse Eigen Sensitivity Method. In order to find the heavy spot, the unbalance in the rotor disc's phase angle can be found using the method of unbalance identification. Numerous spin speeds of rotation have been used in the experimental studies of unbalance identification to determine if there is any effect.

Keywords Influence coefficients · Unbalance identification · Balancing · Finite element (FE) model updating

✉ Dinesh Kumar Pasi
  dkpasi25@gmail.com

[1] Department of Mechanical Engineering, Shri G. S. Institute of Technology and Science, Indore, India

[2] Mechanical Engineering Department, IET-Devi Ahilya University, Indore, India

Introduction

Unbalance is the major contributor of excitation in rotating machines. Some amount of unbalance always remains in the machines even with a precise balancing [1], which is termed as residual unbalance. Vibration signal is used as an indicator to keep track of machinery health. During operation, the balancing state deteriorates for a variety of causes, including dirt accumulation, corrosion, erosion, and particle impact [2]. The need for balancing arose in the late nineteenth century with the development of steam turbines and the current status is that each and every machine need balancing [3]. It is crucial that the vibration levels do not exceed the safe and acceptable levels during run-up and at operating speed, since this would signal the need for balancing [4]. Balancing of rotating machines is a routine practice to minimize the vibrations due to rotating unbalance forces [5]. Often unbalance, if not corrected, causes the occurrence of other types of faults too, e.g., rotor rub, misalignment, etc. Therefore, it is very important to timely diagnose and correct the unbalance in the machines. Rotor may be classified as, namely (i) rigid rotor, (ii) flexible rotor, based on the flexural deflection of the rotor-shaft. It is referred to as a rigid rotor if the flexure caused by the unbalance forces is less than the specified unbalance tolerance at any speed within the maximum operating speed, or as a flexible rotor otherwise [5, 6]. Various methods have been developed over the period of time for unbalance identification and balancing [7–11], e.g., influence coefficient method, modal balancing method and unified approach of balancing. Numerous trial runs are performed in the traditional method of balancing, known as the influence coefficient method, which is an experimental process. The purpose of these runs is to capture rotor response and phase angles in order to make calculations regarding the balancing masses that need to be added in certain planes.

Effect of different crack sizes on the time varying gearmesh stiffness of gear pair

1. Akhilesh Lodwal, Assistant Professor, IET, DAVV, Indore (MP)
2. Dr. Ashesh Tiwari, Professor, IET DAVV, Indore (MP)

Abstract

Gear tooth crack is a type of fault which need monitoring to prevent serious damage to the operating condition of the gear system. In this research work an analytical model is proposed to investigate the effect of gear tooth crack in the form of time varying gear mesh stiffness. In this case the tooth crack propagations is monitored along tooth width, crack depth and crack height are incorporated in this model for simulation of gear tooth root crack. Analysis is started with very small crack size to reflect in results the early stage of fault occurrence Analytical formulation is helpful in finding the mesh stiffness of a spur gear pair with different crack length, width and depth variation. The developed analytical model can predict the change of gear mesh stiffness with presence of a gear tooth crack and also compares the mesh stiffness data with one contact period of gear pair. The analysis is done with the gear pair having more than one tooth in contact during some part of the contact period. This gives single or double tooth contact in one period. Analytical results shows less stiffness when single tooth pair contact occurs for part of TVMS diagram and higher stiffness for remaining part due to double tooth contact.

INTRODUCTION

Gearboxes are the most important mechanism in all automotive application, industries and some daily used system and works on high rotational speed to produce output. Spur gear is mostly used in general gearbox for power transmission. It works at different gear ratios to provide multiple torque ratios. Due to its wide application the monitoring of its health and its early fault detection is very important.

There are many type of fault may arise in gears due to high heat condition, excessive load, bad lubrications etc. like pitting, spalling , crack etc. There are lot of work carried out to investigate gear tooth stiffness with or without faults. Analytical models and Finite element methods are widely used approaches for calculations. Lin Han, Houjanet.al. (2017) determines the effect of crack, pitting, tooth breakage studied on helical gears. Firstly an analytical method is developed to incorporate the faults by combining slicing, integration and potential energy methods. Effect of various parameters on TVMS change was studies [1] Jungho Park et al. (2015) conducted experiment to find the mesh stiffness in faulty state of rotating gears. Transmission error (TE) was used as parameter to make difference between rotation of input and output gear [2]. Fakhar Chaari, Walid Baccar, et. al,(2007) proposed analytical method to quantify the reduction in stiffness due to common teeth faults. The effect of deflection due to bending, contact and fillet foundation was considered to calculate the stiffness. The combined effect of tooth spalling and breakage is observed by frequency and amplitude signal of the system [3]. Ankur Saxena et al. (2016) present computer simulation based analytical approach to quantify the TVMS reduction of gear pair

Determination of Transmission Error and Mesh Stiffness in Spur Gear Pair using CAD-FEM Integration Approach

V K Karma [1], G Maheshwari [2]

[1,2] Mechanical Engineering Department, Institute of Engineering & Technology, Devi Ahilya University, Indore, Madhya Pradesh, 452001, India

vkarma@ietdavv.edu.in

Abstract. Unwanted sound and sensations are key sources of excitations in gear drives. They developed because of Transmission Error (TE). TE is a consequence of geometric or engineering flaws like profile/pitch error etc. or distortions like spall, indentation, crack, rubs etc. arising due to the diverse load conditions. These distortions and various gear parameters like number of teeth, contact ratio, module, pressure angle etc. have huge effects on TE and produce changes in mesh stiffness. This demands to investigate the effects of these parameters on TE and mesh stiffness for the avoidance or early finding of causes of malfunctions in the transmission system using computer models using CAD-CAE (FEM) software. In this paper the TE and mesh stiffness is determined using CAD-FEM integration approach and the impact of some of the gear parameters, tooth tip radius and geometric flaw- pitch error is analyzed. The modeling of spur gears & assembly to form gear pair is done in CAD software SOLIDWORKS. The gear pair formed is then introduced into FEM software Ansys for simulation using transient structural analysis method to find angular deformations and then TE and mesh stiffness. Several charts are drawn amongst rotation angle of one of the gears (driver gear) and TE/mesh stiffness for different gear parameters. The work demonstrated the use of CAD-CAE integration approach and point out that all these parameters affect TE and mesh stiffness in a meaningful way.

Key words: SOLIDWORKS, Pitch Error, Tooth Tip Radius, Tooth Geometry Error, Deformations, Ansys

1. Introduction

Gears are the backbone of the transmission system, and spur gears are the most frequently used elements in it. They are also exposed to distortions because of various engineering/geometric flaws or altering load situations. These distortions are responsible for the development of unsolicited sound and excitations resulting in power or torque loss. To explore the effects of these on power transmission systems such as gear drives, several methods ranging from theoretical or mathematical to experimental or computer simulations are frequently applied successfully. The work presented here shows the use of a CAD and FEM software integration approach developed by [1] for the calculation of mesh stiffness to find the TE and mesh stiffness to analyse the effects of various gear parameters, tooth tip radius and pitch error on TE and mesh stiffness. Pitch error is the difference in theoretically correct pitch and

Analysis of Effects of Change of Gear Parameter Module on Transmission Error in Spur Gear using Interference Volume Method

V Karma [1,4], G Maheshwari [2] and S K Somani [3]

[1,2] Mechanical Engineering Department, Institute of Engineering & Technology, Devi Ahilya University, Indore, Madhya Pradesh, 452001, India   [3] Vice Chancellor, Oriental University, Indore, Madhya Pradesh, India

vkarma@ietdavv.edu.in

Abstract. Gear drives are the most used elements in power transmission systems. Any defect in the gear of these drives leads to noise and vibrations, which affect power/torque transmission. Transmission Error (TE) is one of the critical causes that arises due to the tooth geometry error, cracks in gear, profile error etc. Our work demonstrates, the consequences occurring due to the changes in gear parameter module on TE for spur gear pair of 1:1 gear ratio with pitch error, using the interference volume method. The spur gear without pitch error and with pitch error having the involute profile of standard tooth dimension system and stub tooth dimension system are modelled and assembled in CAD software SOLIDWORKS. The interference volume values obtained from the gear pairs are recorded for one mesh cycle. Various graphs plotted between the angle of rotation and interference volume values for one mesh cycle. It is found from the analysis that as the module and pitch error increase TE also increases. The effect of variation of module and pitch error is more in the standard tooth dimension system than the stub tooth dimension system.

Keywords: CAD, Gear Ratio, Pitch Error, No of Teeth, SOLIDWORKS, Geometry Error

1. Introduction

Gears drives are the most used elements employed to transfer power/torque. The condition to accurately transfer power/torque is that the drive elements such as gears should be free from any error else it could lead to noise and vibrations, which results in the development of Transmission Error (TE) despite of availability of world class manufacturing and design facilities. TE is a show of reading measured of angular or linear displacement by the side of activity on the base circle [1]. Hotait and Kahraman [2] demonstrated experimentally the association connecting dynamic factor and transmission error measurement. The values were obtained from unabated and adapted spur gears using a gear dynamic test set-up. Kohler and Regan [3] concluded that TE has harmonic components of significant amplitude at tooth contact frequency spectrum. Chang and Tang [4] conducted theoretical analysis under the influence of single and cumulative pitch error to investigate the nonlinear vibration response in a double-helical gear set. Velex et al [5] established theoretically a relationship in the middle of active mesh agitation and transmission errors using 3D analysis modal of

Performance Evaluation of Split Air Conditioner with Consideration of Pressure Drop in Evaporator and Condenser

PUNIT MISHRA[1]*, SHUBHAM SONI[2] and GOVIND MAHESHWARI[3]

[1]Mechanical Engineering Department, Shri G S Institute of Technology and Science, Rajiv Gandhi Prodyogiki Vishwavidhyalaya, Indore, India.

[2]Mechanical Engineering Department, Medicaps University, Indore, India.

[3]Mechanical Engineering Department, Institute of Engineering and Technology, Devi Ahilya Vishwavidhyalaya, Indore, India.

Abstract

In this research, a split air conditioner's performance has been evaluated using exergy analysis on three different low global warming potential (GWP) refrigerants, namely R32, R447A, and R447B, to find a replacement for the GWP-high refrigerant R410A. With regard for pressure loss in the evaporator and condenser, a computational model is built to recreate the operational conditions of a split air conditioner. GENETRON Properties 1.4 software is used to calculate performance metrics such as coefficient of performance (COP), exergy destruction ratio, exergetic efficiency, and efficiency defect. Result shows that pressure drop in evaporator alone has an adverse effect on COP and total exergy destruction and it is higher at higher pressure drop. Effect of pressure drop on exergetic efficiency and exergy destruction ratio is found to be less significant with condenser pressure drop compared to evaporator pressure drop. Exergy efficiency is found to be maximum with R447A followed by R447B, R32, and R410A.

Introduction

In looking toward the exponentially rising demand for energy, and environmental protection aspect, researchers from every corner of the globe have been involved to find some new refrigerants with the expectation of improved performance along with eco-friendly aspects considering global warming. Global warming is one of the key concern that should be considered while selecting a refrigerant, as it is one of the major contributor of the undesirable phenomenon known as global warming.[1-2] Global climate change may be caused by a wide range

Theoretical energy analysis of Cascade refrigeration system using low Global warming potential refrigerants

Shubham Soni [a,*], Punit Mishra [a], Govind Maheshwari [b], Devendra S. Verma [b]

[a] Devi Ahilya University, Indore, (M.P.) 452017, India
[b] Department of Mechanical Engineering, Devi Ahilya University, Indore, (M.P.) 452017, India

ARTICLE INFO

ABSTRACT

In the refrigeration sector, refrigerants with low global warming potential (GWP) have become the need of the hour. The presented work aims to investigate the use of low GWP refrigerant pairs like NH_3/CO_2, $R1234yf/CO_2$, and $R1234ze/CO_2$ in the Cascade refrigeration system. This study will help in checking the utility of chosen refrigerants. For the analysis, a mathematical model of a cascade system is prepared and performance parameters like Energy efficiency ratio, compressor power, coefficient of performance are compared for chosen refrigerant pairs. During this study, the Condenser and the evaporator temperature are changed 318 K to 333 K and 228 K to 243 K respectively. It is observed that the highest coefficient of performance is obtained for NH_3/CO_2 which is 8.097% and 4.135 % higher than that obtained for $R1234yf/CO_2$ and $R1234ze/CO_2$ respectively. The compressor power is least consumed for NH_3/CO_2 which is 7.498 % and 3.982 % less than $R1234yf/CO_2$ and $R1234ze/CO_2$ respectively. Thus NH_3/CO_2 is the best choice among all the selected pairs for this study.

1. Introduction

Refrigeration has very wide applications like preservation of food, chemicals, medicine, etc. However, there are some fields, which need very low temperature i.e. lower than 243 K. Single-stage vapour compression refrigeration system cannot be used for obtaining such low temperature as they cannot operate in such a large temperature range hence, two Vapour Compression Refrigeration (VCR) cycles are operated in series as shown in Fig. 1. Such type of arrangement is called cascade refrigeration system (CRS). In the last few decades, the trend of research has been towards finding refrigerants that increase the performance of the system and have a low impact on Ozone and Global warming [11]. During the last few years many researchers have carried out studies on cascade refrigeration system. Researchers like Atkemur et.al, carried out a comparative investigation of energy along with exergy of low global warming potential (GWP) refrigerants and concluded that R41-RE170 performs better in low-temperature regions and has a coefficient of performance (COP) improvement of 13.05%.

[1]. Others like Gholamian et.al, conducted an energy study and exergy study of Cascade refrigeration system using Ammonia and carbon dioxide and highlighted the regions that need improvement [2]. Logesh et.al, analyzed CRS using different refrigerants and concluded that pair of R134a/R170 has better COP and requires less mass flow rate as compared to other considered refrigerant pairs [3]. Z. Sun et.al, did an exergy plus energy investigation of CRS with refrigerants of low GWP and stated that uses of R41/R161 couple is superior as compared to all other selected pair [4]. However, none of the mentioned studies used refrigerant pairs that have negligible GWP. GWP of NH_3, R1234yf, R1234ze, and CO_2 is zero, 4, 7, and 1 respectively.

In the presented work the researchers have done the energy analysis of CRS using refrigerant pair of low GWP NH_3/CO_2, $R1234yf/CO_2$, and $R1234ze/CO_2$ are used as refrigerant pair and performance parameters like Energy Efficiency Ratio (EER), COP, and power consumed in the compressor is calculated using first law of thermodynamics. These parameters are then compared to select the best among the chosen refrigerant pairs. Thus the analysis helps in detecting the use of refrigerants having negligible

Exergetic performance analysis of low GWP refrigerants as an alternative to R410A in split air conditioner

Punit Mishra [a,*], Shubham Soni [a], Govind Maheshwari [b]

[a] Research Scholar, Mechanical Engineering Department, Institute of Engineering and Technology, Devi Ahilya Vishwavidyalaya, Indore 452017, India
[b] Associate Professor, Mechanical Engineering Department, Institute of Engineering and Technology, Devi Ahilya Vishwavidyalaya, Indore 452017, India

ARTICLE INFO

ABSTRACT

In the present analysis, five alternative refrigerants namely R32, R447A, R447B, R452B, and R454B have been analysed based on exergy to find an alternative of high global warming potential refrigerant R410A, in a split air conditioner. Evaporator temperature is considered as 4.5 °C whereas condenser temperature is taken from 40 °C to 60 °C in the interval of 4 °C. Different performance parameters have been calculated like total exergy destruction (TED), exergy destruction ratio (EDR), exergy efficiency, along with the coefficient of performance (COP) and efficiency defect. The result shows that R447A is found to be the potential alternative to replace R410A in the air conditioner as it has 9.24% higher COP and 15.38% less destruction of exergy along with 9.3% higher exergy efficiency compared to R410A at a condenser temperature of 60 °C. TED and EDR, are found to be minimum with the R447A system among all the considered refrigerants.

1. Introduction

HFC410A is used not only in split air conditioners but also in household heat pumps and medium-sized chillers because of its zero ozone depletion potential (ODP). However, it has a rather high Global Warming Potential (GWP) that necessitates the search for its alternatives. As a result, there is a pressing need to identify a replacement for the present R410A (GWP$_{100}$ = 1924) under the Montreal and Kyoto Protocols [1].

Domanski et al. [2] evaluated the system performance using low GWP refrigerants and find that refrigerants with low GWP options are very few, particularly when volumetric capacity is concerned considering R410A or R404A. Blends of refrigerant can meet the desired objective by trade-offs between different performance parameters but the probability to find an ideal best performing refrigerant is minimum. Bell et al. [3] draw a matrix with 13 pure refrigerants having low GWP, alternatives to R134a in air conditioner considering pressure drop in evaporator and condenser with the criteria of non-flammability, higher COP, lower GWP, and volumetric capacity similar to R134a. They concluded that no mixture

was ideal in all the aspects so trade-offs can be made while selecting a refrigerant.

Heredia-Aricapa Y. et al. [4] compares the performance of refrigerant mixture HFC/HFO/HC/R744 on energy basis to find some alternatives of R410A. Among the considered refrigerants R32 along with R446A, R447A, R447B, R452B, R454B, and R459A found to be possible alternatives with improved performance. Fajar T K et al. [5] applied the exergy and energy analysis on small vapour compression refrigeration (VCR) system and obtained higher COP and less exergy destruction with less amount of charge of R290 when retrofitting of R410A. Binbin Yu et al. [6] looked at refrigerant mixes that can deliver equivalent theoretical cycle performance to R410A in air conditioning as well as heat pump applications. They discovered that the R32/R1123/R13I1 mixture increased the volumetric capacity by −4%, 4% to 17%, however the COPs declined slightly from 5 to 10%. To investigate alternatives to the high GWP refrigerant R410A, a performance analysis was conducted utilising six low GWP refrigerants (pure and blends). The binary mix of R32/R1234ze(E) with GWP 300 has the lowest LCCP of the refrigerants tested [7]. Ahmed et al. [8] performs the exergy analysis of VCR system containing R407A, R600A

Comparative energy analysis of R1234yf, R1234ze, R717 and R600a in Vapour Compression Refrigeration system as replacement of R134a

Shubham Soni [a,*], Punit Mishra [a], Govind Maheshwari [b], Devendra S.Verma [b]

[a] Devi Ahilya University, Khandwa road, Indore(M.P.) 452017, India
[b] Department of Mechanical Engineering, Devi Ahilya University, Khandwa road, Indore (M.P) 452017, India

ARTICLE INFO

ABSTRACT

In this study effect of utilization of refrigerants with low Global warming potential is studied theoretically based on first law of thermodynamics and mass balance. Refrigerants like R1234yf, R1234ze, R717, and R600a are used instead of R134a in the Vapour Compression Refrigeration system of 1 TR. The Global Warming Potential of all the refrigerants is negligible (below 4) as compared to that of R134a (1300). The results obtained show that R1234ze and R600a are better refrigerants in the context of COP and power consumed as compared to R134a. Other refrigerants are not very behind and obtain a COP value comparable to that of R134a. R1234yf and R717 may consume slightly more power but their low Global Warming Potential makes them a decent option. R717 requires the least mass flow rate as compared to all the chosen refrigerants.

1. Introduction

The Selection of refrigerant is a complex task. There can be various parameters like cooling capacity, availability, operating temperature, toxicity, etc for the selection of refrigerants. Over the years, however, the criterion has changed to Global Warming Potential (GWP) and Ozone Depletion Potential (ODP). As per Montreal Protocol, 1981 refrigerants that contain Chlorofluorocarbons (CFCs) and Hydrochlorofluorocarbon (HCFCs) were decided to phase out as their ODP values were high. Hydrofluorocarbons (HFC) were considered as replacements of HCFC but they had high GWP. Thus when the decision regarding the refrigerant is made in the context of the environment, low GWP and zero ODP refrigerants are needed. Researchers like Agrawal et. al studied a blend of R290/R600a for replacing R134a in the domestic refrigerator drop-in for domestic refrigerator and found the Performance of R1234yf better than R134a. Gill et al. [6] and Jeema et al. [7] carried study on vapour compression chillers using hydrocarbon-based refrigerants and concluded that hydrocarbons are good alternates for R134a. In this research work the authors have selected refrigerants like R1234yf, R1234ze, R717 and R600a and have carried energy analysis for 1TR of vapour compression refrigeration system[8,9]. Results obtained are then compared with those obtained for R134a. The comparison is done on basis of parameters like Coefficient of performance (COP), Power consumed in compressor (Pc), pressure ratio (Pr), Mass flow rate (m), and Energy Efficiency Ratio (EER). Finally, it is observed that refrigerants like R1234ze, R1234yf, R717, and R600a are better replacements for R134a depending upon different parameters.

Theoretical estimation of efficiency defect in cascade refrigeration system using low global warming potential refrigerant pair

Shubham Soni [a,*], Punit Mishra [a], Govind Maheshwari [b], Devendra S. Verma [b]

[a] Devi Ahilya University, Khandwa Road, Indore (M.P) 452017, India
[b] Department of Mechanical Engineering, Devi Ahilya University, Khandwa Road, Indore (M.P) 452017, India

ARTICLE INFO

ABSTRACT

In the presented work, researchers used Efficiency defect as a parameter for deciding the utility of refrigerants in the Cascade refrigeration system. Cascade refrigeration system's mathematical model is created. Using the first and the second law of thermodynamics energy analysis and exergy analysis are done for different low Global warming potential refrigerant pairs like R134a/CO_2, R1234yf/CO_2, and R1234ze/CO_2. Based on the analysis efficiency defect is calculated for every component of the cascade system individually and the whole system as well. It is found that R1234yf/CO_2 has the highest value of efficiency defect, whereas R134a/CO_2 has the least efficiency defect for the whole cascade system. Change of efficiency defect in various components with evaporator temperature is presented in form of graphs.
Copyright © 2022 Elsevier Ltd. All rights reserved.

Selection and peer-review under responsibility of the scientific committee of the Third International Conference on Recent Advances in Materials and Manufacturing 2021.

1. Introduction

There are various applications in which a temperature lower than − 40 °C is needed. For fulfilling this demand, Cascade Refrigeration System (CRS) is used. The selection of refrigerant pair can be made based on many parameters. However, choosing refrigerant pair of low Global warming potential (GWP) and zero ozone depletion potential (ODP) is the need of the hour [1]. Many studies have been done based on energy analysis of the Cascade refrigeration system. Logesh et al. [2] performed the analysis of the Cascade refrigeration system for various refrigerants and found that the pair of R134a/R170 has better COP and less mass flow rate. Gholamiun et al. [3] performed exergy analysis of CRS using NH3/CO2 and suggested that CO_2- throttling valve, compressor, and heat exchanger are the components where improvements are needed. Atkemur et al. [8] carried a comparative energy & exergy analysis with refrigerants of low GWP. They concluded that R41-R170 performs better in the low-temperature region and has a COP improvement of 13.05%. All these studies made it easier to select the refrigerant. Some researchers like Arora et al. [5] took their research one step ahead. They extended the exergy analysis

of two-stage VCR system and calculated efficiency defect, which is used for determining inter-stage temperature.

In the current study, the authors have used this concept of efficiency defect for the Cascade system. In the submitted work, the exergy analysis of CRS is performed. Based on the results of exergy analysis, the efficiency defect is calculated for different refrigerant pair like R134a/CO_2, R1234yf/CO_2, and R1234ze/CO_2. Refrigerant pair with the least value of efficiency defect is considered the best among chosen refrigerants. Based on the analysis, the variation of efficiency defect of various components of CRS individually with evaporator temperature is presented in graphs.

2. Energy analysis and exergy analysis

A Cascade system is represented in Fig. 1. The compression process is not isentropic. The Efficiency of both compressors is assumed to be 70% [3]. From the concept of energy and mass balance, equations obtained for analysis of each component of CRS are given below [3,4].

$$\sum m_{in} = \sum m_{out} \qquad (1)$$

$$Q + \sum m_{in} h_{in} = W + \sum m_{out} h_{out} \qquad (2)$$

a. Work consumed in low pressure compressor (W_{c1})

* Corresponding author

IET Quantum Communication

ORIGINAL RESEARCH

Deep reinforcement learning-based routing and resource assignment in quantum key distribution-secured optical networks

Purva Sharma[1] | Shubham Gupta[1] | Vimal Bhatia[1,2] | Shashi Prakash[3]

[1]Department of Electrical Engineering, Indian Institute of Technology (IIT) Indore, Indore, India

[2]Faculty of Informatics and Management, University of Hradec Králové, Hradec Králové, Czech Republic

[3]Department of Electronics and Instrumentation Engineering, Institute of Engineering and Technology, Devi Ahilya University, Indore, India

Correspondence

Vimal Bhatia.
Email: vbhatia@iiti.ac.in

Funding information

Indo-US Science and Technology Forum, Grant/Award Number: IUSSTF/JC-089/2019; Ministry of Education, India

Abstract

In quantum key distribution-secured optical networks (QKD-ONs), constrained network resources limit the success probability of QKD lightpath requests (QLRs). Thus, the selection of an appropriate route and the efficient utilisation of network resources for establishment of QLRs are the essential and challenging problems. This work addresses the routing and resource assignment (RRA) problem in the quantum signal channel of QKD-ONs. The RRA problem of QKD-ONs is a complex decision making problem, where appropriate solutions depend on understanding the networking environment. Motivated by the recent advances in deep reinforcement learning (DRL) for complex problems and also because of its capability to learn directly from experiences, DRL is exploited to solve the RRA problem and a DRL-based RRA scheme is proposed. The proposed scheme learns the optimal policy to select an appropriate route and assigns suitable network resources for establishment of QLRs by using deep neural networks. The performance of the proposed scheme is compared with the deep-Q network (DQN) method and two baseline schemes, namely, first-fit (FF) and random-fit (RF) for two different networks, namely The National Science Foundation Network (NSFNET) and UBN24. Simulation results indicate that the proposed scheme reduces blocking by 7.19%, 10.11%, and 33.50% for NSFNET and 2.47%, 3.20%, and 19.60% for UBN24 and improves resource utilisation up to 3.40%, 4.33%, and 7.18% for NSFNET and 1.34%, 1.96%, and 6.44% for UBN24 as compared with DQN, FF, and RF, respectively.

KEYWORDS

deep reinforcement learning, optical network, quantum key distribution, routing and resource assignment

1 | INTRODUCTION

With the rise of various high security-hungry applications, such as finance, cloud-based and several other government services, the importance of optical network security is growing rapidly. This decade will be expected to witness a surge in quantum computers' availability and capability. This evolution of quantum computers is expected to easily break security of the existing and the future optical networks as their security is built on the conventional cryptographic algorithms [1–3]. Thus, to secure the data on optical networks, quantum key distribution (QKD) is proposed as a solution. Quantum keys enhance the security of optical networks, generated by using the QKD technique [4–9] as QKD is based on the fundamental principles of quantum mechanics, namely, the Heisenberg's uncertainty principle [10] and the quantum no-cloning theorem [11], instead of the computational complexity of algorithms [4, 5, 12]. These fundamental principles ensure that a third party trying to eavesdrop on a secret key is easily detected. QKD generates and distributes secret keys over an insecure communication channel using QKD protocols, such as BB84 [13, 14] and others [7, 15–17]. The generated secret keys are then used to encrypt/decrypt the information. The generated quantum keys are impossible to copy because of the

Regular Articles

Implementation of Marin Predators Algorithm for optimizing the position of multiple Optical Network Units in Fiber Wireless Access Networks

Puja Singh [a] [b] ✉ , Shashi Prakash [a] ✉

Show more ⌄

Share   Cite

Abstract

Fiber-Wireless (FiWi) access network is a hybrid network that offers huge bandwidth and ubiquity to the users and is expected to play a dominant role in the emerging next generation communication networks. In this manuscript, a novel Marine Predators algorithm (MPA) is used to optimally place multiple Optical Network Units (ONUs) in FiWi access network. The optimized locations are used in a developed simulation model to assess the performance of FiWi network in terms of throughput and average propagation delay considering peer-to-peer communication. Also, the optimizer's performance was evaluated in terms of fitness value, exploration, exploitation, computational complexity and nature of convergence curve. The MPA's efficiency is benchmarked with respect to a heuristic, Greedy algorithm, as well as existing efficient metaheuristics – Moth-Flame Optimization (MFO), Whale Optimization algorithm (WOA) and Harris-Hawks Optimization (HHO). It was found that MPA outperforms Greedy, MFO, WOA and HHO algorithms in each of the cases.

Introduction

Fiber-Wireless (FiWi) access network is an integrated access network, which provides huge bandwidth and high speed to run quad play applications, such as voice, video, Internet, wireless and premium rich-media applications (e.g., multimedia, interactive gaming and metaverse) [1], [2], [3], [4]. Fiber-Wireless (FiWi) access network [5], [6] or Optical and Wireless Access Network (OWAN) [7] or Wireless and Optical Broadband Access Network (WOBAN) [8] is an ultimate solution to provide cost effectiveness, robustness, flexibility, high capacity and reliability. The advancement of new technologies has also accelerated the development of FiWi networks [9], [10], [11], [12]. Internet of Things (IoT), cloud-based radio access network

Efficient resource provisioning using traffic balancing and crosstalk consideration in multi-core fiber based EONs

Shailendra Kumar Pathak, Shashi Prakash

Show more ⌄

⤳ Share   99 Cite

Abstract

Elastic optical networks technology in combination with space division multiplexing is playing a major role to fulfil the need of increasing internet traffic. However, it suffers from resource sub-utilization due to the traffic heterogeneity in time and bandwidth domains, and the crosstalk between the adjacent cores in a multi-core fiber link. In this paper, we propose time and bandwidth aware traffic balancing strategies with crosstalk consideration to efficiently utilize the spectral resources in MCF based EONs. To this end, we utilize network features and SLA conditions to balance the traffic, in both, the time and the bandwidth domains. In bandwidth domain, we utilize squeezing and splitting with multipath routing, and in time domain, we use sliding and shifting. To further enhance the performance, we use a MCF structure dependent prioritized core allocation based RMCSA strategy. Simulation results indicate superiority of the proposed strategies in terms of different parameters of interest as compared to the benchmark strategies.

Introduction

With the proliferation of high bandwidth applications and services such as grid computing, data center networks and ultra-high definition videos, the internet traffic in the backbone optical network has increased manifold times [1]. At the same time, the transmission capacity of single core fiber (SCF) based optical networks has already reached its physical limit [2]. To address these issues of increasing traffic and capacity crunch in the existing networks, new technologies are required which can efficiently use the available fiber spectrum and further increase the capacity of the optical transport network. Elastic optical networks (EONs) with optical orthogonal frequency division multiplexing (OFDM) modulation technology are promising solution to efficiently and flexibly use the available spectral resources of the optical network. To further

Securing Optical Networks Using Quantum-Secured Blockchain: An Overview

Purva Sharma [1], Kwonhue Choi [2], Ondrej Krejcar [3,4,5,*], Pavel Blazek [3], Vimal Bhatia [1,3] and Shashi Prakash [6]

1   Signals and Software Group, Department of Electrical Engineering, Indian Institute of Technology Indore, Indore 453552, India
2   Department of Information and Communication Engineering, Yeungnam University, Gyeongsan 38541, Republic of Korea
3   Center for Basic and Applied Research, Faculty of Informatics and Management, University of Hradec Kralove, 500 03 Hradec Kralove, Czech Republic
4   Institute of Technology and Business in Ceske Budejovice, 370 01 Ceske Budejovice, Czech Republic
5   Malaysia Japan International Institute of Technology (MJIIT), University Teknologi Malaysia, Kuala Lumpur 54100, Malaysia
6   Photonics Laboratory, Department of Electronics and Instrumentation Engineering, Institute of Engineering and Technology, Devi Ahilya University, Indore 452017, India
*   Correspondence: ondrej.krejcar@uhk.cz

Abstract: The deployment of optical network infrastructure and development of new network services are growing rapidly for beyond 5/6G networks. However, optical networks are vulnerable to several types of security threats, such as single-point failure, wormhole attacks, and Sybil attacks. Since the uptake of e-commerce and e-services has seen an unprecedented surge in recent years, especially during the COVID-19 pandemic, the security of these transactions is essential. Blockchain is one of the most promising solutions because of its decentralized and distributed ledger technology, and has been employed to protect these transactions against such attacks. However, the security of blockchain relies on the computational complexity of certain mathematical functions, and because of the evolution of quantum computers, its security may be breached in real-time in the near future. Therefore, researchers are focusing on combining quantum key distribution (QKD) with blockchain to enhance blockchain network security. This new technology is known as quantum-secured blockchain. This article describes different attacks in optical networks and provides a solution to protect networks against security attacks by employing quantum-secured blockchain in optical networks. It provides a brief overview of blockchain technology with its security loopholes, and focuses on QKD, which makes blockchain technology more robust against quantum attacks. Next, the article provides a broad view of quantum-secured blockchain technology. It presents the network architecture for the future research and development of secure and trusted optical networks using quantum-secured blockchain. The article also highlights some research challenges and opportunities.

Keywords: quantum key distribution; blockchain; quantum-secured blockchain; optical networks; attacks; security

1. Introduction

Optical network infrastructure and services are rapidly growing because of ever-increasing bandwidth-hungry applications such as cloud computing, video conferencing, video messaging, and others. However, optical networks are vulnerable to various types of security breaches, such as service disruption attacks and physical infrastructure attacks [1,2]. Service disruption attacks degrade the performance by inserting interfering signals in the channel for jamming and alien-wavelength attacks. Physical infrastructure attacks, including single component failure, disaster attacks, and critical location attacks, physically damage the optical network infrastructure, such as links or node failure. Currently, in

Efficient ordering policy for secret key assignment in quantum key distribution-secured optical networks

Purva Sharma [a] ⊠ , Vimal Bhatia [a] ⊠ , Shashi Prakash [b] ⊠

Show more ∨

Share　Cite

Get rights and content ↗

Abstract

Quantum key distribution (QKD) is a promising solution to protect data transmission in optical networks against security breaches. Hence, several studies have paid attention on integration of QKD with the existing optical networks. Meanwhile, blocking is a challenging issue for QKD lightpath requests (QLRs) due to limited number of network resources (wavelengths and time-slots) in existing optical networks. In QKD-secured optical networks, the blocking increases with increase in the number of QLRs as well as with the modifications of secret keys for enhancing the security level of QLRs. Hence, the blocking affects the QLRs of different security levels, especially the QLRs of high and moderate security levels. Thus, the prioritization of QLRs based on the security level is essential for reducing the impact of blocking in such networks. In this paper, we propose a secret key assignment priority ordering policy (SKA-POP) for routing, wavelength and time-slot assignment (RWTA) to improve the success probability of QLRs. In the proposed SKA-POP, the resources during assignment and re-assignment are allocated based on the proposed priority criteria. The performance of the proposed SKA-POP is analyzed in terms of the success probability and the probability of secret key update failure (P_{SKUF}). Simulations performed on two different network topologies, namely, NSFNET and UBN24, indicate that the proposed SKA-POP performs better than the non-priority based RWTA (NP-RWTA), priority order-based RWTA (POB-RWTA), partial-priority based RWTA (PP-RWTA), and a version of SKA-POP, i.e., SKA-POP with the longest route first (SKA-POP-LRF) schemes, when the number of QLRs (traffic load) increase in the network. .

Introduction

Optical fiber communication networks are vital for supporting exponential growth in global IP traffic as will be seen in current decade. According to the Cisco Visual Networking Index Report, the global IP traffic will reach an annual rate of 4.8 Zettabytes by 2022 [1]. Meanwhile, it has been observed that the increasing

Deep transfer learning based photonics sensor for assessment of seed-quality

Puneet Singh Thakur [a], Bhavya Tiwari [a], Abhishek Kumar [a], Bhavesh Gedam [a], Vimal Bhatia [a b], Ondrej Krejcar [b c], Michal Dobrovolny [b], Jamel Nebhen [d], Shashi Prakash [e]

Show more ⌄

Share   Cite

Get rights and content

Abstract

Seed-quality is one of the most important factors for achieving the objectives of uniform seedling establishment and high crop yield. In this work, we propose laser backscattering and deep transfer learning (TL) based photonics sensor for automatic identification and classification of high-quality seeds. The proposed sensor is based on capturing a single backscattered image of a seed sample and processing the acquired images by using deep learning (DL) based algorithms. Advantages of the proposed sensor include its ability to characterize morphological and biological changes related to seed-quality, lower memory requirement, robustness against external noise and vibration, easy alignments, and low complexity of acquisition and processing units. Furthermore, use of DL based processing frameworks including convolution neural network (CNN) and various TL models (VGG16, VGG19, InceptionV3, and ResNet50) extract abstract features from the images without any additional image processing and accelerate classification efficiency. Obtained results indicate that all the DL models performed significantly well with higher accuracy; however, InceptionV3 outperformed rest of the models with accuracy reaching up to 98.31%. To validate performance of the proposed sensor standard quality parameters comprising percentage imbibition (PI), radicle length, and germination percentage (GP) were also calculated. Significant change $(p < 0.05)$ in these parameters show that the proposed sensor can accurately monitor the quality of seeds with higher accuracy. Moreover, experimental simplicity and DL based automatic classification make the sensor suitable for real-time applications.

Introduction

Seeds are the foundation for agriculture, and seed quality has a significant impact on crop yield which control the entire seed business including seed producers, breeders, traders, farmers, and distributors

Laser biospeckle technique for characterizing the impact of temperature and initial moisture content on seed germination

Puneet Singh Thakur [a], Amit Chatterjee [a], Laxman Singh Rajput [c], Santosh Rana [d], Vimal Bhatia [a b e], Shashi Prakash [d]

Show more ⌄

∝ Share   ❝ Cite

Get rights and content ↗

Abstract

In this paper, we present laser biospeckle technique for analyzing the impact of temperature regimes and initial moisture content on germination characteristics of soybean seeds. A method is proposed to evaluate the optimum values of recording angle and speckle size for standardizing the experimental parameters. Moreover, to enhance accuracy of the technique, a new procedure based on full-field time history of speckle pattern (FTHSP) for numerical quantification of biospeckle activity (BA) is proposed. Investigations indicate that the BA is significantly ($p<0.05$) dependent on temperature and initial moisture content of seed during germination. Obtained data revealed that these two factors regulated the time required to complete the germination process. The results are benchmarked with standard laboratory test by calculating imbibition rate and germination percentage. These standard laboratory tests are also in agreement with the results acquired by using biospeckle technique. Significant positive correlation ($p<0.01$) between BA and standard germination tests proves applicability of biospeckle analysis as an efficient tool for rapidly evaluating the impact of temperature and initial moisture content on seed germination characteristics. Furthermore, it was also found that both recording angle and size of speckle grains affect the quality of speckle patterns which influence overall accuracy of the analysis. The key advantages of proposed analysis technique are full-field analysis, consideration of optical inhomogeneity present in the samples, lower computation time and complexity (as compared to other full-field techniques), zero standard deviation, and independent of image background.

Introduction

Article

Evaluation of Indian Durum Wheat Genotypes for Yield and Quality Traits Using Additive Main-Effects and Multiplicative Interaction (AMMI) Biplot Analysis under Terminal Heat Stress Conditions

Amit Gautam [1], Sukuru Venkata Sai Prasad [2], Anjana Jajoo [3], Filippo Maria. Bassi [4],*

[1] International Center for Agricultural Research in the Dry Areas (ICARDA)-FLRP, Amlaha, 466113, India

[2] Indian Institute of Rice Research, Hyderabad, 500030, India

[3] School of Biotechnology, Devi Ahiliya University, Indore, 452001, India

[4] International Center for Agricultural Research in the Dry Areas (ICARDA), Rabat, 6929, Morocco

* Correspondence: Filippo Maria. Bassi, Email: F.Bassi@cgiar.org.

ABSTRACT

The abrupt increase of temperatures during and after the flowering period of wheat is defined as terminal heat stress, and it causes severe reductions in productivity. One hundred two durum wheat lines were evaluated against this stress for three consecutive cropping seasons (2014–2017) in Indore, Madya Pradesh (India). The main objectives were to assess their grain yield potential, stability, and rheological quality characteristics under these conditions, and identify other contributing traits to adaptation. Combined ANOVA across environments showed significant differences ($P < 0.01$) for all factors, and high broad sense heritability was recorded for hectoliter weight, 1000-grains weight, grain yield, number of grains per spike, spike length, days to maturity, total carotene and sedimentation values. Grain yield showed significant ($P < 0.01$) positive associated with biomass, harvest index, hectoliter weight and significant negative associations with day to heading and maturity. Genotypes showed explicit variation to environmental condition as supported by significant ($P < 0.01$) for genotype × environment interaction (GEI). The traits like early heading, maturing, high biomass and hectoliter weight were the most critical traits for adaptation under terminal heat stress. To determine effects of GEI data were subjected to GGE biplot analysis, which identified as the most stable and performing across seasons G-30 (GW 1240) for hectoliter weight and G-98 (Vijay) for grain yield. These entries can now be combined via breeding to develop superior heat stress tolerant varieties.

INTRODUCTION

Durum wheat (*Triticum turgidum* spp. *durum*) is the 10th most important cereal crops in the world that is grown on 8 to 10% of the total wheat-cultivated area [1,2]. Durum wheat is mostly cultivated in the Mediterranean basin [3] as it is used in the traditional diet in the form of pasta, couscous, bulgur and many local food products [4–6]. The largest durum wheat growers are the European Union, followed by Canada, Turkey, United States, Algeria, India, Mexico, Kazakhstan, and Syria [7–14]. India is one of the prime producers of durum wheat with some 1.5 million hectares dedicated to its cultivation each year, accounting for approximately 10% of total wheat production [8]. In India during rabi season 2021–22 total cultivated area of wheat was 33.2 million hectare with the record production of around 106 metric ton and total wheat growing area in Madhya Pradesh was 8.71 million hectare with total wheat production was 18 million metric tons whereas durum wheat covered around 1.3 million hectare, with production of 1.5 million metric ton (Progress report State Department of Agriculture Government of India 2023).

The atmospheric temperature plays a critical role in determining the growth and development of the crop. Temperatures exceeding 22 °C detrimental for durum wheat growth, and are hence commonly defined as "heat stress" [15–19]. When temperatures abruptly increase at the end of the growing seasons these are defined as "terminal heat stress". In particular, when this occurs during or immediately after the flowering of the crops it can be extremely damaging [8,14,20,21]. In the optic of the globally raising temperatures, developing better varieties adapted to cope with terminal heat stress is critical to ensure productive farming can continue [22].

Due to the importance and difficulty of the challenge, many studies have been conducted to assess the response of genotypes to this stress in search of novel sources of tolerance [23–27]. The identification of stable and high yielding genotypes is critical to achieve sustainable durum wheat farming in arid and semi-arid regions [28,29], especially when accompanied by strategic agronomical practices [30,31]. Grain yield in wheat is influenced by genotype (G), environment (E), and their interaction Genotype × environment (GEI) [29,32]. Genotypes that respond consistently to different environmental conditions are defined as "stable" and tend to be less influenced by GEI [33]. Because of the unpredictability of climatic conditions, farmers are extremely interested by "stable" varieties capable of tolerating more extreme variations. The identification of traits contributing to stability are important for breeding new cultivars

with improved adaptation to the environmental constraints [34–36]. It was reported that the additive main effects and multiplicative interaction Additive Main-Effects and Multiplicative Interaction (AMMI) model help to distinguish the GEI pattern from the random error components [37,38]. Thus, the present study was conducted to assess the grain yield stability and performance of 102 durum wheat genotypes under terminal heat stress condition during three cropping seasons to identify stable genotypes.

MATERIALS AND METHODS

Genetic Material

Based on the earlier performance under various environmental conditions, 102 genetically diverse durum wheat genotypes were selected from the germplasm developed by the ICAR-Indian Agriculture Research Institute, Regional Station, Indore, India (Supplementary Table S1).

Field Experiments

The field trials were carried out during three consecutive rabi seasons 2014–15, 2015–16, and 2016–17 at the ICAR-Indian Agricultural Research Institute, Regional Station, Indore, Madhya Pradesh India. The experimental field is situated between 22°37' N latitude to 75°50' E longitude at 557 m above Mean Sea Level (MSL) having semi-arid and tropical climate with temperatures shifting from 23 °C to 41 °C and 7 °C to 29 °C in summer and winter seasons, separately, in January before flowering 7 °C to 24 °C and in February after flowering from 23 °C to 31 °C (Figure 1). In this area, most of the rainfall is received during south-west monsoon, i.e., between June to September, with occasional showers in winter. The sowing was done on the 7th of December each season, which corresponds to late sown conditions as a way to maximize exposure to higher temperatures during the flowering transition. Sowing was done in beds having length of 2.5 m in two row plots with a row to row spacing of 18 cm. The experimental design was a randomize block design (RBD) with three replications. Four gravity irrigations of 30 mm were provided during the crop cycle: germination irrigation just after sowing, vegetative stage between 30 to 40 days after sowing, flowering time 55 to 60 days after sowing, and milking stage 80 to 90 days from date of sowing. Recommended agronomical practices were followed to ensure no inputs deficiencies and minimize external effects. All agronomic parameters were recorded (days to heading [39], days to maturity, spike length, number of grains/spike, grain yield/plant, harvest index, and biomass) and several rheological traits (hectoliter weight, yellow pigment, sedimentation value, and 1000 grain weight).
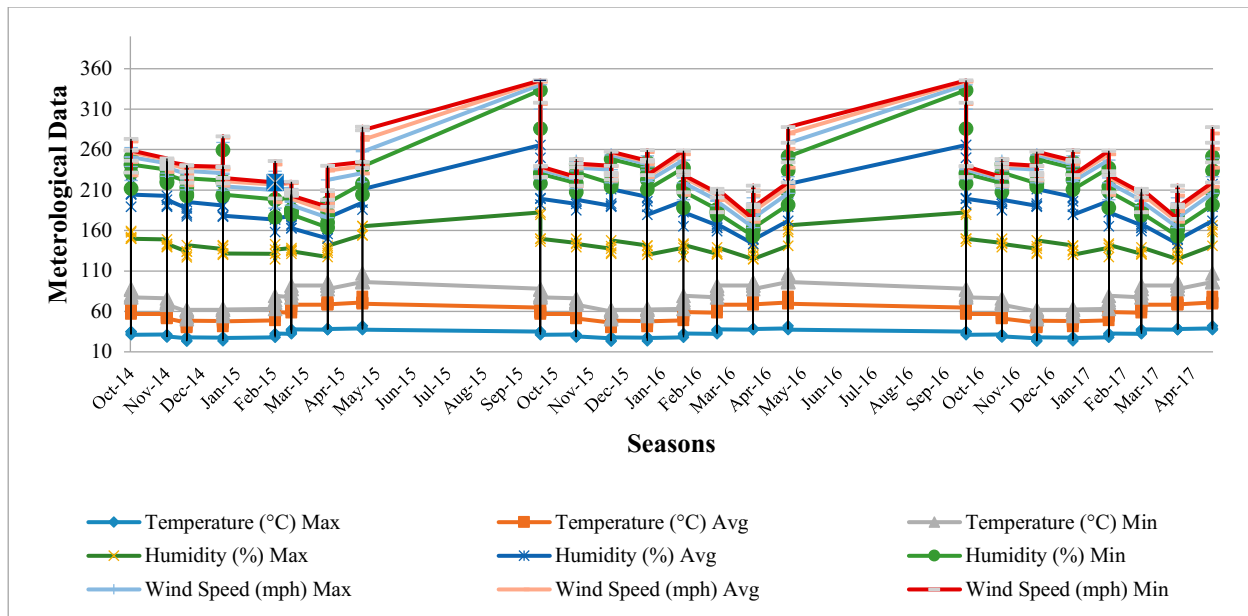
Figure 1. Temperature (°C), Humidity (%), Wind Speed (mph) during crop cycle over the years.

Statistical Analysis

Genstat release 16.1 [40] was used for computing descriptive statistics and correlation analysis. The combined analysis of variance (ANOVA) was performed using Genstat release 16.1 [40], considering genotypes as fixed effects, while years and replications were considered as random effects. The broad sense heritabilities were calculated for each trait using the standard equation [41]. The Additive Main-Effects and Multiplicative Interaction (AMMI) model [42] was run using the Genstat software version 16.1 [40]. The GGE biplot [43,44], was constructed using entry means from each environment for grain yield and quality traits using Genstat software version 16.1 [40]. The GGE biplots model was calculated as follows:

$$\left(Y_{ij} - \overline{Y}j\right) = \lambda_1\xi_{i1}\eta_{j1} + \lambda_2\xi_{i2}\eta_{j2} + e_{ij} \tag{1}$$

Where, Y_{ij} = average yield of ith genotype in j^{th} environment, $\overline{Y}j$ = average yield over all genotypes in j^{th} environment and $\lambda_1\xi_{i1}\eta_{j1}$ and $\lambda_2\xi_{i2}\eta_{j2}$ = collectively the first and second principal component (PC1 and PC2); λ_1 and λ_2 = singular values for the first and second principal components, PC1 and PC2, respectively; ξ_{i1} and ξ_{i2} = PC1 and PC2 scores, respectively for the ith genotype; η_{j1} and η_{j2} = PC1 and PC2 scores, respectively for j^{th} environment; and e_{ij} = residual of the model associated with the ith genotype in the jth environment.

RESULTS

The descriptive results for the combined analysis across seasons are presented in Table 1. Mean value of selected traits based on BLUEs of genotypes 2014–2017 showed diversity among the genotypes. (Supplementary Table S2). The set of genotypes tested generated a

potential genetic gain of 20.8% for grain yield over the mean, and rates ranging from 3.8% for Days to maturity to 38.0% for total carotene.

Table 1. Mean, range, standard error, genetic advance, genetic advance over mean for different traits in durum wheat under terminal heat stress condition.

Traits	Mean	Max	Min	SE±	Genetic advance	GA over mean (%)
DF (days)	74.8	81.8	61.7	0.6	6.6	8.8
DM (days)	113.1	116.2	101.9	0.4	4.3	3.8
SL (cm)	7.3	9.5	5.8	0.0	1.1	15.2
NG	51.6	68.8	33.6	2.9	12	23.3
BM (g)	55.9	71.3	42.5	7.6	8.1	14.5
HI (%)	34.8	45.1	27.1	4.3	6.8	19.6
TGW (g)	48.3	59.7	39.2	1.7	7.8	16.1
HW (g)	78.4	82.1	70.6	1.1	4.0	5.1
T. Car. (ppm)	4.5	7.7	2.7	0.1	1.7	38.0
SDS (mL)	32.4	43.2	22.3	1.6	6.9	21.3
GY (g)	18.8	26.8	13.9	0.4	3.9	20.8

Max: Maximum; Min: Minimum; GA: genetic advance; DF: day to heading; DM: days to maturity; SL: spike length; NG: number of grains/spike; BM: biomass; HI: harvest index; TGM: 1000 grain weight; HW: hectoliter weight; T. Car.: total carotene; SDS: sedimentation value; GY: grain yield/plant.

Table 2. Combined analysis of variance for 102 durum wheat genotypes across three cropping seasons under heat stress conditions.

Statistic	DF	DM	SL	NG	BM	HI	TGW	HW	T. Car.	SDS	GY
H^2	0.88	0.72	0.74	0.77	0.54	0.31	0.78	0.86	0.71	0.70	0.77
GV	10.9**	4.7**	0.4**	36.9**	21.2**	4.2**	16.0**	4.6**	0.8**	12.7**	4.0**
G × E	4.4**	5.3**	0.4**	31.6**	51.9**	26.9**	13.2**	1.9**	1.0**	15.5**	3.6**
RV	0.6	0.4	0.1	2.9	7.6	3.8	1.7	1.1	0.1	1.6	0.4
GM	74.8	113.1	7.3	51.6	55.9	34.8	48.3	78.4	4.5	32.4	18.8
LSD	3.2	3.2	0.8	8.1	8.7	4.7	5.3	2.2	1.4	5.4	2.7
CV (%)	1.0	0.6	3.0	3.3	4.9	5.6	2.7	1.3	8.5	3.9	3.3

** significant at 5% and 1% level of probability, respectively; H^2: Heritability; GV: Genotypic Variance; G × E: Genotypic × Environment; RV: Residual Variance; GM: Grand Mean; LSD: Least significant difference; CV: Coefficient of variation; DF: day to heading; DM: days to maturity; SL: spike length; NG: number of grains/spike; BM: biomass; HI: harvest index; TGW: 1000 grain weight; HW: hectoliter weight; T. Car.: total carotene; SDS: sedimentation value; GY: grain yield/plant.

In Table 2 is summarized the descriptive statistics for the combined analysis. All the studied traits over the years revealed significant effects ($P < 0.01$) for the years. The coefficient of variation (CV) for the investigated traits across environments varied between 0.58% (days to maturity) to 8.49% (total carotene). The lowest CV was observed for number of grains per spike (3.33%), followed by sedimentation value (3.94%), biomass (4.94%), harvest index (5.26%), and highest for total carotene (8.49%). The heritability ranges from 0.31 (harvest index) to 0.88 (days to heading) across the environments. The heritability for grain yield across

environments was 0.77, indicating the influence of environment on grain yield, but also indicating that efficient selection and genetic gain can be made. High estimates of heritabilities were observed for hectolitre weight (0.86), followed by 1000 grain weight (0.78), grain yield (0.77), number of grains per spike (0.77), spike length (0.74) and other traits like days to maturity, total carotene and SDS values were an indicator that these traits have a strong genetic component under limited environmental influence.

Phenotypic Correlation among the Traits under Terminal Heat Stress

Phenotypic correlations between grain yield and the other traits are presented in Table 3 (Supplementary Figure S1). The most significant ($P < 0.01$) contributing traits were biomass (0.63), harvest index (0.45), hectoliter weight (0.23), while significant ($P < 0.01$) negative correlation were identified with day to heading (−0.17) and days to maturity (−0.18). As it can be expected, day to heading showed highly positive association with days to maturity (0.80) but also number of grains/ spike (0.26), total carotene (0.29), and a negative association with spike length (−0.26) and 1000-grains weight (−0.41). The number of grains/spike showed positive association with hectoliter weight (0.41), total carotene (0.26). and sedimentation value (0.24). Biomass showed negative association with harvest index (−0.39).

Table 3. Phenotypic correlation coefficients between mean yield and other traits across three cropping seasons under heat stress conditions.

Traits	DF	DM	SL	NG	BM	HI	TGW	HW	T. Car.	SDS
DM	0.80**									
SL	−0.26**	−0.26**								
NG	0.26**	0.15 [ns]	0.04 [ns]							
BM	−0.13 [ns]	−0.06 [ns]	0.19*	0.19*						
HI	−0.03	−0.10 [ns]	−0.12 [ns]	−0.10 [ns]	−0.39**					
TGW	−0.41**	−0.28**	0.14 [ns]	−0.18*	0.11 [ns]	−0.03 [ns]				
HW	0.05 [ns]	−0.03 [ns]	−0.21**	0.41**	0.19*	0.04 [ns]	0.03 [ns]			
T. Car.	0.29**	0.32**	0.06 [ns]	0.28**	0.05 [ns]	−0.06 [ns]	−0.20*	0.06 [ns]		
SDS	0.08 [ns]	0.04 [ns]	0.02 [ns]	0.24**	−0.08 [ns]	0.17*	−0.02 [ns]	0.21*	0.29**	
GY	−0.17*	−0.18*	0.13 [ns]	0.11 [ns]	0.63**	0.45**	0.07 [ns]	0.23**	0.01 [ns]	0.09 [ns]

*, ** significant at 5% and 1% level of probability, respectively; ns: non-significant; DF: day to heading; DM: days to maturity; SL: spike length; NG: number of grains/spike; BM: biomass; HI: harvest index; TGW: 1000 grain weight; HW: hectoliter weight; T. Car.: total carotene; SDS: sedimentation value; GY: grain yield/plant.

Stability Analysis for Grain Yield and Other Trait by Additive Main-Effects and Multiplicative Interaction (AMMI) Biplot Analysis

Additive Main-Effects and Multiplicative Interaction (AMMI) was performed for grain yield to assess GEI (Supplementary Table S3). Biplot is the most powerful interpretive tool for Additive Main-Effects and

Multiplicative Interaction (AMMI) model. We constructed a biplot for each trait where the main effects and IPCA scores are plotted against each other for genotypes and environments (Supplementary Table S3).

DF: The distribution of the environments indicates that the environments used are distinct for this trait. PCA 1 and PCA 2 were both significant and accounted for 63.4% and 36.6% of the phenotypic variance, respectively. The biplot placed indicated that G-11 (Bijaja Red), G-47 (HI 8653), G-8 (B 4447-BA) and G-81 (NIDW 70) were the most stable genotypes under terminal heat stress condition (Figure 2a,b).

Figure 2. (a) The "which-won-where" view of the GGE biplot based on the G × E data for days to flowering. It explained 100% of the total G + GE. The genotypes are labeled as 1 to 102 and the environments are labeled as E1 to E3. **(b)** The biplot display of days to heading (DtH), biplot explains variability and regression coefficient of genotypes, it also explains adaptability and stability of the genotypes for days to heading, under terminal heat stress conditions.

SL: PCs of Additive Main-Effects and Multiplicative Interaction (AMMI) biplot for spike length showed that PCA 1 and PCA 2 were significant. PC1 and PC2 accounted for 54.4% and 45.6% of variance respectively. It means that by using PC1 and PC2, the analysis could explain 100% variation (Supplementary Table S3). The genotypes G-19 (DWL 5023), G-24 (GW 2), G-26 (GW 1139), G-4 (HI 8550), G-40 (HI 8498), G-42 (HI 8591), G-44 (HI 8627), G-45 (HI 8638), G-48 (HI 8663), G-51 (HI 8691) and G-6 (Amrut) were the most adaptable genotypes for spike length, similarly G-27 (GW 1170), G-4 (AKDW 4240) and G-90 (Raj 6516) were the most stable genotypes and G-4 (AKDW 4240) was the most adaptable and stable genotypes for spike length yield under terminal heat stress condition.

NG: PCs of Additive Main-Effects and Multiplicative Interaction (AMMI) biplot for number of grains/spike showed that PCA 1 and PCA 2 were significant. PC1 and PC2 accounted for 52.3% and 47.7% of variance

respectively. It means that by using PC1 and PC2, the analysis could explain 100 % variation (Supplementary Table S3). The distribution of the environments in the biplot with variable environment means and IPCA scores indicate that the environments behaved very distinct compared each other and selecting of the adaptable and high yielding genotypes among these environments will be useful for terminal heat stress in durum wheat. Among the environments, E2 had short vectors and they did not exert strong interactive forces while E1 and E3 with long vectors were more differentiating environments. The genotypes near the origin are not sensitive to environmental interaction and those distant from the origin are sensitive and have more G × E interactions. The genotypes G-1 (A-9-30-1), G-100 (WH 912), G-3 (AKDW 4151), G-38 (HI 7747), G-39 (HD 4709), G-5 (Altar), G-52 (HI 8722), G-53 (IWP 5004-1), G-56 (IWP 5013), G-74 (MPO 215), G-86 (PDW 233) and G-99 (WH 896) were the most adaptable genotypes for number of grains/spike, similarly G-12 (Bijaga Yellow) and G-55 (IWP 5013) were the most stable genotypes for number of grains/spike under terminal heat stress condition (Figure 3a,b).

Figure 3. (a) The "which-won-where" view of the GGE biplot based on the G × E data for days to flowering. It explained 100% of the total G + GE. The genotypes are labeled as 1 to 102 and the environments are labeled as E1 to E3. **(b)** The biplot display of number of grains per spike (NG), biplot explains variability and regression. coefficient of genotypes, it also explains adaptability and stability of the genotypes for number of grains per spike under terminal heat stress conditions.

BM: PCs of Additive Main-Effects and Multiplicative Interaction (AMMI) biplot for biomass showed that PCA 1 and PCA 2 were significant. PC1 and PC2 accounted for 74.6% and 25.4% of variance respectively. It means that by using PC1 and PC2, the analysis could explain 100% variation (Supplementary Table S3). Among the environments, E2 had short vectors and they did not exert strong interactive forces while E1 and E3 with long

vectors were more differentiating environments. The genotypes near the origin are not sensitive to environmental interaction and those distant from the origin are sensitive and have more G × E interactions. The genotypes G-25 (GW 1114), G-27 (GW 1170), G-30 (GW 1240), G-31 (GW 1244), G-37 (HG 110), G-40 (HI 8498), G-51 (HI 8691), G-55 (IWP 5013), G-6 (Amrut), G-62 (Line 1172), G-77 (N 59), G-82 (NIDW 295), G-89 (Raj 6069) and G-90 (Raj 6516) were the most adaptable genotypes for biomass, similarly only G-12 (Bijaga yellow) was the most stable genotype for biomass under terminal heat stress condition.

HI: PCs of Additive Main-Effects and Multiplicative Interaction (AMMI) biplot for harvest index showed that PCA 1 and PCA 2 were significant. PC1 and PC2 accounted for 66.8% and 33.2% of variance respectively and IPC3 contribute 0.0% variation of the total with Pr. *F* value more than 0.00. It means that by using PC1 and PC2, the analysis could explain 100 % variation (Supplementary Table S3). Among the environments, E2 had short vectors and they did not exert strong interactive forces while E1 and E3 with long vectors were more differentiating environments. The genotypes near the origin are not sensitive to environmental interaction and those distant from the origin are sensitive and have more G × E interactions. The genotypes G-10 (Baxi 228-18), G-15 (DBP 01-09), G-25 (GW 114), G-27 (GW 1170), G-5 (Altar 84), G-50 (HI 8671), G-6 (Amrut), G-71 (Mandsaur local), G-74 (MPO 215), G-77 (N 59), G-89 (Raj 6069), G-9 (Bansi local) and G-97 (VD 97-15) were the most adaptable genotypes for harvest index, similarly G-33 (HD 4502), G-41 (HI 8550), G-77 (N 59) and G-91 (Raj 6562) were the most stable genotypes and G-77 (N 59) was the most adaptable and stable genotypes for harvest index under terminal heat stress condition.

TGW: PCs of Additive Main-Effects and Multiplicative Interaction (AMMI) biplot for 1000 grain weight showed that PCA 1 and PCA 2 were significant. PC1 contribute 52.9% variation to the total whereas PC2 contribute 47.1% to the total variation. It means that by using PC1 and PC2, the analysis could explain 100% variation (Supplementary Table S3). Additive Main-Effects and Multiplicative Interaction (AMMI) biplot placed genotypes G-10 (Baxi 228-18), G-11 (Bijaga Red), G-14 (CPAN 6236), G-29 (GW 1225), G-31 (GW 1244), G-44 (HI 8627), G-45 (HI 8638), G-46 (HI 8645), G-47 (HI 8653), G-48 (HI 8663), G-66 (MACS 2846), G-68 (MACS 3063), G-71 (Mandsaur local) and G-91 (Raj 6562) were the most adaptable genotypes for 1000 grain weight, similarly G-67 (MACS 3061) and G-82 (NIDW 70) were the most stable genotypes and G11 (Bijaga Red) and G-8 (B 4447-BA) were the most adaptable and stable genotypes for 1000 grain weight under terminal heat stress condition (Figure 4a,b).
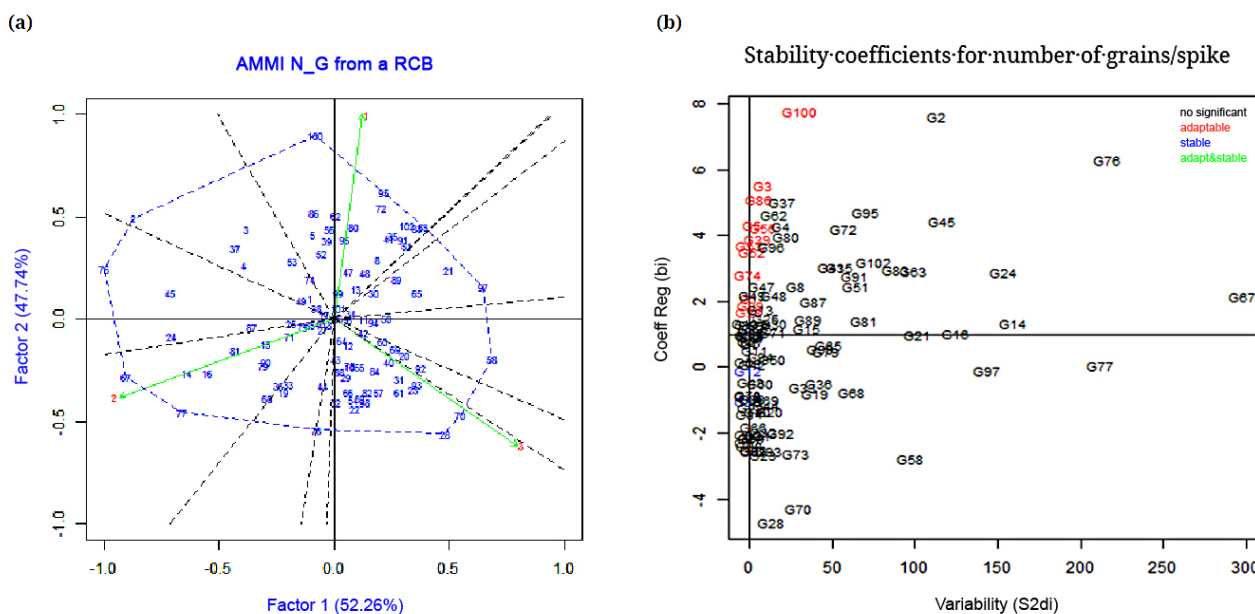
Figure 4. (a) The "which-won-where" view of the GGE biplot based on the G × E data for TGW. It explained 100% of the total G + GE. The genotypes are labeled as 1 to 102 and the environments are labeled as E1 to E3. **(b)** The biplot display of 1000 grain weight, biplot explains variability and regression coefficient of genotypes, it also explains adaptability and stability of the genotypes for 1000 grain weight under terminal heat stress conditions.

HW: PCs of Additive Main-Effects and Multiplicative Interaction (AMMI) biplot for hectoliter weight showed that PCA 1 and PCA 2 were significant. PC1 and PC2 accounted for 69.9% and 30.1% of variance respectively. It means that by using PC1 and PC2, the analysis could explain 100% variation (Supplementary Table S3). Among the environments, E1 had short vectors and they did not exert strong interactive forces while E2 and E3 with long vectors were more differentiating environments. The genotypes G-10 (Baxi 228-18), G-15 (DBP 01-09), G-25 (GW 114), G-27 (GW 1170), G-5 (Altar 84), G-50 (HI 8671), G-6 (Amrut), G-71 (Mandsaur local), G-74 (MPO 1215), G-77 (N 59), G-89 (Raj 6069), G-9 (Bansi local) and G-97 (VD 97-15) were the most adaptable genotypes Hectoliter weight, similarly G-22 (Guji 'S'), G-26 (GW 1139), G-30 (GW 1240), G-50 (HI 8671), G-68 (MACS 3063), G-83 (NP 4) and G-87 (PDW 245) were the most stable genotypes and G-30 (GW 1240) was the most adaptable and stable genotypes for hectoliter weight under terminal heat stress condition.

T. Car.: For total carotene, Additive Main-Effects and Multiplicative Interaction (AMMI) biplot analysis between the mean values and the mean of IPCA scores (Figure 5a,b) indicated that there is no much distinct behavior among the environments. PCs of Additive Main-Effects and Multiplicative Interaction (AMMI) biplot showed that PCA 1 and PCA 2 were significant. PC1 and PC2 accounted for 66.9% and 33.1% of variance respectively. It means that by using PC1 and PC2, the analysis could explain 100% variation (Supplementary Table S3). Additive Main-Effects

and Multiplicative Interaction (AMMI) biplot placed genotypes G-18 (Dohad local), G-19 (DWL 5023), G-24 (GW 2), G-25 (GW 1114), G-30 (GW 1240), G-67 (MACS 3061), G-71 (Mandsaur local), G-74 (MPO 215), G-77 (N 59), G-78 (NI 5759), G-96 (V 21/23) were the most adaptable genotypes for total carotene under terminal heat stress condition.
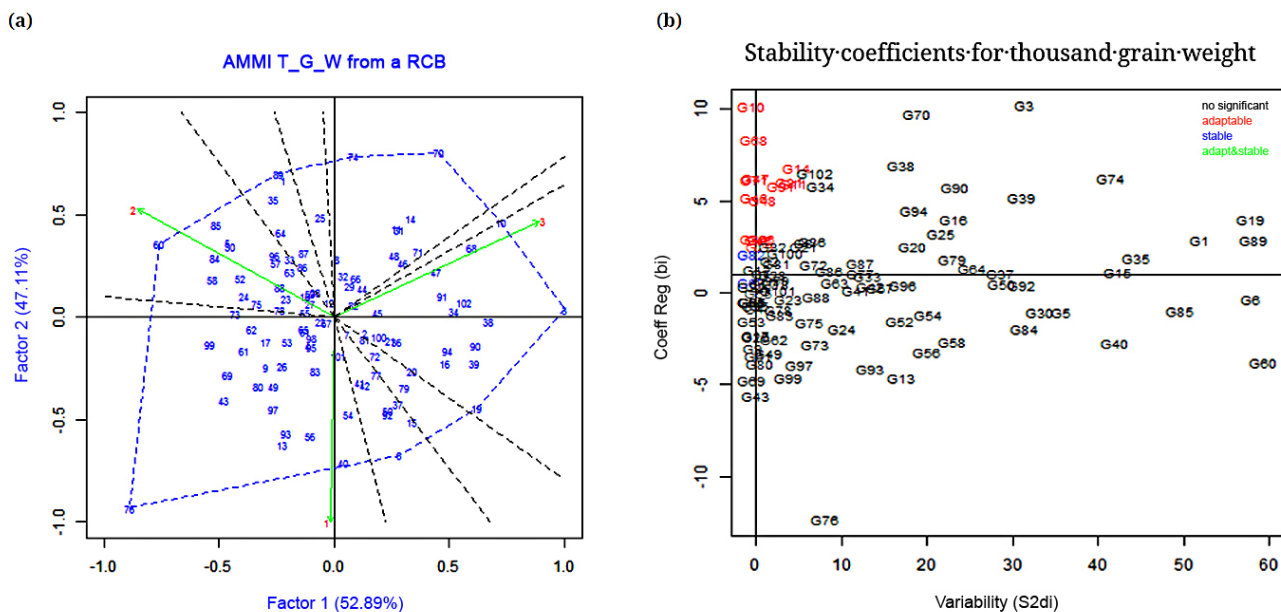

Figure 5. (**a**) The "which-won-where" view of the GGE biplot based on the G × E data for total carotene. It explained 100% of the total G + GE. The genotypes are labeled as 1 to 102 and the environments are labeled as E1 to E3. (**b**) The biplot display of total carotene (T. car.), biplot explains variability and regression. coefficient of genotypes, it also explains adaptability and stability of the genotypes for total carotene under terminal heat stress conditions.

SDS value: For sedimentation value, Additive Main-Effects and Multiplicative Interaction (AMMI) biplot analysis between the mean values and the mean of IPCA scores (Figure 6a,b) indicated that there is no much distinct behavior among the environments. PCs of Additive Main-Effects and Multiplicative Interaction (AMMI) biplot showed that PCA 1 and PCA 2 were significant. PC1 and PC2 accounted for 60.1% and 39.9% of variance respectively. It means that by using PC1 and PC2, the analysis could explain 100% variation (Supplementary Table S3). Additive Main-Effects and Multiplicative Interaction (AMMI) biplot placed genotypes G-19 (DWL 5023), G-24 (GW 2), G-27 (GW 1170), G-31 (GW 1244), G-32 (GW 1245), G-34 (HD 4672), G-5 (Altar 84), G-63 (MACS 9), G-72 (Meghdoot), G-89 (Raj 6069), G-90 (Raj 6516) and G-95 (Trinakria) were the most adaptable genotypes for sedimentation value, similarly G-19 (DWL 5023) and G-52 (HI 8722) were the most stable genotypes and G-19 (DWL 5023) was the most adaptable and stable genotypes for sedimentation value under terminal heat stress condition.(Figure 6a,b).
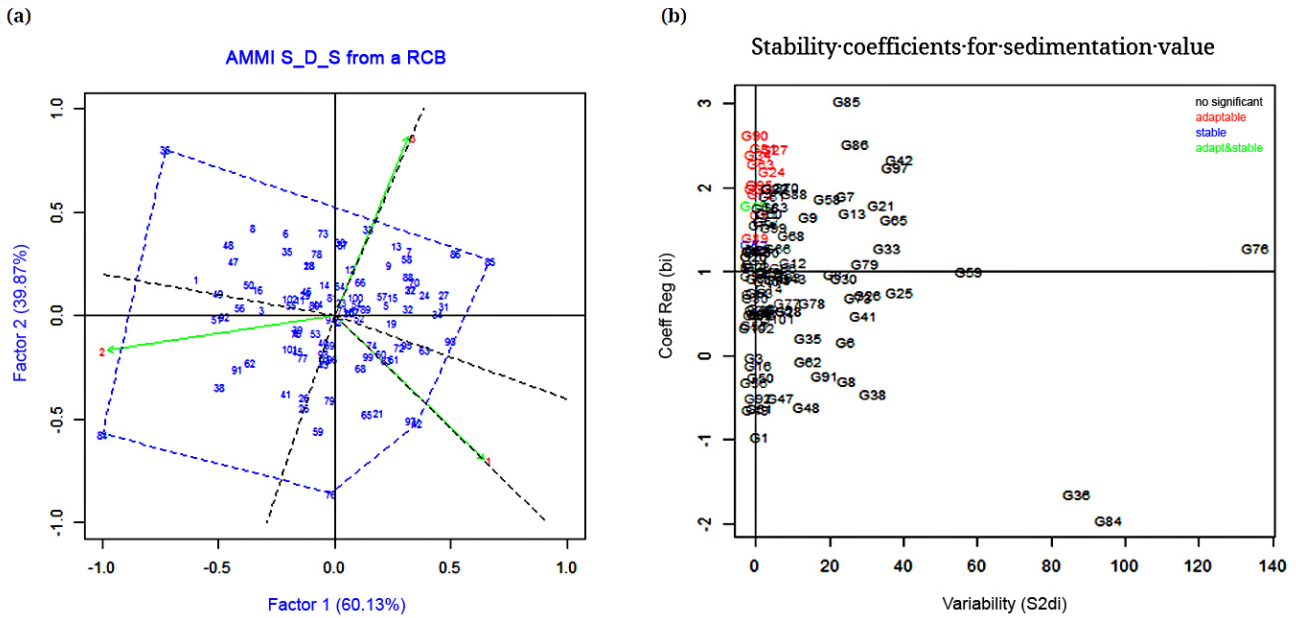
Figure 6. (a) The "which-won-where" view of the GGE biplot based on the G × E data for sedimentation value. It explained 100% of the total G+GE. The genotypes are labeled as 1 to 102 and the environments are labeled as E1 to E3. **(b)** The biplot display of sedimentation value (SDS), biplot explains variability and regression. coefficient of genotypes, it also explains adaptability and stability of the genotypes for sedimentation value under terminal heat stress conditions.
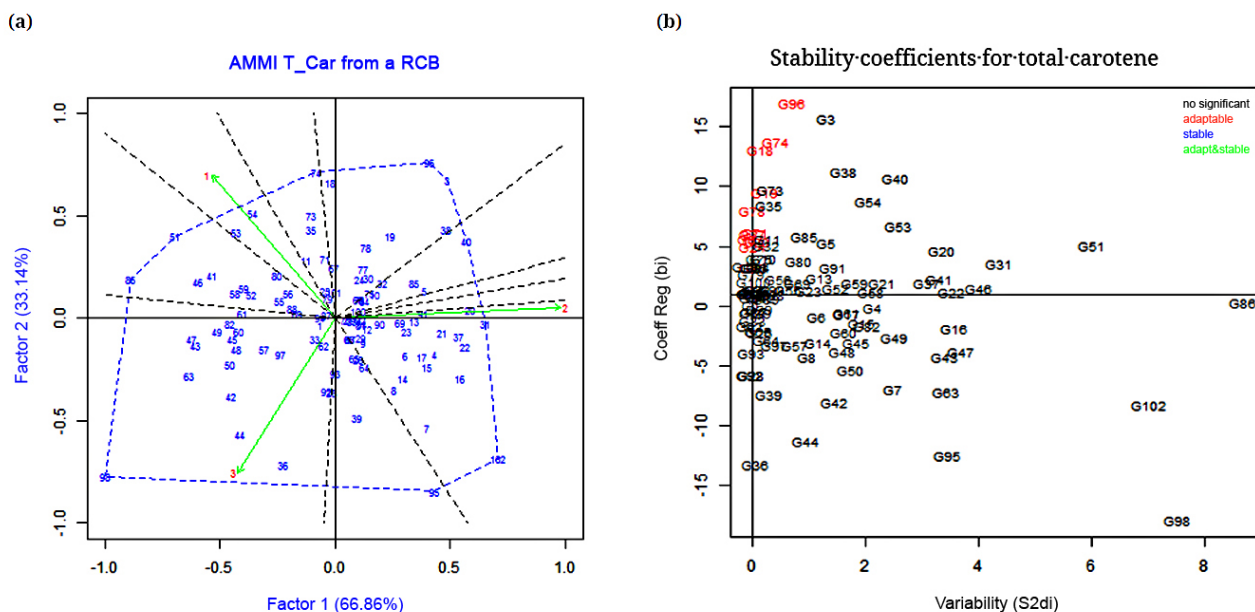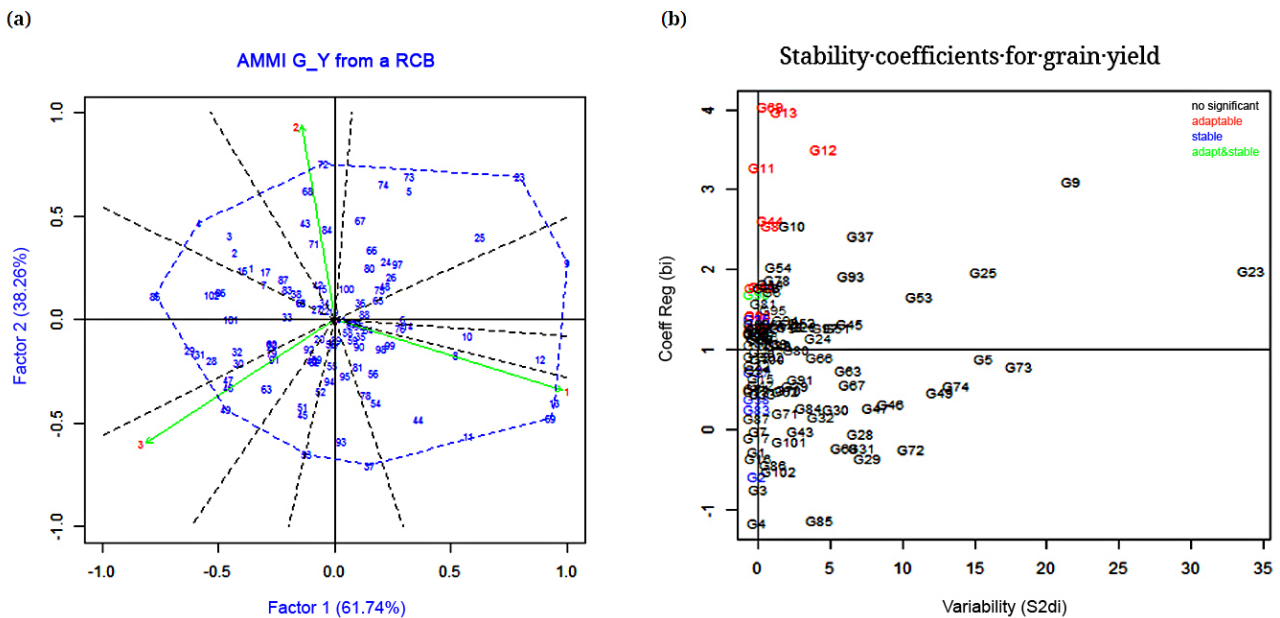

Figure 7. (a) The "which-won-where" view of the GGE biplot based on the G × E data for grain yield. It explained 100% of the total G + GE. The genotypes are labeled as 1 to 102 and the environments are labeled as E1 to E3. **(b)** The biplot display of grain yield (GY), biplot explains variability and regression. coefficient of genotypes, it also explains adaptability and stability of the genotypes for grain yield under terminal heat stress conditions.

Grain yield/plant: PCs of Additive Main-Effects and Multiplicative Interaction (AMMI) biplot for grain yield/plant showed that PCA 1 and PCA 2 were significant. PC1 and PC2 accounted for 61.7% and 38.3% of variance respectively. It means that by using PC1 and PC2, the analysis could explain 100% variation (Supplementary Table S3). Among the environments, E2 had short vectors and they did not exert strong interactive forces while E1 and E3 with long vectors were more differentiating environments. The genotypes near the origin are not sensitive to environmental interaction and those distant from the origin are sensitive and have more G × E interactions.

The genotypes G11 (Bijaga Red), G12 (Bijaga yellow), G-13 (CDW 04), G-44 (HI 8627), G-56 (IWP 5070), G-64 (MACS 1967), G-69 (MACS 3125), G-8 (B 447-BA), G-90 (Raj 6516), G-96 (V 21/23), G-98 (Vijay) and G-99 (WH 912) were the most adaptable genotypes for grain yield, similarly G-2 (A 206), G-27 (GW 1170), G-38 (HI 7747), G-83 (NP 4) and G-98 (Vijay) were the most stable genotypes and G-98 (Vijay) was the most adaptable and stable genotypes for grain yield under terminal heat stress condition. (Supplementary Table S4) (Figure 7a,b). Diversity of most stable genotypes were observed for various traits under terminal heat stress over the years (Table 4).

Table 4. Performance of genotypes for various traits over the years under terminal heat stress conditions.

Overall Yield	Early DtH	BM	TGW	SL	T. Car.	SDS	NG
HI 8627	Bijaja Red	GW 1114	Baxi 228-18	DWL 5023	Dahod local	DWL 5023	A-9-30-1
Bijaga yellow	HI 8653	GW 1170	Bijaga Red	GW 2	DWL 5023	GW 2	WH 912
CDW 04	B 4447-BA	GW 1240	CPAN 6236	Gw 1139	GW 2	GW 1170	AKDW 4151
IWP 5070	NIDW 70	HG 110	GW 1225	HI 8550	GW 1114	GW 1244	HI 7747
MACS 1967		HI 8498	HI 8627	HI 8498	GW 1240	GW 1245	HD 4709
MACS 3125		HI 8691	HI 8645	HI 8591	MACS 3061	MACS 9	Altar
Raj 6516		IWP 5013	HI 8653	HI 8627	MPO 215	Meghdoot	HI 8722
V 21/23		Line 1172	HI 8663	HI 8638	N 59	Raj 6069	IWP 5004-1
HI 7747		Raj 6069	MACS 2846	HI 8663	NI 5759	HD 4672	PDW 233
NP 4		Raj 6516	MACS 3063	HI 8691	V 21/23	HI 8722	WH 896

DISCUSSION

High temperature occurring during reproduction and grain filling period reduce wheat productivity [20,45,46]. The use of delayed sowing ensured that flowering and grain filling stages occurred under warmer conditions (Figure 1) [18]. Our results confirmed that genetic diversity exists for the response to terminal heat stress, with some genotypes better suitable to tolerate this stress. High heritability values were exhibited for

most traits, suggesting that genetic gain is possible for them. This is accordance with what previously reported [47,48]. Low heritability values of traits like biomass and harvest index suggest that selection for these characters would not be effective due to predominant effects of non-additive components and the high influenced by the environmental factors [33,49–52].

Maximum expected genetic advance was observed for total carotene, number of grains per spike, sedimentation value, grain yield/plant and harvest index promoting these for breeding selection [53]. Especially, those traits with high heritability and high genetic advance are the most interesting targets for breeders [54–56]. Bijaga Red, Bijaga yellow, CDW 04, HI 8627, IWP 5070, MACS 1967, MACS 3125, B 447-BA, Raj 6516, V 21/23, Vijay and WH 912 were the most adaptable genotypes for grain yield, were the most adaptable genotypes for grain yield, similarly A 206, GW 1170, HI 7747, NP 4 and Vijay were the most stable genotypes and Vijay was the most adaptable and stable genotypes for grain yield under terminal heat stress condition [57,58].

Under terminal heat stress, our correlation study confirmed that genotypes heading and maturing earlier tend to yield significantly more. Furthermore, high biomass production was confirmed to be a critical trait for adaptation, together with hectoliter weight [59–61]. However, it is valuable to underline that grains number and TGW were not important to determine overall performances of genotypes under terminal heat stress [62,63]. Hence, breeders interested in developing varieties better adapted to terminal heat stress should target short duration types capable of producing high biomass and converting it to yield via seeds having high hectoliter weight, but not TGW [64–71]. Our results also suggest genotypic-dependent heat stress effects on grain quality attributes as suggested by [72–75].

Stability Analysis for Grain Yield and Other Trait by Additive Main-Effects and Multiplicative Interaction (AMMI) Biplot Analysis

Combined analysis of variance showed that both genotype and environment mean sum of squares were significant for grain yield as it was in the ADDITIVE MAIN-EFFECTS AND MULTIPLICATIVE INTERACTION (AMMI) model. Biplot analysis was conducted and visualized to determine the differences among the environments, to evaluate stable and wide adaptable genotypes, and to evaluate the environments which differentiates the genotypes. In this biplot, the usual interpretation of a biplot assay is that if a genotype or an environment has IPCA score nearly zero, it has small interaction effects and found to be stable, results of present study are in conformity with [76–84]. The distribution of the environments in the biplot with variable environment means and IPCA scores indicate that the environments behaved very distinct compared to each other and selection of the adaptable and high yielding genotypes among these environments will be useful for late heat

stress in durum wheat. In the current study, environments E1 and E3 had long vectors which resulted in most variation to differentiate the genotypes [85–95]. A 206, GW 1170, HI 7747, NP 4 and Vijay were the most adaptable and stable genotypes over the years. On the basis of adaptation and stability, genotypes G-11 (Bijga Red), G-8 (B 4447-BA) for day to heading, G-97 (VD 97-15) for days to maturity, G-4 (AKDW 4240) for spike length, G-77 (N 59) for harvest index, G-30 (GW 1240) for hectoliter weight, G-19 (Bansi local for sedimentation value) and G-98 (Vijay) for grain yield were highly adapted and most stable for different traits across the environments, and can be used in convergent durum wheat breeding program to develop heat stress tolerant varieties.

SUPPLEMENTARY MATERIALS

The following supplementary materials are available online at https://doi.org/10.20900/cbgg20230004. Supplementary Table S1: List of genotypes used in the experiment. Supplementary Table S2: Mean value of selected traits based on BLUEs of genotypes 2014–2017. Supplementary Table S3: Analysis of variance of principle components of biplot genotype and location of the traits across three cropping seasons under heat stress conditions. Supplementary Table S4: Performance of genotypes for adaptability, stability and both genotypic adaptability and stability for all the selected traits under terminal heat stress conditions. Supplementary Figure S1: The biplot based on the correlation data for grain yield with other yield contributing traits. It explained 69.74% of the total G + GE where PC1 and PC2 accounted for 42.36% and 27.38% of variance respectively.

DATA AVAILABILITY

The dataset of the study is available from the authors upon reasonable request.

AUTHOR CONTRIBUTIONS

AG: Performed field evaluations and data analyses and writing original draft; SVSP & AJ: Guided during the whole experiment; FB: Provided a critical review of the manuscript and approved the final manuscript.

CONFLICTS OF INTEREST

The authors declare that there is no conflict of interest.

FUNDING

REFERENCES

1. United States Department of Agriculture. Wheat Data. Available from: http://www.ers.usda.gov/dataproducts /wheat-data.aspx. Accessed 2019 Sep 26.

2. FAO. FAOSTAT. Available from: http://faostat.fao.org. Accessed 2022 May 15.

3. Elias EM, Manthey FA, Stack RW, Kianian SF. Breeding efforts to develop fusarium head blight resistant durum wheat in north Dakota. Available from: https://scabusa.org/pdfs/forum05_proc_complete.pdf#page=42. Accessed 2023 Jul 10.

4. Malosetti M, Ribaut JM, Van Euwijk FA. The statistical analysis of multi-environment data: Modeling genotype-by-environment interaction and its genetic basis. Front Physiol. 2013;4:44.

5. Bonjean AP, Angus WJ, van Ginkel M. The world wheat book: A history of wheat breeding. Paris (France): Lavoisier Publishing; 2016.

6. Karabina K, Leonardi E. Turkey grain and feed annual report: TR6015. Available from: http://agriexchange.apeda.gov.in/marketreport/Reports/ Grain%20and%20Feed%20Annual_Ankara_Turkey_3-29-2016.pdf. Accessed 2023 Jul 12.

7. Sakin MA, düzdemir O, Sayaslan A, Yukse F. Stability properties of certain durum wheat genotypes for major quality characteristics. Turk J Agric For. 2011;35(4):343-55.

8. Joshi AK, Mishra B, Chatrath R, Ferrara GO, Singh RP. Wheat improvement in India: present status, emerging challenges and future prospects. Euphytica. 2007;157:431-46.

9. Kadkol GP, Sissons M. Durum wheat: overview. In: Wrigley C, Corke H, Seetharaman K, Faubion J, editors. Encyclopedia of Food Grains. 2nd ed. Oxford (UK): Academic Press; 2016. p. 117-24.

10. Richards RA, Rebetzke GJ, Condon AG, van Herwaarden AF. Breeding opportunities for increasing the efficiency of water use and crop yield in temperate cereals. Crop Sci. 2002;42(1):111-21.

11. Li YF, Wu Y, Hernandez-Espinosa N, Peña RJ. Heat and drought stress on durum wheat: Responses of genotypes, yield, and quality traits. J Cereal Sci. 2013;57(3):398-404.

12. Sissons M, Ovenden B, Adorada D, Milgate A. Durum wheat quality in high input irrigation systems in south eastern Australia. Crop Pasture Sci. 2014;65(5):411-22.

13. Mariani BM, D'Egidio MG, Novaro P. Durum wheat quality evaluation: influence of genotype and environment. Cereal Chem. 1995;72:194-7.

14. Bergkamp B, Impa SM, Asebedo AR, Fritz AK, Jagadish SVK. Prominent winter wheat varieties response to post-flowering heat stress under controlled chambers and field based heat tents. Field Crops Res. 2018;22:143-52.

15. Pradhan GP, Prasad PVV, Fritz AK, Kirkham MB, Gill BS. Effects of Drought and High Temperature Stress on Synthetic Hexaploid Wheat. Funct Plant Biol. 2012;39(3):190-8.

16. De Costa WAJM. A review of the possible impacts of climate change on forests in the humid tropics. J Natl Sci Found. 2011;39(4):281-302.

17. Hennessy K, Fawcett R, Kirono D, Mpelasoka F, Jones D, Bathols J, et al. An assessment of the impact of climate change on the nature and frequency of exceptional climatic events. Available from: http://hdl.handle.net/102.100.100/122078?index=1. Accessed 2023 Jul 10.

18. Fleitas MC, Mondal S, Gerard GS, Hernández-Espinosa N, Singh RP, Crossa J, et al. Identification of CIMMYT spring bread wheat germplasm maintaining superior grain yield and quality under heat-stress. J Cereal Sci. 2020;93:102981.

19. Dias AS, Lidon FC. Evaluation of grain filling rate and duration in bread and durum wheat, under heat stress after anthesis. J Agron Crop Sci. 2009;195(2):137-47.

20. Dwivedi SK, Basu S, Kumar S, Kumar G, Prakash V, Kumar S, et al. Heat stress induced impairment of starch mobilization regulates pollen viability and grain yield in wheat: Study in Eastern Indo-Gangetic Plains. Field Crops Res. 2017;206:106-14.

21. Mahdavi S, Arzani A, Maibody SAMM, Mehrabi AA. Photosynthetic and yield performance of wheat (Triticum aestivum L.) under sowing in hot environment. Acta Physiol Plant. 2021;43(7):106.

22. Farooq M, Bramle H, Palta JA, Siddique KH. Heat stress in wheat during reproductive and grain-filling phases. Crit Rev Plant Sci. 2011;30(6):491-507.

23. Mondal S, Singh RP, Crossa J, Huerta-Espino J, Sharma I, Chatrath R, et al. Earliness in wheat: a key to adaptation under terminal and continual high temperature stress in South Asia. Field Crop Res. 2013;151:19-26.

24. Khan A, Kabir M. Evaluation of spring wheat genotypes (*Triticum aestivum* L.) for heat stress tolerance using different stress tolerance indices. Cercet Agron Mold. 2014;47(4):49-63.

25. Mondal S, Singh RP, Mason ER, Huerta-Espino J, Autrique E, Joshi AK. Grain yield, adaptation and progress in breeding for early-maturing and heat-tolerant wheat lines in South Asia. Field Crops Res. 2016:192;78-85.

26. Kamrani M, Hoseini Y, Ebadollahi A. Evaluation for heat stress tolerance in durum wheat genotypes using stress tolerance indices. Arch Agron Soil Sci. 2017;64(1):38-45.

27. Sunita K, Munjal R, Ram K, Kumar N, Dhanda SS. Heat stress implications on yield and yield component in recombinant inbred lines of bread wheat at reproductive stage. Int J Pure App Biosci. 2017;5(3):1001-7.

28. Nouri A, Etminan A, Teixeira da Silva JA, Mohammadi R. Assessment of yield, yield-related traits and drought tolerance of durum wheat genotypes (*Triticum turjidum* var. *durum* Desf.). Aust J Crop Sci. 2011;5(1):8-16.

29. Rad MRN, Kadir MA, Rafii MY, Jaafar HZE, Naghavi MR, Ahmadi F. Genotype × environment interaction by AMMI and GGE biplot analysis in three consecutive generations of wheat (*Triticum Aestivum*) under normal and drought stress conditions. Aust J Crop Sci. 2013;7(7):956-61.

30. Hagos HG, Abay F. AMMI and GGE biplot analysis of bread wheat genotypes in the Northern part of Ethiopia. Turkish J Field Crops. 2013;6(1):64-8.

31. Kumar B, Hooda E, Hooda BK. GGE biplot analysis of multi-environment yield trials for wheat in northern India. Adv Res. 2018;16(2):1-9.

32. Ashwini KVR, Ramesh S, Sunitha NC. Comparative BLUP, YREM-based performance and AMMI model-based stability of horse gram [*Macrotyloma uniflorum* (Lam.) Verdc.] genotypes differing in growth habit. Genet Resour Crop Evol. 2021;68:457-67.

33. Kumar S, Kumari J, Bansal R, Upadhyay D, Srivastava A, Rana B, et al. Multi-environmental evaluation of wheat genotypes for drought tolerance. Indian J Genet Plant Breed. 2018;78(1):26-35.

34. Mohammadi R, Amri A. Assessment of the suitability of *Triticum turgidum* accessions for incorporation into a durum wheat breeding program. Euphytica. 2022;218(6):70.

35. Ullah A, Nadeem F, Nawaz A, Siddique KHM, Farooq M. Heat stress effects on the reproductive physiology and yield of wheat. J Agron Crop Sci. 2022;208(1):1-17.

36. Yang C, Fraga H, Van Ieperen W, Trindade H, Santos JA. Effects of climate change and adaptation options on winter wheat yield under rainfed Mediterranean conditions in southern Portugal. Clim Chang. 2019;154:159-78.

37. Mohammadi R, Haghparast R, Amri A, Ceccarelli S. Yield stability of rainfed durum wheat and GGE biplot analysis of multi-environment trials. Crop Pasture Sci. 2010;61(1):92-101.

38. Sareen S, Tyagi BS, Sarial AK, Tiwari V, Sharma I. Trait analysis, diversity, and genotype × environment interaction in some wheat landraces evaluated under drought and heat stress conditions. Chilean J Agric Res. 2014;74(2):135-42.

39. Zadoks JC, Chang TT, Konzak CF. A decimal code for the growth stages of cereals. Weed Res. 1974;14(6):415-21.

40. Ltd International VSN. Genstat 1.16 Release (Windows for Genstat 2013). Available from: https://www.shouldiremoveit.com/genstat-16th-edition-64-bit-115275-program.aspx. Accessed 2023 Jul 11.

41. Falconer DS, Mackay TFC. Introduction to Quantitative Genetics. Harlow (UK): Longman; 1996.

42. Gauch HG. Statistical analysis of regional yield trials: AMMI analysis of factorial designs. Amsterdam (Netherlands): Elsevier; 1992.

43. Yan W, Tinker NA. Biplot analysis of multi-environment trial data: Principles and applications. Can J Plant Sci. 2006;86(3):623-45.

44. Yan W. GGE Biplot vs. AMMI Graphs for the Genotype-by-Environment Data Analysis. J Indian Soc Agricul Stat. 2011;65(2):181-93.

45. Asseng S, Cammarano D, Basso B, Chung U, Alderman PD, Sonder K, et al. Hot spots of wheat yield decline with rising temperatures. Glob Change Biol. 2017;23(6):2464-72.

46. Ni Z, Li H, Zhao Y, Peng H, Hu Z, Xin M, et al. Genetic improvement of heat tolerance in wheat: Recent progress in understanding the underlying molecular mechanisms. Crop J. 2017;6(1):32-41.

47. Sachan MS, Singh SP. Genetics of yield and its components in durum wheat (*Triticum durum* Desf.). J Interaca. 2003;7(2):140-3.

48. Kumar A, Daware A, Kumar A, Kumar V, Krishnan SG, Mondal S, et al. Genome-wide analysis of polymorphisms identified domestication-associated long low-diversity region carrying important rice grain size/weight quantitative trait loci. Plant J. 2020;103(4):1525-47.

49. Pinto RS, Reynolds MP, Mathews KL, McIntyre CL, Olivares-Villegas JJ, Chapman SC. Heat and drought adaptive QTL in a wheat population designed to minimize confounding agronomic effects. Theor Appl Genet. 2010;121:1001-21.

50. Mohammed A, Amsalu A, Geremew B. Genetic variability, heritability and trait association in durum wheat (*Triticum turgidum* L. var. *durum*) genotypes. Afri J Agric Res. 2011;6(17):3972-9.

51. Khan A, Munir A, Mukhtar A, Gill KS, Zahid A. Association analysis for agronomic traits in wheat under terminal heat stress. Soudi J Biol Sci. 2021;28(12):7404-15.

52. Gopal K, Patel JA, Prajapati KP, Patel PJ. Estimation of genetic variability, heritability and genetic advance for seed yield and its attributes in sesame (*Sesamum indicum* L.). Int J Bioresour Stress Manag. 2020;11(3):219-24.

53. Kashif M, Ahmad J, Chowdhry MA, Perveen K. Study of genetic architecture of some important agronomic traits in durum wheat (*Triticum durum* Desf.). Asian J Plant Sci. 2003;2:708-12.

54. Johnson HW, Robinson HF, Cornstock RE. Estimates of genetic and environmental variability in Soybeans. Agron J. 1995;47(7):314-8.

55. Kashif M, Khalıq I. Heritability, correlation and path coefficient analysis for some metric traits in wheat. Int J Agri Biol. 2004;6(1):138-42.

56. Hossain MM, Azad MAK, Alam MS, Eaton TEJ. Estimation of Variability, Heritability and Genetic Advance for Phenological, Physiological and Yield Contributing Attributes in Wheat Genotypes under Heat Stress Condition. Am J Plant Sci. 2021;12(4):586-602.

57. Khokhar MI, Hussain M, Zulkiffal M, Sabir W, Mahmood S, Jamil Anwar MW. Studies on genetic variability and inter-relationship among the different traits in wheat (*Triticum aestivum* L.). Krmiva. 2010;52(2):77-84.

58. Manisha S. Genetic variability, heritability, correlation coefficient and path analysis of yield and yield contributing traits in bread wheat (*Triticum aestivum* L.). Int J Plant Sci. 2017;12(2):173-80.

59. Flagella Z, Giuliani MM, Luigia G, Volpi C, Stefania M. Influence of water deficit on durum wheat storage protein composition and technological quality. Eur J Agron. 2010;33(3):197-207.

60. Weber VS, Araus JL, Cairns JE, Sanchez C, Melchinger AE, Orsini E. Prediction of grain yield using reflectance spectra of canopy and leaves in maize plants grown under different water regimes. Field Crops Res. 2012;128:82-90.

61. Mondal S, Joshi AK, Huerta-Espino J, Singh RP. Early Maturity in Wheat for Adaptation to High Temperature Stress. Available from: https://web.archive.org/web/20190318111110id_/https://core.ac.uk/download/pdf/81272886.pdf. Accessed 2023 Jul 10.

62. Ashish VS, Singh SK, Madaan S, Kumar P, Verma A. Divergence of bread wheat genotypes (*Triticum Aestivum* L.) assessed by multivariate biplot analysis based on important markers. J Crop Weed. 2022;18(1):166-73.

63. Gautam A, Sai Prasad SV, Jajoo A, Malviya P. Heritability and correlation of yield and its contributing traits under terminal heat (late sown) situations in durum wheat. Prog Res. 2013;8(2):203-8.

64. Leilah AA, Al-Khateeb SA. Statistical analysis of wheat yield under drought conditions. J Arid Environ. 2005;61(3):483-96.

65. Villegas D, Garcia del Moral LF, Rharrabti Y, Martos V, Royo C. Morphological traits above the flag leaf node as indicators of drought susceptibility index in durum wheat. J Agron Crop Sci. 2007;193(2):103-16.

66. Guoth A, Tari I, Csiszar J, Pecsvaradi A, Cseuz L, Erdei L. Comparison of the drought stress responses of tolerant and sensitive wheat cultivars during grain filling: Changes in flag leaf photosynthetic activity, ABA levels, and grain yield. J Plant Growth Regul. 2009;28:167-76.

67. Jha UC, Bohra A, Singh NP. Heat stress in crop plants: Its nature, impacts and integrated breeding strategies to improve heat tolerance. Plant Breed. 2014;133(6):679-701.

68. Sehgal A, Sita K, Siddique KHM, Kumar R, Bhogireddy S, Varshney RK, et al. Drought or/and heat-stress effects on seed filling in Food Crops: Impacts on functional biochemistry, seed yields, and nutritional quality. Front Plant Sci. 2018;9:1705.

69. Zhang J, Zhang S, Cheng M, Jiang H, Zhang X, Peng C, et al. Effect of drought on agronomic traits of rice and wheat: A meta-analysis. Int J Environ Res Public Health. 2018;15(5):839.

70. El Hassouni K, Belkadi B, Filali-Maltouf A, Tidiane-Sall A, Al-Abdallat A, Nachit M, et al. Loci controlling adaptation to heat stress occurring at the reproductive stage in durum wheat. Agronomy. 2019;9(8):414.

71. Fabian A, Safran E, Szabo-Eitel G, Barnabas B, Jager K. Stigma functionality and fertility are reduced by heat and drought co-stress in Wheat. Front Plant Sci. 2019;10:244.

72. Vargas M, Combs E, Alvarado G, Atlin G, Mathews K, Crossa J. META: A suite of SAs programs to analyze multi-environment breeding trials. Agron J. 2013;105(1):11-9.

73. Balla K, Karsai I, Bonis P, Kiss T, Berki Z, Horvath A, et al. Heat stress responses in a large set of winter wheat cultivars (*Triticum aestivum* L.) depend on the timing and duration of stress. PLoS One. 2019;14(9):e0222639.

74. Kaur V, Singh S, Behl RK. Heat and drought tolerance in wheat: Integration of physiological and genetic platforms for better performance under stress. Ekin J Crop Breed Genet. 2016;2(1):1-14.

75. Reynolds MP, Pask AJD, Hoppitt WJE, Sonder K, Sukumaran S, Molero G, et al. Strategic crossing of biomass and harvest index—source and sink—achieves genetic gains in wheat. Euphytica. 2017;213:1-23.

76. Tahir MA, Tariq A, Muhammad F, Ghulam S. Silicon-induced changes in growth, ionic composition, water relations, chlorophyll contents and membrane permeability in two salt-stressed wheat genotypes. Arch Agron Soil Sci. 2012;58(3):247-56.

77. Zobel RW, Wright MJ, Gauch HG. Statistical analysis of a yield trial. Agron J. 1998;80(3):388-93.

78. Singh C, Gupta A, Gupta V, Kumar P, Sendhil R, Tyagi BS, et al. Genotype × environment interaction analysis of multi-environment wheat trials in India using AMMI and GGE biplot models. Crop Breed Appl Biotechnol. 2019;19:309-18.

79. Bishwas KC, Poudel MR, Regmi D. AMMI and GGE biplot analysis of yield of different elite wheat line under terminal heat stress and irrigated environments. Heliyon. 2021;7:e07206.

80. Dabi A, Alemu G, Geleta N, Delessa A, Solomon T, Zegaye H, et al. Genotype × environment interaction and stability analysis for grain yield of bread wheat (*Triticum aestivum*) genotypes under low moisture stress areas of Ethiopia. Am J Plant Biol. 2021;6(3):44-52.

81. Kumar A, Chand P, Thapa RS, Singh T. Assessment of stability performance and G×E interaction for yield and its attributing characters in bread wheat (*Triticum aestivum* L.). Electron J Plant Breed. 2021;12(1):235-41.

82. Hanif U, Gul A, Amir R, Munir F, Sorrells ME, Gauch HG, et al. Genetic gain and G × E interaction in bread wheat cultivars representing 105 years of breeding in Pakistan. Crop Sci. 2022;62(1):178-91.

83. Alemu G, Dabi A, Geleta N, Duga R, Solomon T, Zegaye H, et al. Genotype × environment interaction and selection of high yielding wheat genotypes for different wheat-growing areas of Ethiopia. Am J Biosci. 2021;9:63-71.

84. Awaad HA. Performance, adaptability and stability of promising bread wheat lines across different environments. In: Awaad H, Abu-hashim M, Negm A, editors. Mitigating Environmental Stresses for Agricultural Sustainability in Egypt. Cham (Switzerland): Springer; 2021. p. 187-213.

85. Adil N, Wani SH, Rafiqee S, Mehrajuddin SOFI, Sofi NR, Shikari AB, et al. Deciphering genotype × environment interaction by AMMI and GGE biplot analysis among elite wheat (*Triticum aestivum* L.) genotypes of himalayan region. Ekin J Crop Breed Genet. 2022;8(1):41-52.

86. Kaya Y, Akcura M, Taner S. GGE-biplot analysis of multi-environment yield trials in bread wheat. Turk J Agric For. 2006;30(5):325-37.

87. Akcura M, Aner MT, Kaya Y. Evaluation of bread wheat genotypes under irrigated multi-environment conditions using GGE biplot analyses. Agriculture. 2011;98(1):35-40.

88. Abate F, Mekbib F, Dessalegn Y. GGE biplot analysis of multi-environment yield trials of durum wheat (*Triticum turgidum* Desf.) genotypes in north western Ethiopia. Am J Exp Agric. 2015;8(2):120-9.

89. Ilker E, Geren H, Unsal R, Sevim D, Fatma AT, Muzaffer T. AMMI-biplot analysis of yield performances of bread wheat cultivars grown at different locations. Int J Curr Microbiol App Sci. 2020;9(5):377-89.

90. Alam MA, Farhad M, Hakim MA, Barma NCD, Malaker PK, Reza MMA, et al. AMMI and GGE biplot analysis for yield stability of promising Bread wheat genotypes in Bangladesh. Pak J Bot. 2017;49(3):1049-56.

91. Bavandpori F, Ahmadi J, Hossaini SM. Yield stability analysis of bread wheat lines using AMMI model. Agric Commun. 2015;3(1):8-15.

92. Khairnar SS, Bagwan JH, Yashavantha KKJ, Baviskar VS, Honrao BK, Surve VD, et al. Studies on genetic variability parameters and character association in bread wheat (*Triticum aestivu*m L.) under timely and late sown environments of irrigated conditions. Electron J Plant Breed. 2018;9(1):190-8.

93. Wardofa GA, Asnake D, Mohammed H. GGE Biplot analysis of genotype by environment interaction and grain yield stability of bread wheat genotypes in central Ethiopia. J Plant Breed Genet. 2019;7(2):75-85.

94. Tekdal S, Kendal E. AMMI model to assess durum wheat genotypes in multi-environment trials. J Agric Sci Technol. 2018;20(1):153-66.

95. Fernandez G. Effective selection criteria for assessing plant stress tolerance. Available from: https://worldveg.tind.io/record/72511#record-files-collapse-header. Accessed 2023 Jul 11.

Diminishing toxicity of pyrene on photosynthetic performance of soybean using *Bacillus subtilis* (NCIM 5594)

Lakshmi Jain[A],* [ID] and Anjana Jajoo[A,B] [ID]

For full list of author affiliations and declarations see end of paper

*Correspondence to:
Lakshmi Jain
School of Life Science, Devi Ahilya University, Indore 452017, India
Email: lakshmijain22@gmail.com

Handling Editor:
Suleyman Allakhverdiev

ABSTRACT

Polycyclic aromatic hydrocarbons are persistent organic pollutants causing serious environmental problems, being toxic to plants and difficult to remediate. Pyrene is one such extremely dangerous compound that is toxic for the environment. This study suggests the use of *Bacillus subtilis* (National Collection of Industrial Microorganisms [NCIM] 5594) to overcome inhibitory effects of pyrene on soybean photosynthesis. The toxicity of pyrene to soybean was evident from a significant decrease in seed germination parameters, photosynthetic performance and biomass during growth of soybean in pyrene contaminated soil. Efficiency of performance index, light absorption, trapping and electron transport were reduced in plants grown in pyrene contaminated soil while significant recovery in these parameters was observed in plants grown in pyrene + *B. subtilis* treated soil. Activity levels of dehydrogenase and lipase enzymes significantly recovered in pyrene + *B. subtilis* treated soil. After extraction of pyrene from soil and soybean plant, concentration of pyrene was lowered in pyrene + *B. subtilis* treated soil and plants. These findings suggest efficient degradation of pyrene by *B. subtilis*. About 70% degradation of pyrene was achieved in soil using *B. subtilis*; thus it is a useful strain for crop improvement in pyrene polluted soil.

Keywords: *Bacillus subtilis*, biomass, Chl *a* fluorescence, photosynthetic performance, polycyclic aromatic hydrocarbons (PAHs), PSII, pyrene, soybean.

Introduction

Polycyclic aromatic hydrocarbons (PAHs) fall under the category of hazardous pollutants that remain in the environment for a long time due to their hydrophobicity and chemical stability. PAH contamination has mutagenic and carcinogenic effects on the environment in addition to acute toxicity (Aksmann *et al.* 2014; Mojiri *et al.* 2019). PAHs, in particular, may be harmful to the flora and fauna of an affected area, resulting in their uptake and accumulation in the food chain (Chauhan *et al.* 2008). The widespread distribution of PAHs, as well as their persistence and potentially deleterious effects on the environment, has piqued researchers' curiosity (Henner *et al.* 1997).

Soil is considered a reservoir of PAHs. Presence of PAHs in soils may influence hazardous effects on several biological constituents of the environment, including plants and microbes (Sverdrup 2001). Persistency of these lipophilic compounds in soil organic matter markedly affects soil biological parameters, e.g. for enzyme activity, which is a reliable indicator of soil quality (Lipińska *et al.* 2015).

Soil enzymatic activity assays are sensitive and are described as 'soil biological fingerprints'. These enzymes have been proposed as potential ecosystem quality indicators and biomarkers for estimating changes in soil management systems. Dehyrogenase (EC 1.1.1) is an oxidoreductase enzyme and its measurement as dehydrogenase activity (DHA) in soil provides a large amount of information about soil biological characteristics (Wolińska *et al.* 2016). Another extracellular enzyme secreted by soil microorganisms is the lipase (EC 3.1.1.3), which is triacylglycerol acyl hydrolase. The ester linkages in fats and oils are hydrolysed into glycerol and free fatty acids by triacylglycerol acyl hydrolases (Treichel *et al.* 2010). The lipases increase the

bioavailability of PAH to soil microbes. In general, products released from hydrocarbon breakdown produce the substrates for hydrolases including esterase-lipase (Kosaric 2001). Estimation of soil lipase activity is a useful tool to monitor the rate of biodegradation in soil (Margesin *et al.* 1999). The hydrocarbon content is negatively correlated with soil lipase activity in natural and bioremediated soil (Margesin *et al.* 2002).

Plants are essential ecosystem components and are exposed to a variety of external factors (Sharma *et al.* 2018). Various environmental factors such as low and high light intensity, extreme temperature conditions, salinisation, lack of some mineral nutrition, water supply, poor soil quality, drought, and different forms of pollution may significantly impact plant photosynthetic function (Allakhverdiev 2020; Brestic *et al.* 2021). PAHs which are extremely toxic pollutants come into contact with plants in a variety of ways, including soil, air, and water. The toxicity of such environmental contaminants has been reported in a variety of plant species, with impacts including germination, growth, photosynthesis and biomass retardation (Marwood *et al.* 2001; Molina and Segura 2021). Previous research has revealed that PAHs show impact on primary and secondary photosynthetic processes (Tomar and Jajoo 2015), by entering plants through stomata or the root system (Kuhn *et al.* 2004). Exposure of plants to PAHs causes significant alterations in the structure and function of photosynthetic machinery (Tomar and Jajoo 2013; Kreslavski *et al.* 2017; Jain and Jajoo 2020). PAH toxicity can impair growth rate, chlorophyll content, and photosynthetic rate of algae and higher plants (Kummerová *et al.* 2006; Aksmann and Tukaj 2008; Jajoo *et al.* 2014). Studies have also reported reduction in the activity of the oxygen evolving complex and electron transport chain in *Pisumsativum* (Kummerová *et al.* 2006; Desalme *et al.* 2013).

Pyrene is a tetracyclic aromatic hydrocarbon with a symmetrical structure. Pyrene has low biodegradability and high persistency in the environment, and is taken into account as a priority pollutant by the US Environmental Protection Authority (EPA) due to its carcinogenic and mutagenic effects (Boll *et al.* 2015). Reduction in root and shoot length and fresh and dry biomass in barley (*Hordeum vulgare*) due to pyrene toxicity has been reported (Khan *et al.* 2014). Decreased root length of wheat was observed with increased concentration of pyrene (Fang *et al.* 2005). It has been also reported that toxicity of pyrene is associated with a reduction in soil dehydrogenase activity (Lipińska *et al.* 2021).

PAHs are chemically stable compounds with half-lives that range from months to years in soil. Considering the toxic and persistent nature of PAHs, researchers have to focus totally on their remediation (Luch 2005; Sivaram *et al.* 2017). Over the last three decades, many bacteria have been found to degrade PAHs by metabolism or co-metabolism. Microbiological treatment of PAH-contaminated soil is an eco-friendly technique which provides complete pollutant degradation and minimal soil disturbance (Habe and Omori 2003; Peng *et al.* 2014). Some previous studies looked into the degradation of PAHs utilising *Bacillus* sp. (Toledo *et al.* 2006; Seo *et al.* 2009). The catabolic enzyme system and spore formation ability of *Bacillus* sp. promote degradation of petroleum compounds (Nanekar *et al.* 2015). The *Bacillus subtilis* strain NCIM 5594, (National Collection of Industrial Microorganisms accession number) was selected for this study due to its biosurfactant production ability and high degradation potential. Biosurfactants are less toxic and environmentally friendly compounds that play an important role in the degradation of PAH compounds by increasing the surface area of substrates, making them suitable for use as green surfactants (Sachdev and Cameotra 2013).

In this study we have evaluated the toxic effect of pyrene (henceforth PYR) on plants' photosynthesis in the presence and absence of *B. subtilis* (NCIM 5594 strain). The majority of the discoveries have been conducted independently, either regarding PAH degradation or about PAH effects on plants, but no integrated research has been done on PAH effects on plant photosynthesis and PAH degradation. This study looked at the effects of bacteria on plant photosynthesis in terms of energy absorption, trapping, electron transport, and photosystem II (PSII) quantum yield, as well as fresh and dry weight in soybean plants growing in PYR treated soil. This research looked at how the soybean plant absorbed and degraded PYR in the presence and absence of bacteria. This is the first comprehensive report, to our knowledge, that explains the protective role of *B. subtilis* (NCIM 5594) on the photosynthetic process of soybeans under PYR stress.

Materials and methods

Pyrene preparation

Pyrene (PYR; Sigma Aldrich, St. Louis, MO, USA) was dissolved in 100% acetone to make 50 mL of stock solution (45 mM). This PYR stock solution was delivered to water to final PYR concentrations of 200 μM. It was found that the concentration of dissolvent did not affect seed germination and growth of seedlings and other physiological parameters (Tomar and Jajoo 2013).

Germination of soybean seeds

Soybean (*Glycine max*) JS-335 seeds were placed into petri dishes (12 cm diameter, 25 seeds per dish) on disks of Whatman filter paper using 15 mL distilled water in control (without PYR) and respective PYR solutions in treatments. These seeds were placed in the dark at $23 \pm 2°C$ for 8 days (Upadhyaya *et al.* 2017). Germination rate was measured

after 4 days and root and shoot lengths were measured after 8 days of germination.

Cultivation of plants

Soybean (*G. max*; JS-335) cultivar was used as plant material. Healthy seeds of uniform size and shape were sowed in 39 cm (length) pots containing 12 kg of medium black soil (pH 7.5); (1:2.5 soil:water ratio); organic carbon (0.05%); Olsen P (6.2 mg/kg); mineral N (6.4 mg/kg). Eight seeds were sown in each pot and allowed to germinate on terrace of Department of Life Sciences, Devi Ahilya University, Indore, India (latitude 22°43′N) (www.accuweather.com) in natural conditions during July to October (28°C; ±0.2°C). Pots were divided into four categories: T1 (Control plants without PYR and *B. subtilis* treatment), T2 (plants with only *B. subtilis* treatment), T3 (plants with only PYR treatment), T4 (plants with both PYR and *B. subtilis* treatment). Four pots were kept for each treatment and the experiment was repeated three times. Plants were replenished daily with normal tap water in T1 and T2, 200 μM PYR in T3 and T4 sets. 10^8 colony forming units (CFU)/mL *B. subtilis* cells were applied after every 5 days in T2 and T4. Measurement of chlorophyll content, chlorophyll *a* (Chl *a*) fluorescence induction kinetics and fresh and dry weight was performed after 50 days of cultivation of plants. Enzymatic activity was measured after every 5 days until 50 days.

Bioinoculum preparation

The *B. subtilis* (NCIM 5594) bacterial strain was used in this study. This bacterial strain was grown to mid-log phase (10^8–10^9 CFU/mL) in nutrient broth medium with continuous shaking at 150 rpm at 37°C to prepare the inoculum. The cells were harvested by centrifuging the broth at 10 000*g* for 10 min to acquire bacterial cells, and washed by sterile water twice to remove the nutrition in bacterial cells. Bacterial suspension was prepared by mixing of purified cell with sterile water. Absorbance of the bacterial suspension was adjusted to 1 at 600 nm (the biomass was approximately of 10^8 CFU/mL).

Measurement of chlorophyll (Chl) *a* fluorescence induction kinetics

Measurement of chlorophyll (Chl) *a* fluorescence was done using Plant Efficiency Analyser (Handy PEA) (Hansatech Norfolk, England, UK). Measurements were taken from the centre of the well-developed leaves (Brestic *et al.* 2018). 15–20 measurements were done for each replicate. Before recording, the plants were dark adapted for 30 min. Leaves show a polyphasic rise where the O–J phase (ends at ~2 ms), the J–I phase (ends at ~30 ms), and I–P phase (ends at ~500 ms) represent the phases of O–J–I–P chlorophyll *a* fluorescence transient in leaves. The O to J phase is

associated with the net photochemical reduction of quinone A to reduced quinone A (Q_A to Q_A^-). The intermediate I step and the final P step have been hypothesised due to presence of a fast and slow reducing plastoquinone (PQ) pool, as well as due to various redox states of the reaction centres (RC) of PS II which facilitate reduction of PQ pool. Also O = F_o for a dark-adapted sample, P = F_m for a dark-adapted sample, J and I = time points taken for J and I step, respectively. An alteration of PSII energy fluxes in response to PYR + *B. subtilis* was also measured using Biolyzer HP-3 software. Various parameters, such as the efficiency of light absorption, trapping, and electron transport and dissipation per cross section of PSII, are indicated by ABS/CSm, TRo/CSm, ETo/CSm and DIo/CSm, respectively (Tsimilli-Micheal and Strasser 2008).

Measurement of total chlorophyll content

The total chlorophyll content of 50 day old plants was measured using a Leaf SPAD chlorophyll meter [FT Green LLC (USA)] according to Zhu *et al.* (2012). Measurements were performed between 11:00 AM and 12:00 PM under natural sunlight (Mathur *et al.* 2018).

Biomass estimation

Fresh and dry weight of shoot and root was determined in four replicates (three plants of each set randomly selected) after 50 days in control and all treatments. Each part was cut into small pieces and weighed for fresh biomass (FM). The same samples were then oven dried at 180°C for 4 h and then weighed for dry mass (DM) (Sharma *et al.* 2018).

Determination of soil enzymatic activities

Measurement of dehydrogenase activity

Soil dehydrogenase activity (DHA) was estimated by reducing 2,3,5-triphenyl-tetrazoliumchloride (TTC), according to the procedure of Casida *et al.* (1964). Soil (1 g) samples (in triplicate) of each treatment were mixed with 0.02 g $CaCl_2$, 0.6% (w/v) TTC, 1% glucose and 1 mL distilled water followed by incubation of 24 h at 37°C. Then, extraction of triphenyltetrazolium formazan (TPF) was performed with ethanol. After filtering the extracts, the absorbance was measured at 485 nm. The amount of triphenyltetrazolium formazan (TPF) formed was calculated using a standard plot.

Measurement of lipase activity

Soil lipase activity was estimated according to Margesin *et al.* (2002). Field-moist soil (0.1 g) was weighed (three replicates), mixed with 5 mL 100 mM NaH_2PO_4/NaOH Buffer (pH 7.2) and pre-warmed at 30°C in a water bath for 10 min. Then 50 μL of substrate solution [100 mM para-nitrophenyl acetate (pNPA) diluted in 2-propanol] was added. The contents were mixed and tubes were incubated

in water bath at 30°C for another 10 min followed by cooling on ice to stop the reaction. Contents were centrifuged at 2000*g* at 4°C for 5 min, the supernatant was pipetted and the test tubes were held on ice. Immediately afterwards, the extinction of released para-nitrophenol (pNP) was measured spectrophotometrically at 400 nm. The amount of para-nitrophenol released was calculated using standard plot.

Extraction of pyrene from soil and plant parts

Extraction of pyrene from soil

Extraction of pyrene (PYR) from soil was performed using a mechanical shaking method (Schwab *et al.* 1999) with some modifications. Soil samples of each treatment were air dried at room temperature, sieved through a 0.5 mm pore sieve and stored at 4°C until analysis. 5 g of sample was weighed, mixed with 30 mL acetonitrile and incubated for overnight shaking at 200 rpm at 30°C. After that, samples were centrifuged for 5 min at 10 000*g*. Supernatant was filtered for quantification of PAH using high performance liquid chromatography (HPLC).

Extraction of pyrene from plant parts

The extraction of pyrene (PYR) from plant parts was done according to Gao and Zhu (2004). Plant samples (leaf, stem and root) of each treatment were washed several times with distilled water, freeze dried, weighed (1 g), homogenised and extracted by ultrasonication with 1:1 (v/v) acetone: hexane. The extracts were then decanted and collected. This process was repeated in triplicate to achieve satisfactory recovery. The extracts were combined and passed through anhydrous Na_2SO_4 column. Solvents were evaporated and dissolved in hexane followed by filtration through silica gel column and eluted using 11.0 mL of 1:1 (v/v) hexane: dichloromethane. The samples were then evaporated, dissolved in 6 mL acetonitrile and quantified by high performance liquid chromatography (HPLC).

HPLC analysis was performed using the JASCO (HPLC) system, with a reverse phase C18 column, (4.6 × 250 mm),

acetonitrile:water (70:30, v/v) as the mobile phase, flow rate – 0.5 mL/min and total run time 20 min.

Statistical analysis

Data was analysed by using GraphPad Prism 5.01 software, Inc. La Jolla, CA, USA. Results were analysed using one-way analysis of variance (ANOVA) followed by Dunnet: comparison of all columns vs control column. Significance was determined at $P < 0.01$ (*$P < 0.05$, **$P < 0.01$ and ***$P < 0.001$) and the results are expressed as mean values and standard deviation (s.d.). All the assays were carried out in replicates (three to four sets for each analysis).

Results

Effects of PYR on seed germination and seedling growth in soybean

Germination ability is an important feature of the seed that can considerably affect crop yield. Seedling growth can be expressed on the basis of shoot length and root length. Exposure of soybean seeds with PYR toxicity inhibit seed germination, shoot length and root length of soybean seeds. 5 µM and 25 µM PYR exerted a non significant effect on the rate of seed germination. There were 12%, 14%, 16%, 18% decreases in the rate of seed germination observed with 50 µM, 100 µM, 200 µM, 500 µM concentrations of PYR respectively (Table 1). After 8 days of germination shoot length of soybean seedlings was not significantly affected with 5 µM and 25 µM PYR while higher concentrations, e.g. 50 µM, 100 µM, 200 µM, 500 µM concentrations of PYR showed 31%, 32%, 35% 39% reduction in shoot length. Root length declined to a non significant degree with 5 µM and 25 µM PYR; whereas it decreased by 24%, 29%, 33%, 43% with 50 µM, 100 µM, 200 µM, 500 µM concentrations of PYR respectively.

Table 1. Effect of PYR on seed germination (4 days) and various growth parameters in soybean seedlings after 8 days of germination.

Treatments	Seed germination rate (%)	Shoot length (cm)	Root length (cm)
Control	84.0 ± 2.3	11.1 ± 1.2 (100%)	4.2 ± 0.3 (100%)
5 µM PYR	78.0 ± 2.3*	10.1 ± 0.3[n.s.] (91%)	3.9 ± 0.5[n.s.] (93%)
25 µM PYR	76.0 ± 4*	9.6 ± 0.5[n.s.] (86%)	3.7 ± 0.1[n.s.] (88%)
50 µM PYR	72.0 ± 2.3***	7.8 ± 0.2*** (69%)	3.2 ± 0.2*** (76%)
100 µM PYR	70.0 ± 2.3***	7.5 ± 0.4*** (68%)	3.0 ± 0.5** (71%)
200 µM PYR	68.0 ± 3.4***	7.2 ± 0.1*** (65%)	2.8 ± 0.05*** (67%)
500 µM PYR	66.0 ± 3.4***	6.8 ± 0.5*** (61%)	2.4 ± 0.1*** (57%)

Data represent the mean of three replications with 25 seeds (for seed germination test) or 10 seeds (root/shoot length) for each measurement. Values are given as mean ± s.d. Significance was determined according to Dunnet comparison of all columns versus control column at $P < 0.01$.
*$P < 0.05$, **$P < 0.01$ and ***$P < 0.001$.
n.s., non significant.

D

Effect of PYR on total chlorophyll content of soybean in the presence and absence of *B. subtilis*

Chlorophyll content reflects the photosynthetic capability and health status of plants. Data represent total chlorophyll content of 50 day old soybean plants. PYR treated soybean plants (T3) showed a 16% reduction in chlorophyll content (Fig. 1). In the T4 sample where *B. subtilis* along with PYR was present, total chlorophyll content was lowered only by 8% in soybean plants in comparison to control. There was no significant change in total chlorophyll content in treated plants treated with *B. subtilis* alone.

Assessment of effect of PYR on photosynthetic process by measuring Chl *a* fluorescence in soybean in the presence and absence of *B. subtilis*

Chl *a* fluorescence transient curves for control and all treatments were measured. A reduction of photosynthetic electron transport chain and its kinetics under PYR stress is reflected by the fluorescence rise curve (OJIP) (Fig. 2). PYR stressed soybean leaves undergo substantial physiological changes, as evidenced by a shift in the form of the Chl *a* transient curve (OJIP). The O–J phase was not affected with PYR in soybean. After PYR treatment in soybean leaves, the J–I and I–P phases were reduced. Application of *B. subtilis* along with PYR in soybean plants, contributes to better photosynthetic capacity and increased photochemical efficiency in PYR treated plants (Fig. 2).

Various Chl *a* fluorescence parameters were measured in control and PYR treated soybean plants (Table 2). Maximum fluorescence is represented by F_m which was nearly 27% decreased in PYR treated soybean plants. Upon addition of bacteria this reduction remained 17% in PYR treated
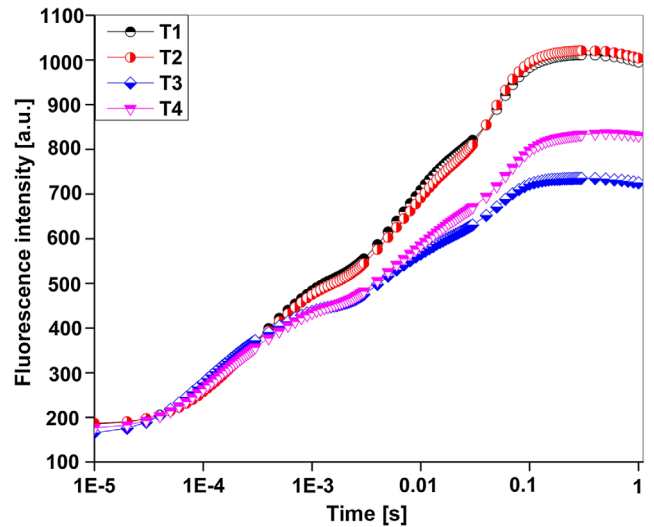

Fig. 2. Change in chlorophyll *a* fluorescence induction curves (OJIP) plotted on logarithmic scale. T1 – Control, T2 – *B. subtilis*, T3 – PYR, T4 – PYR + *B. subtilis* in soybean plants. Each experiment was repeated thrice. Fluorescence intensity is expressed in arbitrary units (a.u.).

soybean plants. Another important parameter F_v/F_m represent quantum efficiency of PSII which was declined by 6% in PYR treated soybean plants. After inoculation of bacteria value of F_v/F_m remains only 4% lowered (Table 2).

Noticeable inhibition in water splitting complex (F_v/F_o) was observed in PYR treated soybean plants. The value of F_v/F_o was decreased by 33% after treatment with PYR. The value of F_v/F_o in the presence of *B. subtilis* in PYR treated soybean leaves remained only 21% reduced as compared to control. Another photosynthetic parameter $(1 - V_j)$ was reduced by 14% in PYR treated soybean plants as compared to control, while this value remains only 3% lowered in PYR + *B. subtilis* treated soybean plants. Hence the recovered value of this parameter suggests a protective role of *B. subtilis* on soybean photosynthesis.

Different energy flux parameters like ABS/CSm, ETo/CSm, TRo/CSm were measured in control and all treatments. Reduction in these parameters was observed in presence of PYR in soybean plants. The value of ABS/CSm in PYR treated soybean plants decreased by 27% (Table 3). The ratio of TRo/CSm and ETo/CSm decreased by 18% and 27% respectively in PYR treated soybean plants. Higher PYR concentration was associated with a decreased ratio of TRo/CSm. All of these parameters were recovered in PYR + *B. subtilis* treated soybean plants. Value of DIo/CSm increased after exposure of PYR in soybean plants. No significant change was observed in the ratio of ABS/CSm, ETo/CSm, TRo/CSm, and DIo/CSm in plants treated with *B. subtilis* alone as compared to control.

Another parameter PI$_{(ABS)}$ stands for performance index measurement on an absorbance basis. Within PSII, it is made
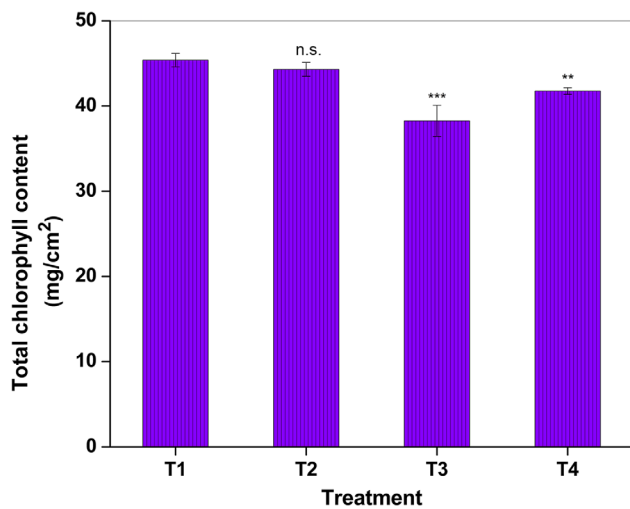

Fig. 1. Change in total chlorophyll content in 50-day-old soybean, where T1 – Control, T2 – *B. subtilis*, T3 – 200 μM PYR, T4 – 200 μM PYR + *B. subtilis*.

Table 2. Effects of 200 µM PYR, *B. subtilis* and PYR + *B. subtilis* on different chlorophyll *a* fluorescence transients in soybean plants.

Treatments	F_m	F_v/F_m	F_v/F_o	$(1 - V_j)$
Control	1011 ± 53 (100%)	0.82 ± 0.01 (100%)	4.79 ± 0.41 (100%)	0.58 ± 0.02 (100%)
B. subtilis	1021 ± 131[n.s.] (101%)	0.82 ± 0.01[n.s.] (100%)	4.85 ± 0.44[n.s.] (102%)	0.60 ± 0.02[n.s.] (103%)
200 µM PYR	735 ± 22[***] (73%)	0.77 ± 0.01[**] (94%)	3.21 ± 0.18[**] (67%)	0.50 ± 0.03[*] (86%)
200 µM PYR + *B. subtilis*	836 ± 131[**] (83%)	0.79 ± 0.01[*] (96%)	3.78 ± 0.44[*] (79%)	0.56 ± 0.02[n.s.] (97%)

Data represent the mean of three replications with five measurements from each of the four pots for each treatment. Values are given as mean ± s.d. Significance was determined according to Dunnet comparison of all columns versus control column at $P < 0.01$.
[*]$P < 0.05$, [**]$P < 0.01$ and [***]$P < 0.001$.
n.s., non significant.

Table 3. Effects of 200 µM PYR, *B. subtilis* and PYR + *B. subtilis* on different energy flux parameters in soybean plants.

Treatments	ABS/CSm	TRo/CSm	ETo/CSm	DIo/CSm
Control	1011 ± 53 (100%)	1593 ± 64 (100%)	976 ± 69 (100%)	429 ± 30 (100%)
B. subtilis	1021 ± 131[n.s.] (101%)	1577 ± 75[n.s.] (99%)	993 ± 53[n.s.] (102%)	418 ± 42[n.s.] (97%)
200 µM PYR	735 ± 22[***] (73%)	1312 ± 23[**] (82%)	711 ± 55[*] (73%)	554 ± 21[n.s.] (129%)
200 µM PYR + *B. subtilis*	836 ± 131[**] (83%)	1425 ± 124[n.s.] (89%)	862 ± 127[n.s.] (88%)	490 ± 91[n.s.] (114%)

Data represent the mean of three replications with five measurements from each of the four pots for each treatment. Values are given as mean ± s.d. Significance was determined according to Dunnet comparison of all columns versus control column at $P < 0.01$.
[*]$P < 0.05$, [**]$P < 0.01$ and [***]$P < 0.001$.
n.s., non significant.

up of three basic components (1) a component referring to the density of active PSII reaction centres per Chl (RC/ABS), (2) a component describing light reaction performance as $\Phi_{Po}/(1 - \Phi_{Po})$, and (3) a component describing dark redox reaction performance as $\Psi_o/(1 - \Psi_o)$.

The value of RC/ABS declined by 39% due to toxicity of PYR in soybean plant (Table 4), while in PYR + *B. subtilis* treated plant this value reduced only by 19%. PYR treated soybean plants shows 36% reduction in $\Phi_{Po}/(1 - \Phi_{Po})$. This value reduced in PYR + *B. subtilis* by 22%. Value of $\Psi_o/(1 - \Psi_o)$ represents the vitality of plants, it decreased by 25% in PYR treated soybean plants. Recovery by *B. subtilis* revealed less damage in all the three components of performance index. No significant change was observed in these parameters in plants treated with *B. subtilis* alone as compared to control.

Effects of PYR on biomass production of soybean in the presence and absence of *B. subtilis*

Measurement of biomass in terms of fresh and dry weight of shoot and root was done in control and all treatments. In PYR treated soybean plants, fresh weight of shoot and root declined by 64% and 50% respectively while the value of fresh weight of shoot and root in PYR + *B. subtilis* treated soybean plants was 18% and 26% lowered respectively (Fig. 3). Dry weight of shoot and root in PYR treated plants was also affected negatively and it decreased by 70% and 59% respectively in comparison with control. PYR + *B. subtilis* treated soybean plants showed recovery in dry weight as compared to PYR treated soybean plants. The value of shoot and root dry weight in PYR + *B. subtilis* treated plants decreased only by 20% and 32%.

Table 4. Effects of 200 µM PYR, *B. subtilis* and PYR + *B. subtilis* on components of Performance Index $PI_{(ABS)}$ in soybean plants.

Treatments	RC/ABS	$\Phi_{Po}/(1 - \Phi_{Po})$	$\Psi_o/(1 - \Psi_o)$
Control	0.88 ± 0.09 (100%)	3.71 ± 0.38 (100%)	1.58 ± 0.14 (100%)
B. subtilis	0.90 ± 0.09[n.s.] (102%)	3.77 ± 0.36[n.s.] (102%)	1.62 ± 0.18[n.s.] (103%)
200 µM PYR	0.54 ± 0.03[**] (61%)	2.36 ± 0.11[*] (64%)	1.18 ± 0.18[n.s.] (75%)
200 µM PYR + *B. subtilis*	0.71 ± 0.09[n.s.] (81%)	2.90 ± 0.72[n.s.] (78%)	1.53 ± 0.37[n.s.] (97%)

$PI_{(ABS)}$ as derived from chlorophyll *a* fluorescence induction kinetics.
Data represent the mean of three replications with five measurements from each of the four pots for each treatment. Values are given as mean ± s.d. Significance was determined according to Dunnet comparison of all columns versus control column at $P < 0.01$.
[*]$P < 0.05$, [**]$P < 0.01$ and [***]$P < 0.001$.
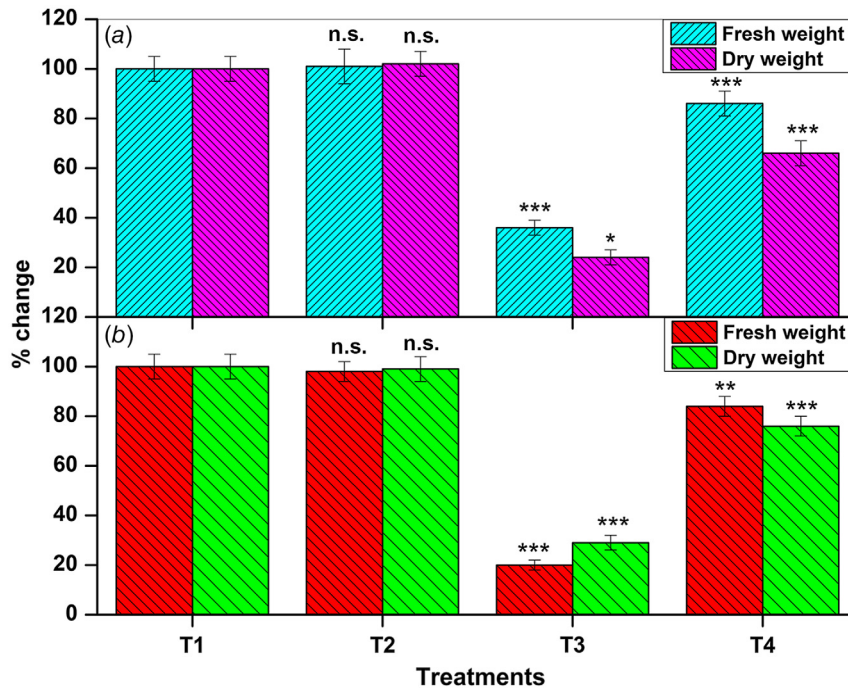n.s., non significant.

F

Fig. 3. Change in fresh and dry weight of (*a*) shoot, (*b*) root in 50 days old soybean plant in control and all treatments where T1 – Control, T2 – *B. subtilis*, T3 – 200 μM PYR, T4 – 200 μM PYR + *B. subtilis*. *$P < 0.05$, **$P < 0.01$ and ***$P < 0.001$, n.s., non significant.

Effects of PYR on soil enzymes in the presence and absence of *B. subtilis*

Activity of dehydrogenase and lipase enzyme was measured in soybean cultivated soil after every 5 day intervals until 50 days, and a gradual increase in activity of both enzymes was observed in all treatments until the end of the study. A positive correlation was found in number of days and activity of both enzymes in control and treated soil. Dehydrogenase and lipase activities both were significantly influenced by the dose of PYR and a negative correlation was observed between PYR treatment and enzyme activity.

PYR treated soybean cultivated soil exhibited 15% and 10% reductions in dehydrogenase and lipase activity respectively as compared to control soil after 50 days of treatment (Fig. 4). In PYR + *B. subtilis* treated soybean cultivated soil, activity of dehydrogenase and lipase was increased by 11% and 16% respectively as compared to control.

Extraction of PYR from remediated and unremediated soil cultivated with soybean

Further study was conducted to extract PYR from soil samples. The amount of PYR extracted from PYR treated soybean cultivated soil was 1.30 ± 0.02 μM/g (100%). Content of PYR extracted from PYR + *B. subtilis* treated soybean cultivated soil was only 0.39 ± 0.04 μM/g, which was 30% of PYR treated soil, which suggests that 70% of PYR was degraded by bacteria in 50 days (Fig. 5, Table 5). These results suggest that PYR was degraded by *B. subtilis*.

Degradation of PYR observed in PYR + *B. subtilis* treated soil supported recovery in photosynthetic parameters.

Extraction of PYR from soybean plants growing in remediated and unremediated soil

PYR was extracted from PYR and PYR + *B. subtilis* treated soybean plants. The amount of PYR extracted from roots of PYR treated soybean plants was taken as 100% (Table 5). Only 67% of PYR remained in roots of PYR + *B. subtilis* treated soybean plants. The amount of PYR extracted from stems of PYR treated soybean plant was taken as 100%, while no PYR was detected in PYR treated soybean leaves. PYR was also not detected in stem and leaves of PYR + *B. subtilis* soybean plants.

Discussion

PAHs can impair any stage of plant growth from germination to reproduction. Germination is a key parameter that is important for total yield and biomass. It consists of a complex phenomenon involving several physiological and biochemical changes leading to activation of the embryo (Parihar *et al.* 2015). The rate of seed germination can be used as a bio indicator of pollutant contamination because this process is very sensitive to various kinds of pollutants. Seedling growth can be expressed on the basis of shoot length and root length. Seedling growth, apart from seed germination, is a convenient indicator of environmental phytotoxicity.
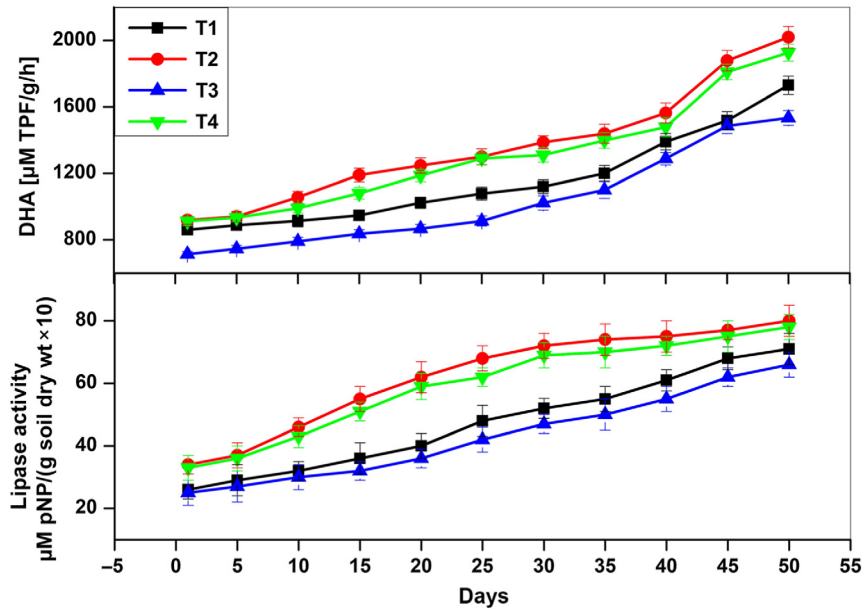
Fig. 4. Dehydrogenase (DHA) activity (µM TPF/g/h) and Lipase activity [µM pNP/ (g soil dry wt × 10)] in 50 day old soil cultivated with soybean with PYR treatment and *B. subtilis* where T1 − Control, T2 − *B. subtilis*, T3 − 200 µM PYR, T4 − 200 µM PYR + *B. subtilis*.
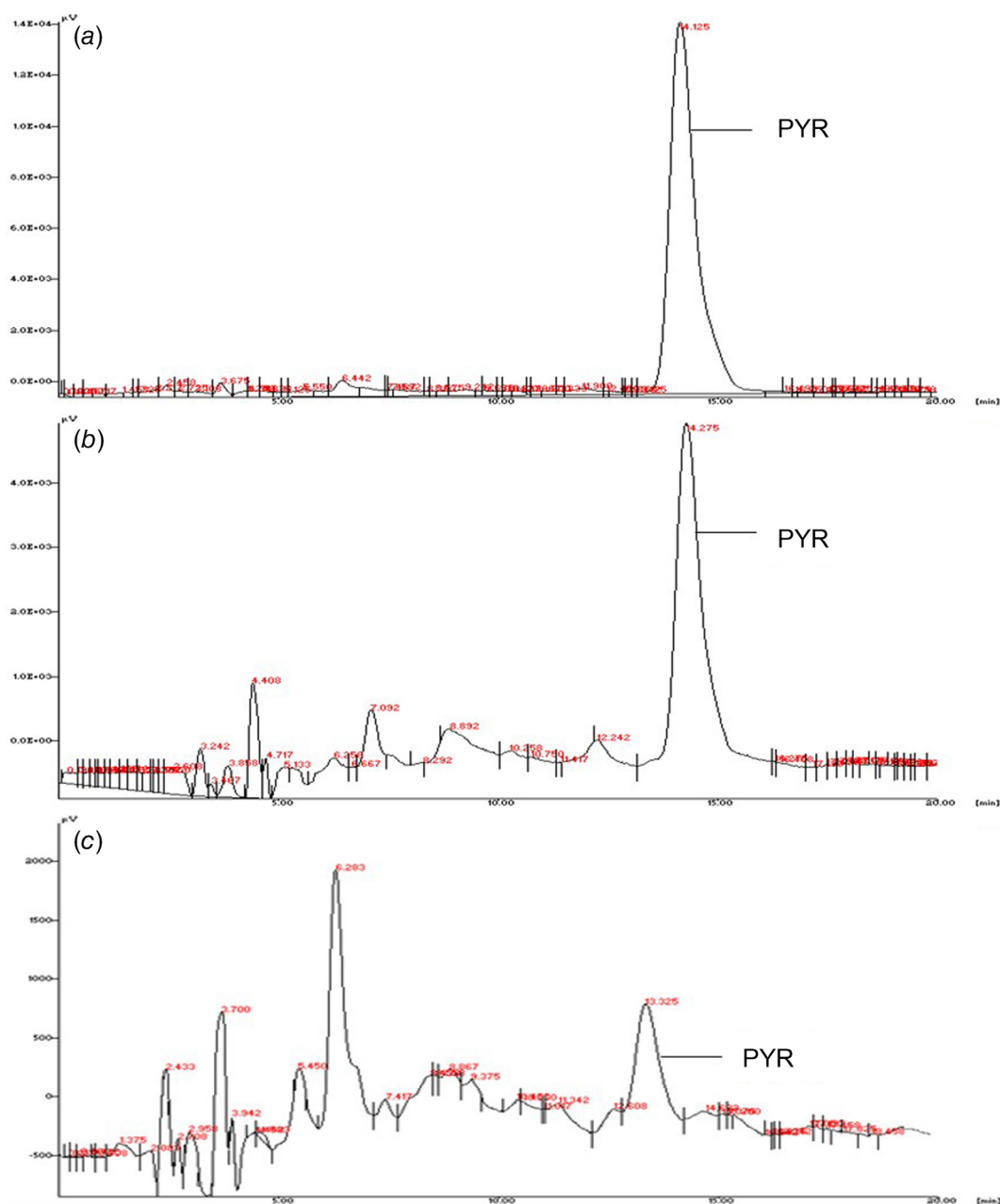
Destruction of the seed embryo by hydrocarbons can be an important reason for the prevention of seed germination in presence of PYR (Reynoso-Cuevas *et al.* 2008). Change in germination rate of soybean seeds may be because of changes in the endogenous level of hormones (cytokinin, gibberellin, ethylene and ABA) in the presence of PYR. Another reason may be inactivation of mobilisation of protein and saccharide reserves in the seed during germination. The possible cause of inhibition of shoot and root length of soybean plant may be the lipophilic nature of PYR, which may interact with biological membranes leading to changes in its structure and function, resulting in impaired growth and metabolic activity of the cell.

Reduction in total chlorophyll content in PYR treated soybean plants is due to decomposition of chlorophyll. Less reduced chlorophyll content was observed in PYR + *B. subtilis* treated plants. These observations suggest that the bacterium is suppressing the structural and functional damage of the chloroplast, eventually leading to less decomposition of chlorophyll.

Chlorophyll *a* fluorescence (ChlF) is used to study the relationship between light-dependent processes and fluorescence (Goltsev *et al.* 2016). It provides sophisticated and non-invasive methods for studying photosynthetic dynamics. It is based on the theory of 'energy flow' across thylakoid membranes (Strasser *et al.* 2000). The name OJIP comes from the points on the induction curve created by the recorded chlorophyll fluorescence signal, which correlate to the decline of Q_A and the primary electron acceptor of photosystem II. Phases are calculated on a $\log_{10}$ time scale. A first step rises from the origin (O) to an intermediate step (J step, 2 ms), followed by a second, slower rise from the origin (O) to a second intermediate (I step, 30 ms) to a peak P (Strauss *et al.* 2006; Tu *et al.* 2016). The O–J part of

the fluorescence rise is due to closure of some of the PSII reaction centres in response to the reduction of Q_A to a level determined by the ratio between the trapping rate and Q_A reoxidation rate by the secondary electron acceptor Q_B as well as rest of the electron transfer chain. The J–I and I–P phases were reduced in PYR treated soybean plants. The reduction of the secondary electron acceptor Q_B, plastoquinone (PQ), cytochrome (Cyt $b_6 f$), and plastocyanin (PC) is represented by the J–I section of the curve (Strasser *et al.* 1995; Hill *et al.* 2004). The reduction of electron transporters (ferredoxin, intermediary acceptors, and NADP [nicotinamide adenine dinucleotide phosphate]) on the photosystem I acceptor side is usually linked to the increase in chlorophyll fluorescence in the I–P region of the induction curve (Kalaji *et al.* 2014). Damage to the PSII reaction centres, lower photosynthetic capacity and photochemical efficiency, or impairment of the leaf photosynthetic system, as well as reduced photosynthetic CO_2 fixation, are all seen when these phases are reduced in PYR treated leaves (Percival and Henderson 2003).

Values of maximum fluorescence (F_m) and quantum efficiency of PSII (F_v/F_m) were decreased in PYR treated soybean plants. The decrease in these parameters is due to the presence of a large population of inactive PSII centres due to degradation of the D1 protein, thus reducing electron transport capacity in PSII. Recovery in these parameters in the presence of *B. subtilis* suggests an important role of the bacterium in protection of D1 protein from toxic effects of PYR. Inhibition in the water splitting complex (F_v/F_o) was observed in PYR treated soybean plants. Damage in the water splitting complex was observed resulting in impairment in PSII photochemistry (Pereira *et al.* 2000; Kalaji *et al.* 2011). The higher value of F_v/F_o in the presence of *B. subtilis* suggests that the water splitting complex was less damaged due to

Fig. 5. HPLC chromatogram of PYR treated soil cultivated with soybean. (*a*) Standard PYR; (*b*) soil sample treated with PYR; (*c*) soil sample treated with PYR + *B. subtilis*.

Table 5. PYR content in different soil and soybean plants growing in PYR and PYR + *B. subtilis* treated soil.

Treatments	PYR content (µM/g) in different samples			
	Soil	Root	Stem	Leaf
Control	ND	ND	ND	ND
B. subtilis	ND	ND	ND	ND
200 µM PYR	1.30 ± 0.02 (100%)	0.009 ± 0.002 (100%)	0.001 ± 0.001 (100%)	ND
200 µM PYR + *B. subtilis*	0.39 ± 0.04 (30%)	0.006 ± 0.002 (67%)	ND	ND

Data represent the mean of three replications from each of the four pots for each treatment. Values are given as mean ± s.d.
ND, not detected.

lowered toxicity of PYR in the presence of this bacterium. The V_j parameter provides information about the acceptor side of PSII and is equivalent to ($F_j - F_o/F_m - F_o$). The efficiency with which trapped electrons are able to proceed beyond Q_A^- is equal to ($1 - V_j$) or ψ_o (Singh Tomar and Jajoo 2013). In PYR + *B. subtilis* treated plants the recovered value of this parameter suggests that toxic effects of PYR on photosynthesis of soybean plant were reduced by *B. subtilis*.

The lowered value of ABS/CSm stipulates a reduction in the energy absorbed per excited cross section (Tsimilli-Micheal and Strasser 2008). The decrease in electron transport per cross section in PYR treated plants as compared with the control plants reflects a reduction in absorption of energy by antenna pigments (ABS/CSm) and inactivation of reaction centre complexes. Action of PYR on active reaction centres may generate a dissipative sink for excitation energy. A decreased ratio of TRo/CSm illustrates diminished trapping of energy by reaction centres. A decrease in the density of active reaction centres is also responsible for the decrease in TRo/CSm. All of these parameters were recovered in PYR + *B. subtilis* treated soybean plants. These observations were also supported by increased chlorophyll content in PYR + *B. subtilis* treated soybean plants. The increased value of DIo/CSm in PYR treated soybean plants indicates that energy was dissipated in the form of heat. Presence of *B. subtilis* along with PYR could recover the disruption caused by PYR in all these parameters.

PI(ABS) is a highly sensitive measure that is used to determine stress and used as a plant vitality indicator. It is a popular tool for comparing primary photochemical reactions (Chen and Cheng 2009). The value of RC/ABS declined in PYR in soybean plants (Table 4), and recovered in PYR + *B. subtilis* treated plants. Changes in RC/ABS indicate change in active PSII reaction centres (RCs), as well as a reduction in the size of the chlorophyll antenna servicing each RC and the density of reaction centres. $\Phi_{Po}/(1 - \Phi_{Po})$ illustrate damage in the water splitting complex of PSII and PSII photochemistry. PYR treated soybean plants showed damage in the water splitting complex; this interpretation is also supported by a reduction in value of the F_v/F_o parameter. Recovery in this parameter was observed in PYR + *B. subtilis* treated plants. The value of $\Psi_o/(1 - \Psi_o)$ represents the vitality of plants. The decrease in the value of $\Psi_o/(1 - \Psi_o)$ in PYR treated soybean plants suggests that these compounds reduce the trapping and absorption of efficient electrons resulting in downregulation of electron transport from Q_A^- to the PSI end acceptor. These findings are also supported by decreased absorption and trapping of energy in PYR treated soybean plants.

Biomass is the mass of living biological organisms in a given area at a given time. Biomass production is regarded as a reliable external indicator of the internal status of plant (Rai-Kalal and Jajoo 2021). Fresh or dry weight is used to describe a species' biomass. Biomass production is considered an important and commonly used indicator for assessment of plant growth. Fresh and dry weight of shoot and root were decreased in PYR treated plants. The reason behind this reduction in fresh and dry weight is decreased chlorophyll content and photosynthetic performance of PYR treated plants. The recovered value in fresh and dry weight in soybean plants in the presence of *B. subtilis* suggests that *B. subtilis* protects plants from PYR toxicity by reducing its concentration in soil and can be considered as beneficial for soybean crop improvement in PYR polluted soil.

The activity of soil enzymes (dehydrogenase and lipase) was decreased in PYR treated soybean cultivated soil. Toxicity of PYR exerts a direct effect on soil microflora by killing the microorganisms or decreasing the availability of substrate, this may cause reduced activity of both enzymes in PYR treated soil. Activity of these enzymes represents soil quality and fertility. Reduced fertility of PYR contaminated soil is supported by reduced photosynthesis and biomass production in PYR treated soybean plants. In PYR + *B. subtilis* treated soybean cultivated soil, activity of dehydrogenase and lipase was observed increased as compared to control. In PYR + *B. subtilis* treated soil PYR seems to be utilised by *B. subtilis* as a substrate for a source of energy, thus *B. subtilis* shows capability to degrade PYR. It has been reported in previous findings that three- or four-ring containing organic compounds constitute a rich source of energy and carbon for microorganisms (Baran *et al.* 2004; Sheng *et al.* 2008; Lipińska *et al.* 2015). *Bacillus subtilis* has shown great potential in production of biosurfactants, which facilitate the easy availability of PAHs as substrate; thus it could degrade PYR more efficiently. Activity of dehydrogenase and lipase were found to be higher in soil treated with *B. subtilis* alone as compared to control soil, due to the presence of a large microbial population. This explanation finds support from earlier observations in which dehydrogenase activity was considered equivalent to metabolic ability of the soil and it is thought to be proportional to the biomass of soil microorganisms (Wolińska and Stępniewska 2012). *B. subtilis* efficiently degrade PYR from soil. However, PYR was additionally utilised by bacterium in soil treated with this compound along with *B. subtilis*. Decreased enzyme activities in soil treated with PYR alone also suggest that the naturally occurring microflora was not able to degrade PYR efficiently.

The latter part of the study involved extraction and quantification of PYR from soil samples. The amount of PYR extracted from PYR treated soybean cultivated soil was greater than the amount of PYR extracted from PYR + *B. subtilis* treated soybean cultivated soil, which suggests that efficient degradation of PYR was achieved by bacteria in 50 days (Fig. 5, Table 5). Degradation of PYR achieved in PYR + *B. subtilis* treated soybean cultivated soil supported recovery in the photosynthetic parameters. A greater amount of PYR was extracted from roots, because roots are the first tissue to be exposed to PYR. These PAH compounds cause retardation in root growth, root extension and proliferation. The authors also reported that PYR causes inhibition in

length of roots of soybean plants (Tomar and Jajoo 2015). Reduced root growth is due to PYR toxicity, which directly inhibits photosynthetic efficiency of plants and may affect seed yield due to a lack of initial uptake and transport of water and nutrients to the plants (Cui *et al.* 2016). The content of PYR extracted from stem and leaf were less in comparison with roots. That observation may be due to reduced translocation of this hydrophobic compound (PYR) through xylem vessels and enzymatic degradation of such PAH compounds in stem and leaves. A positive correlation was observed between PAH concentration in soil and plant parts. PYR was not detected in the control nor in soil treated with *B. subtilis* alone cultivated with soybean. Declines in photosynthetic efficiency in leaves of soybean plants growing in PYR treated soil suggest that PYR caused destruction in the photosynthetic apparatus. This may be because of hindered nutrient uptake from soil. Enhanced photosynthesis in plants growing in PYR + *B. subtilis* treated soil, demonstrated the bioremediation potential of bacteria and recovery in photosynthetic apparatus by reducing the amount of PYR in soil. A negative correlation was found between the concentration of PYR in soil and photosynthetic efficiency of soybean plants. In the present investigation the applied bacteria showed auspicious results in PYR degradation. Hence the use of *B. subtilis* can play an important role in remediation of PYR contaminated sites and is beneficial for the protection of soybean crop growing in PYR contaminated soil.

Conclusion

We conclude that photosynthetic efficiency of soybean plants was significantly decreased by PYR; whereas PYR + *B. subtilis* treated plants shows noticeable recovery on this metric. The kinetics of chlorophyll *a* fluorescence were measured to monitor the fluorescence of chlorophyll *a*. Seed germination, chlorophyll *a* fluorescence induction kinetics, ABS/CSm, ETo/CSm, TRo/CSm, performance index and activity of soil enzymes (dehydrogenase and lipase) were measured in controls, and in soybean plants treated with PYR, PYR + *B. subtilis* and *B. subtilis* alone. Inhibitory effects of PYR on all these parameters were observed, whereas a recovery in the majority of the parameters was observed in PYR + *B. subtilis* plants. This surfactant producing bacterium facilitates the degradation of PYR in soil, hence reducing its concentration and thereby its inhibitory effects. 70% degradation of PYR was achieved by bacterium in soil. Because of the low concentration of PYR in the soil treated with PYR + *B. subtilis*, there was less PYR translocation via the roots in PYR + *B. subtilis* treated plants compared to PYR treated plants. These observations imply that the presence of *B. subtilis* in PYR treated plants protected the photosynthetic machinery from PYR induced damage. *B. subtilis* could help plants to cope

with PYR toxicity. However, we recognise that *B. subtilis* alone can only mitigate the harmful effects of PYR to some extent. It would be beneficial to use a consortium of bacteria to degrade PYR completely. We also suggest that Chl *a* fluorescence measurement can be authentically used to study effects of pollutants and remedial strategies on plants.

References

Aksmann A, Tukaj Z (2008) Intact anthracene inhibits photosynthesis in algal cells: a fluorescence induction study on *Chlamydomonas reinhardtii cw*92 strain. *Chemosphere* **74**, 26–32. doi:10.1016/j.chemosphere.2008.09.064

Aksmann A, Pokora W, Baścik-Remisiewicz A, Dettlaff-Pokora A, Wielgomas B, Dziadziuszko M, Tukaj Z (2014) Time-dependent changes in antioxidative enzyme expression and photosynthetic activity of *Chlamydomonas reinhardtii* cells under acute exposure to cadmium and anthracene. *Ecotoxicology and Environmental Safety* **110**, 31–40. doi:10.1016/j.ecoenv.2014.08.005

Allakhverdiev SI (2020) Optimising photosynthesis for environmental fitness. *Functional Plant Biology* **47**, iii–vii. doi:10.1071/FPv47n11_FO

Baran S, Bielińska JE, Oleszczuk P (2004) Enzymatic activity in an airfield soil polluted with polycyclic aromatic hydrocarbons. *Geoderma* **118**, 221–232. doi:10.1016/S0016-7061(03)00205-2

Boll ES, Johnsen AR, Christensen JH (2015) Polar metabolites of polycyclic aromatic compounds from fungi are potential soil and ground-water contaminants. *Chemosphere* **119**, 250–257. doi:10.1016/j.chemosphere.2014.06.033

Brestic M, Zivcak M, Hauptvogel P, Misheva S, Kocheva K, Yang X, Li X, Allakhverdiev SI (2018) Wheat plant selection for high yields entailed improvement of leaf anatomical and biochemical traits including tolerance to non-optimal temperature conditions. *Photosynthesis Research* **136**, 245–255. doi:10.1007/s11120-018-0486-z

Brestic M, Yang X, Li X, Allakhverdiev SI (2021) Crop photosynthesis for the twenty-first century. *Photosynthesis Research* **150**, 1–3. doi:10.1007/s11120-021-00869-5

Casida LE Jr, Klein DA, Santoro T (1964) Soil dehydrogenase activity. *Soil Science* **98**, 371–376. doi:10.1097/00010694-196412000-00004

Chauhan A, Fazlurrahman, Oakeshott JG, Jain RK (2008) Bacterial metabolism of polycyclic aromatic hydrocarbons: strategies for bioremediation. *Indian Journal of Microbiology* **48**, 95–113. doi:10.1007/s12088-008-0010-9

Chen LS, Cheng L (2009) Photosystem 2 is more tolerant to high temperature in apple (*Malus domestica* Borkh.) leaves than in fruit peel. *Photosynthetica* **47**, 112–120. doi:10.1007/s11099-009-0017-4

Cui X, Dong Y, Gi P, Wang H, Xu K, Zhang Z (2016) Relationship between root vigour, photosynthesis and biomass in soybean cultivars during 87 years of genetic improvement in the northern China. *Photosynthetica* **54**, 81–86. doi:10.1007/s11099-015-0160-z

Desalme D, Binet P, Chiapusio G (2013) Challenges in tracing the fate and effects of atmospheric polycyclic aromatic hydrocarbon deposition in vascular plants. *Environmental Science &Technology* **47**, 3967–3981. doi:10.1021/es304964b

Fang GC, Wu YS, Chen JC, Fu PP, Chang CN, Ho TT, Chen MH (2005) Characteristic study of polycyclic aromatic hydrocarbons for fine and coarse particulates at Pastureland near Industrial Park sampling site of central Taiwan. *Chemosphere* **60**, 427–433. doi:10.1016/j.chemosphere.2004.12.034

Gao Y, Zhu L (2004) Plant uptake, accumulation and translocation of phenanthrene and pyrene in soils. *Chemosphere* **55**, 1169–1178. doi:10.1016/j.chemosphere.2004.01.037

Goltsev VN, Kalaji HM, Paunov M, Bąba W, Horaczek T, Mojski J, Kociel H, Allakhverdiev SI (2016) Variable chlorophyll fluorescence and its use for assessing physiological condition of plant photosynthetic apparatus. *Russian Journal of Plant Physiology* **63**, 869–893. doi:10.1134/S1021443716050058

Habe H, Omori T (2003) Genetics of polycyclic aromatic hydrocarbon metabolism in diverse aerobic bacteria. *Bioscience, Biotechnology, and Biochemistry* **67**, 225–243. doi:10.1271/bbb.67.225

Henner P, Schiavon M, Morel J-L, Lichtfouse E (1997) Polycyclic aromatic hydrocarbon (PAH) occurrence and remediation methods. *Analysis* **25**, 56–59.

Hill R, Larkum AWD, Frankart C, Kühl M, Ralph PJ (2004) Loss of functional photosystem II reaction centres in zooxanthellae of corals exposed to bleaching conditions: using fluorescence rise kinetics. *Photosynthesis Research* **82**, 59–72. doi:10.1023/B:PRES.0000040444.41179.09

Jain L, Jajoo A (2020) Protection of PSI and PSII complexes of wheat from toxic effect of anthracene by *Bacillus subtilis* (NCIM 5594). *Photosynthesis Research* **146**, 197–211. doi:10.1007/s11120-019-00692-z

Jajoo A, Mekala NR, Tomar RS, Grieco M, Tikkanen M, Aro E-M (2014) Inhibitory effects of polycyclic aromatic hydrocarbons (PAHs) on photosynthetic performance are not related to their aromaticity. *Journal of Photochemistry and Photobiology B: Biology* **137**, 151–155. doi:10.1016/j.jphotobiol.2014.03.011

Kalaji HM, Bosa K, Kościelniak J, Hossain Z (2011) Chlorophyll *a* fluorescence—a useful tool for the early detection of temperature stress in spring barley (*Hordeum vulgare* L.). *Omics: A Journal of Integrative Biology* **15**, 925–934. doi:10.1089/omi.2011.0070

Kalaji HM, Oukarroum A, Alexandrov V, Kouzmanova M, Brestic M, Zivcak M, Samborska IA, Cetner MD, Allakhverdiev SI, Goltsev V (2014) Identification of nutrient deficiency in maize and tomato plants by *in vivo* chlorophyll *a* fluorescence measurements. *Plant Physiology and Biochemistry* **81**, 16–25. doi:10.1016/j.plaphy.2014.03.029

Khan MI, Cheema SA, Shen C, Hassan I, Chen Y (2014) Phytotoxicity assessment of phenanthrene and pyrene in soil using two barley genotypes. *Toxicological & Environmental Chemistry* **96**, 94–105. doi:10.1080/02772248.2014.923425

Kosaric N (2001) Biosurfactant application for soil bioremediation. *Food Technology and Biotechnology* **39**, 295–304.

Kreslavski VD, Brestic M, Zharmukhamedov SK, Lyubimov VY, Lankin AV, Jajoo A, Allakhverdiev SI (2017) Mechanisms of inhibitory effects of polycyclic aromatic hydrocarbons in photosynthetic primary processes in pea leaves and thylakoid preparations. *Plant Biology* **19**, 683–688. doi:10.1111/plb.12598

Kuhn A, Ballach H-J, Wittig R (2004) Studies in the biodegradation of 5 PAHs (phenanthrene, pyrene, fluoranthene, chrysene und benzo(a) pyrene) in the presence of rooted poplar cuttings. *Environmental Science and Pollution Research* **11**, 22–32. doi:10.1065/espr2003.11.178

Kummerová M, Barták M, Dubová J, Tříska J, Zubrová E, Zezulka S (2006) Inhibitory effect of fluoranthene on photosynthetic processes in lichens detected by chlorophyll fluorescence. *Ecotoxicology* **15**, 121–131. doi:10.1007/s10646-005-0037-1

Lipińska A, Wyszkowska J, Kucharski J (2015) Diversity of organotrophic bacteria, activity of dehydrogenases and urease as well as seed germination and root growth *Lepidium sativum, Sorghum saccharatum* and *Sinapis alba* under the influence of polycyclic aromatic hydrocarbons. *Environmental Science and Pollution Research* **22**, 18519–18530. doi:10.1007/s11356-015-5329-2

Lipińska A, Wyszkowska J, Kucharski J (2021) Microbiological and biochemical activity in soil contaminated with pyrene subjected to bioaugmentation. *Water, Air, & Soil Pollution* **232**, 45. doi:10.1007/s11270-020-04950-y

Luch A (2005) 'The carcinogenic effects of polycyclic aromatic hydrocarbons.' (Imperial College 470 Press: London)

Margesin R, Zimmerbauer A, Schinner F (1999) Soil lipase activity – a useful indicator of oil biodegradation. *Biotechnology Techniques* **13**, 859–863. doi:10.1023/A:1008928308695

Margesin R, Feller G, Hämmerle M, Stegner U, Schinner F (2002) A colorimetric method for the determination of lipase activity in soil. *Biotechnology Letters* **24**, 27–33. doi:10.1023/A:1013801131553

Marwood CA, Solomon KR, Greenberg BM (2001) Chlorophyll fluorescence as a bioindicator of effects on growth in aquatic macrophytes from mixtures of polycyclic aromatic hydrocarbons. *Environmental Toxicology and Chemistry* **20**, 890–898. doi:10.1002/etc.5620200425

Mathur S, Sharma MP, Jajoo A (2018) Improved photosynthetic efficacy of maize (*Zea mays*) plants with arbuscular mycorrhizal fungi (AMF) under high temperature stress. *Journal of Photochemistry and*

Photobiology B: Biology **180**, 149–154. doi:10.1016/j.jphotobiol.2018.02.002

Mojiri A, Zhou JL, Ohashi A, Ozaki N, Kindaichi T (2019) Comprehensive review of polycyclic aromatic hydrocarbons in water sources, their effects and treatments. *Science of the Total Environment* **696**, 133971. doi:10.1016/j.scitotenv.2019.133971

Molina L, Segura A (2021) Biochemical and metabolic plant responses toward polycyclic aromatic hydrocarbons and heavy metals present in atmospheric pollution. *Plants* **10**, 2305. doi:10.3390/plants10112305

Nanekar S, Dhote M, Kashyap S, Singh SK, Juwarkar AA (2015) Microbe assisted phytoremediation of oil sludge and role of amendments: a mesocosm study. *International Journal of Environmental Science and Technology* **12**, 193–202. doi:10.1007/s13762-013-0400-3

Parihar P, Singh S, Singh R, Singh VP, Prasad SM (2015) Effect of salinity stress on plants and its tolerance strategies: a review. *Environmental Science and Pollution Research* **22**(6), 4056–4075. doi:10.1007/s11356-014-3739-1

Peng R, Fu X, Tian Y, Zhao W, Zhu B, Xu J, Wang B, Wang L, Yao Q (2014) Metabolic engineering of Arabidopsis for remediation of different polycyclic aromatic hydrocarbons using a hybrid bacterial dioxygenase complex. *Metabolic Engineering* **26**, 100–110. doi:10.1016/j.ymben.2014.09.005

Percival GC, Henderson A (2003) An assessment of the freezing tolerance of urban trees using chlorophyll fluorescence. *The Journal of Horticultural Science and Biotechnology* **78**, 254–260. doi:10.1080/14620316.2003.11511614

Pereira WE, de Siqueira DL, Martínez CA, Puiatti M (2000) Gas exchange and chlorophyll fluorescence in four citrus rootstocks under aluminium stress. *Journal of Plant Physiology* **157**, 513–520. doi:10.1016/S0176-1617(00)80106-6

Rai-Kalal P, Jajoo A (2021) Priming with zinc oxide nanoparticles improve germination and photosynthetic performance in wheat. *Plant Physiology and Biochemistry* **160**, 341–351. doi:10.1016/j.plaphy.2021.01.032

Reynoso-Cuevas L, Gallegos-Martínez ME, Cruz-Sosa F, Gutiérrez-Rojas M (2008) *In vitro* evaluation of germination and growth of five plant species on medium supplemented with hydrocarbons associated with contaminated soils. *Bioresource Technology* **99**, 6379–6385. doi:10.1016/j.biortech.2007.11.074

Sachdev DP, Cameotra SS (2013) Biosurfactants in agriculture. *Applied Microbiology and Biotechnology* **97**, 1005–1016. doi:10.1007/s00253-012-4641-8

Schwab AP, Su J, Wetzel S, Pekarek S, Banks MK (1999) Extraction of petroleum hydrocarbons from soil by mechanical shaking. *Environmental Science & Technology* **33**, 1940–1945. doi:10.1021/es9809758

Seo J-S, Keum Y-S, Li QX (2009) Bacterial degradation of aromatic compounds. *International Journal of Environmental Research and Public Health* **6**, 278–309. doi:10.3390/ijerph6010278

Sharma C, Mathur S, Tomar RS, Jajoo A (2018) Investigating role of Triton X-100 in ameliorating deleterious effects of anthracene in wheat plants. *Photosynthetica* **56**, 652–659. doi:10.1007/s11099-017-0715-2

Sheng M, Tang M, Chen H, Yang B, Zhang F, Huang Y (2008) Influence of arbuscular mycorrhizae on photosynthesis and water status of maize plants under salt stress. *Mycorrhiza* **18**, 287–296. doi:10.1007/s00572-008-0180-7

Sivaram AK, Logeshwaran P, Lockington R, Naidu R, Megharaj M (2017) Impact of plant photosystems in the remediation of benzo[a]pyrene and pyrene spiked soils. *Chemosphere* **193**, 625–634. doi:10.1016/j.chemosphere.2017.11.081

Strasser RJ, Srivastava A, Govindjee (1995) Polyphasic chlorophyll *a* fluorescence transient in plants and cyanobacteria. *Photochemistry and Photobiology* **61**, 32–42. doi:10.1111/j.1751-1097.1995.tb09240.x

Strasser RJ, Srivastava A, Tsimilli-Michael M (2000) The fluorescence transient as a tool to characterize and screen photosynthetic samples. In 'Probing photosynthesis: mechanisms, regulation and adaptation'. (Eds M Yunus, U Pathre, P Mohanty) pp. 445–483. (Taylor & Francis)

Strauss AJ, Krüger GHJ, Strasser RJ, Van Heerden PDR (2006) Ranking of dark chilling tolerance in soybean genotypes probed by the chlorophyll *a* fluorescence transient O-J-I-P. *Environmental and*

Experimental Botany **56**, 147–157. doi:10.1016/j.envexpbot.2005.01.011

Sverdrup LE (2001) Toxicity of tar constituents in terrestrial ecosystem. Effects of eight polycyclic aromatic compounds on terrestrial plants, soil invertebrates and microorganisms. PhD thesis, Faculty of Mathematics and Natural Sciences, University of Oslo, Norway.

Toledo FL, Calvo C, Rodelas B, González-López J (2006) Selection and identification of bacteria isolated from waste crude oil with polycyclic aromatic hydrocarbons removal capacities. *Systematic and Applied Microbiology* **29**, 244–252. doi:10.1016/j.syapm.2005.09.003

Tomar RS, Jajoo A (2013) A quick investigation of the detrimental effects of environmental pollutant polycyclic aromatic hydrocarbon fluoranthene on the photosynthetic efficiency of wheat (*Triticum aestivum*). *Ecotoxicology* **22**, 1313–1318. doi:10.1007/s10646-013-1118-1

Tomar RS, Jajoo A (2015) Photomodified fluoranthene exerts more harmful effects as compared to intact fluoranthene by inhibiting growth and photosynthetic processes in wheat. *Ecotoxicology and Environmental Safety* **122**, 31–36. doi:10.1016/j.ecoenv.2015.07.002

Treichel H, de Oliveira D, Mazutti MA, Di Luccio M, Oliveira JV (2010) A review on microbial lipases production. *Food and Bioprocess Technology* **3**, 182–196. doi:10.1007/s11947-009-0202-2

Tsimilli-Micheal M, Strasser RJ (2008) In vivo assessment of stress impact on plant's vitality: applications in detecting and evaluating the beneficial role of mycorrhization on host plants. In 'Mycorrhiza'. (Ed. A Varma) pp. 679–703. (Springer)

Tu W, Li Y, Liu W, Wu L, Xie X, Zhang Y, Wilhelm C, Yang C (2016) Spring ephemerals adapt to extremely high light conditions via an unusual stabilization of Photosystem II. *Frontiers in Plant Science* **6**, 1189. doi:10.3389/fpls.2015.01189

Upadhyaya H, Roy H, Shome S, Tewari S, Bhattacharya MK, Panda SK (2017) Physiological impact of Zinc nanoparticle on germination of rice (*Oryza sativa* L) seed. *Journal of Plant Science and Phytopathology* **1**, 62–70. doi:10.29328/journal.jpsp.1001008

Wolińska A, Stępniewska Z (2012) Dehydrogenase activity in the soil environment. In 'Biochemistry, genetics and molecular biology, dehydrogenases'. (Ed. RA Canuto) pp. 183–210. (Lublin)

Wolińska A, Kuźniar A, Szafranek-Nakonieczna A, Jastrzębska N, Roguska E, Stępniewska Z (2016) Biological activity of autochthonic bacterial community in oil-contaminated soil. *Water, Air, & Soil Pollution* **227**, 130. doi:10.1007/s11270-016-2825-z

Zhu J, Tremblay N, Liang Y (2012) Comparing SPAD and atLEAF values for chlorophyll assessment in crop species. *Canadian Journal of Soil Science* **92**, 645–648. doi:10.4141/cjss2011-100

Author affiliations
[A]School of Life Science, Devi Ahilya University, Indore 452017, India.
[B]School of Biotechnology, Devi Ahilya University, Indore 452017, India.

Moderate photoinhibition of PSII and oxidation of P700 contribute to chilling tolerance of tropical tree species in subtropics of China

V.S.J. SUNOJ[*,+] (iD), Y. WEN[*], A. JAJOO[**], A.W. SHORT[*,***], W.H. ZENG[*], N.I. ELSHEERY[#], and K.F. CAO[*,+] (iD)

State Key Laboratory for Conservation and Utilization of Subtropical Agri-Bioresources and Guangxi Key Laboratory of Forest Ecology and Conservation, College of Forestry, Guangxi University, 530004 Nanning, Guangxi, China[*]
School of Life Science, Devi Ahilya University, 452017 Indore, India[**]
Department of Agricultural Botany, Tanta University, 72513 Tanta, Egypt[#]
Institute of Ecology and Evolution, University of Oregon, Eugene, OR 97403, USA[***]

Abstract

In the subtropics, a few tropical tree species are distributed and planted for ornamental and horticultural purposes; however, the photosynthesis of these species can be impaired by chilling. This study aimed to understand how these species respond to chilling. Light-dependent and CO_2 assimilation reactions of six tropical tree species from geographically diverse areas, but grown at a lower subtropical site in China, were monitored during a chilling ($\leq 10°C$). Chilling induced stomatal and nonstomatal effects and moderate photoinhibition of PSII, with severe effect in *Ixora chinensis*. *Woodfordia fruticosa* was little affected by chilling, with negligible reduction of photosynthesis and PSII activity, higher cyclic electron flow (CEF), and oxidation state of P700 (P700⁺). Photoinhibition of PSII thus reduced electron flow to P700, while active CEF reduced oxidative damage of PSI and maintained photosynthesis during chilling. Studied parameters revealed that coupling between light-dependent and CO_2 assimilation reactions was enhanced under chilling.

Highlights

- Chilling induced stomatal and nonstomatal effects and moderate photoinhibition of PSII
- Photoinhibition of PSII, photosynthesis control, and CEF sustained oxidation of P700
- Oxidation of P700 reduced oxidative damage and maintained photosynthesis during chilling

Introduction

Tropical plants grow in hot and humid climatic conditions with minor seasonal temperature variations. However, the chilling tolerance of some tropical plant species enables them to survive in marginal tropical and lower subtropical areas (subtropics with relatively low latitudes), where short-term chilling events ($\leq 10°C$ for a few days) frequently occur during winter. A few selected tropical tree species have been planted in marginal tropical and lower subtropical areas for ornamental and horticultural purposes (Jalili *et al.* 2010, Li *et al.* 2016, Mau *et al.* 2018). Chilling during winter in the lower subtropics is a major factor limiting the latitudinal distribution and poleward migration of tropical plant species, despite global warming (Li *et al.* 2016, Wen *et al.* 2018). Chilling stress is complex and adversely affects the morphological, physio-biochemical, and molecular processes in plants, thus it reduces their growth and development (Allen and Ort 2001, Liu *et al.* 2018, Elsheery *et al.* 2020, Li *et al.* 2021, Mathur *et al.* 2021). Earlier studies have revealed the influence of chilling in combination with varying incident light intensities on photosynthesis and photo-protection mechanisms of plants, including diverse tropical tree species (Someralo and Krause 1990, Barth and Krause 1999, Elsheery *et al.* 2008, Huang *et al.* 2010a,b; 2011, 2017; Zheng *et al.* 2016, Yang *et al.* 2017).

During photosynthesis, the antenna complexes of PSII and PSI absorb light energy and drive the electron flow to generate energy-rich compounds (ATP and NADPH), which are utilized to fix CO_2, converting it into carbohydrates (Miyake 2020). Under chilling, due to stomatal and nonstomatal control of CO_2 fixation, Chl *a* of reaction centers of the photosystems (P700 in PSI [excited; P700*] and P680 in PSII [excited; P680*]) cannot be de-excited to their ground state (Allen and Ort 2001). The failure of de-excitation of reaction centers of photosystems alters the photosynthetic electron transport. Such circumstances result in a reduction of O_2 (Mehler reaction) and produce reactive oxygen species (ROS) such as superoxide ($O_2^{\bullet-}$) and hydrogen peroxide (H_2O_2). The production of ROS contributes to the generation of hydroxyl radicals ($^{\bullet}OH$), which can damage DNA, proteins, and lipids. In contrast, the oxidized reaction centers of chlorophyll P680 in PSII (P680$^+$) are reduced by accepting electrons, resulting from the oxidation of water and forming singlet P680 (^{1}P680*). Failure to de-excite ^{1}P680* leads to the production of triplet chlorophyll (^{3}P680*), which can transfer the energy to ground state oxygen ($^3O_2$), resulting in the production of singlet oxygen ($^1O_2$), a harmful ROS similar to $O_2^{\bullet-}$. High concentrations of ROS trigger a higher level of photoinhibition or inactivation of photosystems which is detrimental to plant survival under chilling (Allen and Ort 2001, Müller *et al.* 2001, Rutherford and Krieger-Liszkay 2001, Miyake 2010, 2020). However, among photosystems, PSII is more sensitive to chilling than PSI in a range of tropical tree species (Someralo and Krause 1990, Barth and Krause 1999, Huang *et al.* 2010a,b).

Photoinhibition of PSI occurs when PSII transfers electrons beyond the electron-accepting capacity of PSI. Compared with PSII, the PSI reaction centers require more time to recover from ROS-mediated oxidative damage (Zhang *et al.* 2004, Zivcak *et al.* 2015), which can be lethal due to the inefficiency of plants to cope with extensive loss/inhibition of PSI (Sonoike 1996, 2011; Guidi *et al.* 2019). Therefore, protection of PSI from oxidative damage by keeping P700 in an oxidized state (P700$^+$) is crucial to the survival of plants under chilling (Kubo *et al.* 2011, Sonoike 2011). Photoinhibition of PSII and subsequent reduction of electron flow to PSI in tropical trees under chilling protects PSI from chilling injury by supporting a sustainable P700$^+$ state (Huang *et al.* 2010a, Sonoike 2011, Miyake 2020). Hence, mode-rate photoinhibition of PSII throughout unfavorable conditions is considered a first-level photoprotection mechanism (Murchie and Niyogi 2011, Tikkanen *et al.* 2014). However, higher, and prolonged photoinhibition of PSII and PSI leads to the accumulation of ROS, which damages DNA, proteins, and lipids. Damage to the lipids of the thylakoid membrane increase membrane fluidity, resulting in the destruction of the photosynthetic apparatus and thus the impairment of photosynthesis and growth (Derks *et al.* 2015, Elsheery *et al.* 2020).

Irrespective of the photosystems, the change in the magnitude of photoinhibition from moderate to severe is a consequence of the intensity and duration of chilling, the high intensity of incident light during the stress period, lower CO_2 fixation, and linear electron flow (LEF) between PSII to PSI and the failed de-excitation of photosystem reaction centers (P700* and P680*) to an oxidized state (P700$^+$ and P680$^+$). In other words, the extent of photoinhibition is intensified by a combination of the longer duration of excitation status of P700 and P680, high content of ROS, inability to avoid oxidative damage by activation of various photoprotection mecha-nisms, nonenzymatic scavenging of ROS, and delayed recovery from chilling injuries (Asada 2006, Khatoon *et al.* 2009, Murata *et al.* 2007, 2012; Miyake 2010, 2020; Huang *et al.* 2011).

ROS are strong signaling molecules involved in plant growth and development as well as primary signals for stress responses; their excess production and high content can have a negative impact on plant development (Foyer and Shigeoka 2011, Zheng *et al.* 2019). Effective regulation of the excess energy in photosystems before the surplus production of ROS, and timely removal of ROS, relies on photoprotection mechanisms such as (*1*) cyclic electron flow (CEF) around PSI, (*2*) nonphotochemical quenching (NPQ) to dissipate excess absorbed light energy, (*3*) water–water cycle (WWC) or the Mehler–ascorbate peroxidase pathway (MAP) (Miyake 2010, Neto *et al.* 2017), and (*4*) photorespiration (Asada 2006). Hence, CEF, NPQ, and WWC under stress conditions are vital for stress tolerance and the subsequent recovery from stress. The activation of the above-mentioned photoprotective mechanisms under chilling is entirely dependent on the magnitude of the chilling tolerance of a plant, and the efficiency of such

mechanisms determines the chilling tolerance of a plant. Other important mechanisms, such as regulation of the stomatal opening and closing (stomatal behavior) (Raven 2014, Jurczyk *et al.* 2019) and reducing side heterogeneity of PSII, antenna size heterogeneity of PSII (Bukhov and Carpentier 2000, Belgio *et al.* 2014, Mathur *et al.* 2021), and anatomical and morphological alterations (Gratani *et al.* 2013, Wu *et al.* 2022), are equally crucial for chilling tolerance. The chilling tolerance of plant species can be genetic, which is permanent within the lifespan of a plant species, and phenotypic, which is reversible according to the existing microclimatic conditions, called evolutionary adaptation and acclimation or morphophysiological adjustments, respectively (Körner 2016).

A few studies have been conducted to understand the photoprotection mechanisms and sensitivity of photo-systems in tropical tree species found in the marginal tropics of China (Huang *et al.* 2010a,b; 2011, 2017; Zheng *et al.* 2016, Yang *et al.* 2017). However, such studies were conducted at the seedling stage with artificial chilling treatments for a short duration (hours), and their results demonstrate the activation of photoprotection mechanisms, *i.e.*, CEF and NPQ. Furthermore, these studies have also demonstrated reduced maximum photochemical efficiency of PSII (F_v/F_m), the effective photochemical quantum yield of PSII [$Y_{(II)}$] and PSI [$Y_{(I)}$], nonphotochemical quenching (NPQ), PSI acceptor-side limitation [$Y_{(NA)}$] and foliar gas exchange along with higher PSI donor-side limitation [$Y_{(ND)}$] and quantum yield of nonregulated energy dissipation [$Y_{(NO)}$] in response to chilling. At the same time, maximum photooxidizable P700 (P_m) was higher or stable in tropical trees under chilling. In this study, we sought to provide photosynthetic responses of geographically diverse tropical tree species to a realistic seasonal chilling event under the prevailing ambient microclimatic conditions in open fields of a lower subtropical site in China during winter, rather than using seedlings and artificial induction of chilling. Our primary target was to grade the tested tropical plant species in a lower subtropical site in China according to the magnitude of their chilling tolerance and compare and validate the physiological response of the current study with the earlier studies. The specific objectives of this study were to address the following questions: (*1*) How is the magnitude of chilling tolerance of tropical tree species in the lower subtropics related to the physiological mechanisms involved in photosynthesis?

And (*2*) how are light-dependent and CO_2 assimilation reactions coupled to each other in tested tropical trees under a chilling event during winter as compared with summer? We tested the hypothesis that, under chilling, maintaining the P700$^+$ state in PSI and related suppression of oxidative damage retains limited photosynthesis, and the tight coupling of light-dependent and CO_2 assimilation reactions support the chilling survival of tropical trees in the lower subtropics.

Materials and methods

Plant materials and growth conditions: The present study was conducted in January 2018 (winter; average day/night temperature: 13/11°C) and July 2018 (summer; average day/night temperature: 28/25°C) on the campus of Guangxi University, Nanning, China (22.83°N, 108.28°E). For this experiment, adult plants of six tropical tree species grown in an open field were selected based on geographical diversity (*see* text table below).

Physiological traits were recorded for fully mature leaves, which were exposed to sunlight during winter and summer. Before the physiological traits were recorded the experimental site received 11.7 mm of rainfall from 4 to 7 January 2018 and 78.9 mm from 1 to 15 July 2018 (Fig. 1S, *supplement*). Therefore, the soil was wet during the measurements in both seasons. A temperature drop to ≤ 10/≤ 6°C in day/night for four days during winter was considered a chilling event.

Photosynthetic rate, stomatal conductance, and carbo-xylation efficiency: In both seasons (winter and summer), photosynthetic rate (P_N), stomatal conductance (g_s), and internal CO_2 concentration (C_i) of six tree species were recorded using a portable photosynthesis system (*LI-6800*, *LICOR*, Lincoln, NE, USA). From each species, a minimum of nine measurements were recorded between 9:00 to 11:00 h from three individual plants. The leaf was illuminated by PAR of 1,000 µmol(photon) m^{-2} s^{-1} provided by a red-blue light-emitting diode (LED), whereas ambient CO_2, temperature, and relative humidity (RH) were used during the measurement of gas exchange. Carboxylation efficiency (CE) was calculated from the ratio of P_N to C_i (Rymbai *et al.* 2014).

Chlorophyll (Chl *a*) fluorescence and P700 measure-ments: Chl fluorescence and P700 measurements were

Botanical name	Family	Geographic distribution
Ixora chinensis Lam.	Rubiaceae	Southern China and southeastern Asia
Aglaia odorata Lour.	Meliaceae	Native to Taiwan and subtropical mountain regions of southern China
Lagerstroemia speciosa L.	Lythraceae	Tropical southern Asia
Dypsis lutescens (H. Wendl.)	Arecaceae	Madagascar, Andaman Islands, Reunion, El Salvador, Cuba, Puerto Rico, the Canary Islands, southern Florida, Haiti, the Dominican Republic, Jamaica, the Leeward Islands, and the Venezuelan Antilles
Markhamia stipulata (Wall.)	Bignoniaceae	South China to Southeast Asia
Woodfordia fruticosa L.	Lythraceae	Tanzania, Madagascar, Comores, Saudi Arabia, Oman, Myanmar (Burma), Bhutan, Indonesia, China, India, Sri Lanka, Nepal, Pakistan, and Vietnam

performed in both seasons using a *Dual PAM-100* (*Heinz Walz*, Effeltrich, Germany). The transients were recorded at 25°C from the leaves of six detached branches of three individual trees. Immediately after detaching branches from the trees, basal parts of branches were immersed in distilled water and transported to the laboratory. First, dark-adapted F_0 and F_m were determined in fully exposed mature leaves after 30 min of dark adaptation and by applying a saturation pulse of 10,000 μmol(photon) m^{-2} s^{-1} for 300 ms. Photochemical efficiency of PSII (F_v/F_m) was calculated as $F_v/F_m = (F_m - F_0)/F_m$; where F_0 is the minimum fluorescence and F_m the maximum in the dark-adapted state.

After determining F_0 and F_m, light-adapted Chl fluorescence transients and P700 measurements were measured. The mode of collection of branches, number of replications, and recording temperature was the same as for dark-adapted measurements. Before the light-adapted measurements, leaves were light-adapted for 30 min under PAR of 500 μmol(photon) m^{-2} s^{-1}; and then Chl fluorescence and P700 transients were recorded after 3 min exposure to light intensity of 10,000 μmol(photon) m^{-2} s^{-1} by placing the leaf between the measuring head of the *Dual PAM-100*. The light-adapted Chl fluorescence transients were calculated as $Y_{(II)} = (F_m' - F_s)/F_m'$, $Y_{(NO)} = F_s/F_m'$, and $Y_{(NPQ)} = 1 - Y_{(II)} - Y_{(NO)}$ (Genty *et al.* 1989, Oxborough and Baker 1997, Kramer *et al.* 2004); where $Y_{(II)}$ is the effective photochemical quantum yield of PSII, $Y_{(NO)}$ is the quantum yield of nonregulated energy dissipation, $Y_{(NPQ)}$ is the fraction of energy dissipated as heat through regulated nonphotochemical quenching (NPQ), F_m' is light-adapted state maximum fluorescence, and F_s is light-adapted state steady-state fluorescence (Kramer *et al.* 2004).

The maximum photooxidizable P700 in PSI (P_m) was determined by applying far-red light for 10 s, followed by a saturation pulse of 10,000 μmol(photon) m^{-2} s^{-1} for 300 ms after 30 min of dark adaptation. The P_m represents the maximum change of the P700 signal from fully reduced state P700 (minimum signal; P700) to the fully oxidized state P700 (maximum; P700$^+$) upon application of a saturation pulse. P_m allows the scaling of the P700 signal and is an essential prerequisite for the determination of P700 transients, similar to F_m of chlorophyll fluorescence transient. Other PSI transients were calculated from the light-adapted transients and predetermined P700$^+$ as follows: $Y_{(I)} = 1 - Y_{(ND)} - Y_{(NA)}$; where $Y_{(ND)} = 1 - P700(red)$ $[Y_{(ND)} = 1 - Y_{(I)}]$, $Y_{(NA)} = (P_m - P_m')/P_m$; $Y_{(I)}$ is the effective photochemical quantum yield of PSI, which is defined by the fraction of overall P700 reduced in a given state and not limited by the acceptor side $[Y_{(NA)}]$. Donor-side limitation $[Y_{(ND)}]$ is the fraction of overall P700 oxidized in a given state and $Y_{(NA)}$ (acceptor-side limitation) represents the fraction of P700 that cannot be oxidized by a saturation pulse in a given state due to a lack of acceptors; $Y_{(NA)}$ reflects the inability of far-red light to oxidize all P700. At the same time, maximum photooxidizable P700 in a given light state (P_m') upon application of the saturation pulse is similar to F_m' of Chl fluorescence at light-adapted state. P700(red),

which was determined in a given state with the help of the saturation pulse, represents the fraction of overall P700 reduced for a given state (Klughammer and Schreiber 1994, 2008).

Estimation of LEF and CEF: Linear electron flow from PSII to PSI (LEF [μmol(e^-) m^{-2} s^{-1}]; electron transport rate of PSII [ETR$_{(II)}$] [μmol(e^-) m^{-2} s^{-1}] and electron transport rate of PSI [ETR$_{(I)}$] [μmol(e^-) m^{-2} s^{-1}], respectively) in the six selected species were calculated using the following formula: ETR$_{(II)}$ = $Y_{(II)}$ × ab I × PAR × 0.5 and ETR$_{(I)}$ = $Y_{(I)}$ × ab I × PAR × 0.5; where, ab I (0.84) is the light absorptance ratio of a leaf and 0.5 is a theoretical factor based on the assumption that reaction centers of the chlorophylls in both photosystems absorb 50% of incident light (Maxwell and Johnson 2000). The value of CEF was estimated as: CEF = ETR$_{(I)}$ − ETR$_{(II)}$ [data not shown in the manuscript as $Y_{(CEF)}$ is representative of CEF], and $Y_{(CEF)}$ was estimated as: $Y_{(CEF)}$ = $Y_{(I)}$ − $Y_{(II)}$ (Miyake *et al.* 2005a,b).

The outputs from the *Dual PAM-100* may somewhat underestimate LEF; consequently, they overestimate CEF as the *Dual PAM-100* measures Chl *a* fluorescence from leaf mesophyll cells near the leaf surface while P700 comprises the signal from the whole leaf (Huang *et al.* 2011). Despite this inaccuracy, earlier researchers and we believe that relative changes in LEF and CEF in response to chilling are reliable to understand the relative seasonal changes (Miyake *et al.* 2005a,b; Huang *et al.* 2010a,b; 2011, 2015; Gao and Wang 2012).

Statistical analysis: Correlation analysis between actual ambient light-independent reaction values and potential light-dependent reaction values of both seasons was executed using *Sigma Plot* (*ver. 10, Systat Inc.*, USA). For statistical analysis of the data, three biological replications per species were used for each collected parameter and season. We used analysis of variance (*ANOVA*) to test for significant differences in all measured physiological parameters among species and between seasons. Generalized linear models (GLM) in *SPSS* (*ver. 10, SPSS Inc.*, USA) were used to assess the effects of species and season on the measured physiological parameters. For the statistical comparison between the two seasons for each species, a *Student*'s *t*-test was conducted.

Results

We observed significant differences in various physiological parameters and responses of the studied tree species between seasons (Table 1). F_v/F_m was significantly reduced under chilling in all species, except for *Woodfordia fruticosa*, which displayed no change in F_v/F_m and the smallest reduction in photosynthesis compared to the other species (Fig. 1). Among the six species, three species had F_v/F_m values of 0.6–0.7 during the chilling period; *Ixora chinensis* had an F_v/F_m value of 0.43, and *W. fruticosa* maintained an F_v/F_m value above 0.78 during both seasons. $Y_{(NPQ)}$ was reduced in all species studied and the smallest reduction was observed in *Aglaia odorata* and *W. fruticosa*

Table 1. Effect of chilling event on light-energy utilization in PSII, redox state of PSI, and cyclic electron flow (CEF) in comparison with those in summer. The values in parentheses indicate the percentage change in winter compared with summer. Statistical comparison between both seasons for individual species indicated by * and ** corresponding to significance at $P<0.05$ and $P<0.01$, respectively. NS indicates nonsignificant. $ETR_{(I)}$ – photosynthetic electron flow through PSI; $ETR_{(II)}$ – photosynthetic electron flow through PSII; LEF – linear electron flow; P_m – maximum photooxidizable P700; $Y_{(I)}$ – effective photochemical quantum yield of PSI; $Y_{(II)}$ – effective photochemical quantum yield of PSII; $Y_{(CEF)}$ – effective quantum yield of CEF; $Y_{(NA)}$ – acceptor-side limitation of PSI; $Y_{(ND)}$ – donor-side limitation of PSI; $Y_{(NO)}$ – yield of regulated heat dissipation of PSII; $Y_{(NPQ)}$ – effective quantum yield of NPQ or regulated nonphotochemical quenching.

	Ixora chinensis		Aglaia odorata		Lagerstroemia speciosa		Dypsis lutescens		Markhamia stipulata		Woodfordia fruticosa	
	Winter	Summer	Winter	Summer	Winter	Summer	Winter	Summer	Winter	Summer	Winter	Summer
$Y_{(II)}$	0.03 (−57%)*	0.07	0.04 (−33%)*	0.06	0.09 (−19%)*	0.11	0.05 (−29%)*	0.07	0.06 (−14%)*	0.07	0.22 (+57%)*	0.14
$Y_{(I)}$	0.07 (−50%)*	0.14	0.08 (−38%)*	0.13	0.16 (−6%)NS	0.17	0.08 (−38%)*	0.13	0.09 (−36%)*	0.14	0.35 (+67%)*	0.21
$Y_{(NPQ)}$	0.23 (−68%)*	0.71	0.32 (−55%)*	0.71	0.12 (−83%)**	0.69	0.17 (−75%)**	0.68	0.14 (−81%)**	0.73	0.28 (−57%)*	0.65
$Y_{(NO)}$	0.74 (+236%)**	0.22	0.64 (+178%)**	0.23	0.81 (+268%)**	0.22	0.78 (+212%)**	0.25	0.80 (+321%)**	0.19	0.50 (+138%)**	0.21
P_m	2.4 (+322%)**	0.6	1.8 (+239%)**	0.5	2.7 (+435%)**	0.5	1.3 (+306%)**	0.3	2.0 (+115%)**	0.9	2.5 (+462%)**	0.4
$Y_{(CEF)}$	0.04 (−33%)*	0.06	0.04 (−43%)*	0.07	0.08 (+1%)NS	0.08	0.05 (−7%)*	0.06	0.03 (−57%)*	0.07	0.13 (+86%)*	0.07
$Y_{(ND)}$	0.85 (+21%)*	0.70	0.85 (+35%)*	0.63	0.71 (+13%)*	0.63	0.84 (+14%)*	0.74	0.85 (+29%)*	0.66	0.55 (+15%)*	0.48
$Y_{(NA)}$	0.08 (−53%)*	0.17	0.07 (−71%)**	0.24	0.14 (−26%)*	0.19	0.09 (−31%)*	0.13	0.06 (−70%)**	0.20	0.11 (−65%)*	0.31
LEF [μmol(e⁻) m⁻² s⁻¹]	37.9 (−53%)*	80.4	47.5 (−36%)*	74.1	106.0 (+2%)NS	104.0	50.3 (−35%)**	77.8	59.0 (−29%)*	83.0	127.0 (−7%)*	136.0
$ETR_{(I)}$ [μmol(e⁻) m⁻² s⁻¹]	26.0 (−50%)*	52.5	31.8 (−36%)*	49.9	65.4 (−3%)NS	67.6	34.1 (−33%)*	51.0	35.5 (−35%)*	54.7	77.5 (−5%)*	81.8
$ETR_{(II)}$ [μmol(e⁻) m⁻² s⁻¹]	11.9 (−57%)*	27.9	15.7 (−35%)*	24.1	40.1 (+12%)*	35.9	16.2 (−40%)*	26.8	23.5 (−17%)*	28.3	49.7 (−10%)*	54.1
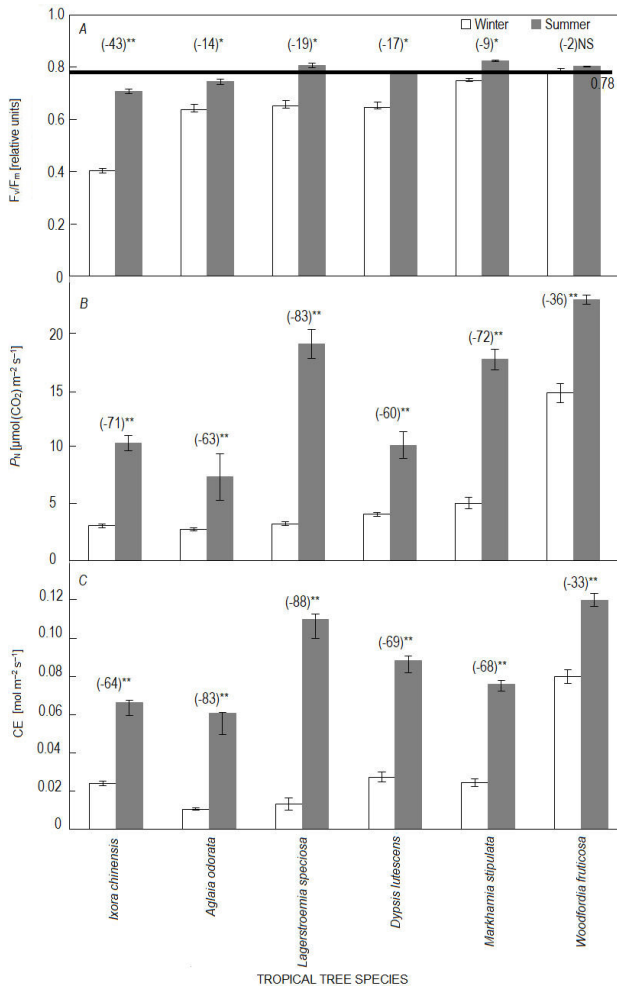
Fig. 1. Differences in (*A*) maximum photochemical efficiency of PSII (F_v/F_m), (*B*) net photosynthetic rate (P_N), and (*C*) carboxylation efficiency (CE) during the chilling event ($\leq 10°C$; *white bars*) and summer ($\geq 27°C$; *gray bars*) among six tropical tree species. *The white and gray bars* indicate the means and standard errors. The values in the parentheses indicate a relative change in the winter values compared with the summer. *The black line* across Fig. 1*A* indicates F_v/F_m value of 0.78. Statistical comparison between both seasons for individual species indicated by NS, *, and ** corresponding to non-significance, significance at $P<0.05$ and $P<0.01$, respectively.

(Table 1). In contrast, P_m was 15 to 462% higher across species under chilling compared to measurements made in summer (Table 1). CEF under chilling was the highest in *W. fruticosa* followed by *Lagerstroemia speciosa*, and lower in *Markhamia stipulata*, *A. odorata*, and *I. chinensis*.

Effect of chilling event on gas exchange and their relationship with F_v/F_m: Besides the significant reduction of F_v/F_m in five of the species (Fig. 1), P_N, g_s, and CE were significantly reduced in all species under chilling, and positively correlated with F_v/F_m across species during
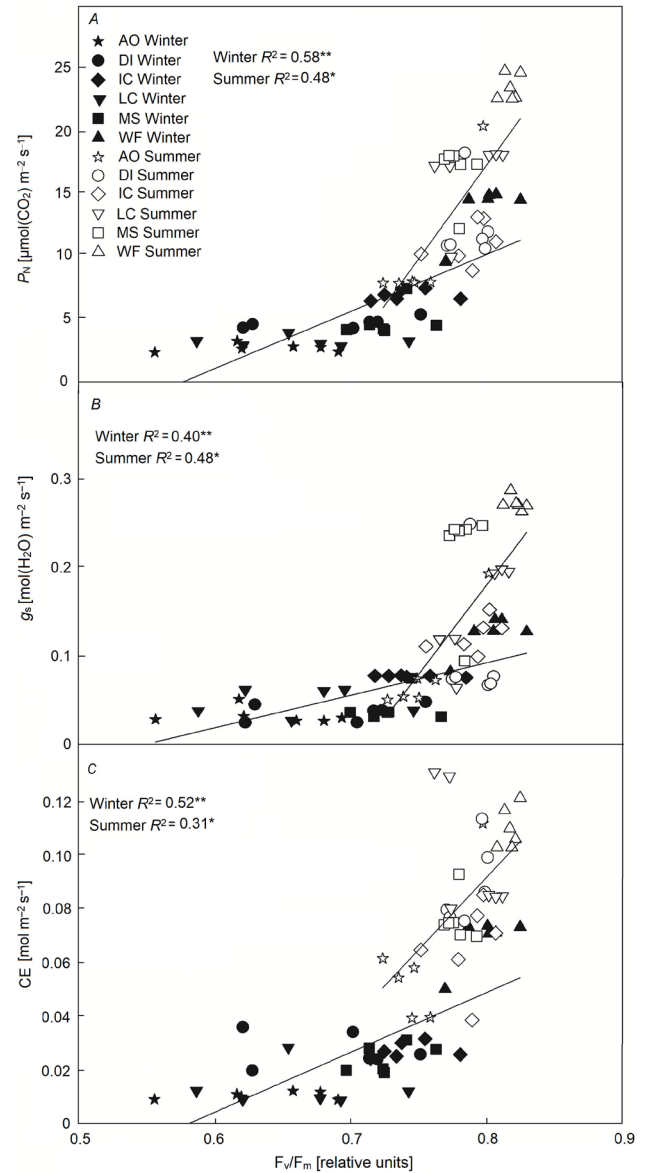
Fig. 2. Correlation of maximum quantum yield of PSII in the dark-adapted state (F_v/F_m) with (*A*) net photosynthetic rate (P_N), (*B*) stomatal conductance (g_s), and (*C*) carboxylation efficiency (CE) during the chilling event ($\leq 10°C$; *closed symbols*) and summer ($\geq 27°C$; *open symbols*) among six tropical tree species. Coefficient of determination (R^2) followed by * and ** corresponding to significance at $P<0.05$ and $P<0.01$, respectively. AO – *Aglaia odorata*; DI – *Dypsis lutescens*; IC – *Ixora chinensis*; LS – *Lagerstroemia speciosa*; MS – *Markhamia stipulata*; WF – *Woodfordia fruticosa*.

each season, respectively (Fig. 2). *Lagerstroemia speciosa* showed the greatest reduction in P_N and CE, while *W. fruticosa* showed higher P_N and CE than any other species in both seasons, with the lowest reduction under chilling; and the lowest P_N and CE was in *A. odorata* (Fig. 1).

Effect of chilling event on light-energy utilization by PSII, redox state of PSI, and CEF: We observed lower values of $Y_{(II)}$ and $Y_{(I)}$ under chilling across species, except for *W. fruticosa*, which had higher values than any of the other species for the above parameters (Table 1; Fig. 2S, *supplement*). Concomitantly, $Y_{(NPQ)}$ was reduced across all species, whereas $Y_{(NO)}$ increased. The difference in $Y_{(NO)}$ and CEF among species was minimal during summer compared with the difference under chilling. A faster rate of photosynthetic electron flow through PSII and PSI [LEF; $ETR_{(II)}$ and $ETR_{(I)}$] was recorded in *W. fruticosa* during both seasons among all species studied. In contrast, LEF was low in *I. chinensis* under chilling. Furthermore, we measured a higher CEF during summer compared to chilling in all species except for *W. fruticosa* and *L. speciosa*. Finally, $Y_{(ND)}$ and P_m increased, whereas $Y_{(NA)}$ decreased in all species under chilling. In contrast, $Y_{(ND)}$ and P_m were lower in *W. fruticosa* (Table 1).

Relationship of light energy utilization in PSII with the redox state of PSI and CEF: We detected negative correlations between $Y_{(ND)}$ and $Y_{(II)}$ and $Y_{(ND)}$ and LEF across species in each season; however, the correlation was stronger during winter. Furthermore, the negative correlation between $Y_{(ND)}$ and CEF across species was only observed during winter (Fig. 3). In contrast, there were no correlations between $Y_{(NA)}$ and the above parameters in either season, whereas CEF showed significant positive correlations with LEF and $Y_{(II)}$ only during winter (Fig. 4). We observed negative correlations between $Y_{(NO)}$ and $Y_{(NPQ)}$ (Fig. 5*A*), and between $Y_{(NA)}$ and $Y_{(ND)}$ (Fig. 5*C*) across species in each season, whereas $Y_{(I)}$ and $Y_{(II)}$ were significantly and positively correlated across species in each season (Fig. 5*B*).

Discussion

Chilling affects many components related to photosynthesis (Allen *et al.* 2000, Allen and Ort 2001), including nonstomatal regulation, *i.e.*, electron transport between photosystems in thylakoid membrane and activities of CO_2 assimilation reactions of photosynthesis, photorespiration, and stomatal functioning. Both CO_2 fixation and PSII and PSI reactions of photosynthesis are inhibited by chilling. Seasonal chilling during winter induced photoinhibition of PSII in five of the six tropical tree species (not in *W. fruticosa*), which was evident from the significant reduction in F_v/F_m and $Y_{(II)}$ (Fig. 1, Table 1). However, the reduction of F_v/F_m during chilling was less than 20% for all species, except for *I. chinensis*, which showed a 43% reduction (Fig. 1). This suggests that photoinhibition was moderate (Huang *et al.* 2010a,b; 2016a,b). On the other hand, maximum oxidizable P700 in PSI as indicated by P_m was significantly higher across all species under chilling compared to summer. $Y_{(I)}$ was reduced in five of the six species (not in *W. fruticosa*). Regardless of species, the magnitude of changes in F_v/F_m, $Y_{(II)}$, $Y_{(I)}$, and P_m in adult trees corresponded to the response of seedlings of tropical tree species under artificially induced short-duration

chilling (Elsheery *et al.* 2007, 2008; Huang *et al.* 2010a,b; 2016a,b). The higher F_v/F_m, $Y_{(II)}$, and $Y_{(I)}$ values and lower inhibition of CO_2 assimilation reaction parameters, particularly P_N and CE, of *W. fruticosa* suggest that it is the most chilling-tolerant of the tested species (Fig. 1, Table 1). Hence, responses of the light-dependent and CO_2 assimilation reactions of photosynthesis in *W. fruticosa* during chilling enabled *W. fruticosa* to cope with chilling, as discussed by comparing it with the moderate and sensitive species included in this study.

Positive correlations of F_v/F_m with P_N, g_s, and CE in both seasons (Fig. 2) revealed the strong coupling between the light-dependent and CO_2 assimilation reactions of photosynthesis. At the same time, relationships between these parameters were stronger during winter than summer. In contrast, there was no significant correlation between P_m and the above-mentioned CO_2 assimilation reaction parameters (data not shown). Furthermore, all the above positive correlations (Fig. 2) also suggest that the initial target of chilling was CO_2 assimilation reactions of photosynthesis (evident from lower P_N, g_s, and CE; Figs. 1, 2) across all species and subsequently caused moderate photoinhibition of PSII and lower electron flow (evident from lower F_v/F_m and LEF; Fig. 1). This was evident from the increased C_i and reduced g_s and the positive correlation of g_s with F_v/F_m (Fig. 2). An increase in C_i occurred at the time of slower CO_2 fixation associated with the inactivation of CO_2 assimilation reactions (as discussed above) or nonstomatal limitation. Further, higher C_i was associated with a partial closure of the stomata which suggests the simultaneous engagement of both stomatal and nonstomatal effects on P_N under chilling (Allen and Ort 2001, Raven 2014, Huang *et al.* 2016a,b; Jurczyk *et al.* 2019). Partial closure of the stomata under chilling was evident from lower g_s resulting from higher C_i.

Lower P_N and reduction of LEF between photosystems led to the moderate photoinhibition of PSII across the species and *W. fruticosa* showed the smallest reduction in LEF in winter compared to summer (Table 1). The lower rate of LEF was due to the inhibition of electron transfer from plastoquinone (PQ) to plastocyanin (PC), resulting in the increased reduction of the PQ pool. The reduced PQ pool was caused by the lower CO_2 fixation known as photosynthesis control (West and Wiskich 1968, Baker *et al.* 2007, Miyake 2020). Over-reduction of the PQ pool, which induces an inhibition of the Q-cycle in the cytochrome (Cyt) b_6/f complex and P700 oxidation is known as reduction-induced suppression of electron flow (RISE), which is also a part of photosynthesis control in cyanobacteria (Shaku *et al.* 2016, Miyake 2020). Photosynthesis control and RISE are important mechanisms to prevent deleterious photoinhibition of PSI by reducing the electron flow from PSII to PSI along with activation of alternative electron flows (CEF and WWC). Electron flow from PSII to PSI is a prerequisite for the photoinhibition of PSI and consequent secondary damages (Sonoike 2011, Miyake 2020). Because of photosynthesis control and RISE, the higher oxidation state of PSI (P700$^+$) as indicated by higher
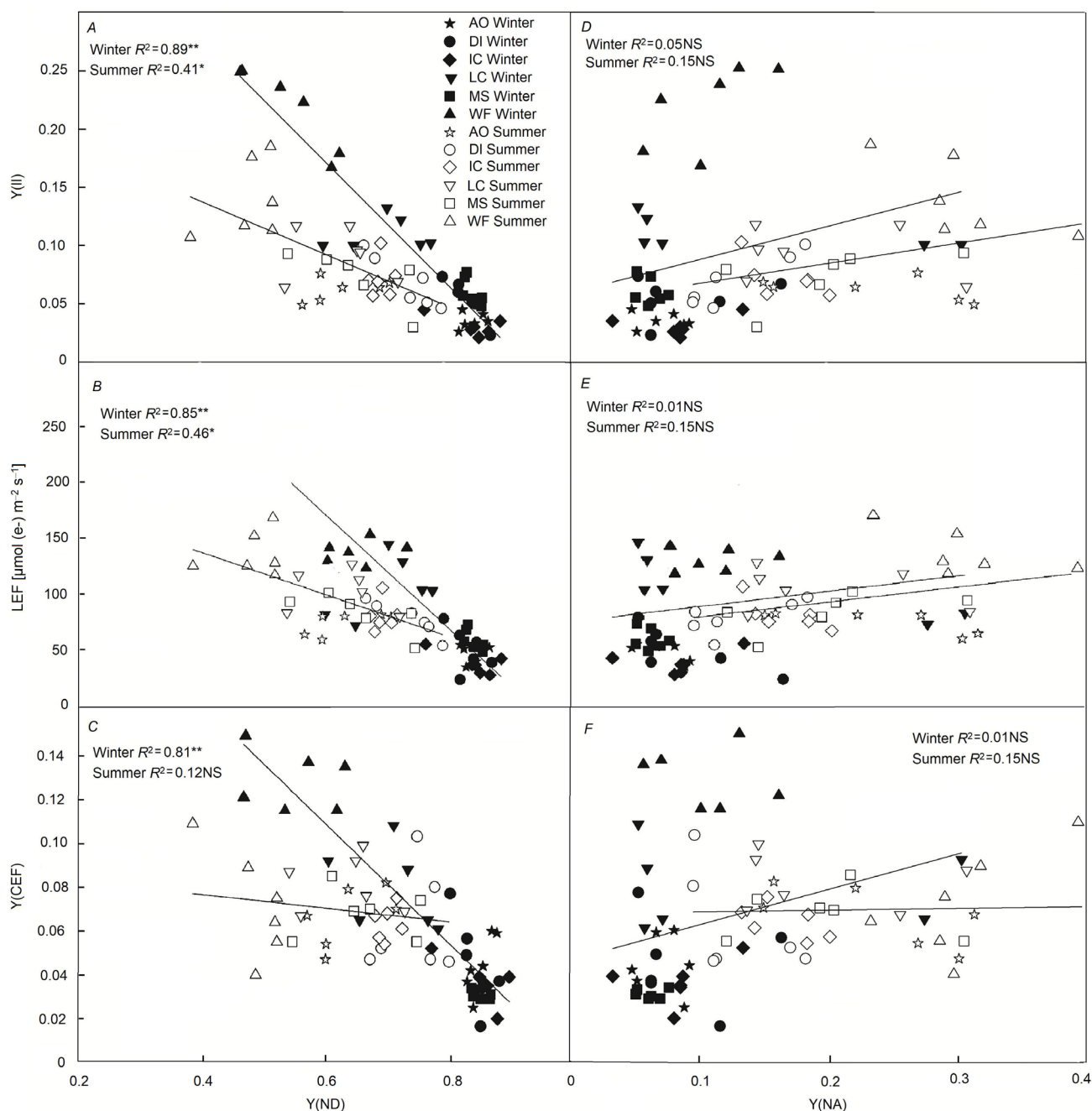
Fig. 3. Correlation of donor-side limitation of PSI [$Y_{(ND)}$] and acceptor-side limitation of PSI [$Y_{(NA)}$] with (*A,D*) effective photochemical quantum yield of PSII [$Y_{(II)}$], (*B,E*) linear electron flow (LEF), and (*C,F*) effective quantum yield of CEF [$Y_{(CEF)}$] during the chilling event (≤ 10°C; *closed symbols*) and summer (≥ 27°C; *open symbols*) among six tropical tree species. Coefficient of determination (R^2) followed by NS, *, and ** corresponding to non-significance, significance at $P<0.05$ and $P<0.01$, respectively. AO – *Aglaia odorata*; DI – *Dypsis lutescens*; IC – *Ixora chinensis*; LS – *Lagerstroemia speciosa*; MS – *Markhamia stipulata*; WF – *Woodfordia fruticosa*.

P_m is maintained by potential balancing of absorption and utilization of energy, and inhibition of ROS production (Miyake 2010, 2020; Sonoike 2011, Takagi *et al.* 2017, Kadota *et al.* 2019).

In this study, we assumed the existence of RISE and confirmed the photosynthesis control in all tested species with higher $Y_{(ND)}$ (Table 1), from its strong negative correlation with $Y_{(II)}$, LEF, and $Y_{(CEF)}$ under winter compared with summer (Figs. 3, 4*A*). $Y_{(ND)}$ is the electron-donor side (plastoquinone; PQ) limitation of PSI. A negative correlation of $Y_{(ND)}$ with LEF and $Y_{(II)}$ under chilling implies that the $Y_{(ND)}$ has mediated reduced electron flow between photosystems and lower efficiency of PSII to utilize light energy for photosynthesis,
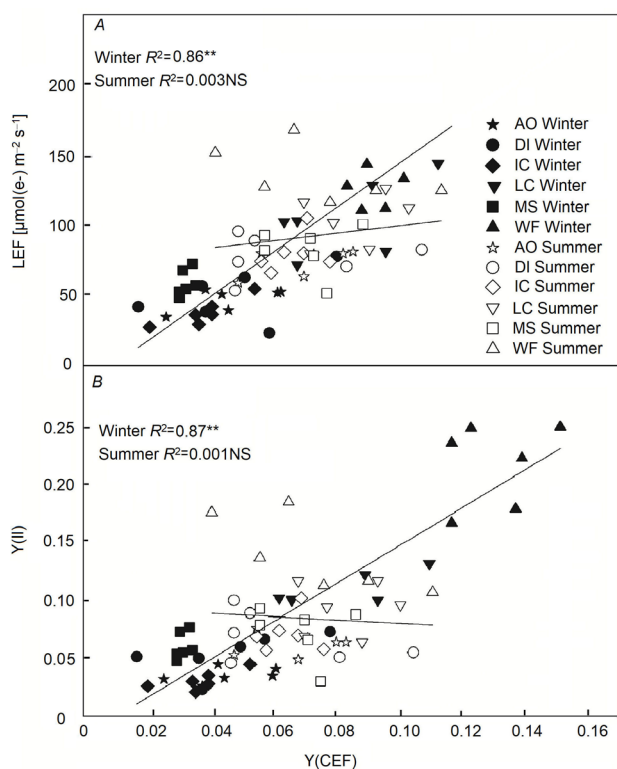
Fig. 4. Correlation of effective quantum yield of CEF [$Y_{(CEF)}$] with (*A*) linear electron flow (LEF) and (*B*) effective photochemical quantum yield of PSII [$Y_{(II)}$] during the chilling event ($\leq 10°C$; *closed symbols*) and summer ($\geq 27°C$; *open symbols*) among six tropical tree species. Coefficient of determination (R^2) followed by NS, *, and ** corresponding to non-significance, significance at $P<0.05$ and $P<0.01$, respectively. AO – *Aglaia odorata*; DI – *Dypsis lutescens*; IC – *Ixora chinensis*; LS – *Lagerstroemia speciosa*; MS – *Markhamia stipulata*; WF – *Woodfordia fruticosa*.

respectively. At the same time, a minor increase in $Y_{(ND)}$ was observed in the chilling-tolerant species *W. fruticosa* (Table 1). Similar trends were observed in seedlings of tropical trees exposed to chilling temperatures (Huang *et al.* 2010a,b; 2011).

A decrease in the ratio of oxidized PQ to total PQ [higher reduction of PQ (photosynthesis control and RISE) or higher $Y_{(ND)}$] supports important alternative electron flow, *i.e.*, CEF (Miyake *et al.* 2005a,b; Kubo *et al.* 2011). The correlation between $Y_{(ND)}$ and $Y_{(CEF)}$ was negative in the current study (Fig. 3C), which confirms the involvement of photosynthesis control and RISE in the activation or enhancement of CEF (in *W. fruticosa*), and maintenance of minimum CEF across all other species. Despite the varying degree of CEF during winter across the tree species, CEF allowed PSII to manage the electron load (Joliot and Johnson 2011) to a certain extent as evidenced by the positive correlation of $Y_{(CEF)}$ with $Y_{(II)}$ and LEF (Fig. 4).

Higher $Y_{(NA)}$ values imply that a portion of reduced electron carriers on the acceptor side of PSI could not be oxidized due to the limitation of CO_2 assimilation
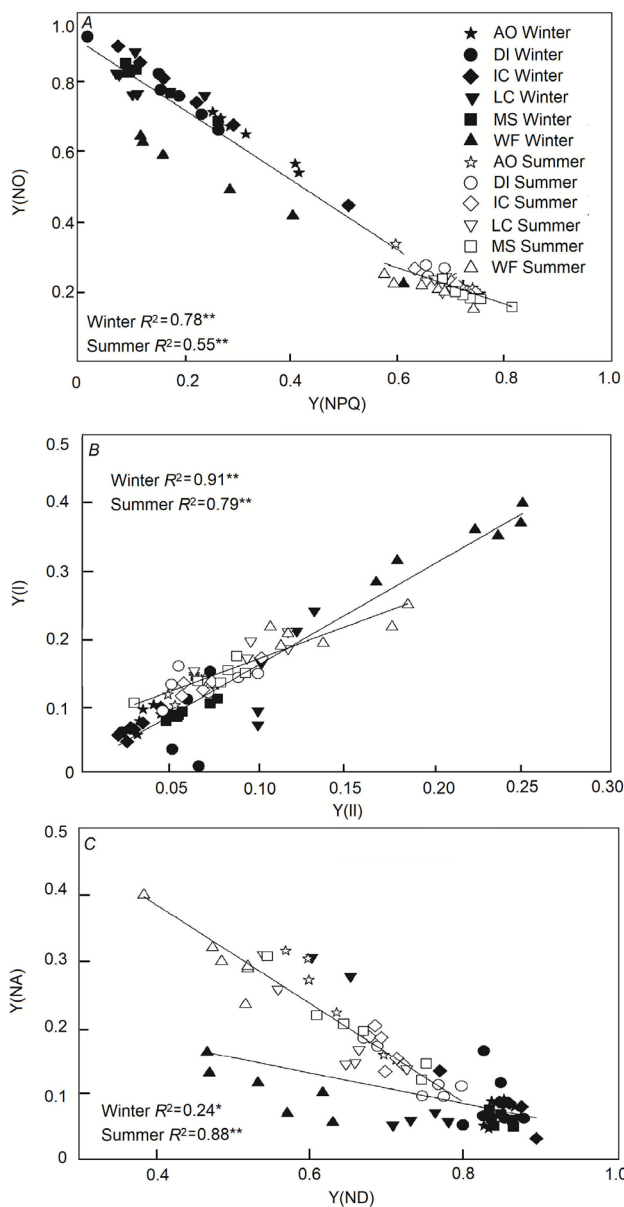
Fig. 5. Correlation between (*A*) effective quantum yield of nonphotochemical quenching [$Y_{(NPQ)}$] and yield of regulated heat dissipation of PSII [$Y_{(NO)}$], (*B*) effective photochemical quantum yield of PSII [$Y_{(II)}$] and effective photochemical quantum yield of PSI [$Y_{(I)}$], and (*C*) donor-side limitation of PSI [$Y_{(ND)}$] and acceptor-side limitation of PSI [$Y_{(NA)}$] during a chilling event ($\leq 10°C$; *closed symbols*) and summer ($\geq 27°C$; *open symbols*) among six tropical tree species. Coefficient of determination (R^2) followed by NS, *, and ** corresponding to non-significance, significance at $P<0.05$ and $P<0.01$, respectively. AO – *Aglaia odorata*; DI – *Dypsis lutescens*; IC – *Ixora chinensis*; LS – *Lagerstroemia speciosa*; MS – *Markhamia stipulata*; WF – *Woodfordia fruticosa*.

reactions, particularly caused by lower P_N and higher C_i (Shimakawa and Miyake 2018, Miyake 2020). While in this study, similar to the response of seedlings of tropical tree species observed in earlier studies by Huang *et al.*

(2010a,b; 2011), $Y_{(NA)}$ was lower during winter than in summer (Table 1). This contradiction in $Y_{(NA)}$ under chilling across species with lower P_N and higher C_i can be attributed to lower F_v/F_m, higher $Y_{(ND)}$, and CEF, which supported the oxidative status of P700 in PSI (P700$^+$). In contrast to $Y_{(ND)}$, there was no correlation between $Y_{(NA)}$ and any of the other measured physiological parameters in both seasons, except P_m (Fig. 3).

A weak negative correlation between $Y_{(ND)}$ and LEF, $Y_{(CEF)}$ and $Y_{(II)}$ during summer, compared to winter, was due to the favorable weather conditions, which enabled faster photosynthesis, thus leading to unclogged electron flow between photosystems (Figs. 1B, 3; Table 1). On the other hand, lower $Y_{(ND)}$ and P_m and higher $Y_{(NA)}$ and CEF in four of the six species during summer (Table 1) can be attributed to the high ambient light intensity as PSI is susceptible to high light intensity in summer or due to the acclimation and higher PSII to PSI ratio (Fig. 1S) (Barth and Krause 1999, Miyake et al. 2004, 2005a,b; Kubo et al. 2011, Kono and Terashima 2016).

CEF may be negligible in favorable growth conditions (Kou et al. 2013, Kadota et al. 2019), under chilling greater significance of CEF was evident from the response of tolerant W. fruticosa compared with the other four moderately tolerant species, whereas no significant change in CEF was observed in the L. speciosa (Table 1). This is consistent with the previous finding of activation of CEF with increased photoinhibition and limited photosynthesis (Miyake et al. 2004, 2005a,b; Takahashi et al. 2009, Agrawal et al. 2016, Neto et al. 2017). There are several main functions of CEF involved in the mitigation of the impact of stress, thereby preventing severe damage to PSII and ultimately PSI: (1) to synthesize ATP to support LEF and to maintain the balance of ATP and NADPH consumption; (2) to generate a higher proton gradient (ΔpH) along with LEF for the activation of NPQ to protect PSII thereby maintaining electron flow; (3) to protect the oxygen-evolving complex (OEC) inside the thylakoid lumen, which is the primary site for photodamage in PSII and de novo synthesis of D1 protein; (4) to maintain the balance of $Y_{(ND)}$ and $Y_{(NA)}$ to protect PSI from photoinhibition; and (5) to limit ROS production at PSII and PSI (Müller et al. 2001, Mohanty et al. 2007, Miyake 2010, 2020; Allakhverdiev 2011, Joliot and Johnson 2011, Sonoike 2011, Kono and Terashima 2016, Huang et al. 2018, Kadota et al. 2019).

The reduced $Y_{(NPQ)}$ and its significant negative correlation with $Y_{(NO)}$ across species under chilling indicates a lower level of stimulation of NPQ during photoinhibition of PSII, and thereby an intensified inhibition of the chain of reactions of photosynthesis (Table 1, Fig. 5A), which was similar to the trend in seedlings of tropical trees exposed to chilling temperatures (Huang et al. 2010a,b; 2011). The higher $Y_{(NO)}$ indicates that both photochemical energy conversion and protective regulatory mechanisms were not effective in preventing the photoinhibition of PSII. Low values of $Y_{(NPQ)}$ under chilling across the six species indicate lower regulated photoprotective activity through the xanthophyll cycle. Such a state of NPQ can take place when the ΔpH between thylakoid lumen and stroma is inadequate due to reduced LEF and inactive or insufficient CEF for the conformational change of PsbS protein structure, which acts as a ΔpH sensor to activate NPQ (Joliot and Joliot 2006, Miyake 2010, Yamori and Shikanai 2016, Zheng et al. 2019). However, low $Y_{(NO)}$ and high $Y_{(NPQ)}$ values in W. fruticosa compared with the other species (except A. odorata which showed higher $Y_{(NPQ)}$ than W. fruticosa) further confirms the importance of CEF for chilling tolerance. Conversely, L. speciosa showed higher CEF next to W. fruticosa, but lower $Y_{(NPQ)}$, F_v/F_m, P_N, CE, and $Y_{(II)}$ and higher $Y_{(NO)}$ and $Y_{(I)}$ under chilling across all species (Table 1). Interestingly, stimulation of CEF should trigger an NPQ-mediated ΔpH with assistance from PsbS protein, which was not observed in L. speciosa. This can be due to the inadequacy of the ΔpH created by the stimulation of CEF in L. speciosa to increase NPQ. Alternatively, it may be due to the conformational changes in PsbS protein structure that led to a lower degree of NPQ, thereby resulting in higher photoinhibition of PSII. Meanwhile, A. odorata showed an opposite trend to L. speciosa (Table 1). This species showed lower CEF, but higher $Y_{(NPQ)}$ than W. fruticosa, with lower F_v/F_m, P_N, CE, $Y_{(II)}$, and $Y_{(I)}$ and higher $Y_{(NO)}$. This might be explained by the higher level of structural damage in PSII in A. odorata which impaired efficient management of excess energy even after a higher activation of NPQ. Further studies are required to clarify these controversial results and to understand the mechanisms underlying photodamage.

In summary, a seasonal chilling event induced moderate photoinhibition of PSII in the majority of the tested tropical tree species. Stomatal and nonstomatal regulations on photosynthesis under chilling resulted in reduced fixation and light-dependent reactions, such as a slower rate of LEF by increasing photosynthesis control and thereby higher oxidation state of PSI that prevented photoinhibition of PSI. Woodfordia fruticosa was the least affected by chilling as demonstrated by a lower reduction of photosynthetic rate and photochemical efficiency of PSII and higher CEF and oxidation state of P700 in PSI compared with the other species. Correlation analysis suggested that the light-dependent and CO_2 assimilation reactions of photosynthesis were closely coupled across all tree species in each season, with stronger coupling in winter. The tropical tree species demonstrated a range of strategies to regulate photosynthesis by rearranging the degree of photoprotection mechanisms according to seasonal meteorological conditions. The present results have implications for screening tropical plant species to improve planning for the management of urban landscapes based on future climatic predictions.

References

Agrawal D., Allakhverdiev S.I., Jajoo A.: Cyclic electron flow plays an important role in protection of spinach leaves under high temperature stress. – Russ. J. Plant Physiol. **63**: 210-215, 2016.

Allakhverdiev S.I.: Recent progress in the studies of structure and function of photosystem II. – J. Photoch. Photobio. B **104**: 1-8, 2011.

Allen D.J., Ort D.R.: Impacts of chilling temperatures on photosynthesis in warm-climate plants. – Trends Plant Sci. **6**: 36-42, 2001.

Allen D.J., Ratner K., Giller Y.E. *et al.*: An overnight chill induces a delayed inhibition of photosynthesis at midday in mango (*Mangifera indica* L.). – J. Exp. Bot. **51**: 1893-902, 2000.

Asada K.: Production and scavenging of reactive oxygen species in chloroplasts and their functions. – Plant Physiol. **141**: 391-396, 2006.

Baker N.R., Harbinson J., Kramer D.M.: Determining the limitations and regulation of photosynthetic energy transduction in leaves. – Plant Cell Environ. **30**: 1107-1125, 2007.

Barth C., Krause G.H.: Inhibition of photosystems I and II in chilling-sensitive and chilling-tolerant plants under light and low-temperature stress. – Z. Naturforsch. **54c**: 645-657, 1999.

Belgio E., Kapitonova E., Chmeliov J. *et al.*: Economic photoprotection in photosystem II that retains a complete light-harvesting system with slow energy traps. – Nat. Commun. **5**: 4433, 2014.

Bukhov N.G., Carpentier R.: Heterogeneity of photosystem II reaction centers as influenced by heat treatment of barley leaves. – Physiol. Plantarum **110**: 279-285, 2000.

Derks A., Schaven K., Bruce D.: Diverse mechanisms for photoprotection in photosynthesis. Dynamic regulation of photosystem II excitation in response to rapid environmental change. – BBA-Bioenergetics **1847**: 468-485, 2015.

Elsheery N.I., Sunoj V.S.J., Wen Y. *et al.*: Foliar application of nanoparticles mitigates the chilling effect on photosynthesis and photoprotection in sugarcane. – Plant Physiol. Bioch. **149**: 50-60, 2020.

Elsheery N.I., Wilske B., Cao K.F.: The effect of night chilling on gas exchange and chlorophyll fluorescence of two mango cultivars growing under two irradiances. – Acta Bot. Yunnan. **30**: 447-456, 2008.

Elsheery N.I., Wilske B., Zhang J.L., Cao K.F.: Seasonal variations in gas exchange and chlorophyll fluorescence in the leaves of five mango cultivars in southern Yunnan, China. – J. Hortic. Sci. Biotech. **82**: 855-862, 2007.

Foyer C.H., Shigeoka S.: Understanding oxidative stress and antioxidant functions to enhance photosynthesis. – Plant Physiol. **155**: 93-100, 2011.

Gao S., Wang G.: The enhancement of cyclic electron flow around photosystem I improves the recovery of severely desiccated *Porphyra yezoensis* (Bangiales, Rhodophyta). – J. Exp. Bot. **12**: 4349-4358, 2012.

Genty B., Briantais J.M., Baker N.R.: The relationship between the quantum yield of photosynthetic electron transport and quenching of chlorophyll fluorescence. – BBA-Gen. Subjects **990**: 87-92, 1989.

Gratani L., Catoni R., Varone L.: Morphological, anatomical and physiological leaf traits of *Q. ilex*, *P. latifolia*, *P. lentiscus*, and *M. communis* and their response to Mediterranean climate stress factors. – Bot. Stud. **54**: 35, 2013.

Guidi L., Lo Piccolo E., Landi M.: Chlorophyll fluorescence, photoinhibition and abiotic stress: Does it make any difference the fact to be a C_3 or C_4 species? – Front. Plant Sci. **10**: 174, 2019.

Huang W., Hu H., Zhang S.: Photosynthesis and photosynthetic electron flow in the alpine evergreen species *Quercus guyavifolia* in winter. – Front. Plant Sci. **7**: 1511, 2016b.

Huang W., Quan X., Zhang S.B., Liu T.: *In vivo* regulation of proton motive force during photosynthetic induction. – Environ. Exp. Bot. **148**: 109-116, 2018.

Huang W., Yang Y.J., Hu H. *et al.*: Sustained diurnal stimulation of cyclic electron flow in two tropical tree species *Erythrophleum guineense* and *Khaya ivorensis*. – Front. Plant Sci. **7**: 1068, 2016a.

Huang W., Zhang S.B., Cao K.F.: Stimulation of cyclic electron flow during recovery after chilling-induced photoinhibition of PSII. – Plant Cell Physiol. **51**: 1922-1928, 2010a.

Huang W., Zhang S.B., Cao K.F.: The different effects of chilling stress under moderate light intensity on photosystem II compared with photosystem I and subsequent recovery in tropical tree species. – Photosynth. Res. **103**: 175-182, 2010b.

Huang W., Zhang S.B., Cao K.F.: Cyclic electron flow plays an important role in photoprotection of tropical trees illuminated at temporal chilling temperature. – Plant Cell Physiol. **52**: 297-305, 2011.

Huang W., Zhang S.B., Xu J.C., Liu T.: Plasticity in roles of cyclic electron flow around photosystem I at contrasting temperatures in the chilling-sensitive plant *Calotropis gigantea*. – Environ. Exp. Bot. **141**: 145-153, 2017.

Huang W., Zhang S.B., Zhang J.L., Hu H.: Photoinhibition of photosystem I under high light in the shade-established tropical tree species *Psychotria rubra*. – Front. Plant Sci. **6**: 801, 2015.

Jalili A., Jamzad Z., Thompson K. *et al.*: Climate change, unpredictable cold waves and possible brakes on plant migration. – Global Ecol. Biogeogr. **19**: 642-648, 2010.

Joliot P., Johnson G.N.: Regulation of cyclic and linear electron flow in higher plants. – P. Natl. Acad. Sci. USA **108**: 13317-13322, 2011.

Joliot P., Joliot A.: Cyclic electron flow in C_3 plants. – BBA-Bioenergetics **1757**: 362-368, 2006.

Jurczyk B., Grzesiak M., Pociecha E. *et al.*: Diverse stomatal behaviors mediating photosynthetic acclimation to low temperatures in *Hordeum vulgare*. – Front. Plant Sci. **9**: 1963, 2019.

Kadota K., Furutani R., Makino A. *et al.*: Oxidation of P700 induces alternative electron flow in photosystem I in wheat leaves. – Plants-Basel **8**: 152, 2019.

Khatoon M., Inagawa K., Pospíšil P. *et al.*: Quality control of photosystem II: Thylakoid unstacking is necessary to avoid further damage to the D1 protein and to facilitate D1 degradation under light stress in spinach thylakoids. – J. Biol. Chem. **284**: 25343-25352, 2009.

Klughammer C., Schreiber U.: An improved method, using saturating light pulses, for the determination of photosystem-I quantum yield via P700$^+$ absorbance changes at 830 nm. – Planta **192**: 261-268, 1994.

Klughammer C., Schreiber U.: Complementary PSII quantum yields calculated from simple fluorescence parameters measured by PAM fluorometry and the Saturation Pulse method. – PAM Appl. Notes **1**: 27-35, 2008.

Kono M., Terashima I.: Elucidation of photoprotective mechanisms of PSI against fluctuating light photoinhibition. – Plant Cell Physiol. **57**: 1405-1414, 2016.

Körner C.: Plant adaptation to cold climates. – F1000Research **5**: 2769, 2016.

Kou J., Takahashi S., Oguchi R. *et al.*: Estimation of the steady-state cyclic electron flux around PSI in spinach leaf discs in white light, CO_2-enriched air and other varied conditions. – Funct. Plant Biol. **4**: 1018-1028, 2013.

Kramer D.M., Johnson G., Kiirats O., Edwards G.E.: New fluorescence parameters for the determination of Q_A redox state and excitation energy fluxes. – Photosynth. Res. **79**: 209-218, 2004.

Kubo S., Masumura T., Saito Y. *et al.*: Cyclic electron flow

around PSI functions in the photoinhibited rice leaves. – Soil Sci. Plant Nutr. **57**: 105-113, 2011.

Li Y., Liu J., Zhou G. *et al.*: Warming effects on photosynthesis of subtropical tree species: a translocation experiment along an altitudinal gradient. – Sci. Rep.-UK **6**: 24895, 2016.

Li Y., Sunoj V.S.J., Short A.W. *et al.*: Correlations between allocation to foliar phosphorus fractions and maintenance of photosynthetic integrity in six mangrove populations as affected by chilling. – New Phytol. **232**: 2267-2282, 2021.

Liu X., Zhou Y., Xiao J., Bao F.: Effects of chilling on the structure, function and development of chloroplasts. – Front Plant Sci. **9**: 1715, 2018.

Mathur S., Sunoj V.S.J., Elsheery N.I. *et al.*: Regulation of photosystem II heterogeneity and photochemistry in two cultivars of C_4 crop sugarcane under chilling stress. – Front. Plant Sci. **12**: 627012, 2021.

Mau A.C., Reed S.C., Wood T.E., Cavaleri M.A.: Temperate and tropical forest canopies are already functioning beyond their thermal thresholds for photosynthesis. – Forests **9**: 47, 2018.

Maxwell K., Johnson G.N.: Chlorophyll fluorescence – a practical guide. – J. Exp. Bot. **51**: 659-668, 2000.

Miyake C.: Alternative electron flows (water–water cycle and cyclic electron flow around PSI) in photosynthesis: Molecular mechanisms and physiological functions. – Plant Cell Physiol. **51**: 1951-1963, 2010.

Miyake C.: Molecular mechanism of oxidation of P700 and suppression of ROS production in photosystem I in response to electron-sink limitations in C_3 plants. – Antioxidants **9**: 230, 2020.

Miyake C., Horiguchi S., Makino A. *et al.*: Effects of light intensity on cyclic electron flow around PSI and its relationship to non-photochemical quenching of Chl fluorescence in tobacco leaves. – Plant Cell Physiol. **l46**: 1819-1830, 2005b.

Miyake C., Miyata M., Shinzaki Y., Tomizawa K.: CO_2 response of cyclic electron flow around PSI (CEF-PSI) in tobacco leaves: Relative electron fluxes through PSI and PSII determine the magnitude of non-photochemical quenching (NPQ) of Chl fluorescence. – Plant Cell Physiol. **46**: 629-637, 2005a.

Miyake C., Shinzaki Y., Miyata M., Tomizawa K.: Enhancement of cyclic electron flow around PSI at high light and its contribution to the induction of non-photochemical quenching of Chl fluorescence in intact leaves of tobacco plants. – Plant Cell Physiol. **45**: 1426-1433, 2004.

Mohanty P., Allakhverdiev S.I., Murata N.: Application of low temperatures during photoinhibition allows characterization of individual steps in photodamage and the repair of photosystem II. – Photosynth. Res. **94**: 217-224, 2007.

Müller P., Li X.-P., Niyogi K.K.: Non-photochemical quenching. A response to excess light energy. – Plant Physiol. **125**: 1558-1566, 2001.

Murata N., Allakhverdiev S.I., Nishiyama Y.: The mechanism of photoinhibition *in vivo*: Re-evaluation of the roles of catalase, α-tocopherol, non-photochemical quenching, and electron transport. – BBA-Bioenergetics **1817**: 1127-1133, 2012.

Murata N., Takahashi S., Nishiyama Y., Allakhverdiev S.I.: Photoinhibition of photosystem II under environmental stress. – BBA-Bioenergetics **1767**: 414-421, 2007.

Murchie E.H., Niyogi K.K.: Manipulation of photoprotection to improve plant photosynthesis. – Plant Physiol. **155**: 86-92, 2011.

Neto M.C.L., Cerqueira J.V.A., da Cunha J.R. *et al.*: Cyclic electron flow, NPQ and photorespiration are crucial for the establishment of young plants of *Ricinus communis* and *Jatropha curcas* exposed to drought. – Plant Biol. **19**: 650-659, 2017.

Oxborough K., Baker N.R.: Resolving chlorophyll *a* fluorescence images of photosynthetic efficiency into photochemical and non-photochemical components – calculation of q_P and F_v'/F_m' without measuring F_o'. – Photosynth. Res. **54**: 135-142, 1997.

Raven J.A.: Speedy small stomata? – J. Exp. Bot. **65**: 1415-1424, 2014.

Rutherford A.W., Krieger-Liszkay A.: Herbicide-induced oxidative stress in photosystem II. – Trends Biochem. Sci. **26**: 648-653, 2001.

Rymbai H., Laxman R.H., Dinesh M.R. *et al.*: Diversity in leaf morphology and physiological characteristics among mango (*Mangifera indica*) cultivars popular in different agro-climatic regions of India. – Sci. Hortic.-Amsterdam **176**: 189-193, 2014.

Shaku K., Shimakawa G., Hashiguchi M., Miyake C.: Reduction-induced suppression of electron flow (RISE) in the photosynthetic electron transport system of *Synechococcus elongatus* PCC 7942. – Plant Cell Physiol. **57**: 1443-1453, 2016.

Shimakawa G., Miyake C.: Oxidation of P700 ensures robust photosynthesis. – Front. Plant. Sci. **9**: 1617, 2018.

Someralo S., Krause G.H.: Photoinhibition at chilling temperatures and effects of freezing stress on cold acclimated spinach leaves in the field. A fluorescence study. – Physiol. Plantarum **79**: 617-622, 1990.

Sonoike K.: Degradation of *psa B* gene product, the reaction center subunit of photosystem I, is caused during photoinhibition of photosystem I: possible involvement of active oxygen species. – Plant Sci. **115**: 157-164, 1996.

Sonoike K.: Photoinhibition of photosystem I. – Physiol. Plantarum **142**: 56-64, 2011.

Takagi D., Ishizaki K., Hanawa H. *et al.*: Diversity of strategies for escaping reactive oxygen species production within photosystem I among land plants: P700 oxidation system is prerequisite for alleviating photoinhibition in photosystem I. – Physiol. Plantarum **161**: 56-74, 2017.

Takahashi S., Milward S.E., Fan D.Y. *et al.*: How does cyclic electron flow alleviate photoinhibition in *Arabidopsis*? – Plant Physiol. **149**: 1560-1567, 2009.

Tikkanen M., Mekala N.R., Aro E.M.: Photosystem II photoinhibition-repair cycle protects Photosystem I from irreversible damage. – BBA-Bioenergetics **1837**: 210-215, 2014.

Wen Y., Qin D.W., Leng B. *et al.*: The physiological cold tolerance of warm-climate plants is correlated with their latitudinal range limit. – Biol. Lett. **14**: 20180277, 2018.

West K.R., Wiskich J.T.: Photosynthetic control by isolated pea chloroplasts. – Biochem. J. **109**: 527-532, 1968.

Wu J., Nadeem M., Galagedara L. *et al.*: Effects of chilling stress on morphological, physiological, and biochemical attributes of silage corn genotypes during seedling establishment. – Plants-Basel **11**: 1217, 2022.

Yamori W., Shikanai T.: Physiological functions of cyclic electron transport around photosystem I in sustaining photosynthesis and plant growth. – Annu. Rev. Plant Biol. **67**: 81-106, 2016.

Yang Y.J., Chang W., Huang W. *et al.*: The effects of chilling-light stress on photosystems I and II in three *Paphiopedilum* species. – Bot. Stud. **58**: 53, 2017.

Zhang S., Scheller H.V.: Photoinhibition of photosystem I at chilling temperature and subsequent recovery in *Arabidopsis thaliana*. – Plant Cell Physiol. **45**: 1595-1602, 2004.

Zheng C., Tang J., Chen J. *et al.*: Mechanisms on inhibition of photosynthesis in *Kandelia obovata* due to extreme cold events under climate change. – Ecol. Process. **5**: 20, 2016.

Zheng X.-T., Chen Y.-L., Zhang X.-H. *et al.*: ANS-deficient *Arabidopsis* is sensitive to high light due to impaired anthocyanin photoprotection. – Funct. Plant Biol. **46**: 756-765, 2019.

Zivcak M., Brestic M., Kunderlikova K. *et al.*: Repetitive light pulse-induced photoinhibition of photosystem I severely affects CO_2 assimilation and photoprotection in wheat leaves. – Photosynth. Res. **126**: 449-463, 2015.

Shielding of Photosynthetic Apparatus by Consortia of Bacterial Endophytes in Tomato Plants Suffering From Fusarium Wilt

Himani Chaturvedi[1], Bhupendra Singh[2], Anjana Jajoo[2,3] and Anil Prakash[1]*

[1] Department of Microbiology, Barkatullah University, Bhopal, India, [2] School of Life Science, Devi Ahilya University, Indore, India, [3] School of Biotechnology, Devi Ahilya University, Indore, India

Fusarium oxysporum is one of the most damaging plant pathogens causing Fusarium wilt in many plants leading to serious economic loss. The fungus colonizes the xylem, which leads to resistance in water flow in the plant thereby affecting the rate of photosynthesis. The present study focuses on the selection of bacterial endophytes isolated from tomato plants and evaluating their potential to antagonize *Fusarium oxysporum* in tomato *in vivo*. The results obtained indicated that two endophytic isolates, namely *Pseudomonas fluorescens* BUMD5 and *Bacillus velezensis* BUMD9, could act as efficient biocontrol agents (BCAs) as they inhibited the growth of pathogen by 67.2 and 69.1%, respectively, *in vitro*. Both the isolates were found to produce hydrolytic enzymes chitinase and protease. They also produced siderophore and hydrogen cyanide (HCN). The consortia of both the isolates significantly reduced the infection percentage by about 67% and a 3-fold decrease in disease severity was observed as compared to pathogen control. The treatment of infected plants with these potent isolates was also beneficial in improving the overall photosynthetic performance index (PI). Thus, plants treated with consortia of these isolates exhibited better overall plant growth despite being infected by the pathogen.

Keywords: biological control, endophytes, photosynthetic apparatus, tomato plant, Fusarium wilt

INTRODUCTION

Fusarium oxysporum, an ascomycete, is a major disease-causing pathogen affecting plants in agricultural settings (Fisher et al., 2012). It is listed among the topmost devastating pathogens worldwide. Fusarium wilt is one of the major plant diseases caused by pathogenic *Fusarium oxysporum* strains (Dean et al., 2012). The spores produced by the fungus are known to remain in the soil for decades in a viable form thereby leading to the failure of crop rotation schemes (Nelson, 1981). The spores germinate after encountering plant root exudates and initiate the colonization of the host plant, followed by an invasion of vascular bundles. The water uptake system of the plant gets affected thereby causing severe wilting and sometimes death of the host plant (Altinok, 2005).

Tomato is also vulnerable to Fusarium wilt. The symptoms observed in infected plants include stunted growth, wilting, yellowing of leaves and stems, defoliation, marginal leaf necrosis, and vascular necrosis (Singh et al., 2017). The effect of a pathogen can be traced through the entire plant including shoot tips and fruits. The xylem discoloration might be observed only on one side initially but eventually leads to browning of the entire xylem (Cerkauskas, 2017). There are three

protein complexes that are responsible for mediating the primary reactions of photosynthesis in the thylakoid membranes of chloroplasts. These include PSII, the cytochrome b_6f complex (Cytb_6f), and PSI, which are connected in series through the photosynthetic electron transport chain. The light-harvesting systems of PSII and PSI capture light energy and transfer it to the reaction center chlorophylls to create a charge separation across the membrane. This leads to the formation of a strong oxidant on the donor side of PSII capable of splitting water into molecular oxygen, protons, and electrons (Eberhard et al., 2008). The obstruction in the water transport system affects the rate of photosynthesis due to stomatal closure induced by water deficit. It is also found to affect the metabolic pathways of photosynthesis, Rubisco is one of the examples (Duniway and Slatyer, 1971; Lorenzini et al., 1997; Saeed et al., 1999; Pedrosa et al., 2011). Fusarium wilt is responsible for affecting three crucial processes in photosynthesis- the thylakoid electron transport, the carbon reduction cycle, and the stomatal control of the CO_2 supply (Allen et al., 1997).

The present-day strategies used to control wilt include the use of chemical fungicides, heat sterilization of soil, and the use of resistant plant varieties; however, none of them proved to be completely successful. Chemical control methods include the application of some broad-spectrum biocides like carbendazim before planting. These chemicals are preventive in nature but cannot treat an infection. These are also found to be harmful to other beneficial soil microbes and can also enter the food chain thereby causing detrimental health (López-Aranda et al., 2016). The application of heat is non-selective and can affect the quality of soil (Mahmood et al., 2014). Developing resistant plant varieties is the most effective method but genetically encoded resistance is not durable for a longer period of time and leads to the emergence of new resistant strains (Takken and Rep, 2010; De Sain and Rep, 2015).

In recent years, endophytic micro-organisms which colonize host tissues internally without causing damage or eliciting disease symptoms, have received increased attention (Sturz et al., 2000; Chaturvedi et al., 2016). Endophytes have been considered successful candidates to be used as BCAs because of their ability to colonize a plant and have a more protective and less competitive environment as compared to their rhizospheric colleagues. The use of BCAs in an efficient manner is a self-sustaining and long-term method to control plant diseases and pests. Bacterial BCAs showing antagonistic actions against plant pathogenic fungi that cause a wide spectrum of plant diseases have been reported. Different mechanisms remain responsible for the antagonism of biocontrol agents that include the production of antifungal metabolites, competition for space and nutrients, mycoparasitism, and induction of the defense responses in plants (Glick, 1995; Howell, 2003; Chaturvedi and Prakash, 2020).

In the present study, we aimed to explore beneficial endophytic bacteria as potent biocontrol agents against Fusarium wilt of tomato. The isolates were selected on the basis of their antagonistic potential against *Fusarium oxysporum in vitro*. The selected isolates were tested for their capability of producing hydrolytic enzymes like chitinase and protease and plant growth promoting attributes like siderophore and HCN

production. Furthermore, this study aims to understand the biocontrol effect of bacterial endophytes on Fusarium wilt in tomato plants and therefore, the photosynthetic apparatus which is affected during wilting. We also analyzed the amount of chlorophyll a (Chl a), chlorophyll b (Chl b), and total chlorophyll content (a+b) in plants treated with pathogen and biocontrol agents. By measuring Chl fluorescence kinetics, the efficiency of Photosystem II (PSII) photochemistry was measured. Energy pipeline models of photosynthetic apparatus visualized the alterations of PSII energy fluxes in response to the pathogen and its recovery by biocontrol agents. In summary, the isolates identified in the present study can be useful in controlling Fusarium wilt of tomato, the consortia of them being even more efficient.

MATERIALS AND METHODS

Plants, Bacteria, Fungi, and Growth Conditions

The tomato wilt pathogen *Fusarium oxysporum* f. sp. *lycopersici* (ITCC 6859) was collected from the Indian type culture collection (ITCC), IARI, Delhi. The pathogen was maintained in Potato Dextrose Agar (PDA) (López-Martínez et al., 1999) at 4°C and periodically sub-cultured in PDA.

The tomato plants were collected from the Bhopal region (23.165964°N 77.328515°E) of Madhya Pradesh. Endophytic bacteria were isolated from roots, stems, and leaves (five samples each) of plants according to the method described by Hallmann et al. (1997) and Sturz et al. (1998). All the isolates were maintained in the nutrient agar slants at 4°C. The efficiency of the surface sterilization process was checked according to Hallmann et al. (1997) (detailed procedure and images in **Supplementary File 1**).

Antifungal Activity of Isolated Strains

The isolated microbes were screened for their antagonistic potential against *Fusarium oxysporum* by dual culture assay (Shabanamol et al., 2017). About 2 mm of *Fusarium* mycelia plug grown on PDA was placed at 2 cm from the edge of the agar plate and challenged on the other end of the plate at 2 cm from the edge with a single streak of the bacterial isolates. Petri plates were incubated at 28 ± 2°C for 7 days and percent (%) inhibition was calculated using the following formula:

$$I = \frac{(C - T) \times 100}{C}$$

where, I = % inhibition in mycelia growth; C = growth of pathogen in control plates; T = growth of pathogen in dual culture plates.

Identification of Selected Endophytes

Total two isolates showing maximum inhibition for the fungal pathogen were selected and identified by molecular means using 16S rRNA sequencing. Twenty-four-hours old cultures of the selected bacterial isolates were subjected to DNA extraction using a bacterial genomic DNA isolation kit (HiMedia) following the manufacturer's instructions. The extracted DNA was used

to amplify 16S genes. The polymerase chain reaction (PCR) product was purified by using a PCR product purification kit (HiMedia) and was sent for sequencing (Bio-innovations, Mumbai, Maharashtra). The sequence obtained was analyzed using BLAST and was deposited in NCBI GenBank. The phylogenetic tree had been constructed using the MEGA7 software (Midhun et al., 2017).

Screening for Attributes Aiding to Antagonism

Production of Hydrolytic Enzymes-Chitinase and Protease

The ability of endophytic isolates to produce chitinase was determined by inoculating on a minimal medium amended with colloidal chitin as the sole carbon source (Renwick et al., 1991). Plates were incubated at $28 \pm 2°C$ and analyzed for the zone of clearance for up to 10 days. Protease production was observed according to Smibert et al. (1994). The development of a clear zone around the bacterial colony inoculated in the skimmed milk agar indicated a positive result.

Siderophore Production

The Chrome Azurol S (CAS) agar medium was prepared as described by Schwyn and Neilands (1987) for the qualitative detection of siderophore production. The strain was inoculated in the Chromo Azurol S (CAS) (blue agar) plate and kept for incubation at $37°C$ for 48 h. The presence of a yellow to light orange halo zone in the medium surrounding the colony indicates the production of siderophore.

HCN Production

The production of HCN was observed according to Bakker and Schippers (1987). The log phase culture (50 µl) of the bacterial strain was spread on a nutrient medium containing glycine (4.5 gL^{-1}). The change of color of the Filter paper (Whatman filter paper 1) soaked in 0.5% picric acid in 1% sodium bicarbonate placed in the upper lid of the Petri plate incubated at $28°C$ for 96 h from yellow to reddish brown was recorded as an index of positive for cyanogenic activity.

Effect of Selected Isolates on Vigor Index and Seed Germination

Surface sterilized tomato seeds were inoculated in bacteria broth with a final concentration of $\sim 10^8$ CFU per seed and were incubated for 24 h at $28 \pm 2°C$. Among them, 20 seeds were randomly selected by discarding the broth. They were transferred to the Petri plate containing sterile moistened blotting paper. Seeds treated with sterile distilled water (SDW) served as control. The Petri plates were incubated at $28 \pm 2°C$ for 7 days under the dark condition for germination (Xia et al., 2015). The germination percentage was calculated using the formula:

$$Germination\ Percentage = \frac{Number\ of\ Seeds\ Germinated}{Total\ Number\ of\ Seeds} \times 100$$

The seedling vigor index was calculated using the following formula:

$$Seedling\ Vigour = Seedling\ Length\ in\ cm \\ \times Germination\ Percentage$$

Evaluation of Biocontrol Efficacy of Selected Isolates *in-vivo*

Seed treatment was done as mentioned in section Effect of Selected Isolates on Vigor Index and Seed Germination. For treatment with the consortia of isolates, 10 ml of one culture was combined with 10 ml of another. The confirmation of endophytic colonization was done as mentioned in **Supplementary File 2**. About three treatments and two controls were considered for the experiment as mentioned in the table. The bacteria-treated tomato seeds were sown in the paper cups. After attaining the two true leaf stage the seedlings were transferred to the individual pots (12.5×14.5 cm) containing autoclaved soil. The treatments included in the study are as follows: T1- Plant uninoculated (Healthy Control), T2- Plant inoculated with pathogen, T3- Plant treated with BUMD5 and *Fusarium*, T4- Plant treated with BUMD9 and *Fusarium*, and T5- Plant treated with consortia and *Fusarium*.

Pathogen Inoculation

The *Fusarium oxysporum* spore suspension of inoculum was prepared by pouring 20 ml of SDW in each culture plate of 5–7 days old fungal mycelium and then gently scraped using the spore harvester. The concentration of conidia was adjusted to 10^7 conidia ml^{-1}. Then, about 5 ml of prepared spore suspension was used to inoculate each seedling in all five treatments using the soil drenching method (Patil et al., 2011). In the soil drenching method, 5 ml of fungal suspension (i.e., water containing conidia of the pathogen) was inoculated to each of the seedlings by drenching the soil around the root zone with the help of a pipette. Before inoculation, the roots were slightly severed (wounded) by inserting a needle, 1 cm away from the stem. Root severing was done to ensure pathogen penetration through roots.

Symptom severity of the shoot system of the plants was assessed (6 weeks after pathogen inoculation) using the following scales: 0- no symptoms,1-yellowing 1–25% of the leaves near the stem base, 2-Yellowing, and wilt 26–50% of leaves with a simple brown discoloration in the xylem vessels, 3-Yellowing, and wilt 51–75% of the leaves with dark brown coloring in the xylem vessels and 4-Wilt and die 76–100% of leaves (Souza et al., 2010).

The disease severity index and infection percentage were calculated using the following formulae:

$$Disease\ Severity\ Index\ (\%) = \frac{ni \times si}{4n} \times 100$$

$$Infection\ (\%) = \frac{ni}{n} \times 100$$

where, ni: is the number of plants affected by each degree of severity, si: the degree of severity of the attack (0–4), n: the total number of plants used for each energy level applied.
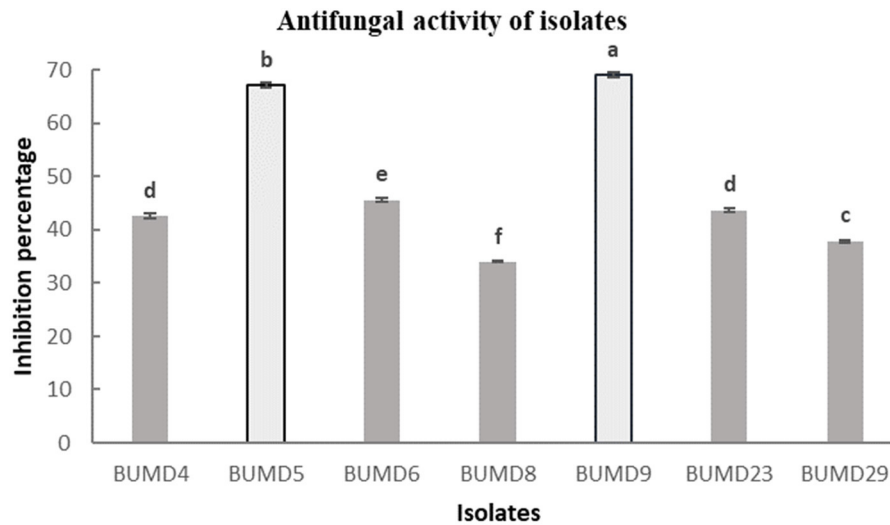
FIGURE 1 | *In vitro* antifungal activity against *Fusarium oxysporum*. The strains showing maximum percentage inhibition BUMD5 and BUMD9 were selected for further studies.

Estimation of Chlorophyll Content

Sample preparation was done according to Pérez-Patricio et al. (2018). Absorbance readings were performed at wavelengths of 663 and 645 nm. The control was acetone/ethanol (2:1 v/v). The obtained values were substituted in the following formulas, for the estimation of photosynthetic pigments:

$$Chlorophyll\ a\ (mg/g) = (12.7 \times A663) - (2.59 \times A645)$$
$$Chlorophyll\ b\ (mg/g) = (22.9 \times A645) - (4.7 \times A663)$$
$$Chlorophyll\ Total\ (mg/g) = (8.2 \times A663) + (20.2 \times A645)$$

Where, A663 and A645 are the absorbance measured from 663 and 645 nm, respectively.

Measurement of Fluorescence Induction Kinetics

Polyphasic chlorophyll a fluorescence transient called O-J-I-P (JIP-test) was measured using a plant efficiency analyzer (PEA, Hansatech, England) in tomato plants. In order to provide a homogeneous illumination, excitation light of 650 nm was focused on the surface of the leaf from an array of three light-emitting diodes. The intensity of light reaching the leaf was 3,000 μmol (photon) m^{-2} s^{-1}, which was sufficient to produce maximum fluorescence (Fm). Plants were adapted to dark for 20 min prior to measurements. The Biolyzer HP 3 software (the chlorophyll fluorescence analysis program of the Bioenergetics Laboratory, gifted by the University of Geneva, Switzerland) was used to prepare the energy pipeline model.

Statistical Analysis

The data were subjected to one-way ANOVA and Tukey's HSD test at the level of $p \leq 0.05$. All the statistical analyses were performed using the SPSS version 16 statistical package (IBM SPSS, USA).

RESULTS

Selection of Potent Strains to Be Used as Biocontrol Agents Against Fusarium Wilt

A total of 36 isolates were collected from the different parts of the plant, viz. roots (17), stem (11), and leaves (8). All the isolates were tested for antifungal activity. A total of eight isolates showed anti-fungal activity in the dual culture method (**Supplementary File 3**) out of which two isolates, BUMD5 and BUMD9, showing maximum inhibition percentage, i.e., 67.2 and 69.1%, respectively, were chosen for further studies (**Figure 1**). Both the isolates were found to produce hydrolytic enzymes chitinase and protease (**Figures 2A,B**). Also, both the strains were positive for siderophore and HCN production (**Figures 2C,D**). The sequences were submitted in NCBI GenBank and accession numbers MZ223450 and MZ223454 were obtained. The isolate MZ223450 was found to have 99.06% similarity to *Pseudomonas fluorescens* P21(FJ605510.1) and MZ223454 was found to have 99.9% similarity to *Bacillus velezensis* HFBPR51 (MT539153.1), respectively, using sequencing and BLAST results. **Figure 3** shows the phylogenetic trees obtained using MEGA software.

Effect of Selected Isolates on Vigor Index and Seed Germination

The isolates were assessed individually as well in combination for seed germination potential. They showed an enhanced seed germination percentage and vigor index when compared to the uninoculated control after 7 days of incubation. It could be
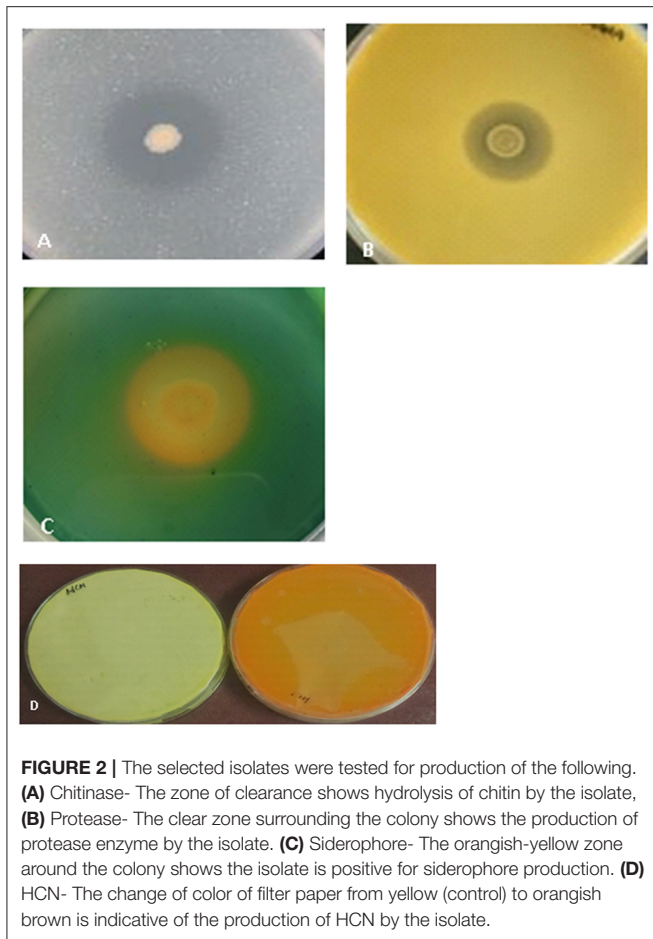
FIGURE 2 | The selected isolates were tested for production of the following. (A) Chitinase- The zone of clearance shows hydrolysis of chitin by the isolate, (B) Protease- The clear zone surrounding the colony shows the production of protease enzyme by the isolate. (C) Siderophore- The orangish-yellow zone around the colony shows the isolate is positive for siderophore production. (D) HCN- The change of color of filter paper from yellow (control) to orangish brown is indicative of the production of HCN by the isolate.

inferred that the seed germination and vigor index was influenced by the seed treatment with the isolates (**Table 1**).

Evaluation of Biocontrol Efficacy of Selected Isolates *in vivo*

Effect of Different Treatments on Plant Growth Parameters

It was observed that during the study, treatment T5 significantly reduced the infection by 67% when compared to control followed by treatments T3 and T4, which reduced by 26.7 and 33.3%, respectively (**Table 2**). Although there was no significant difference observed in the reduction in disease severity between T3, T4, and T5, there is an almost 3-fold reduction in disease severity when compared to the plant only inoculated with the pathogen (T2).

The growth parameters were observed for the plants after 45 days of pathogen inoculation (**Figure 4**). Maximum root length and shoot length, i.e., 18.1 ± 0.11 cm and 39.7 ± 0.5 cm (**Figures 5A,B**, respectively), were observed in T5, which is almost equal to that observed in an uninoculated or healthy plant (T1). However, a significant increase in fresh weight and dry weight (**Figures 5C,D**) was clearly observed in plants under the treatment T5 when compared to a healthy plant (T1).
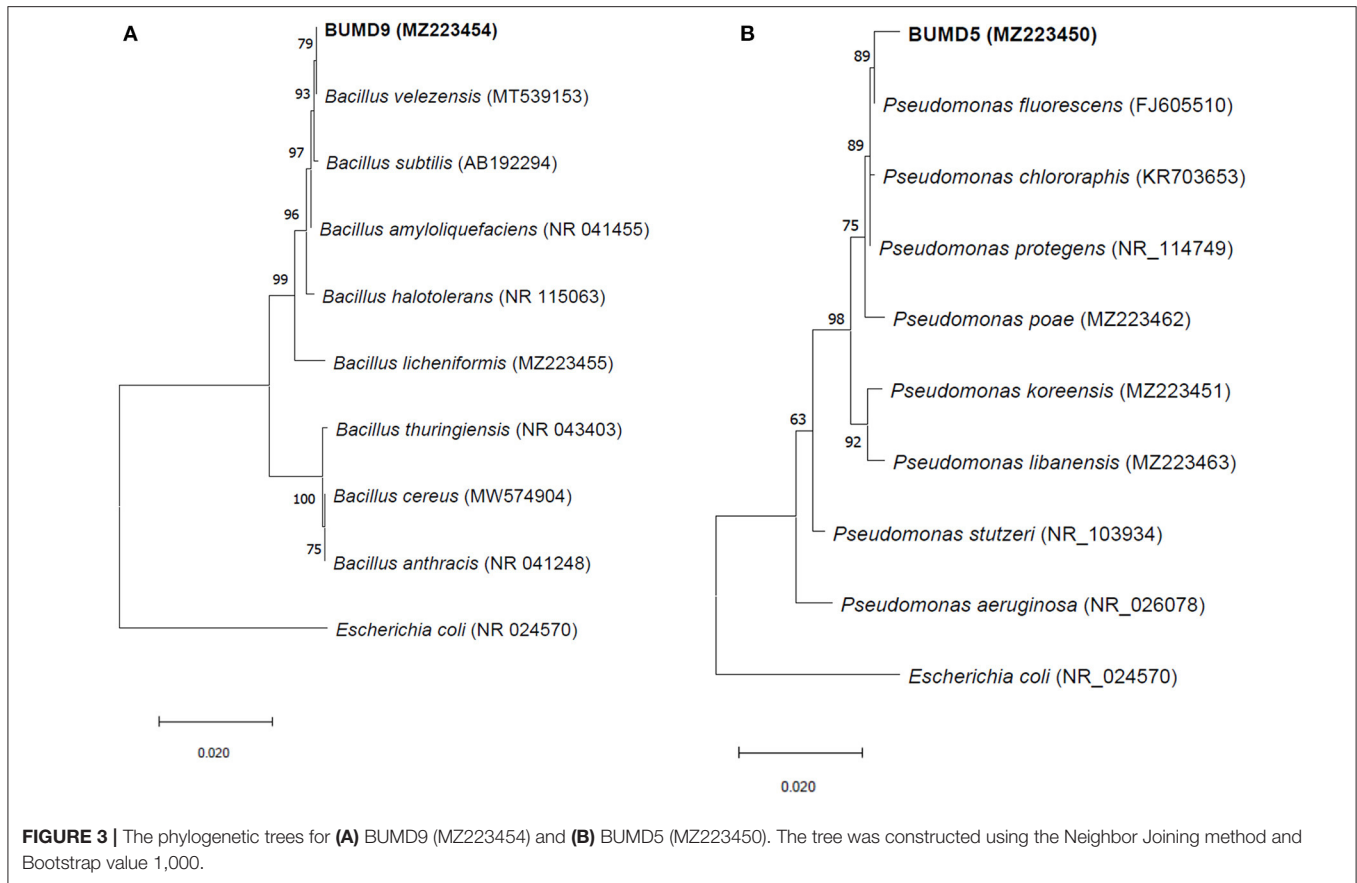
Estimation of Chlorophyll Content

The effect of different treatments on leaves can be seen in **Figure 6**. However, no significant difference in concentration of chl a was observed among T1, T4, and T5 ($20.05 \pm 0.65\,\mu\mu g/ml$, $20.17 \pm 1.99\,\mu g/ml$, and $20.90 \pm 0.19\,\mu g/ml$, respectively) whereas the lowest concentration of the same was observed in the pathogen induced T2 ($13.92 \pm 1.57\,\mu g/ml$) as seen in **Figure 7A**. In the case of chlorophyll b, maximum concentration was seen in T4 and T5 ($13.76 \pm 1.27\,\mu g/ml$ and $13.78 \pm 1.07\,\mu g/ml$, respectively) followed by T1 ($12.55 \pm 0.70\,\mu g/ml$) and lowest concentration was observed in T2 ($10.24 \pm 1.16\,\mu g/ml$) as shown in **Figure 7B**. Total chlorophyll content (a+b) was found to be highest in T5 ($34.69 \pm 0.25\,\mu g/ml$) followed by T4 ($33.95 \pm 2.85\,\mu g/ml$) and the lowest concentrations were again observed in T2 ($21.91 \pm 1.33\,\mu g/ml$) as seen in **Figure 7C**.

Measurement of Fluorescence Induction Kinetics

The chlorophyll fluorescence transient curves are shown in **Figure 8** and the parameters derived from them are shown in **Table 3**. A change in the shape of the curve and the fluorescence intensity of the OJIP transient were observed in control and treated plants. This was correlated with a change in the transport of photosynthetic electrons in the tomato plants treated with a pathogen and potent bacteria. As seen in **Figure 8**, in comparison to T1 (Control), the quantum efficiency of PSII photochemistry (as inferred from the Fv/Fm ratio) significantly decreased by about 13% in T2. Infected plants receiving biocontrol treatment decreased the damaging effect of the pathogen on plants and were least damaged (T5). In T2 plants, the efficiency of the water splitting complex (Fv/Fo) on the donor side of PSII was decreased significantly by 38% in comparison to control plants (T1). It is steadily recovered after the biocontrol treatments. In this study, RC/ABS, which reflects the number of active reaction centers decreased significantly in T2 by 21.5% as opposed to T1 (Control). The efficiency by which an electron trapped can pass further ahead of Q_A- is equivalent to $(1-V_J)$ or Ψo (Tomar and Jajoo, 2013). No significant variation in the value of a 1-Vj was observed for different treatments except a decrease of around 13% in T2. The performance index (PI) sensitively reflects the function and vitality of the photosynthetic apparatus (Mathur et al., 2018). PI tremendously decreased by 57.1% in infected plants (T2) as compared to T1 (control) (**Table 3**). However, the application of biocontrol agents improved the PI and the effect was more pronounced in T5 where bacterial consortia could protect photosynthetic apparatus in plants from pathogenic effects.

Relevant activities, such as ABS/CS, TR/CS, ET/CS, and DI/CS, indicating the efficiency of light absorption, trapping, electron transport, and dissipation per cross section of PSII, respectively, have been demonstrated in the form of energy pipeline models for various treatments (**Figure 9**). This model gives information about the efficiency of the flow of energy from antennae to the electron transport chain components through the RC of PSII. As compared to control (T1), T2 showed a decrease of 20% in ABS/CS, 27% in TRo/CS, and 29% in ETo/CS. However, the application of biocontrol treatments (T3, T4, and T5) led to improvement in the number of active reaction centers (indicated

FIGURE 3 | The phylogenetic trees for **(A)** BUMD9 (MZ223454) and **(B)** BUMD5 (MZ223450). The tree was constructed using the Neighbor Joining method and Bootstrap value 1,000.

by open circles) as well as better rates of electron transport (indicated by the width of the blue line). T5 was found to be best with regard to the performance of the photosynthetic parameters.

DISCUSSION

Fusarium wilt is among the most devastating diseases of tomato. The xylem colonization by the pathogen is known to increase water flow resistance in the plant, resulting in the leaf water deficit that is responsible for reducing the leaf photosynthesis and transpiration (Nogués et al., 2002). Therefore, it is necessary to seek an effective prevention and control strategy to control the Fusarium wilt disease during crop production. Using endophytes as biological control agents for plant diseases is an efficient and environmental-friendly approach.

In the present study, we have identified two potential strains, *Pseudomonas fluorescens* BUMD5 and *Bacillus velezensis* BUMD9, which when used individually as well as in combination can act as potent biocontrol agents for controlling the fusarium wilt in tomato plants. Both the isolates have shown significant antagonistic activity against Fusarium *in vitro*. They have also been demonstrated to produce hydrolytic enzymes, which aid the endophytes in the initial colonization process. The selected strains also produced HCN and siderophores, which help the endophytes in outcompeting the phytopathogens in the ecological niche. Several studies have shown *Bacillus velezensis* as

TABLE 1 | Effect of seed bio-priming on seed germination and vigor indices.

	Control	BUMD5	BUMD9	Consortia
Germination %age	43.3 ± 1.67^c	63.3 ± 1.67^b	71.7 ± 3.33^b	81.7 ± 1.67^a
Seedling length	1.63 ± 0.12^c	3.53 ± 0.12^b	3.83 ± 0.176^{ab}	4.5 ± 0.208^a
Vigour index	70.5 ± 3.97^d	230 ± 11.5^c	294 ± 18.9^b	374 ± 10.1^a

Values are means ± SEM, n = 3 per treatment group. Means in a row without a common superscript letter differ (P < 0.05) as analyzed by one-way ANOVA and the TUKEY HSD test.

TABLE 2 | Effect of isolates on infection percentage and disease severity index.

	T1	T2	T3	T4	T5
Infection %age	0 ± 0^d	100 ± 0^a	73.3 ± 6.67^b	66.7 ± 6.67^b	33.3 ± 6.67^c
DSI	0 ± 0^c	83.3 ± 1.67^a	33.3 ± 1.67^b	36.7 ± 1.67^b	25 ± 5^b

Values are means ± SEM, n = 3 per treatment group. Means in a row without a common superscript letter differ (P < 0.05) as analyzed by one-way ANOVA and the TUKEY HSD test.

a potential plant growth promoter and biocontrol agent. *Bacillus velezensis* NKG-2 was found to secrete fungal cell wall degrading enzymes, volatile organic compounds (VOCs), and indole-3-acetic acid and siderophore and also helped in reducing the disease severity of *Fusarium oxysporum* wilt disease on tomato
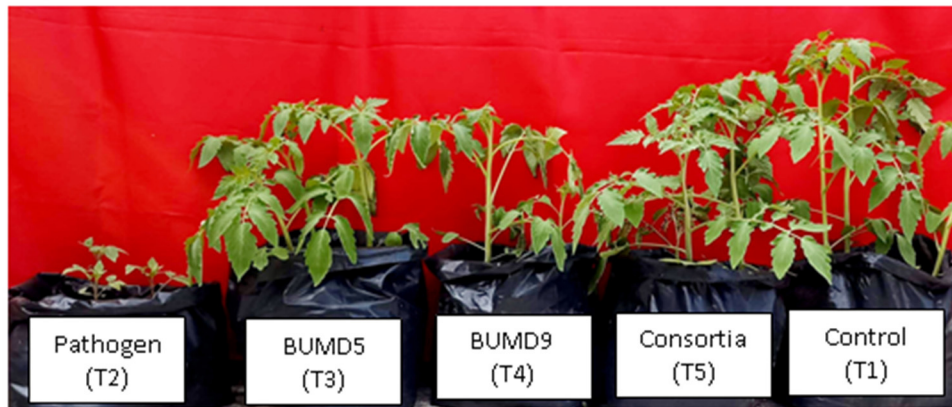
FIGURE 4 | Effect of different treatments on plant growth in a pot experiment. T1- Plant uninoculated (Healthy Control), T2- Plant inoculated with *Fusarium*, T3- Plant treated with BUMD5 and *Fusarium*, T4- Plant treated with BUMD9 and *Fusarium,* and T5- Plant treated with consortia and *Fusarium*.
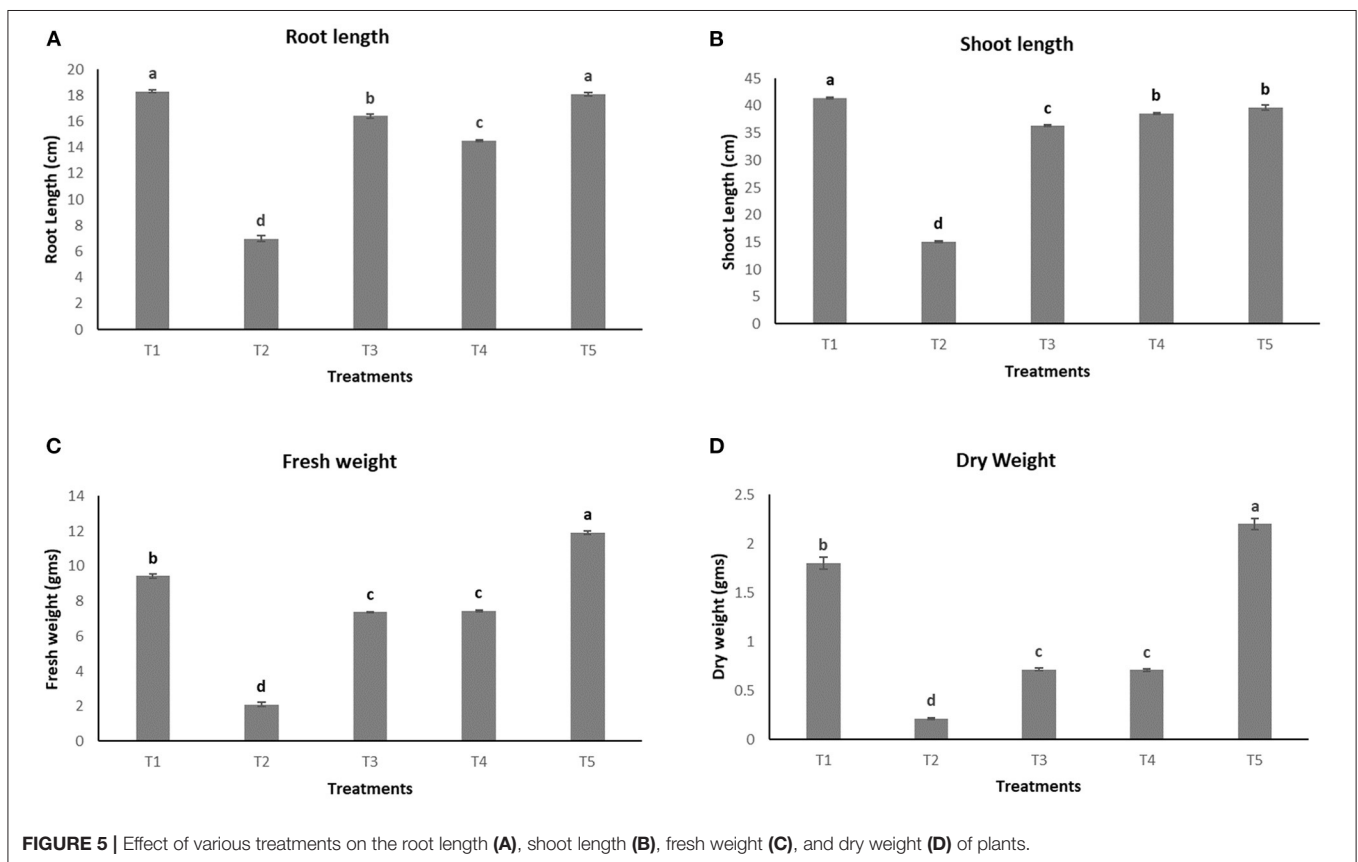
FIGURE 5 | Effect of various treatments on the root length **(A)**, shoot length **(B)**, fresh weight **(C)**, and dry weight **(D)** of plants.

plants both under *in vitro* and *in vivo* conditions (Myo et al., 2019). The strains also improved the chlorophyll content of plants as compared to diseased plants. *Bacillus velezensis* GF267 reduced the intensity of tomato bacterial spots and increased the chlorophyll content in plants as reported by Mates et al. (2019). Various strains of *Pseudomonas fluorescens* have also been shown to be effective biocontrol agents against multiple plant diseases (Yendyo et al., 2017; Kulimushi et al., 2021; Mosahaneh et al.,

2021). As observed in the current study, the combination of these two isolates was more effective in controlling wilt as compared to the treatments containing these isolates alone. It has been evident that mixed inoculants interact synergistically, with a different or complementary mode of action and provide increased disease resistance. Various combinations of microbes have been shown to increase plant productivity and provide better disease resistance to plants. As reported by Pacheco et al. (2021), the microbial

FIGURE 6 | Yellowing of leaves as observed after various treatments.
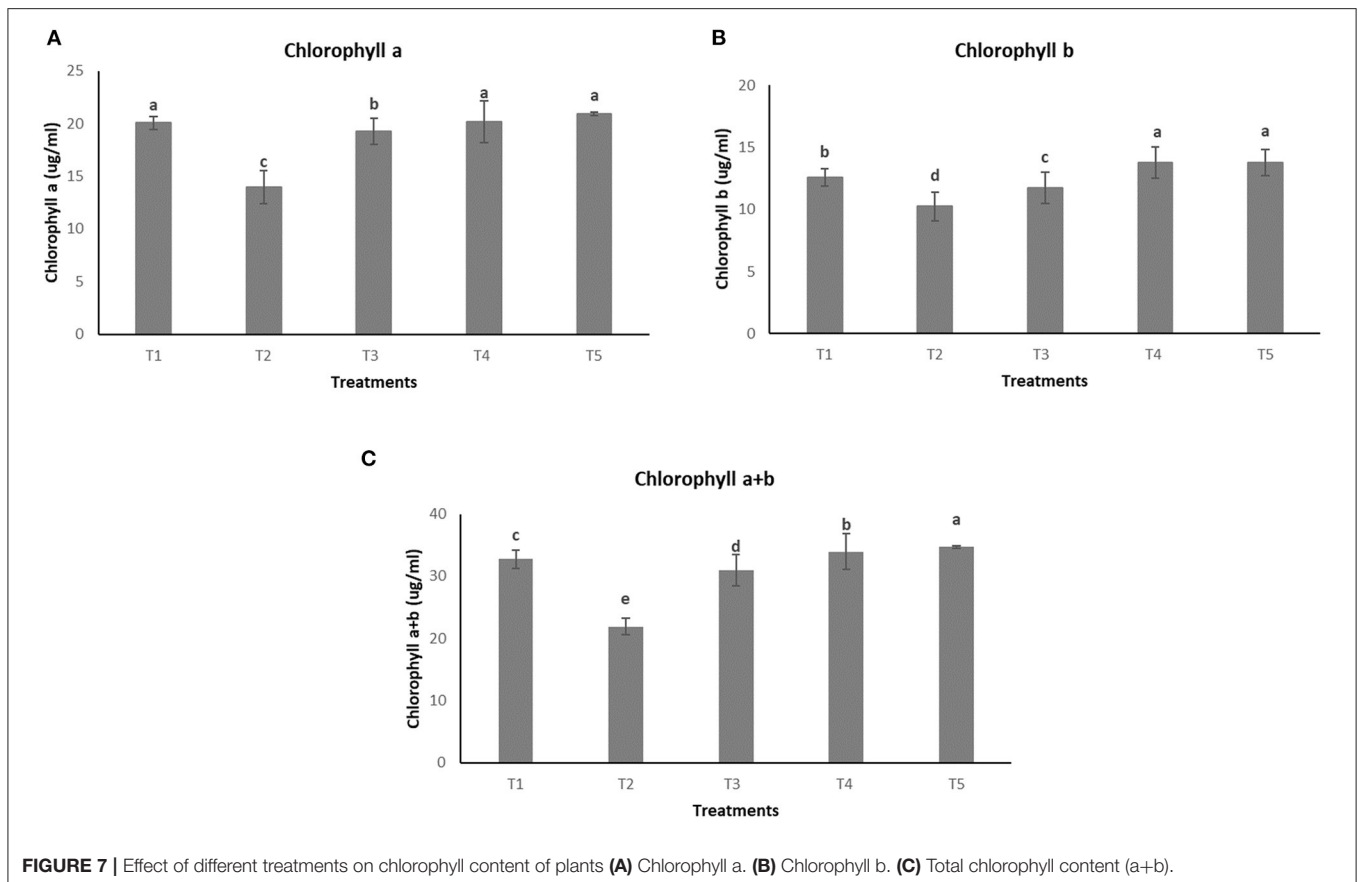
FIGURE 7 | Effect of different treatments on chlorophyll content of plants **(A)** Chlorophyll a. **(B)** Chlorophyll b. **(C)** Total chlorophyll content (a+b).

consortium increased maize productivity, and at the same time improved Phosphate use efficiency as compared to individual strains. To the best of our knowledge, the use of a combination of two selected isolates, *Pseudomonas fluorescens* and *Bacillus velezensis,* has not been reported earlier.

Endophytes have also been studied extensively for plant growth promotion. They have been considered better candidates as compared to rhizospheric microbes because of their close association with plants (Gupta et al., 2015). Many bacterial species including *Bacillus, Pseudomonas,* etc., have been used to improve plant productivity (Gupta et al., 2019). We have also obtained similar results in which better growth parameters like root length, shoot length, fresh weight, and dry weight have been observed in plants treated with BUMD5, BUMD9,

and their consortia despite being treated with the pathogen *Fusarium oxysporum*.

Improved growth parameters are generally related to the better photosynthetic performance of the plant. To monitor the efficiency of photosynthesis, we used a non-invasive method of Chl a fluorescence kinetics. Chl a fluorescence kinetics parameters have been recognized as ideal predictors of photosynthetic performance and energy conversion efficiency of Photosystem II (PSII) (Mathur et al., 2018). **Figure 9** shows the effect of treatments on the shape of chlorophyll a fluorescence transient to analyze changes in electron transfer reactions occurring at PSII (Papageorgiou, 2012). In the present study, decreased Fv/Fm values indicate stress due to a pathogen that damages the photosynthetic apparatus (Goltsev et al., 2016). To localize the effects of treatments on the acceptor side of PSII, the kinetics of relative variable fluorescence (Vj) were calculated. The efficiency by which a trapped electron can move further ahead of Q_{A-} is equal to (1 - Vj) or Ψo (Tomar and Jajoo, 2013). Not much variation in the values of (1 - Vj) were observed in plants treated with or without bacteria except for a decline

of 13% in T2. It suggests that Q_A- re-oxidation and electron transport at the acceptor side of PSII was not much affected (Tomar and Jajoo, 2013). The photosynthetic performance index (PI) is an indicator of plant vitality. PI_{total} is an overall parameter that incorporates biophysical parameters, determined from the JIP-test (Maliba et al., 2019). PI is the product of a dependent parameter for an antenna, reaction center, and electron transport. In the tomato plants under the pathogenic influence, biological treatment has resulted in an improved overall performance index (PI) (**Figure 9**). It can also be observed in other plant growth parameters and chlorophyll content.

Energy pipeline models of photosynthetic apparatus further visualized the alterations of PSII energy fluxes in response to the pathogen and its recovery by biocontrol agents (**Figure 8**). This model gives information about the efficiency of the flow of energy from antennae to the electron transport chain components through the cross-section of PSII (Li et al., 2014). It has been shown that ABS/CSm, ETo/CSm, TR$_o$/CSm declined with T2 treatment. ETo/CSm decreased due to lower energy absorption by antenna pigments (ABS/CSm), lower energy trapping by RCs (TRo/CSm), and higher energy loss as heat (DIo/CSm). The decrease in TRo/CSm is mainly due to the decrease in the density of the active RCs and this is an indication that downregulation of PSII is accomplished by the inactivation of the RCs. As a negative effect of the pathogen, a decrease in the density of active reaction centers (indicated as open circles) and a rise in the density of closed reaction centers (indicated as full circles) have been observed (T2). Biological treatments may retrieve the negative effects of pathogens on the overall photochemistry. However, bacterial consortia could protect tomato plants better from the damaging effects of pathogens.
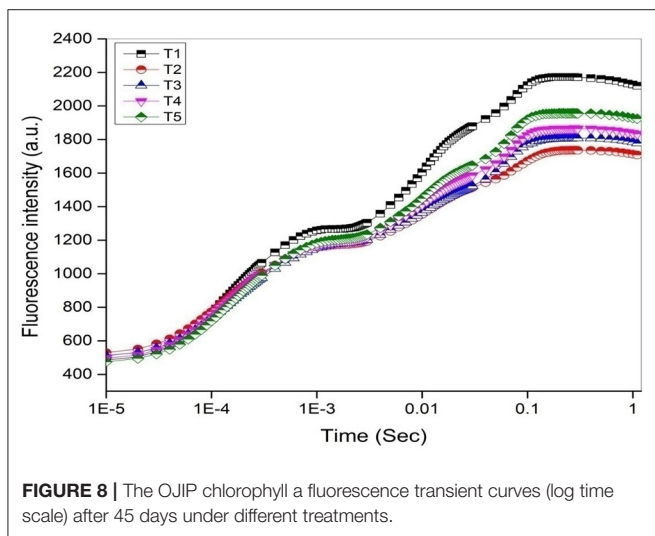
CONCLUSION

Fusarium wilt is a major disease affecting crops leading to severe economic loss every year. The clogging of the xylem is responsible for wilting leading to the death of the plant. *Bacillus velezensis* and *Pseudomonas fluorescens* can be considered potent biocontrol agents to control the disease. They have significantly reduced the deleterious effect on the photosynthetic apparatus, thereby

FIGURE 8 | The OJIP chlorophyll a fluorescence transient curves (log time scale) after 45 days under different treatments.

TABLE 3 | Parameters obtained from fluorescence transient curves measured on day 45 under different treatments on tomato plant.

Treatments	Fv/Fm	RC/ABS	Fv/Fo	1-vj	PI
T1	0.78 ± 0.01[a] (100)	0.56 ± 0.03[a] (100)	3.56 ± 0.13[a] (100)	0.53 ± 0.01[a] (100)	1.07 ± 0.13[a] (100)
T2	0.68 ± 0.02[e] (87.1)	0.44 ± 0.04[d] (78.5)	2.20 ± 0.21[c] (61.7)	0.46 ± 0.01[d] (86.7)	0.46 ± 0.09[e] (42.9)
T3	0.71 ± 0.0[d] (91)	0.50 ± 0.02[c] (89.2)	2.52 ± 0.01[c] (70.7)	0.48 ± 0.02[c] (90.5)	0.61 ± 0.05[d] (57)
T4	0.73 ± 0.02[c] (93.5)	0.49 ± 0.04[c] (87.5)	2.77 ± 0.37[b] (77.8)	0.48 ± 0.01[c] (90.5)	0.68 ± 0.16[c] (63.5)
T5	0.76 ± 0.01[b] (97.4)	0.54 ± 0.04[b] (96.4)	3.20 ± 0.15[a] (89.8)	0.50 ± 0.02[b] (94.3)	0.88 ± 0.13[b] (82.2)

Values are means ± SEM, n = 3 per treatment group. Means in a row without a common superscript letter differ (P < 0.05) as analyzed by one-way ANOVA and the TUKEY HSD test.
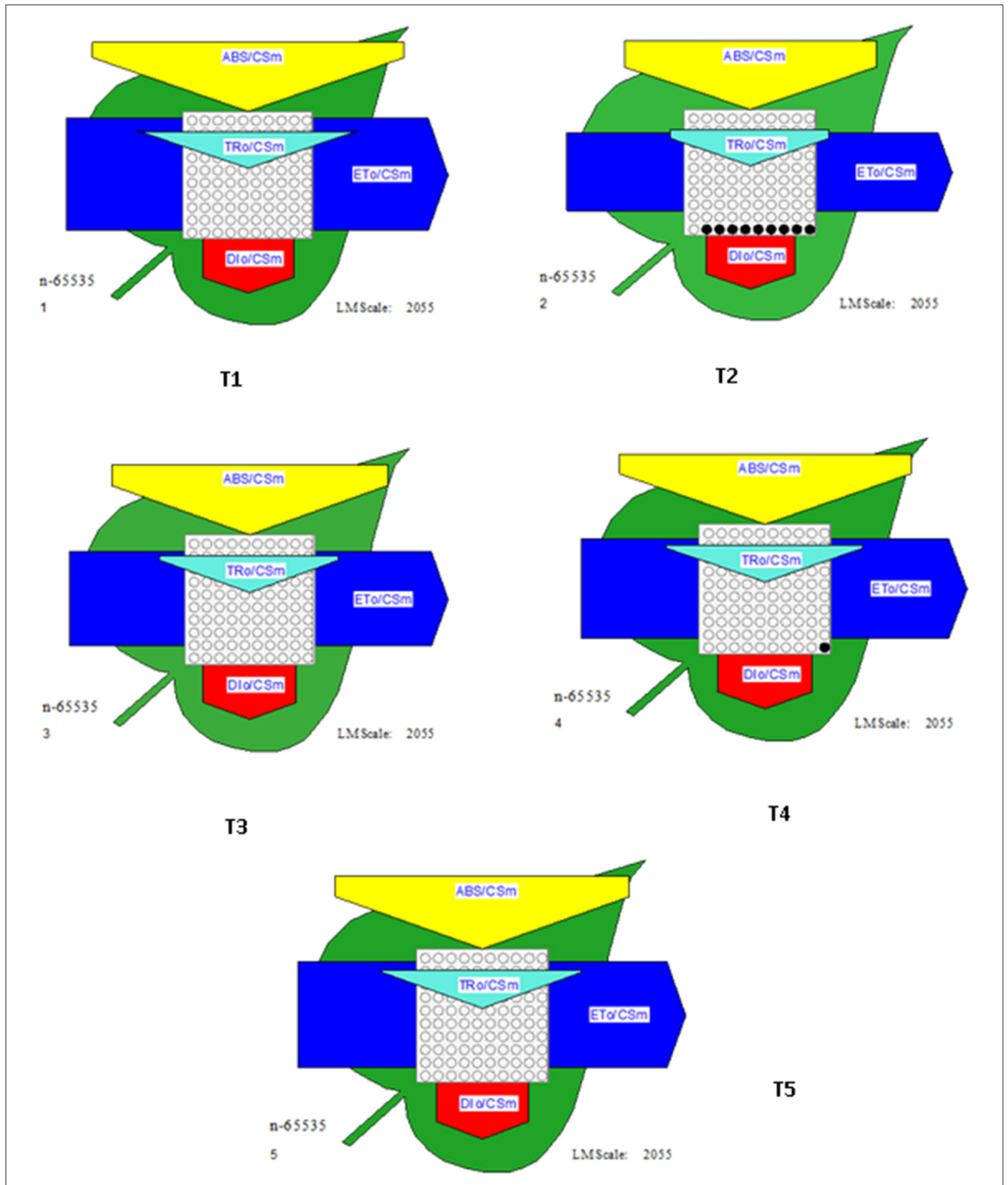
FIGURE 9 | Energy pipeline leaf model showing proportions of phenomenological energy flux parameters within a leaf, calculated per cross-section (CSm) in different treatments. The width of the corresponding arrow denotes the activity of that parameter. Empty and filled black circles indicate the percentage of active and inactive reaction centers of PSII, respectively. ABS/CSm, Absorption per cross section; TRo/CSm, Trapping per cross section; ETo/CSm, electron transport per cross section; Dlo/CSm, Dissipation per cross section.

improving plant growth. However, a better understanding of the impact of these isolates on the genes regulating photosynthesis is required for a more focused approach toward their development as bio-control agents on large scale.

DATA AVAILABILITY STATEMENT

The datasets presented in this study can be found in online repositories. The names of the repository/repositories and accession number(s) can be found below: NCBI (accession: MZ223450 and MZ223454).

AUTHOR CONTRIBUTIONS

HC, AJ, and AP contributed to conception and design of the study. HC organized the database, wrote the manuscript, and performed the statistical analysis. BS wrote sections of the manuscript. All authors contributed to manuscript revision, read, and approved the submitted version.

FUNDING

SUPPLEMENTARY MATERIAL

The Supplementary Material for this article can be found online at: https://www.frontiersin.org/articles/10.3389/fagro.2022.831731/full#supplementary-material

REFERENCES

Allen, D. J., McKee, I. F., Farage, P. K., and Baker, N. R. (1997). Analysis of limitations to CO2 assimilation on exposure of leaves of two *Brassica napus* cultivars to UV-B. *Plant Cell Environ.* 20, 633–640. doi: 10.1111/j.1365-3040.1997.00093.x

Altinok, H. H. (2005). First report of Fusarium wilt of eggplant caused by *Fusarium oxysporum* f. sp. melongenae in Turkey. *Plant Pathol.* 54, 577–577. doi: 10.1111/j.1365-3059.2005.01235.x

Bakker, A. W., and Schippers, B. O. B. (1987). Microbial cyanide production in the rhizosphere in relation to potato yield reduction and *Pseudomonas* spp-mediated plant growth-stimulation. *Soil Biol. Biochem.* 19, 451–457. doi: 10.1016/0038-0717(87)90037-X

Cerkauskas, R. F. (2017). Etiology and management of Fusarium crown and root rot (*Fusarium oxysporum*) on greenhouse pepper in Ontario, Canada. *Can. J. Plant Pathol.* 39, 121–132. doi: 10.1080/07060661.2017.1321044

Chaturvedi, H., and Prakash, A. (2020). "Exploitation of plant tissue Invading Rhizospheric microbes as bio-fertilizers," in *Rhizosphere Microbes*, eds S. K. Sharma, U. B. Singh, P. K. Sahu, H. V. Singh, and P. K. Sharma (Singapore: Springer Nature), 315–329.

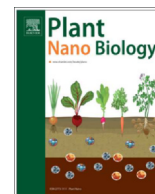Chaturvedi, H., Singh, V., and Gupta, G. (2016). Potential of bacterial endophytes as plant growth promoting factors. *J. Plant Pathol. Microbiol.* 7, 1–6. doi: 10.4172/2157-7471.1000376

De Sain, M., and Rep, M. (2015). The role of pathogen-secreted proteins in fungalvascular wilt diseases. *Int. J. Mol. Sci.* 16, 23970–23993. doi: 10.3390/ijms161023970

Dean, R., Van Kan, J. A. L., Pretorius, Z. A., Hammond-Kosack, K. E., DiPietro, A., Spanu, P. D., et al. (2012). The top 10 fungal pathogens in molecular plant pathology. *Mol. Plant Pathol.* 13, 414–430. doi: 10.1111/j.1364-3703.2011.00783.x

Duniway, J. M., and Slatyer, R. O. (1971). Gas exchange studies on the transpiration and photosynthesis of tomato leaves affected by *Fusarium oxysporum* f. sp. lycopersici. *Phytopathology* 61, 1377–1381. doi: 10.1094/Phyto-61-1377

Eberhard, S., Finazzi, G., and Wollman, F. A. (2008). The dynamics of photosynthesis. *Annu. Rev. Genet.* 42, 463–515. doi: 10.1146/annurev.genet.42.110807.091452

Fisher, M. C., Henk, D. A., Briggs, C. J., Brownstein, J. S., Madoff, L. C., McCraw, S. L., et al. (2012). Emerging fungal threats to animal, plant and ecosystem health. *Nature* 484, 186–194. doi: 10.1038/nature10947

Glick, B. R. (1995). The enhancement of plant growth by free-living bacteria. *Can. J. Microbiol.* 41, 109–117. doi: 10.1139/m95-015

Goltsev, V. N., Kalaji, H. M., Paunov, M., Baba, W., Horaczek, T., Mojski, J., et al. (2016). Variable chlorophyll fluorescence and its use for assessing physiological condition of plant photosynthetic apparatus. *Russ. J. Plant Physiol.* 63, 869–893. doi: 10.1134/S1021443716050058

Gupta, G., Chaturvedi, H., Snehi, S. K., and Prakash, A. (2019). *Role of Plant Growth Promoting Rhizobacteria (PGPR) for Improvement of Sustainable Agriculture in Plant Growth Promoting Microorganisms: Microbial Resources for Enhanced Agricultural Productivity*, eds S. R. Niranjan and A. C. Udayashankar. Hauppauge, NY: Nova Publisher.

Gupta, G., Parihar, S. S., Ahirwar, N. K., Snehi, S. K., and Singh, V. (2015). Plant growth promoting rhizobacteria (pgpr): current and future prospects for development of sustainable agriculture. *J. Microb. Biochem. Technol.* 7,096–102. doi: 10.4172/1948-5948.1000188

Hallmann, J., Quadt-Hallmann, A., Mahaffee, W. F., and Kloepper, J. W. (1997). Bacterial endophytes in agricultural crops. *Can. J. Microbiol.* 43, 895–914. doi: 10.1139/m97-131

Howell, C. R. (2003). Mechanisms employed by Trichoderma species in the biological control of plant diseases: the history and evolution of current concepts. *Plant Dis.* 87, 4–10. doi: 10.1094/PDIS.2003.87.1.4

Kulimushi, S. M., Muiru, W. M., and Mutitu, E. W. (2021). Potential of Trichoderma spp., Bacillus subtilis and Pseudomonas fluorescens in the management of early blight in tomato. *Biocontrol Sci. Technol.* 31, 1–12. doi: 10.1080/09583157.2021.1900784

Li, T., Hu, Y., Du, X., Tang, H., Shen, C., and Wu, J. (2014). Salicylic acid alleviates the adverse effects of salt stress in *Torreya grandis* cv. Merrillii seedlings by activating photosynthesis and enhancing antioxidant systems. *PLoS ONE* 9, e109492. doi: 10.1371/journal.pone.0109492

López-Aranda, J. M., Domínguez, P., Miranda, L., de los Santos, B., Talavera, M., Daugovish, O., et al. (2016). Fumigant use for strawberry production in Europe: the current landscape and solutions. *Int. J. Fruit Sci.* 16, 1–15. doi: 10.1080/15538362.2016.1199995

López-Martínez, R., Hernández-Hernández, F., Bazán-Moraand, E., and Castañón-Olivares, L. R. (1999). Comparative study of two culture conservation methods in medical mycology. *World J. Microbiol. Biotechnol.* 15, 471–474. doi: 10.1023/A:1008983217783

Lorenzini, G., Guidi, L., Nali, C., Ciompi, S., and Soldatini, G. F. (1997). Photosynthetic response of tomato plants to vascular wilt diseases. *Plant Sci.* 124, 143–152. doi: 10.1016/S0168-9452(97)04600-1

Mahmood, T., Mehnaz, S., Fleischmann, F., Ali, R., Hashmi, Z. H., and Iqbal, Z. (2014). Soil sterilization effects on root growth and formation of rhizosheaths in wheat seedlings. *Pedobiologia* 57, 123–130. doi: 10.1016/j.pedobi.2013.12.005

Maliba, B. G., Inbaraj, P. M., and Berner, J. M. (2019). Photosynthetic responses of canola and wheat to elevated levels of CO2, O3 and water deficit in open-top chambers. *Plants* 8, 171. doi: 10.3390/plants8060171

Mates, A. D. P. K., de Carvalho Pontes, N., and de Almeida Halfeld-Vieira, B. (2019). *Bacillus velezensis* GF267 as a multi-site antagonist for the control of tomato bacterial spot. *Biol. Control* 137, 104013. doi: 10.1016/j.biocontrol.2019.104013

Mathur, S., Jain, L., and Jajoo, A. (2018). Photosynthetic efficiency in sun and shade plants. *Photosynthetica* 56, 354–365. doi: 10.1007/s11099-018-0767-y

Midhun, S. J., Neethu, S., Vysakh, A., Sunil, M. A., Radhakrishnan, E. K., and Jyothis, M. (2017). Antibacterial activity of autochthonous bacteria isolated from *Anabas testudineus* (Bloch, 1792) and it's *in vitro* probiotic characterization. *Microb. Pathog.* 113, 312–320. doi: 10.1016/j.micpath.2017.10.058

Mosahaneh, L., Charehgani, H., Abdollahi, M., and Rezaei, R. (2021). Biological control agents in the management of different initial population densities of *Meloidogyne javanica* in tomato. *Acta Phytopathol. Entomol. Hung.* 55, 151–159. doi: 10.1556/038.55.2020.016

Myo, E. M., Liu, B., Ma, J., Shi, L., Jiang, M., Zhang, K., et al. (2019). Evaluation of *Bacillus velezensis* NKG-2 for bio-control activities against fungal diseases and potential plant growth promotion. *Biol. Control* 134, 23–31. doi: 10.1016/j.biocontrol.2019.03.017

Nelson, P. E. (1981). Chapter 3 - life cycle and epidemiology of *Fusarium oxysporum*. *Fungal Wilt. Dis. Plants* 51–80. doi: 10.1016/B978-0-12-464450-2.50008-5

Nogués, S., Cotxarrera, L., Alegre, L., and Trillas, M. I. (2002). Limitations to photosynthesis in tomato leaves induced by Fusarium wilt. *New Phytol.* 154, 461–470. doi: 10.1046/j.1469-8137.2002.00379.x

Pacheco, I., Ferreira, R., Correia, P., Carvalho, L., Dias, T., and Cruz, C. (2021). Microbial consortium increases maize productivity and reduces grain phosphorus concentration under field conditions. *Saudi J. Biol. Sci.* 28, 232–237. doi: 10.1016/j.sjbs.2020.09.053

Papageorgiou, G. C. (2012). "Fluorescence emission from the photosynthetic apparatus," in *Photosynthesis* (Dordrecht: Springer), 415–443.

Patil, S., Sriram, S., and Savitha, M. J. (2011). Evaluation of non-pathogenic Fusarium for antagonistic activity against Fusarium wilt of tomato. *Biol. Control* 25, 118–123.doi: 10.18311/jbc/2011/3739

Pedrosa, F. O., Monteiro, R. A., Wassem, R., Cruz, L. M., Ayub, R. A., Colauto, N. B., et al. (2011). Genome of Herbaspirillum seropedicae strain SmR1, a specialized diazotrophic endophyte of tropical grasses. *PLoS genetics* 7, e1002064.

Pérez-Patricio, M., Camas-Anzueto, J. L., Sanchez-Alegría, A., Aguilar-González, A., Gutiérrez-Miceli, F., Escobar-Gómez, E., et al. (2018). Optical method for estimating the chlorophyll contents in plant leaves. *Sensors* 18, 650. doi: 10.3390/s18020650

Renwick, A., Campbell, R., and Coe, S. (1991). Assessment of *in vivo* screening systems for potential biocontrol agents of Gaeumannomycesgraminis. *Plant Pathol.* 40, 524–532. doi: 10.1111/j.1365-3059.1991.tb02415.x

Saeed, I. A. M., MacGuidwin, A. E., Rouse, D. I., and Sharkey, T. D. (1999). Limitation to photosynthesis in *Pratylenchus penetrans*- and *Verticillium dahliae*-infected potato. *Crop Sci.* 39, 1340–1346. doi: 10.2135/cropsci1999.3951340x

Schwyn, B., and Neilands, J. B. (1987). Universal chemical assay for the detection and determination of siderophores. *Anal. Biochem.* 160, 47–56. doi: 10.1016/0003-2697(87)90612-9

Shabanamol, S., Sreekumar, J., and Jisha, M. S. (2017). Bioprospecting endophytic diazotrophic Lysinibacillussphaericus as biocontrol agents of rice sheath blight disease. *3 Biotech* 7, 1–11. doi: 10.1007/s13205-017-0956-6

Singh, V. K., Singh, H. B., and Upadhyay, R. S. (2017). Role of fusaric acid in the development of 'Fusarium wilt' symptoms in tomato: physiological, biochemical and proteomic perspectives. *Plant Physiol. Biochem.* 118, 320–332. doi: 10.1016/j.plaphy.2017.06.028

Smibert, R. M., Krieg, N. R., Gerhardt, P., Murray, R., and Wood, W. (1994). *Methods for General and Molecular Bacteriology*. Washington, DC: American Society for Microbiology, 607–654.

Souza, L. T., Michereff, S. J., Laranjeira, D., Andrade, D. E., Ferraz, E., Lima, G. S., et al. (2010). Reaction of tomato genotypes to races 2 and 3 of *Fusarium oxysporum* f. sp. lycopersici. *Hortic. Bras.* 28, 102–106. doi: 10.1590/S0102-05362010000100019

Sturz, A. V., Christie, B. R., and Matheson, B. G. (1998). Associations of bacterial endophyte populations from red clover and potato crops with potential for beneficial allelopathy. *Can. J. Microbiol.* 44, 162–167. doi: 10.1139/w97-146

Sturz, A. V., Christie, B. R., and Nowak, J. (2000). Bacterial endophytes: potential role in developing sustainable systems of crop production. *CRC. Crit. Rev. Plant Sci.* 19, 1–30. doi: 10.1080/07352680091139169

Takken, F. L. W., and Rep, M. (2010). The arms race between tomato and *Fusarium oxysporum*. *Mol. Plant Pathol.* 11, 309–314. doi: 10.1111/j.1364-3703.2009.00605.x

Tomar, R. S., and Jajoo, A. (2013). A quick investigation of the detrimental effects of environmental pollutant polycyclic aromatic hydrocarbon fluoranthene on the photosynthetic efficiency of wheat (*Triticum aestivum*). *Ecotoxicology* 22, 1313. doi: 10.1007/s10646-013-1118-1

Xia, Y., DeBolt, S., Dreyer, J., Scott, D., and Williams, M. A. (2015). Characterization of culturable bacterial endophytes and their capacity to promote plant growth from plants grown using organic or conventional practices. *Front. Plant Sci.* 6, 490. doi: 10.3389/fpls.2015.00490

Yendyo, S., Ramesh, G. C., and Pandey, B. R. (2017). Evaluation of *Trichoderma* spp., Pseudomonas fluorescens and *Bacillus subtilis* for biological control of Ralstonia wilt of tomato. *F1000Research* 6:2028. doi: 10.12688/f1000research.12448.1

ELSEVIER

SiO₂ nanopriming protects PS I and PSII complexes in wheat under drought stress

Prabha Rai Kalal[a], Rupal Singh Tomar[a], Anjana Jajoo[a,b,*]

[a] *School of Life Sciences, Devi Ahilya University, Indore, India*
[b] *School of Biotechnology, Devi Ahilya University, Indore, India*

A B S T R A C T

Drought is an important abiotic stress that hampers the growth of plants by inhibiting photosynthesis resulting in major crop losses. Silicon is known for its role to alleviate impact of various abiotic stresses in plants. In the present study, drought sensitive wheat variety HI-1544 was subjected to drought stress (DS) by withholding irrigation. The aim of this study was to evaluate the impact of SiO₂ nanopriming in protecting photosynthesis, particularly photosystems (PSI and PSII), under drought condition. DS significantly reduced the quantum yield of PSII (YII) and PSI (YI) in unprimed drought stressed (UP + DS) plants but non-significant reduction was observed in NP + DS wheat plants. Likewise a severe impairment in the electron transport rate of PSII and PSI (ETRII and ETRI) in UP + DS was noticed as compared to NP + DS plants. Among energy dissipation parameters, regulated and non-regulated energy dissipation [Y(NPQ) and Y(NO) respectively] showed prominent increase in UP + DS plants when compared to NP + DS wheat plants. Decrease in YI was accompanied by significant increase in donor Y(ND) and acceptor side Y(NA) limitation of PSI in UP + DS plants. These parameters were less affected in NP + DS wheat plants. A remarkable inhibition in the oxidation reduction kinetics of P700 was observed in UP + DS plants while it were less affected in NP + DS wheat plants. The data suggests that the impact of drought stress (DS) was more prominent on PSII than PSI. SiO₂ nanopriming conferred more protection to PSII complex, thereby improving photosynthetic efficiency under DS.

1. Introduction

The ever changing environmental conditions have resulted in various abiotic stress conditions exhibiting major impact on global vegetation and crop productivity. Drought is amongst the prime abiotic stress that has affected crop productivity in agricultural lands worldwide (Waraich et al., 2011). Looking at the current trend of increasing population and changing climatic conditions, majority of regions will be facing chronic shortage of freshwater to satisfy agricultural requirements. The problem will intensify in near future resulting in major crop losses each year.

A prolonged period of drought has major impact on developmental process and metabolism ultimately affecting growth of the plant (Dhakal, 2021). Prominent effect of water stress is seen on plant photosynthesis which is one of the important phenomenon for plant growth (Ashraf and Harris, 2013). Impact of drought stress on light harvesting, rate of electron transport and dark reactions may result in overall reduction in photosynthesis. Drought stress results in substantial damage

to photosynthetic pigments and deterioration of thylakoid membranes (Kannan and Kulandaivelu, 2011). Moreover, stomatal closure under drought stress limits carbon dioxide (CO₂) uptake in leaves thereby inhibiting the process of CO₂ reduction and accumulation of reduced photosynthetic electron transport components (Wahid and Rasul, 2005). The accumulation of these compounds reduce molecular oxygen leading to overproduction of reactive oxygen species (ROS) such as superoxide and hydroxyl radicals as well as H₂O₂ provoking oxidative damage to the photosynthetic apparatus (Fahad et al., 2017). Explicitly, ROS accumulation is related to severe damage caused to both photosystems (PSI and PSII) in chloroplasts hampering the cyclic as well as noncyclic electron transport (Abdelmoneim et al., 2014). It ultimately affects the synthesis of ATP and NADPH, thereby retarding overall photosynthesis (Teskey et al., 2015).

Developing drought tolerance in crop varieties might be a promising approach to tackle this problem. One of such approaches is seed nanopriming. Priming is a pre-sowing treatment technique that regulates biochemical and physiological processes of seeds for enhancing

---

germination and mitigation of stress (Rai-Kalal et al., 2021; Sherin et al., 2022). Nanomaterials have range of applications and a great potential to contribute to the agricultural revolution. Various nano-formulations in the form of nanofertilizer, nanopesticides, nanoherbicides are being used to enhance agricultural productivity and to lower the impact of chemical based products on agriculture and environment (Mahakham et al., 2017). These effects depend on the physico-chemical properties of nanoparticles such as size, zeta potential, and concentration of nanoparticles which play a key role in their uptake and translocation in plants (Nile et al., 2022). Previous studies have reported application of various metal based nanoparticles including Zn, Fe, Ag, Hg etc. (Mahakham et al., 2017) to enhance crop performance and improved yield. In our recent work, nanopriming of seeds to enhance germination rate, germination synchronization, and seedling growth was reported (Rai-Kalal and Jajoo, 2021; Pereira et al., 2021). However effect of seed nanopriming in enhancing abiotic stress tolerance potential in plants remains unexplored. Very few nanomaterials have been tested so far for their ability to induce tolerance to abiotic stress.

Silicon (Si) is known to be a part of non-essential element for higher plants. The beneficial role of silicon in growth and development has been observed in some of the plant species including rice (Song et al., 2014). However, there are many studies reporting the role of silicon in ameliorating various abiotic and biotic stresses in plants indicating its protective role (Rastogi et al., 2021). Studies report that Si acts as a plant protectant and bio stimulant maintaining hormonal homeostasis, balancing the osmotic potential and adjusting the antioxidants machinery to keep a check on ROS content under wide range of abiotic stresses (Hameed et al., 2021). Although silicon is present in bulk form in abundance in soil, plants lack ability of Si uptake from soil which is further reflected in physiological and yield traits of the plant (Souri et al., 2021). Therefore uptake of silicon by plants in nanoform may be a better option.

The above facts invoked our interest to evaluate the effect of increasing silicon availability to plants via seed nanopriming. In our previous study, we have reported effects of SiO_2 NPs as seed priming agent in improving wheat seed quality in terms of improved germination and seedling growth and enhanced seedling vigor (Rai-Kalal et al., 2021). Drought stress has a major impact on plant photosynthesis inhibiting the normal functioning of the two photosystems. A fine tuning of working of both photosystem is essential for plant to perform optimum photosynthesis. However, role of Si nanopriming on wheat plant photosynthetic apparatus under water stress conditions remains unexplored. Considering these aspects, we hypothesize that SiO_2 nanopriming alleviates the effect of drought stress in nanoprimed plants by maintaining the photosynthetic efficiency of plants and protecting plant photosynthetic machinery (mainly photosystem I and photosystem II) from oxidative damage when subjected to drought stress. To our knowledge the present work is the first attempt to study the impact of seed priming Si nanoparticles on plant photosynthetic apparatus focusing on relative performance of the two photosystems under drought stress.

2. Materials and methods

2.1. Priming of wheat seeds with SiO_2 nanoparticles

Wheat seeds HI-1544, a drought sensitive cultivar, was obtained from IARI (Indian Agriculture research institute) Indore. Silicon oxide nanoparticles (SiO_2 NPs) were procured from Nano Research Lab, Jamshedpur, having size range of 20–30 nm. All the chemicals required in this study are analytical grade purchased from Sigma and HiMedia. Seeds were primed with SiO_2 NPs. Additionally to study the significance of using Si in nanoform as priming agent, another set of seeds were primed with Bulk SiO_2 following (Rai-Kalal and Jajoo, 2021). Briefly, 50 wheat seeds were primed by soaking the seeds in nanoparticle solution (15 mg/L). The seeds were kept for continuous agitation for 12 h

of priming time (Rai-Kalal et al., 2021). After the priming these seeds were given repeated wash with distilled water and air dried to bring them back to their original moisture content. For comparison, unprimed (UP) seeds were taken as control.

2.2. Staining of internalized SiO_2 nanoparticles using methyl red (MR)

To study the internalization of Si NPs in nanoprimed wheat seeds, methyl red (MR) dye staining method by Dayanandan et al. (1983) was followed. According to this, MR makes a red color complex with silanol group. Briefly, 1 g of primed and unprimed seeds was rinsed in water followed by 1 min wash with 1% HCl to remove surface bound impurities. When dissolved in benzene, MR appears colorless. When adsorbed by silica; MR imparts a dark red color. Seed samples of approximately 1 g were cut into halves placed in glass test tubes, and the sample were stained with 5 ml of methyl red in benzene for 30 min in freshly prepared 0.1% MR solution in benzene. Samples were then incubated for 30 min for color development (Images shown in Supplementary Fig. S1).

2.3. Determination of hydrolytic enzyme activity in nanoprimed wheat seeds

2.3.1. α-Amylase activity
In seeds germinated for 72 h, the activity of α-amylase (as mg starch hydrolyzed h^{-1} protein mg $^{-1}$) was measured following the method described in Sawhney et al. (1970).

2.3.2. Protease activity
In seeds germinated for 72 h, activity of protease enzyme (as mg protein hydrolyzed g^{-1} fresh weight) was measured as described by Kunitz (1947).

2.4. Determination of soluble sugar content

The total soluble sugars were estimated by following the method of Hedge and Hofreiter(1962).

2.5. Effect of drought stress on quantum efficiency of PSI and PSII in nanoprimed wheat plants

2.5.1. Drought stress application
Pot experiments were conducted to study the effect of drought stress on wheat plants. For growing wheat, black garden soil mixed with sand in the ratio 3:1 was used. Pots were kept in natural sunlight in open to subject them to natural field conditions. The temperature conditions during experimental days (January) had maximum day temperature around 25 °C. In the beginning, plants were kept fully irrigated. Drought stress (DS) was given after 20 days of germination. Relative soil water content was measured as described by (Pebriansyah et al., 2012). In DS plants, after 10 days, relative soil water content was reduced to 20% as that of control. In order to understand significance of using nano-Si for priming in enhancing drought tolerance, additional pot experiments with Bulk Si were also conducted. Experimental setup mainly consisted of fully irrigated unprimed (UP + W), irrigated nano-primed (NP + W), and irrigated Bulk primed (Bulk + W) plants including drought stressed unprimed (UP + DS), drought stressed nanoprimed (NP + DS) and drought stressed Bulk (Bulk + DS) wheat plants. Fully irrigated unprimed wheat (UP + W) plants were considered as control.

2.5.2. Relative water content (RWC)
RWC in wheat leaf was determined following Ashkavand et al. (2015) following equation.

RWC = (Wf– Wd /Wt– Wd)× 100

W_f: fresh weight of leaf, W_t: leaf turgid weight, W_d: leaf dry weight.

Table 1

Chlorophyll fluorescence measurements using Dual-PAM100 (Tomar and Jajoo, 2014).

Parameters	Description
Y(II)	Effective quantum yield of PSII
Y(I)	Effective quantum yield of PSI
ETR(I)	PSI electron transport rate
ETR(II)	PSII electron transport rate
NPQ	Non-photochemical quenching or Quantum Yield of regulated energy dissipation
Y(NO)	Quantum yield of non-regulated dissipation of energy in PSI
Y(NA)	Fraction of total P700 that cannot be oxidized due to lack of acceptors
Y(ND)	Fraction of total P700 that is oxidized due to donor-side limitation

These were measured after keeping leaves in oven at 60 °C for 48 h.

2.5.3. Measurement of energy conversion of PSI and PSII in drought stressed nanoprimed wheat plants

Quantum yields of energy conversion in PSI and PSII were measured by saturation pulse (SP) technique using Pulse Amplitude Modulated system (Dual-PAM-100, Walz, Germany) in intact leaves of wheat plants. The protocol as described in (Klughammer and Schreiber, 1994; Kalaji et al., 2016; Nath et al., 2017) was followed. Description of some of the parameters of PSI and PSII obtained from using DUAL-PAM100 are listed in Table 1.

2.5.4. Oxidation-reduction kinetics of P700

To calculate redox state of P700, the light induced changes in absorption at 830–875 nm (ΔA830–875) were measured by dual wavelength unit connected via Dual- PAM-100 (Walz) (Nath et al., 2016). Single-turnover (ST, 14 µs) and multiple-turnover (MT, 50 ms) saturating flashes were used for calculation of the pool size of intersystem electrons on P700 reaction centre (Ivanov et al., 2006). The half-life of P700 re-reduction ($t_{1/2}$) was calculated with Origin 8.0 (Origin Lab Corporation).

2.6. Data analysis

Data were analyzed using Graphpad Prism 5.01 Software (GraphPad Software, Inc.). Results were analyzed using one-way ANOVA and then Duncans test to determine significance between mean value. Significance was determined at $p < 0.01$ (* $p < 0.05$, ** $p < 0.01$, and *** $p < 0.001$). The results are shown as mean values and standard deviation (SD). All the measurements were carried out three times in triplicate. Different alphabets indicate significant difference among treatments.

3. Results

3.1. Staining of SiO₂ nanoparticles in nanoprimed seeds

Methyl red (MR) was used for silica staining in plants. When dissolved in benzene, MR appears light yellow-orange in color, while when adsorbed by silica MR imparts red color (Nondek et al., 1986). Results showed formation of intense red colored complex in nanoprimed and Bulk SiO_2 primed wheat seeds. No color change was formed in unprimed seeds which can be correlated with presence of Si in nanoprimed seeds and its absence in unprimed seeds (results shown as Supplementary Fig. S1).

3.2. Determination of hydrolytic enzyme activity and soluble sugar content

Effect of SiO_2 NP priming on hydrolytic enzyme activity and total soluble sugar content in 72 h germinated UP, NP and Si Bulk primed wheat seeds are shown in Table 2. An increase in the activity of seed hydrolytic enzymes was observed in nanoprimed wheat seeds. Activity of α- amylase showed a significant increase by 80% followed by a prominent increase by 57% in protease activity in nanoprimed wheat seeds as compared to control. On the contrary, the activity of both amylase and protease increased by only 25% and 28% respectively in Bulk SiO_2 primed wheat seeds. Further, effect of nanopriming on starch metabolism in seeds was also evaluated in terms of total soluble sugar content. The results showed 73% increase in the total soluble sugar content of nanoprimed seed whereas an increase of only 18% was observed in Bulk SiO_2 primed seeds, as compared to control.

3.3. Effect of drought stress on relative water content (RWC) of leaves

Drought stress results in a drastic reduction in relative water content of plant leaves. Table 3 shows RWC in fully irrigated and drought stressed wheat leaves. NP + W wheat leaves showed maximum RWC (95%) as compared to UP + W (84%) and Bulk + W (86%)wheat leaves. Subjecting to DS significantly changed the leaf water status. RWC in UP + DS leaves were reduced to 48% followed by a prominent decrease in Bulk + DS plant leaves to 66%. However, RWC in NP + DS was 73% which was comparatively better in comparison to UP + DS wheat leaves.

3.4. Effect of drought stress on quantum yield of PSI and PSII

Effect of drought stress on the efficiency of energy conversion of PSI and PSII in UP + DS, NP + DS, Bulk + DS wheat plants was monitored using Saturation Pulse (SP) method. Optimum plant performance requires a balance in the rate of energy conversion processes of PSII and PSI. The study of Chl *a* fluorescence yield parameters relates to the distribution of the absorbed energy between its utilization for photosynthesis and wastage in the form of heat (regulated and non-regulated). The amplitude of Fm and Pm which represents maximum activity of PSII and PSI respectively was significantly increased in NP + W as compared to control (Fig. 1). Exposure of wheat plants to 10 days of drought conditions drastically affected Fm. Fm was significantly reduced being minimum in UP + DS plants (57% reduction) while showing only 10% reduction in NP + DS plants when compared with UP + W wheat plants (Fig. 1). The amplitude of Pm representing the quantity of maximum photo-oxidisable P700 (Fu and Huang 2001) is considered one of the most reliable parameters to measure the amount of efficient PSI complexes. Pm was attained maximum for NP + W compared to UP + W and Bulk + W wheat plants. However in response to DS, Pm dropped significantly in UP + DS plants (reduced by 55%)

Table 2

Effect of priming on activity of α-amylase, protease and soluble sugar content of UP (unprimed), NP (nanoprimed) and Bulk (SiO₂ Bulk primed) wheat seedlings. Statistical details as explained in M & M.

Treatment	α-Amylase (mg starch hydrolyzed h⁻¹ protein mg⁻¹)	Protease (unit/mg protein)	Soluble sugar (mg/g fresh weight)
UP	19.34 ± 0.1[c]	0.43 ± 0.02[c]	2.2 ± 0.01[c]
NP	34.8 ± 0.2[***a]	0.69 ± 0.03[***a]	3.8 ± 0.01[***a]
Bulk	24.19 ± 0.3[***b]	0.54 ± 0.02[***b]	2.6 ± 0.02[***b]

Table 3
Effect of drought stress on leaf relative water content (RWC) in control (UP + W), nanoprimed irrigated (NP + W), Bulk SiO$_2$ primed irrigated (Bulk + W), unprimed drought (UP + DS), nanoprimed drought (NP + DS) and Bulk SiO$_2$ primed drought stressed (Bulk + DS) wheat plants. Statistical details given in M & M.

Treatment	Fresh weight (g)	Turgid weight (g)	Dry weight (g)	RWC (%)
UP + W	0.219 ± 0.03[b]	0.275 ± 0.02[b]	0.028 ± 0.02[c]	84 ± 0.7[b]
NP + W	0.305 ± 0.01[***a]	0.317 ± 0.02[***a]	0.039 ± 0.01[***a]	95 ± 0.5[***a]
Bulk + W	0.211 ± 0.02[nsb]	0.240 ± 0.03[***c]	0.026 ± 0.01[nsc]	86 ± 0.5[nsb]
UP + DS	0.144 ± 0.03[***]	0.245 ± 0.03[***c]	0.023 ± 0.04[***d]	48 ± 0.4[***e]
NP + DS	0.237 ± 0.02[***b]	0.314 ± 0.02[***a]	0.033 ± 0.03[***b]	73 ± 0.7[***c]
Bulk + DS	0.193 ± 0.03[***c]	0.265 ± 0.02[nsb]	0.020 ± 0.03[***d]	66 ± 0.5[***d]
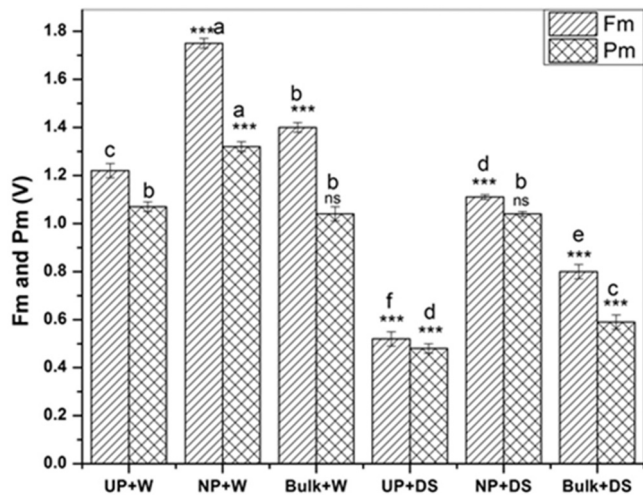
Fig. 1. Effect of drought stress on maximum fluorescence (Fm) and maximal change in P700 (Pm) signal in UP + W (unprimed irrigated), NP + W (nanoprimed irrigated), Bulk + W (Bulk irrigated), UP + DS (unprimed drought), NP + DS (nanoprimed drought) and Bulk + DS (Bulk drought) wheat plants. Statistical details given in M & M.

while showing non-significant change in NP + DS compared to control plants.

The quantum yield efficiency (YII and YI) and electron transport rate (ETRII and ETRI) of PSII and PSI in irrigated UP + W (control), NP + W, Bulk + W and drought stressed UP + DS, NP + DS and Bulk + DS wheat plants is shown in Figs. 2,3. The quantum yield efficiency of both PSII (YII) and PSI (YI) were significantly enhanced in NP + W as

compared to UP + W and Bulk + W primed wheat plants. Likewise, the measurement of electron transport around PSII (ETR II) and PSI (ETRI) also showed a prominent increased in NP + W wheat plants as compared to UP + W control. However, exposure to DS, resulted in a prominent decrease in YII and YI in all the drought stressed plants compared to UP + W wheat plants. Results obtained show a drastic reduction in Y(II) parameters in UP + DS plants followed by significant decrease in Bulk + DS wheat plants. Decrease in YII was further accompanied by a simultaneous increase in Y(NO) and Y(NPQ) representing non-regulated and regulated energy dissipation in UP + DS wheat plants Fig. 4. On the contrary, damage in YII was non-significant in NP + DS wheat plants. Lower reduction in YII in NP + DS plants resulted in considerably non-significant change in Y(NO) followed by lesser increase in Y(NPQ) in NP + DS plants in comparison to UP + DS.

Likewise, Y(I) representing the quantum yield efficiency of PSI was reduced in UP + DS wheat plants (Fig. 2). In UP + DS plants decrease in YI was followed by significant increase in Y(ND) and Y (NA) representing the quantum yield of non-photochemical energy dissipation caused by donor side limitation and acceptor side limitation respectively as compared to control UP + W plants (Fig. 5). However, in NP + DS plants reduction under DS was non-significant followed by non-significant reduction Y(NA) and considerably lesser reduction in Y(ND) than in UP + DS wheat plants. Further, the rate of electron transport was down regulated due to DS. A dramatic decline in ETRI and ETRII was observed in UP + DS and Bulk + DS wheat plants but less decline in NP + DS plants was observed as compared to UP + W wheat plants.

3.5. Effect of drought stress on P700 redox kinetics

Efficiency of energy conversion of PS I can be estimated the redox state of PSI reaction center (P700) which can be measured by noting absorbance
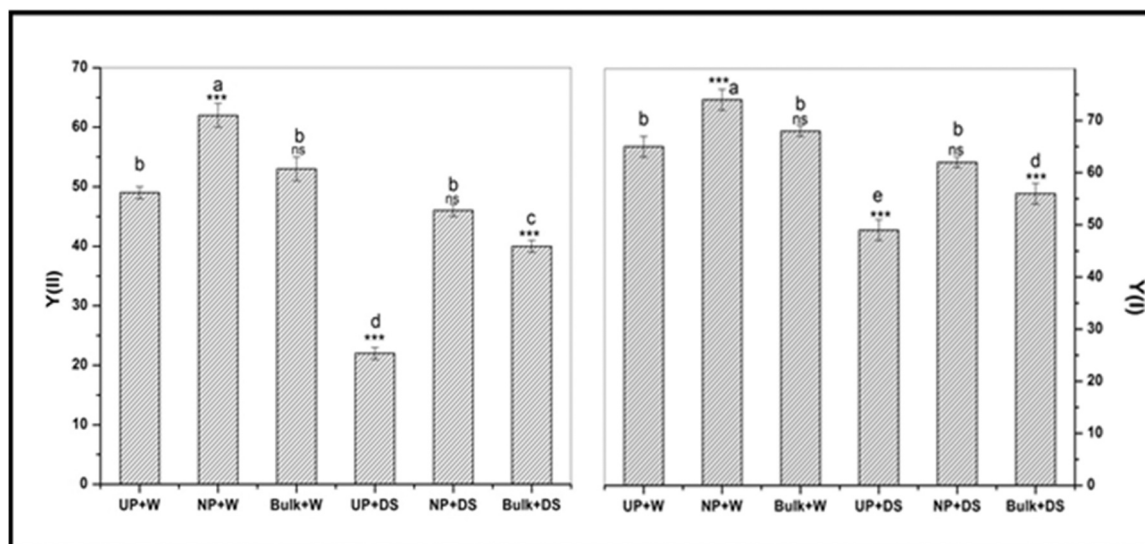
Fig. 2. Effect of drought stress on quantum yield of PSII (YII) and PSI (YI) in UP + W (unprimed irrigated); (NP + W) (nanoprimed irrigated); Bulk + W (Bulk irrigated); UP + DS (unprimed drought); NP + DS (nanoprimed drought) and Bulk + DS (Bulk drought) stressed wheat plants. Statistical details given in M & M.
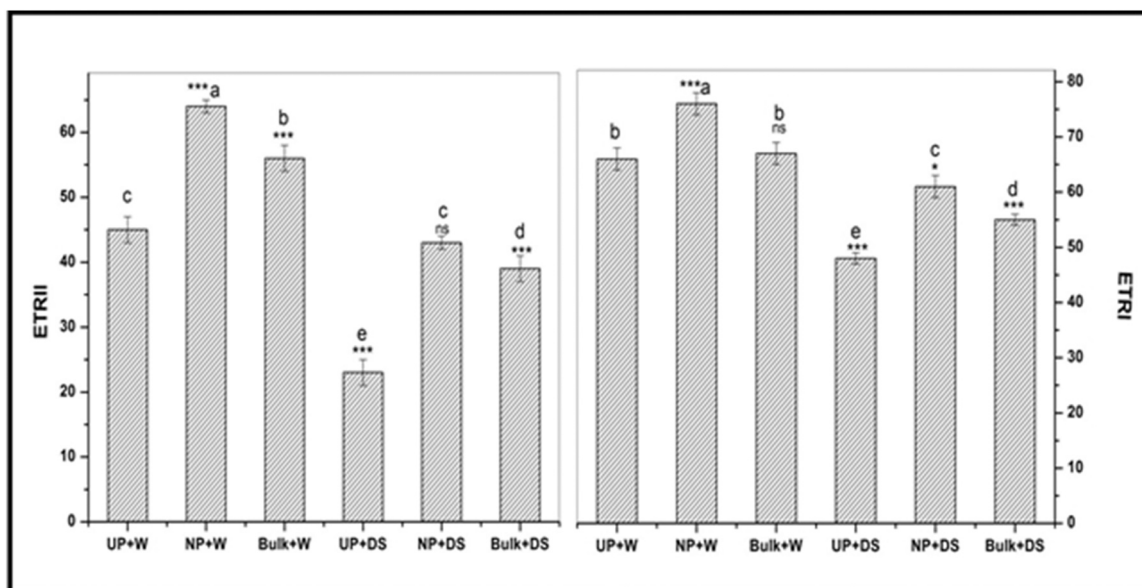
Fig. 3. Effect of drought stress on electron transport rate of PSII (ETRII) and PSI (ETRI) in UP + W (unprimed irrigated); NP + W (nanoprimed irrigated); Bulk + W (Bulk irrigated); UP + DS (unprimed drought); NP + DS (nanoprimed drought) and Bulk + DS (Bulk drought) stressed wheat plants. Statistical details given in M & M.

change caused by $P700^+$ cation-radical between 830 and 875 nm (Klughammer and Schreiber, 1994).Table 4 shows absorbance change at $\Delta A_{830-875}$ after application of FR (far red light) in wheat leaves in response to DS. In fully irrigated wheat plants the rise of absorbance at $\Delta A_{830-875}$ nm was very high. The amplitude of absorbance change at $\Delta A_{830-875}$ reached highest in NP + W followed by Bulk + W and UP + W wheat leaves.

As an effect of DS, $\Delta A_{830-875}$ showed drastic decline in UP + DS (reduced by 57%) and Bulk + DS (reduced by 53%) wheat plants as compared to UP + W plants. However, the observed reduction in $\Delta A_{830-875}$ was less in NP + DS (by only 36%) wheat plants. Further, the intersystem electron pool size of PSI was estimated by the application of ST and MT flashes in control and DS plants. The value of MT: ST area was found to be minimum in all irrigated wheat plants however, showing maximum increase in UP + DS plants. In NP + DS plants this ratio was showed non-significant changes compared to that of control.

Further, the kinetics of $P700^+$ re-reduction with a half-life ($t_{1/2}$) is represented in Table 4. The $t_{1/2}$ value for control plants UP + W was observed to be 0.88 s which was 0.76 s for NP + W plants. As an effect of DS $t_{1/2}$ values were increased to 0.99 s in both UP + DS and Bulk + DS plants, while no significant change in NP + DS wheat plants respectively as compared to UP + W wheat plants.

4. Discussion

The potential effects of SiO_2 nanoparticles as seed priming agent in enhancing various seed germination parameters including increased germination percentage, seedling length and seedling vigor in nano-primed wheat seeds are already been reported (Rai-Kalal et al., 2021). This increase can be explained based on a hypothetical mechanism proposing penetration of nanoparticles in seed coat by creating small
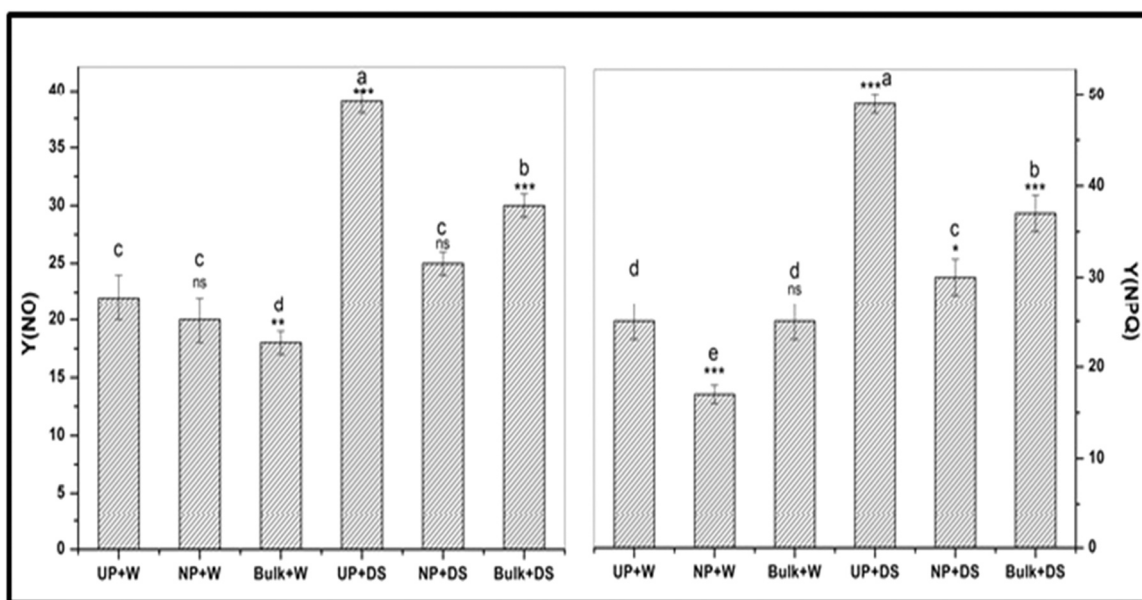
Fig. 4. Effect of drought stress on the quantum yield of non-regulated energy dissipation Y(NO) and the quantum yield of regulated energy dissipation Y(NPQ) in UP + W (unprimed irrigated); NP + W (nanoprimed irrigated); Bulk + W (Bulk irrigated); UP + DS (unprimed drought); NP + DS (nanoprimed drought) and Bulk + DS (Bulk drought) stressed wheat plants. Statistical details given in M & M.

Fig. 5. Effect of drought stress on the quantum yield of non-photochemical energy dissipation due to acceptor side limitation Y(NA) and the quantum yield of non-photochemical energy dissipation due to donor side limitation Y(ND) in UP + W (unprimed irrigated); NP + W (nanoprimed irrigated); Bulk + W (Bulk irrigated); UP + DS (unprimed drought); NP + DS (nanoprimed drought) and Bulk + DS (Bulk drought) stressed wheat plants Statistical details given in M & M.
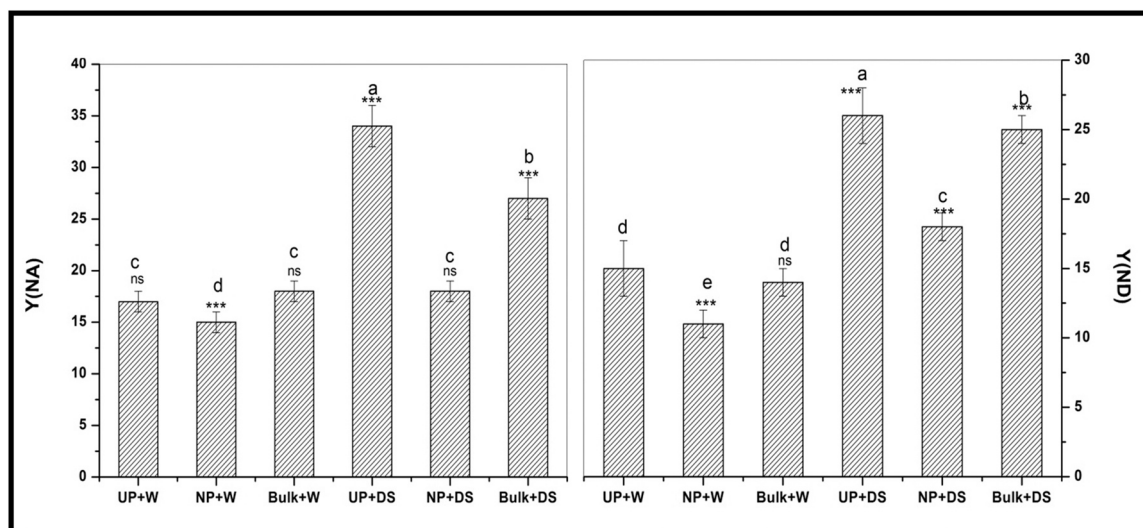
Table 4

Effect of drought stress on the steady-state oxidation of P700 ($\Delta A_{(830-875)}$), electron donor pool size to PS I (multiple turnover (MT): single turnover (ST) area) and dark reduction kinetics ($t_{1/2}$ in s) in UP + W, NP + W, Bulk + W, UP + DS, NP + DS and Bulk + DS wheat plants. Statistical details given in M & M.

Treatment	$\Delta A_{(830-875)}$	MT/ST area	$t_{1/2}$
UP + W	1.75 ± 0.01^b	9.6 ± 0.3^b	0.88 ± 0.01^b
NP + W	$2.25 \pm 0.02^{***a}$	9.5 ± 0.3^{nsb}	$0.76 \pm 0.01^{***c}$
Bulk + W	$1.55 \pm 0.02^{**c}$	9.5 ± 0.4^{nsb}	0.91 ± 0.02^{nsb}
UP + DS	$0.75 \pm 0.03^{***f}$	$11.5 \pm 0.3^{***a}$	$0.99 \pm 0.02^{***a}$
NP + DS	$1.12 \pm 0.02^{***d}$	9.3 ± 0.2^{nsb}	0.85 ± 0.03^{nsb}
Bulk + DS	$0.82 \pm 0.02^{***e}$	10.2 ± 0.2^{nsb}	$0.99 \pm 0.01^{***a}$

pores. Formation of nanopores is accompanied with up-regulation of aquaporin genes involved in rapid water uptake. Increase in seed water uptake can induce higher metabolic activity of various seed hydrolytic enzymes like amylase and protease involved in starch and protein hydrolysis during initial phase of imbibition in nanoprimed seeds (Mahakham et al., 2017). Increase in the activity of these germination related hydrolytic enzymes corresponds well with an increase in total soluble sugar content (Table 2) required to support early seedling growth in NP seeds compared to UP and Bulk primed wheat seeds. Overall, owing to the smaller size and high surface area to volume ratio, bioavailability of Si nanoparticles is increased leading to easy penetration in the seeds, thus improving seed quality in terms of rapid water uptake, higher germination percentage and enhanced seed vigor in comparison to their bulk counterparts (Mansoor et al., 2019). Seed vigor forms an important aspect in the process of seed germination thereby promoting better seedling growth and enhanced recovery when subjected to any abiotic stress in its entire life cycle (Rai-Kalal et al., 2021).

Drought stress has a major impact on plant photosynthesis disturbing the membrane permeability of chloroplast. Water deficiency in drought condition induces negative change in photosynthetic pigment content, impairing normal functioning of photosynthetic machinery (Fu and Huang 2001). Severity of drought stress can be estimated from leaf relative water content. Leaf RWC was drastically reduced by 52% in UP + DS plants; however this reduction was only 22% in leaves of NP + DS plants (Table 3). Considerable less reduction in water content in NP leaves under DS can be explained as a result of marked enhancement in root and shoot ratio resulting in greater water uptake capacity and reduced water loss through transpiration (Rai-Kalal and Jajoo, 2021). Thus, better water status in NP plants could be positively correlated with improved drought tolerance potential.

It is well established that under water stress condition plant tend to close their stomata in order to maintain a relative plant water status (Lawlor and Cornic, 2002). However, long-term stomatal closure to avoid water loss results in the accumulation of harmful ROS species resulting in oxidative stress. Photosynthetic apparatus of plant is the major victim of such oxidative damage. The present work was aimed to evaluate the impact of DS on photosynthetic efficiency of PSI and PSII complexes in nanoprimed wheat plants. Information obtained from the study of saturation pulse kinetics provides a precise knowledge about the complex process of PSI and PSII photochemistry and their efficiency of energy conversion. Application of a saturating pulse to a dark-adapted leaf induces a maximum value of fluorescence (Fm) by closing reaction centers in non-stressed plants (Murchie and Lawson, 2013). The amplitude of Fm, representing the number of active (photo-oxidisable) reaction centers of PSII, was significantly increased in NP + W as compared to UP + W wheat plants. However on subjecting to DS a drastic reduction in amplitude of Fm was observed in UP + DS plants (Fig. 1). Decrease in Fm in UP + DS plants suggest drought induced oxidative damage of photosynthetic apparatus at structural and functional level resulting in severe to damage to PSII reaction centers (Tomar and Jajoo, 2019). On the contrary, Fm was less affected in NP + DS plants indicating positive role of SiO$_2$ nanoparticle in preventing the photosynthetic apparatus from being damaged under DS.

Likewise, the maximum level of P700$^+$ signal is denoted by Pm (which is analogous to Fm in PSII) (Tikkanen et al., 2014). Our results showed significant increase in Pm in NP + W as compared to UP + W wheat plants (Fig. 1). However, Pm was significantly decreased in UP + DS wheat as a response towards drought stress. The measured decrease in Pm in UP + DS plants suggest a drastic reduction in photoactive reaction centers of PSI and decrease in the amount of photo-oxidisable PSI per unit leaf area (Brestic et al., 2015). On the contrary, in NP + DS plant reduction in Pm was non-significant as compared to UP + W plants indicating better availability of number photo-oxidisable PSI complexes to perform photochemistry even under DS (Mathur et al., 2018).

The increase in Fm and Pm can be directly correlated with increase in quantum yield efficiency of PSII and PSI respectively. The quantum yield of PSII (YII) and PSI (YI) is positively associated with photosynthetic rate in plants related to fraction of photo chemically active reaction centers of both photosystems (Mathur et al.,2018). Therefore

Fig. 6. Diagrammatic representation showing the effects of drought stress on photosynthetic efficiency of PSII and PSI in unprimed and nanoprimed wheat plants.

any damage to photosynthetic reaction centers of PSII and PSI in response to DS is a reduction in YII and YI (Fig. 2). Results obtained show significant increase in Y (II) in NP+W followed by increase in Bulk+W plants as compared to UP+W wheat plants. However, Y(II) was drastically reduced in UP+DS wheat plants representing increase in the number of 'inactive' reaction centers as a result of photo-oxidative damage of D1 protein in response to DS (Tomar and Jajoo, 2015). On the contrary, the damage in YII was significantly less in NP+DS plants. The lesser extent of decrease in YII in NP+DS plants is in corroboration with our previous findings (Rai Kalal et al.,2021) that reported increase in total Chl pigment content in SiO_2 nanoprimed plants resulting in increase in number of active reaction center involved in maximum absorption of photons in performing photochemistry under DS.

The efficiency of linear electron transport rate in PSII (ETRII) showed a prominent increase in NP+W plants as compared to UP+W wheat plants. Subjecting the plants to DS resulted in significant reduction in ETR(II) in UP+DS and Bulk+DS plants (Fig. 3). However, this reduction was more pronounced in UP+DS wheat plants, showing considerably less reduction in NP+DS wheat plants. The efficiency of photochemical energy conversion of PSII is directly proportional to linear electron transport (Jain and Jajoo, 2019). Thus non-significant reduction in ETRII in NP+DS plants can be explained by non-significant reduction in YII (discussed above). Further, decrease in the extent of Y (II) and ETRII in UP+DS plants occurred in expense of considerable increase in Y(NO) accompanied with simultaneous increase in Y(NPQ) (Fig. 4). Increase in Y(NO) in UP+DS plants is mainly associated with reduced efficiency of PSII and increase in fraction of inactive reaction centers thus explains severe damage to PSII in UP+DS plants leading to excess of heat dissipation (Suzuki et al., 2011). Our results indicated less change in Y(NO) followed by an increase in Y (NPQ) in NP+DS plants compared to that of UP+DS plant. Y(NPQ) represents the physiological means to dissipate the excessive light energy in regulated form as a protective mechanism against damage under drought stress (Mathur et al.,2019). This explains maximum utilization of harvested light to perform photochemistry and least dissipated in the form of heat in NP+DS wheat plants.

Compared to PSII, PSI parameters were less sensitive to DS. The quantum yield efficiency of PSI (YI) was maximum in NP+W plants followed by a substantial increase in ETRI (Figs. 2,3). This increase could be directly correlated to an increase in root to shoot ratio in nanoprimed plants (Rai Kalal et al., 2021) which helped the plant for better water and nutrient uptake from soil thereby improving PSI

efficiency and an enhanced electron transport rate in NP+W plants as compared to UP+W (Mathur et al., 2019). However, exposure to DS resulted in a significant reduction in YI in UP+DS plants whereas showing considerably less reduction in NP+DS wheat plants. Likewise, ETRI was also substantially decreased in UP+DS wheat plants. However, NP+DS plants sustained a better physiological status of PSI which is evident from a lesser extent of reduction in ETRI and YI even under DS conditions.

Decrease in YI in UP+DS plants is related to an increase in Y(ND) and Y(NA). Increase in the non-photochemical quantum yield Y(ND) explains the increase in donor-side limitation of PSI due to lower light energy absorption and electron transport from PSII to PSI antenna complex as a result of PSII photo-inhibition under DS (Tikkanen et al., 2014). Increase in Y(NA) in UP+DS plants represents the non-photochemical quantum yield with acceptor side limitation which represents the fraction of P700 that cannot be oxidized due to lack of electron acceptor. However, increase in both Y(NA) and Y(ND) was less in NP+DS plants comparison to UP+DS wheat plants. This explains that both PSI and PSII antenna complexes are in a better state of light absorption thereby sustaining their efficiency to perform improved photochemistry even under DS (Tomar and Jajoo, 2017).

Further studies were conducted to measure P700 oxidation kinetics using the ST and MT white flashes during far-red illumination. The oxidation-reduction kinetics of P700 was measured as the absorbance changes at 830–875 nm with the application of single turnover and multiple turnover flash (ST and MT flash) in dark adapted leaves of control and all the drought treated plants. A significant decrease in $\Delta A_{830-875}$ was seen in UP+DS plants illustrating decrease in the overall level of photo-oxidisable P700 (Table 4). The reduction in the level of photo-oxidisable P700 in UP+DS plants directly reflects the functional impairment of LEF (Linear electron flow). However, comparatively higher $\Delta A_{830-875}$ was observed in NP+DS in comparison to UP+DS plants. The application of ST and MT flashes during far red illumination gives information about the size of the intersystem electron pool. The application of ST flash transiently reduce $P700^+$ during far-red illumination upon arrival of an electron from PSII, whereas the MT flash completely reduced the PQ pool and also all the oxidized P700 (Jain and Jajoo, 2019). Further, the MT: ST area ratio increased significantly in UP+DS plants reflecting a higher intersystem carrier pool thereby suggesting acceptor side limitation of PSI. This increase can also be attributed to significantly higher Y(NA) in UP+DS plants. On the other hand, no significant change in MT:ST ratio was observed in NP+DS

plants which is in accordance with comparatively lesser increase in Y (NA) under DS (Fig. 5). Further, $t_{1/2}$ which represents the time required for re-reduction of P700 + was comparatively less for NP + W than $t_{1/2}$ for UP + W wheat plants. This decrease can be explained as result of prominent increase in ETRI, YI and a prominent decrease in Y (NA) in NP + W plants as compared to control. Efficient transfer of electrons from PSI to ferrdoxin generates higher NAPDH and ATP molecules for efficient dark reactions. However, in UP + DS plants $t_{1/2}$ was significantly increased suggesting impairment of ETRI (Fig. 3). On the contrary, in case of NP + DS plants, the $t_{1/2}$ was almost similar to the control suggesting restoration of efficiency of YI and ETRI in nano-primed plants under DS. Thus, the analysis of above results showed the effects of SiO_2 nanopriming in improving drought tolerance potential in nanoprimed wheat plants by protecting both PSII and PSI. Thus from results obtain we can say that SiO_2 nanopriming of wheat seeds helped plants to cope up even under water stressed conditions by maintaining a better photosynthetic efficiency of both the photosystems particularly PSII. These results are summarized diagrammatically in Fig. 6.

5. Conclusion

On the basis of results obtained, it is concluded that seed nano-priming with SiO_2 NPs promotes improved drought tolerance potential in drought sensitive wheat plants. Drought stress showed a major impact on photosynthetic efficiency of unprimed plants resulting in significant impairment of its PSII and PSI complexes. The inhibiting effects of DS suppressed both PSII and PSI but the inhibiting effect was more prominent in PSII. Results obtained strongly imply that SiO_2 nano-priming protected the plant photosystems showing no significant effects on the quantum yield efficiency as well as electron transport rate of both PSII and PSI, in nanoprimed wheat plants. Decrease in quantum yield of PSII and PSI in UP + DS plants are directly correlated to increase in non-regulated heat dissipation Y(NO) and donor side limitation Y (ND) of PSII and PSI respectively. However nanopriming efficiently alleviated the effects of DS showing non-significant increase in heat dissipation suggesting better utilization of absorbed energy in performing photochemistry. The effect of SiO_2 nanopriming in mitigating the effects of drought stress on photosynthesis can be related to increase in root to shoot ratio which enhanced the uptake and translocation of water and essential nutrients indirectly resulting in increased chlorophyll content. SiO_2 nanopriming thereby helped the plants to maintain the integrity and stability of both the photosystems under DS. Consequently, we propose SiO_2 nanoparticles as an effective priming agent to enhance drought tolerance in wheat.

CRediT authorship contribution statement

Study was conceptualized and designed by AJ, PR. Experiments were performed by PR, RST, and analyzed by PR and AJ. Manuscript was written by PR, RST and edited by AJ.

Data Availability

Data will be made available on request.

Declaration of Competing Interest

The authors declare that they have no known competing financial interests or personal relationships that could have appeared to influence the work reported in this paper.

Acknowledgement

Appendix A. Supporting information

References

Abdelmoneim, T.S., Tarek, A.A.M., Almaghrabi, O.A., Alzahrani, H.S., Abdelbagi, I., 2014. Increasing plant tolerance to drought stress by inoculation with arbuscular mycorrhizal fungi. Life Sci. J. 11, 10–17 (http://www.lifesciencesite.com/).

Ashkavand, P., Tabari, M., Zarafshar, M., Tomaskova, I., Struve, D., 2015. Effect of SiO_2 nanoparticles on drought resistance in hawthorn seedlings. Res Pap. 76, 350–359. https://doi.org/10.1515/frp-2015-0034

Ashraf, M., Harris, P.J.C., 2013. Photosynthesis under stressful environments: an overview. Photosynthetica 51, 163–190. https://doi.org/10.1007/s11099-013-0021-6

Brestic, M., Zivcak, M., Kunderlikova, K., Sytar, O., Shao, H.-B., Kalaji, H.M., Allakhverdiev, S., 2015. Low PSI content limits the photo protection of PSI and PSII in early growth stages of chlorophyll b-deficient wheat mutant lines. Photosynth. Res. 125, 151–166. https://doi.org/10.1007/s11120-015-0093-1

Dayanandan, P., Kaufman, P.B., Franklin, C.I., 1983. Detection of silica in plants. Am. J. Bot. 70, 1079–1084.

Dhakal, A., 2021. Effect of drought stress and management in wheat - a review. Food Agribus. Manag. 2, 62–66. https://doi.org/10.26480/fabm.02.2021.62.66

Fahad, S., Bajwa, A.A., Nazir, U., Anjum, A.A., Farooq, A., Zohaib, A., Sadia, S., Nazim, W., Akins, S., Suad, S., Ihsan, M.S., Alharby, H., Wu, C., Wang, D., Huang, J., 2017. Crop production under drought and heat stress: plant responses and management options. Front. Plant Sci. https://doi.org/10.3389/fpls.2017.01147

Fu, J., Huang, B., 2001. Involvement of antioxidants and lipid peroxidation in the adaptation of two cool-season grasses to localized drought stress. Environ. Exp. Bot. 45, 105–114. https://doi.org/10.1016/S0098-8472(00)00084-8

Hameed, A., Farooq, T., Hameed, A., Sheikh, M.A., 2021. Silicon-mediated priming induces acclimation to mild water-deficit stress by altering physio-biochemical attributes in wheat plants. Front. Plant Sci. https://doi.org/10.3389/fpls.2021.625541

Hedge, J.E., Hofreiter, B.T., 1962. In: Whistler, R.L., BeMiller, J.N. (Eds.), Methods in Carbohydrate Chemistry Vol.17. Academic Press, New York, pp. 420.

Ivanov, A.G., Hendrickson, L., Krol, M., Selstam, E., Oquist, G., Hurry, V., Huner, N.P.A., 2006. Digalactosyl-Diacylglycerol deficiency impairs the capacity for photosynthetic intersystem electron transport and state transitions in *Arabidopsis thaliana* due to Photosystem I acceptor-side limitations. Plant Cell Physiol. 47, 1146–1157 https://doi.org/10.1093/pcp/pcj08 9.

Jain, L., Jajoo, A., 2019. Protection of PSI and PSII complexes of wheat from toxic effect of anthracene by *Bacillus subtilis* (NCIM 5594). Photosynth. Res. https://doi.org/10.1007/s11120-019-00692-z

Kalaji, H.M., Jajoo, A., Oukarroum, A., Brestic, M., Zivcak, M., Samborska, I.A., Cetner, M.D., Lukasik, I., Goltsev, V., Ladle, R.J., 2016. Chlorophyll *a* fluorescence as a tool to monitor physiological status of plants under abiotic stress conditions. Acta Physiol. Plant 38, 102. https://doi.org/10.1007/s11738-016-2113-y

Kannan, N.D., Kulandaivelu, G., 2011. Drought induced changes in physiological, biochemical and phytochemical properties of *Withania somnifera Dun.* J. of Med. Plant Res. 5, 3929–3935. https://doi.org/10.5897/JMPR.9000462

Klughammer, C., Schreiber, U., 1994. An improved method, using saturating light pulses, for the determination of photosystem-I quantum yield via P700+ absorbance changes at 830 nm. Planta 192, 261–268. https://doi.org/10.1007/BF01890043

Kunitz, M., 1947. Crystalline soybean trypsin inhibitor: II. General properties. J. Gen. Physiol. 30, 291–310. https://doi.org/10.1085/jgp.30.4.291

Lawlor, D.W., Cornic, G., 2002. Photosynthetic carbon assimilation and associated metabolism in relation to water deficits in higher plants. Plant Cell Environ. 25, 275–294. https://doi.org/10.1046/j.0016-8025.2001.00814.x

Mahakham, W., Sarmah, A.K., Maensiri, S., Theerakulsiput, P., 2017. Nanopriming technology for enhancing germination and starch metabolism of aged rice seeds using phytosynthesized silver nanoparticles. Sci. Rep. 7, 8263. https://doi.org/10.1038/s41598-017-08669-5

Mansoor, N., Younus, A.1, Jamil, Y., Shahid, M., 2019. Impact of nanosized and bulk ZnO on germination and early growth response of *Triticum aestivum*. Pak. J. Agric. Sci. 56, 879–884.

Mathur, S., Tomar, R.S., Jajoo, A., 2019. Arbuscular Mycorrhizal fungi (AMF) protects photosynthetic apparatus of wheat under drought stress. Photosynth. Res https://link.springer.com/article/10.1007/s11120-018-0538-4.

Murchie, E.H., Lawson, T., 2013. Chlorophyll fluorescence analysis: a guide to good practice and understanding some new applications. J. Exp. Bot. 64, 3983–3998. https://doi.org/10.1093/jxb/ert208

Nath, K., O'Donnell, J.P., Lu, Y., 2017. Chloroplastic iron-sulfur scaffold protein NFU3 is essential to overall plant fitness. Plant Signal Behav. 12, 6 https://doi.org/10.1080/15592 324.2017.12820 23.

Nath, K., Ryan, L., Wessendorf, R.L., Lu, Y., 2016. A nitrogen-fixing subunit essential for accumulating 4Fe-4S-containing photosystem I core proteins. Plant Physiol. 172, 2459–2470 https://doi.org/10.1104/pp.16.01564.

Nile, H.S., Thiruvengadam, M., Wang, Y., Samynathan, R., Shariati, M.A., Rebezov, M., Arti Nile, A., Sun, M., Venkidasamy, B., Xiao, J., Kai, G., 2022. Nano-priming as

emerging seed priming technology for sustainable agriculture—recent developments and future perspectives. J. Nano 20, 254. https://doi.org/10.1186/s12951-022-01423-8

Nondek, L., Buszewski, B., Berek, D., 1986. Retention of pyridine and 2,6-dimethylpyridine on silanized silica: a simple test on residual silanols? J. Chromatogr. A 360, 241–246. https://doi.org/10.1016/S0021-9673(00)91669-8

Pebriansyah, A., Karti, P.D.M.H., Permana, A.T., 2012. Effect of drought stress and addition of Arbuscula mycorrhizal fungi (AMF) on growth and productivity of tropical grasses (*Chloris gayana, Paspalumdilatatum,* and *Paspalum notatum*). Pastura 2, 41–48.

Pereira, A., Oliveira, H.C., Fraceto, L.F., Santaella, C., 2021. Nanotechnology potential in seed priming for sustainable agriculture. Nanomaterials 11, 267.

Rai-Kalal, P., Jajoo, A., 2021. Priming with zinc oxide nanoparticles improve germination and photosynthetic performance in wheat. Plant Physiol. Biochem 160, 341–351.

Rai-Kalal, P., Tomar, R.S., Jajoo, A., 2021. Seed nanopriming by silicon oxide improves drought stress alleviation potential in wheat plants. Funct. Plant Biol. 48.

Rastogi, A., Yadav, S., Hussain, S., Kataria, S., Hajihashemi, S., Ku, P., 2021. Does silicon really matter for the photosynthetic machinery in plants…? Plant Physiol. Biochem 169, 40–48.

Sawhney, S., Tokyo, K.L., Nanda, K.K., 1970. Changes in amylase activity during extension growth and floral induction in *Impatiens balsamina*. a Qual. Short. Day Plant. Indian J. Plant. Physiol. 13, 198–205.

Sherin, G., Aswathi, K.P., Puthur, J., 2022. Photosynthetic functions in plants subjected to stresses are positively influenced by priming. Plant Stress. 4, 100079.

Song, A., Li, P., Fan, F., Li, Z., Liang, Y., 2014. The effect of silicon on photosynthesis and expression of its relevant genes in rice (*Oryza sativa* L.) under high-zinc stress. PLoS One 9, e113782 https:// doi.org/10.1371/journal.pone.0113782.

Souri, Z., Khanna, K., Karimi, N., Ahmad, P., 2021. Silicon and plants: current knowledge and future prospects. J. Plant Growth Regul. 3, 906–925. https://doi.org/10.1007/s00344-020-10172-7

Suzuki, N., Miller, G., Morales, J., Shulaev, V., Torres, M.A., Mittler, R., 2011. Respiratory burst oxidases: the engines of ROS signaling. Curr. Opin. Plant Biol. 14, 691–699. https://doi.org/10.1016/j.pbi.2011.07.014

Teskey, R., Wertin, T., Bauweraerts, I., Ameye, M., McGuire, M.A., Steppe, K., 2015. Responses of tree species to heat waves and extreme heat events. Plant Cell Environ. 38, 1699–1712. https://doi.org/10.1111/pce.12417

Tikkanen, M., Mekala, N.R., Aro, E.M., 2014. Photosystem II photoinhibition–repair cycle protects photosystem I from irreversible damage. Biochim. Et. Biophys. Acta 1837, 210–215. https://doi.org/10.1016/j.bbabio.2013.10.001

Tomar, R.S., Jajoo, A., 2014. Fluoranthene,apolycyclicaromatichydrocarbon,inhibitslightaswell as darkreactionsofphotosynthesisinwheat(*Triticumaestivum*). Ecotoxicol. Environ. Saf. 109, 110–115.

Tomar, R.S., Jajoo, A., 2015. Photomodified fluoranthene exerts more harmful effects as compared to intact fluoranthene by inhibiting growth and photosynthetic processes. Ecotoxicol. Environ. Saf. 122, 31–36 https://doi.org/10.1016/j.ecoen v.2015.07.002.

Tomar, R.S., Jajoo, A., 2017. PSI becomes more tolerant to fluoranthene through the initiation of cyclic electron flow. Funct. Plant Biol. 44, 978–984 https://doi.org/10.1071/FP171 21.

Tomar, R.S., Jajoo, A., 2019. Photosynthetic response in wheat plants caused by the phototoxicity of fluoranthene. Funct. Plant Biol. 46, 725–731. https://doi.org/10.1071/FP18328

Wahid, A., Rasul, E., 2005. Photosynthesis in Leaf, Stem, Fower and Fruit. In: Pessarakli, M. (Ed.), Handbook of Photosynthesis. CRC Press, Florida, pp. 479–497.

Waraich, E.A., Ahamad, R., Asharf, M.Y., 2011. Role of mineral nutrition in alleviation of drought stress in plants. Aust. J. Crop Sci. 5, 764–777.

Impact of polycyclic aromatic hydrocarbons on photosynthetic and biochemical functions and its bioremediation by *Chlorella vulgaris*

Rupal Singh Tomar [a,b,*], Prabha Rai-Kalal [a], Anjana Jajoo [a,c]

[a] *School of Life Sciences, Devi Ahilya University, Indore, India*
[b] *Department of Biology, Washington University, St. Louis, MO, USA*
[c] *School of Biotechnology, Devi Ahilya University, Indore, India*

A B S T R A C T

Among several pollutants found in the aquatic environment, polycyclic aromatic hydrocarbons (PAHs) can interfere with the normal functioning of the aquatic organisms. The aim of this study was to investigate the application of *Chlorella vulgaris* for bioremediation of different type of PAHs [2-ring Naphthalene (NAP), 3-ring Anthracene (ANT), and 4-ring Pyrene (PYR)] and their impact on photosynthesis and growth of *C. vulgaris*. After 7 days of exposure of PAHs, growth of *C. vulgaris* was affected in the order PYR > ANT > NAP. With regard to biomolecules, all PAHs treatments showed a significant decrease in lipid content, but the toxic effect of PYR was more pronounced. Chl *a* fluorescence study of algal samples indicated that photosystem II (PSII) performance was unaffected by NAP and ANT toxicity, however, severe disruption of PSII activity by PYR was noted. Interestingly, *C. vulgaris* was able to remove all three PAHs from the media (~90–92 % NAP, ~90–94 % ANT and ~76 % PYR) within 7 days. After 3 days of cultivation, activity of dehydrogenase was increased in NAP and ANT inoculated culture, reflecting metabolization of these compounds which reduced after 7 days. As compared to control culture (no PAHs) a sharp decline in dehydrogenase activity was noted in PYR treated culture (after 3 and 7 days). Based on the results obtained, *C. vulgaris* could absorb NAP and ANT (linear PAHs) more efficiently than PYR (angular PAH). These results imply that ability of *C. vulgaris* to degrade PAHs depends in part on the configuration of the ring structure.

1. Introduction

Polycyclic aromatic hydrocarbons (PAHs) are persistent organic pollutants which pose potential risks to plant and animal life [1]. Hundreds of PAHs have been identified out of which 16 PAHs have been listed as priority pollutants by the Environmental Protection Agency of US (US EPA) and the European Union [2]. Incautious release of PAHs into the aquatic environment has put aquatic organisms in high risk. PAHs show toxic, carcinogenic, mutagenic effects, particularly by generating singlet oxygen and other ROS. For this reason, they are considered aquatic contaminants of high concern [2].

After absorption, PAHs substantially affects cellular processes *e.g.*, photosynthesis and growth rates [3,4] which is detrimental to entire aquatic ecosystem and food chains. PAHs are able to inhibit algal growth, where the extent of inhibition varied among various algal species [3–8]. Because of small size with a large surface area, algae have proven to be an excellent aquatic test organism for assessing environmental toxicity of such pollutants. Toxic effects of PAHs on growth, photosynthesis, and respiration in higher plants with emphasis on interaction with PAH with solar and ultraviolet (UV) radiation have been reported [9,10]. Most of by-products of PAHs are quinones [3]. Due to their structural resemblance to natural quinones found in photosynthetic cells, they have the potential to replace these elements and thereby disturbing electron transport processes essential for cellular energy generation. Many studies have reported the inhibition of the photosynthetic electron transport chain and down regulation of PS II, most likely at the cytochrome *b6f* level by PAHs in algae and higher plants [3,9–11].

Previous studies have demonstrated that PAHs can be degraded by various microorganism [4,12–14]. Moreover, bioremediation by microalgae is regarded as one of the major mechanisms for removal of PAHs from the environment and is affected by properties of the pollutant and the catabolic ability of microalgae [15,16]. Among the microalgal strains, green algae such as *Chlorella vulgaris* [4], *Chlorella* and

---

Oscillatoria [2], *Chlorella sp. MM3* [17,18], *Scenedesmus platydiscus*, *Scenedesmus quadricauda* [19], and *Selenastrum capricornutum* [20] have been tested as potential bio-degraders for PAHs.

The present study attempts to assess the potential of *C. vulgaris* for bioremediation for three different PAHs and compare their effects on biomolecules and photosynthesis of *C. vulgaris*. Experiments were conducted to gain more insight into various biological processes that regulate cell progression responding to introduction of tested PAHs *i.e.* Naphthalene (NAP), Anthracene (ANT) and Pyrene (PYR). These 3 PAHs were chosen on the basis of molecular weight (NAP-128.2 g mol^{-1}, ANT-178.23 g mol^{-1} and PYR-202.25 g mol^{-1} respectively), number of rings (NAP-2 ring, ANT-3 ring and PYR-4 ring) and structure (NAP, ANT linear and PYR angular). At the same time, they have been detected with high frequency and concentration, ranging from ηg L^{-1} in surface water or groundwater to μg L^{-1} in oil spill areas [21]. It was reported that small size and low molecular weight PAHs are more reactive because of their high specific surface area and ability to penetrate organisms [22]. Furthermore, it has been reported that physico-chemical properties of PAHs have impact on contaminant toxicity and their degradability [23]. Much of the published research focused on the removal of the low molecular weight (LMW) PAHs, such as naphthalene and phenanthrene [24,25]. However, little is known about impact and biodegradation of high molecular weight (HMW) PAHs. So, the aim of the present research was to investigate whether ring number and structure of PAHs affect *C. vulgaris* ability to i) survive in PAHs rich environment, ii) absorb different PAH and iii) degrade PAH. This study provides evidence for toxicological effects of NAP, ANT and PYR on photosynthesis, biomolecules and bioremediation efficiency of *C. vulgaris*.

2. Materials and methods

2.1. Algal species and culture conditions

Freshwater microalgal species *C. vulgaris* was obtained by Phycospectrum Environmental Research Centre, Chennai India. Cells were grown in BG11 media (Himedia, M1958, India). Cultures were illuminated with cool white fluorescent tubes (20 W) at a light intensity of 60 μmol photon m^{-2}s^{-1} at 25 °C and a diurnal cycle of 16 h light and 8 h dark on shakers (130 rpm) in algal culture room. After 7–10 days (exponential growth phase) cells were harvested by centrifugation at 2500g for 5 min for further experiments.

2.2. Experimental setup

For each treatment, 3 conical flasks (250 mL, Erlenmeyer flasks), containing 150 mL culture medium were prepared and autoclaved. Appropriate amount of algal mass was then inoculated to each conical flask to obtain an initial optical density 0.1 at 680 nm. Optical density was measured by UV–VIS spectrophotometer (Thermo Scientific, Evolution 201, USA). After inoculation, 75 μL of stock solution (10 gL^{-1} of NAP, ANT and PYR in Acetone) were added into 150 mL media to obtain 5 mgL^{-1} concentrations. The flasks without addition of any PAHs were used as the control. The growing conditions were the same as mentioned above. After 3 and 7 days of incubation, algal samples of control and PAHs treatments were retrieved for various experiments.

2.3. Determination of growth and biomass

Microalgal growth was monitored regularly at an interval of 24 h by measuring optical density (OD) at 680 nm using a UV–VIS spectrophotometer (Thermo Scientific, Evolution 201, USA). Dry biomass was estimated after drying of 100 mL culture in a pre-weigh centrifuge tube in a hot air oven at 80 °C for 4 to 6 h. The growth rate (d^{-1}) was calculated using the following equation:

$$GR\ \left(d^{-1}\right) = \left(\ln N_2 - \ln N_0\right)/\left(t_2 - t_0\right) \tag{1}$$

where N$_2$ is the OD at time t$_2$ and N$_0$ is the OD at time t$_0$ (day 0).

2.4. Determination of lipid, carbohydrate and protein content

Lipid content was estimated by sulpho-phospho-vanillin (SPV) colorimetric method as described in Mishra et al. [26]. Carbohydrate content was estimated by Phenol−Sulfuric Acid method as described in Laurens et al. [27]. Protein estimation was done according to Slocombe et al. [28] with some changes. In brief, protein extraction was done by 6 % TCA (Trichloro acetic acid) and kept at room temperature overnight. Protein content was measured by Foline reagent.

2.5. Determination of chlorophyll content

Pigment content was determined using the following method. 5 mL of culture was taken and centrifuged at 2500g for 5 min. The supernatant was discarded and 5 mL of 99.9 % methanol was added to the pellet, mixed properly and incubated at 90 °C for 5 min. The culture was centrifuged at 9000g for 5 min and the supernatant was used for pigment estimation [4]. Calculations were done as mentioned in Dere et al. [29].

2.6. Measurement of Chl a fluorescence

Measurements of the quantum yields of energy conversion in photosystem II (PSII) were carried out through saturation pulse technique, using a Pulse amplitude modulator (Dual PAM-100, Walz, Effeltrich, Germany) system in intact algal cell culture. Algal sample were dark adapted for 30 min at 23 ± 2 °C before measurements then 1.5 mL of cell culture was taken in cuvette for induction curve recording. A weak modulated light (12 μmol photon m^{-2} s^{-1}) was given to get minimal fluorescence (Fo), followed by actinic light (53 μmol photon m^{-2} s^{-1}), and saturating pulse (SP) (6000 μmol photon m^{-2} s^{-1}) to achieve maximum fluorescence (Fm). After determination of Fo and Fm, the induction curve was recorded with the routine program of the Dual-PAM-100 software. Induction curve was recorded with SP for 5 min to achieve the steady state of the photosynthetic apparatus, and then the actinic light was turned off.

2.7. Extraction of polycyclic aromatic hydrocarbons (PAHs) from media

Extraction of PAHs was performed by ethyl acetate according to Tomar and Jajoo [4] and was analyzed by UV–VIS spectrophotometer (Thermo Scientific, Evolution 201, USA) at 230–380 nm and reduction was calculated. Algal sample was separated from the medium by centrifugation at 1000g for 10 min. The 10 mL supernatant was extracted twice with 20 mL ethyl acetate (HPLC grade Sigma Aldrich) in a separating funnel on a shaker for 2 h and then concentrated by a vacuum rotary evaporator. Standard absorption spectra were measured by same concentration of PAHs in ethyl acetate. Sample extraction was performed at day of inoculation (0th day), 3rd day and 7th day of cultivation. Experimental samples were compared with the standard spectra.

2.8. Determination of dehydrogenase enzyme activity

Dehydrogenase activity was determined according to Tomar and Jajoo [4]. Four tubes each containing 20 mL of algal sample were centrifuged at 2500g for 5 min and pallet were mixed with 2 mL Tris-HCl and 1 mL 0.8 % TTC (2,3,5-triphenyl tetrazolium chloride). Three to four drops of formaldehyde were added to one tube of each treatment (blank control tubes) to stop the reaction then all tubes were put into a water bath at 32 °C for color development in dark. After 60 min, 3–4 drops of formaldehyde were added to the other tubes to stop the reaction. Acetone (4 mL) and petroleum ether (5 mL) were added in each tube and shaken by hand for 10 min. The petroleum ether layers were

moved to a color matching dish and the absorbance was measured by spectrophotometer at 492 nm compared to pure petroleum ether. Dehydrogenase activity was calculated by the preparation of calibration curve of triphenylformazane (TF) in microgram of TF formation mL^{-1} h^{-1}.

$$DHA \left(\mu g \text{ of TF } mL^{-1} h^{-1} \right) = C/t \times v \qquad (2)$$

C = TF amount on the calibration curve to corresponding absorbance; t = duration of color development in h; v = volume algal sample in mL.

2.9. Statistical analysis

Data was analyzed using GraphPad Prism 5.01 software, Inc., La Jolla, CA, USA. Results were analyzed using one-way analysis of variance (ANOVA) followed by Newman-Keuls Multiple Comparison Test. Significance was determined at $P < 0.001$ (*$P < 0.05$, **$P < 0.01$, ***$P < 0.001$) and results expressed as mean values SD. Different letters indicates significant difference among treatments. All the experiments were done five times in replicates of three.

3. Results and discussion

3.1. Comparative effects of three polycyclic aromatic hydrocarbons (PAHs) on the growth of C. vulgaris

To evaluate the impact of three different PAHs on *C. vulgaris*, specific growth of algal culture with various treatments was measured. *C. vulgaris* was grown in culture medium spiked with 5 mg L^{-1} concentration of NAP, ANT, and PYR in separate flasks. The experiments were conducted in control laboratory conditions. Growth of *C. vulgaris* was monitored for 7 days in control and PAHs treated cultures (Fig. 1). Spectrophotometric data (Fig. 1) of algal cell density illustrated that exposure to NAP did not have significant effect on the population of *C. vulgaris*, when compared with the absorbance (680 nm) values of control cell population. However, 7 days exposure of ANT and PYR, caused a reduction in the growth of algal cells and almost 50 % of reduction in PYR treated culture was observed (Fig. 1). The tolerance level of *C. vulgaris* to tested PAHs was in the order NAP > ANT > PYR.

Biomass was quantified as dry weight, after 7 days of cultivation in control and different PAHs treatments and it followed same trend as growth. The dry weight of *C. vulgaris* was reduced by all the three PAHs (not significant in NAP), indicating that PAHs inhibited the growth of
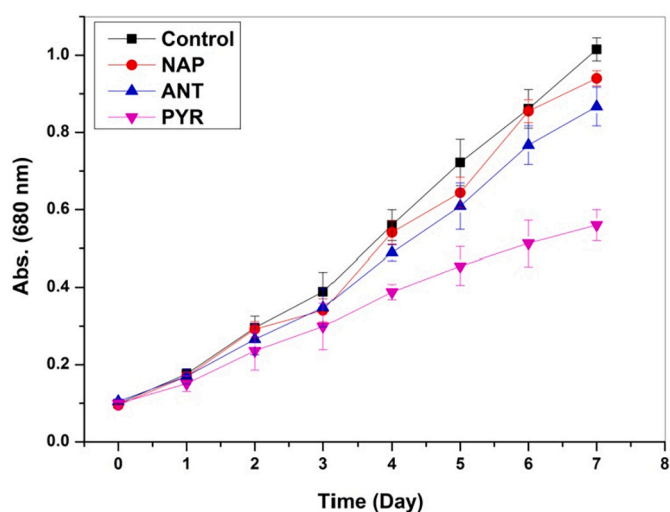
algal cells (Fig. 2). In addition, the growth rate per day (change in OD per day) of *C. vulgaris* was reduced with all tested PAHs at 5 mgL^{-1} concentrations (0.130 d^{-1} in control, 0.120 d^{-1} in NAP, 0.108 d^{-1} in ANT and 0.068 d^{-1} in PYR). It should be noted that the dry weight and growth rate of algal cells were most prominently diminished by PYR (Fig. 2). The incompetent performance of *C. vulgaris* in PYR inoculated medium can be related to toxicity of high molecular weight and cluster benzene ring arrangement of PAH which is difficult to metabolize [17,18]. It has been observed that low molecular weight (LMW) PAHs and heterocyclic compounds were degraded more quickly than the high molecular weight (HMW) PAHs [30]. In agreement with current results, decreasing cell growth rate of various algal species with different PAHs was previously reported [31,32].

3.2. Comparative effect of three polycyclic aromatic hydrocarbons (PAHs) on photosynthetic pigments content

Photosynthetic pigments such as chlorophyll are main components that absorb light energy and activate primary photochemical reactions which directly affect the ability of photosynthesis. Thus, change in chlorophyll content alters the photosynthetic efficiency. Photosynthetic pigments (chlorophyll *a*, chlorophyll *b* and total chlorophyll) of *C. vulgaris* were measured to assess the influence of NAP, ANT and PYR on photosynthetic process of algae (Table 1). As compared to control, the concentration of Chl *a* and Chl *b* did not change significantly ($p < 0.05$) after 7 days of incubation with tested concentration of NAP. However, Chl *a* and *b* concentration increased after 7 days of incubation with ANT (16 % and 10 % respectively) and decreased with PYR cultivation (53 % and 57 % respectively) with respect to control. Moreover, Chl *a/b* ratio increased with exposure of ANT and PYR in *C. vulgaris* cells (Table 1). Pigments analysis of *C. vulgaris* cells with three PAHs showed changes in their relative concentration indicating that reduction of the pigment content was associated with an increase in the molecular weight of the PAHs. These results indicated that PYR exhibited more severe effects on photosynthesis of algae.

3.3. Comparative effects of three polycyclic aromatic hydrocarbons (PAHs) on Photosystem II (PSII) activity

To evaluate the light energy utilization efficiency of PSII, we compared the quantum yields of energy conversion within PSII in control, NAP, ANT and PYR exposed algal cell culture. Measurement of Chl *a*
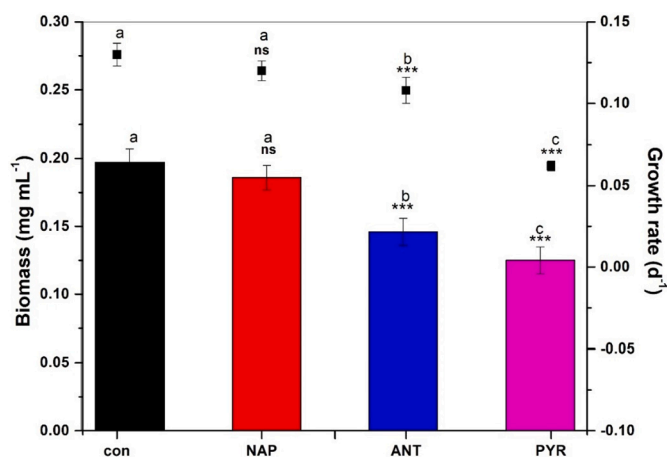

Fig. 1. Effects of Naphthalene (NAP), Anthracene (ANT) and Pyrene (PYR) on the growth curve of *C. vulgaris* during 7 days of cultivation. Error bars represent standard deviation (SD, $n = 3$).

Fig. 2. Growth rate (black square symbol) and dry biomass (in column) of *C. vulgaris*, after 7 days exposure to different PAHs, Naphthalene (NAP), Anthracene (ANT) and Pyrene (PYR). Error bars represent standard deviation ($n = 3$). *** ($p < 0.001$), ** ($p < 0.01$) and * ($p < 0.05$) represent significant differences between the control and treatment. Different alphabets indicate significant difference among treatments.

Table 1

Effects on photosynthetic pigments content (Chlorophyll *a* (Chl *a*), Chlorophyll *b* (Chl *b*), total chlorophyll in (μg mg^{-1}DW) in *C. vulgaris* after 7 days exposure to different PAHs (Naphthalene (NAP), Anthracene (ANT) and Pyrene (PYR). Data are presented as the mean value for five replicates ($n = 3$) ± standard deviation (SD). Significant differences were calculated according to Newman-Keuls multiple comparison test. (ns = non-significant, *p < 0.05, *p < 0.01 and ***p < 0.001). Different alphabets indicate significant difference among treatments.

Treatments	Chl *a*	Chl *b*	Total Chl	Chl *a*/Chl *b*
Control	41.62 ± 2.2[b]	21.62 ± 2.1[a]	63.24 ± 4.6[b]	1.92 ± 0.03[c]
NAP	41.9 ± 3.1[ns,b]	21.82 ± 3.2[ns,a]	63.72 ± 5.2[ns,b]	1.92 ± 0.01[ns,c]
ANT	48.6 ± 4.1[*,a]	23.97 ± 2.8[ns,a]	72.6 ± 5.2[***,a]	2.02 ± 0.01[**,b]
PYR	19.2 ± 2.4[***,c]	9.12 ± 1.8[***,b]	28.32 ± 3.1[***,c]	2.2 ± 0.02[**,a]

fluorescence by Dual PAM-100 revealed essential information about the photosynthetic apparatus, mainly quantum yield of photosystem II (PSII). The addition of NAP and ANT did not cause any significant change in Y(II) while it significantly reduced in PYR exposed cell (55 % of control) (Table 2). The values of non-photochemical quenching [Y(NPQ)] and photochemical quenching [Y(NO)] were unaffected by NAP and ANT exposure, while an increase was observed in Y(NPQ) with PYR treatment which was related to higher degree of PSII inhibition (Table 2). Compared with the control, PYR exposed cells showed 4 times higher value of Y(NPQ) (Table 2). After 7 days of exposure to PAHs, the electron transport rates of PSII [ETR(II)] was significantly reduced in PYR inoculated cell culture. ETR(II) declined by 57 % with PYR treatment, while it did not show any change with NAP and ANT treatments. Thus the values of ETR(II) reflected same trend as Y(II). The drop in Y(NO) and high rise in Y(NPQ) in PYR exposed cell, reflect damage to PSII but still with a protective mechanism through NPQ it protects itself against photochemical damage. The decrease in Y(II) and ETR(II) also show the reduction in the number of active PSII centers and it may also be associated with a decrease in Chl *a* content in PYR treated cells [10,33,34]. Moreover, a significant increase in Chl *a/b* ratio was reported, which indicated that antenna size was affected [35] due to the toxicity of higher molecular weight PYR [36].

Besides the quantum yield, the most important information obtained from Chl *a* fluorescence is contained in various quenching parameters (qL, qN, and qP) [37]. In this context the parameter qL is particularly useful, as it provides information about fractions of open PSII reaction centers [38]. Table 2 shows the changes in qL, with different PAHs inoculation of algal cells. A gradual reduction was observed in qL with increasing molecular weight of PAHs. As compared to control cells qL was decreased by 6 %, 10 % and 24 % with NAP, ANT and PYR respectively and the maximum decrease in qL was observed in PYR treated cell culture. From analysis of qL values, it is apparent that the number of active PSII reaction centers decreased with PAHs inoculation and the amplitude of this decrease being larger in PYR inoculated cell culture. Coefficient of photochemical quenching (qP) indicates efficiency of open PSII reaction centers which can vary between 1 and 0. After 7 days, qP did not change significantly in NAP (Table 2) but was affected significantly ($p < 0.05$) by ANT and PYR spiked culture. PYR treated cells showed lowest value suggesting that efficiency of PSII reaction centers was more susceptible to PYR. The difference between two coefficients of photochemical quenching parameters (qP-qL) reflects

connectivity of PSII reaction centers [39]. Therefore, estimation of connectivity may be derived from comparison of qL and qP. In the present study, NAP and ANT had negligible effect on connectivity of PSII centers while it was inhibited significantly in PYR exposed cells. Based on these results it is suggested that with high molecular weight PAH (PYR), the antenna of individual PSII reaction centers lost connectivity so the excitation energy cannot be transferred with high probability. This difference may be due to difference in the structure and size of the tested PAHs.

qN is an indicator of stress induced limitations and has proven to be the most sensitive parameter for early detection of any limitations by fluorescence measurements [40–42]. In algal cells of control culture, the amplitude of qN (coefficient of non-photochemical quenching) was 0.189, and it was not affected significantly by NAP (0.192) and ANT (0.182) but was significantly enhanced in PYR treated cell culture (0.526). The coefficient of non-photochemical quenching qN is sensitive to changes in the energy status of the chloroplasts (energy-dependent quenching). Our results suggest when algal cells were exposed to PYR, down-regulation of the rate of energy conversion in PSII was enhanced and O$_2$-dependent electron flow was inhibited. During PYR exposure an increase in qN is also associated with stress induced damage, which is often reflected by an increase of Y(NPQ) to compensate for decreased PSII activity.

3.4. Comparative effects of polycyclic aromatic hydrocarbons (PAHs) on biomolecules of algal cells

Chemical composition of microalgae depends on the environmental conditions; that is, they produce a large array of compounds under abiotic stress conditions to adapt and survive. For example, unfavourable conditions such as temperature, pH, salinity, and nutrients lead to change in the content of lipid and carbohydrates as well as pigments and ultimately the growth of microalgae [43,44]. PAHs are hydrophobic in nature, therefore their toxic effects on green algae may result from interference with cell biomolecules [4]. In the present study the impact on cell protein, lipid and carbohydrate content in response to NAP, ANT and PYR was measured (Fig. 3). After 7 days of cultivation, in control cells, protein content was 159 μg mg^{-1}DW and it was found to be 156 μg mg^{-1}DW in NAP, 125 μg mg^{-1}DW in ANT and 99 μg mg^{-1}DW in PYR exposed cells after 7 days of cultivation. It was seen that maximum amount of protein was obtained from control cells culture, and the

Table 2

Comparative analysis of Chl *a* fluorescence parameter of *C. vulgaris* cells after 7 days exposure to Naphthalene (NAP), Anthracene (ANT) and Pyrene (PYR). Data are presented as the mean value for five replicates ($n = 3$) ± standard deviation (SD). Significant differences were calculated according to Newman-Keuls multiple comparison test. (ns = non-significant, *p < 0.05, *p < 0.01 and ***p < 0.001). Different alphabets indicate significant difference among treatments.

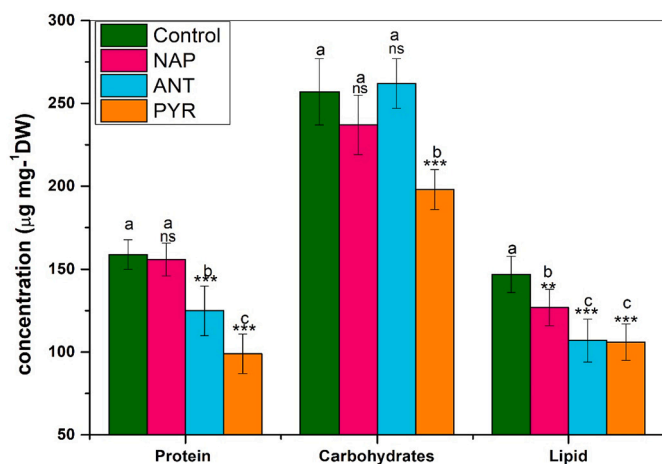| Parameters	Control	NAP	ANT	PYR
ETR(II)	31.5 ± 1.3[ns,a]	30.4 ± 1.1[ns,a]	30 ± 1.2[ns,a]	16.8 ± 2.1[***,b]
Y(II)	0.555 ± 0.01[a]	0.553 ± 0.02[ns,a]	0.546 ± 0.01[ns,a]	0.305 ± 0.06[***,b]
Y(NO)	0.376 ± 0.03[a]	0.375 ± 0.02[ns,a]	0.371 ± 0.02[ns,a]	0.355 ± 0.01[*,b]
Y(NPQ)	0.068 ± 0.006[b]	0.078 ± 0.008[ns,b]	0.06 ± 0.008[ns,b]	0.298 ± 0.01[***,a]
qN	0.189 ± 0.02[b]	0.192 ± 0.01[ns,b]	0.162 ± 0.02[ns,b]	0.526 ± 0.01[***,a]
qP	0.761 ± 0.03[a]	0.755 ± 0.01[ns,a]	0.735 ± 0.02[*,b]	0.538 ± 0.03[***,c]
qL	0.462 ± 0.01[a]	0.435 ± 0.02[ns,a]	0.417 ± 0.02[*,b]	0.335 ± 0.01[***,c]
qP-qL	0.299 ± 0.01[a]	0.322 ± 0.03[ns,a]	0.318 ± 0.03[ns,a]	0.203 ± 0.01[***,b]

Fig. 3. Toxic effects of different polycyclic aromatic hydrocarbons (PAHs) on the biomolecules content (protein, carbohydrates, and lipids) of *C. vulgaris* after 7 days of cultivation. Error bars represent standard deviation (SD, $n = 3$). *** ($p < 0.001$), ** ($p < 0.01$) and * ($p < 0.05$) represent significant differences between the control and treatments. Different alphabets indicate significant difference among treatments.

protein content was not altered by NAP exposure. Carbohydrate and lipid also play important roles in carbon partitioning, osmotic homeostasis and metabolism in algal cells [45]. In the present study, after 7 days carbohydrate content decreased from 257 µg mg^{-1}DW (control culture) to 236 µg mg^{-1}DW in NAP, 262 µg mg^{-1}DW in ANT and 198 µg mg^{-1}DW in PYR inoculated culture media (Fig. 3). Similarly, lipid content was decreased with all tested PAHs, indicating that PAHs have negative impact on energy rich compounds. In algae cells, selectively permeable membranes are the first line of defence against external stress factors. PAHs may alter the cell membranes permeability by affecting cell membrane proteins and lipids. As PAHs easily combines with proteins and lipids *in vivo* [46] and PAHs can alter functioning of the algal cells. In the present study, exposure to three PAHs caused significant reduction in lipid content in proportion to molecular weight of PAHs. High molecular weight PYR shows maximum reduction in lipid molecules. The cell growth rate and biomass productivity play a major role in determining the microalgal carbohydrates and lipid productivity. Decreased carbohydrate and lipid content with PAHs might be ascribed to inhibition of cell division and osmotic imbalance [47]. Synthesis of biomolecules such as protein, carbohydrates and lipid is directly related to photosynthesis and responsible for the growth and development of microalgae organism. Obtained results showed some alteration in biomolecules with NAP and ANT treatments, however photosynthesis performance of NAP and ANT exposed cell did not show any significant change. These results indicated that low molecular weight PAHs have more effect on synthesis of different biomolecules of algal cell compared to photosynthetic machinery which seems to be survival and tolerance mechanism of algae. In case of PYR, cells fail to protect its photosynthesis machinery and other metabolic processes.

3.5. Removal efficiency of C. vulgaris for Naphthalene (NAP), Anthracene (ANT) and Pyrene (PYR)

To know the removal efficiency of *C. vulgaris* for three tested PAHs remaining amount of PAHs in the media was studied. PAHs uptake from media through *C. vulgaris* cells was studied by measurement of absorption spectra following 3rd and 7th day of incubation with 5 mgL^{-1} concentration of PAHs. Fig. 4A shows that the amount of NAP remaining in the media dropped sharply, with 90–92 % of it being metabolized at the end of 7th day cultivation. Similar results of PAHs removal were found in ANT (92–95 %) (Fig. 4B) and PYR (~75 %) (Fig. 4C)

treatments, suggesting that all the three PAHs could be rapidly absorbed by *C. vulgaris* cells. The remaining amount of NAP and ANT at end of the experiment was only 5 to 10 %, indicating that almost all NAP and ANT taken up by *C. vulgaris* cells within 7 days. The percentage of PYR remaining in the media in presence of *C. vulgaris* was ~25 % after 7 days of cultivation. Spectrophotometric study confirms that the absorbance of PAHs in the culture media decreased with the incubation time. PAHs content in the medium dropped sharply during 1 to 7 days incubation and maximum percentage of PAHs uptake occurs during the first 3–4 days. The abiotic loss of all three PAHs in the present culture condition was negligible (data not shown). Result obtained indicated that *C. vulgaris* was able to take up all PAHs substantially and could grow efficiently with NAP and ANT, although the growth of *C. vulgaris* was reduced by 50 % with PYR exposure. The removal efficiency of the *C. vulgaris* was much higher for NAP and ANT than that for PYR.

3.6. Comparative effect of three different polycyclic aromatic hydrocarbons (PAHs) on dehydrogenase activity

When algal cells grow in presence of any organic compound it can induce changes in enzymatic reactions. In algal cells, dehydrogenase is an important oxidoreductase enzyme which metabolizes organic compounds. It is a vital part of the electron transport system of a cell. Therefore, the possible involvement of this catabolic enzyme in different PAHs degradation by *C. vulgaris* was investigated. A prominent rise in dehydrogenase activity was observed in NAP and ANT treated cell culture after 3 days of incubation (Table 3). Average dehydrogenase activity after 3 days of exposure was calculated to be 0.106 µg of TF mL^{-1} h^{-1} in control, 0.135 µg of TF mL^{-1} h^{-1} in NAP and it was 0.165 µg of TF mL^{-1} h^{-1} in ANT exposed algal cells. This initiation of enzyme activity was accompanied by a significant reduction in the amount of PAHs from the media within three days. After 7 days of cultivation the highest value of dehydrogenase activity was observed in control cells and it declined in NAP and ANT cell culture (Table 3). Maximum absorption of NAP and ANT occurred within 3 days of cultivation, therefore higher dehydrogenase activity was observed at 3rd day of cultivation. Dehydrogenase activity was found to be lowest in PYR exposed cell even after 3rd (0.052 µg of TF mL^{-1} h^{-1}) and 7th day (0.062 µg of TF mL^{-1} h^{-1}) of cultivation.

This result implies that the detoxification mechanism of algae exhibited by, production of dehydrogenase [4,17,18] was more effective for NAP and ANT treatment, leading to a higher tolerance to intracellular concentration of both PAHs. Moreover, results indicate that PYR was more recalcitrant, and more difficult to be metabolized by *C. vulgaris*, although absorption of PYR by *C. vulgaris* was considerably good. A loss of ability by the cells to metabolize HMW PAHs resulting from irreparable damage to the catabolic system responsible for degradation, is possibly because of loss of essential biomolecules or enzyme damage due to low photosynthetic rate. On the basis of these results, we conclude that *C. vulgaris* efficiently metabolizes low molecular weight PAH within the cell and has good prospects for its application for bioremediation of hydrocarbons from petroleum industry wastewater. A schematic diagram showing the summary of the results obtained above is presented in Fig. 5. Algal cells were negatively affected by ANT and PYR treatments with the tested concentration, however, PYR proved to be most toxic to *C. vulgaris* growth. PAHs influence growth of algal cells by affecting its chlorophyll contents, which in turn affects the accumulation of organic matter during photosynthesis. The decline in the productivity of biomolecules may lead to its density reduction.

4. Conclusion

This study describes the impact of PAHs with evidence of physiological and biochemical changes in microalgae cells. Study revealed the interaction of algal cells with different PAHs which negatively influence growth and biomass yield. However, the removal efficiency of *C. vulgaris*
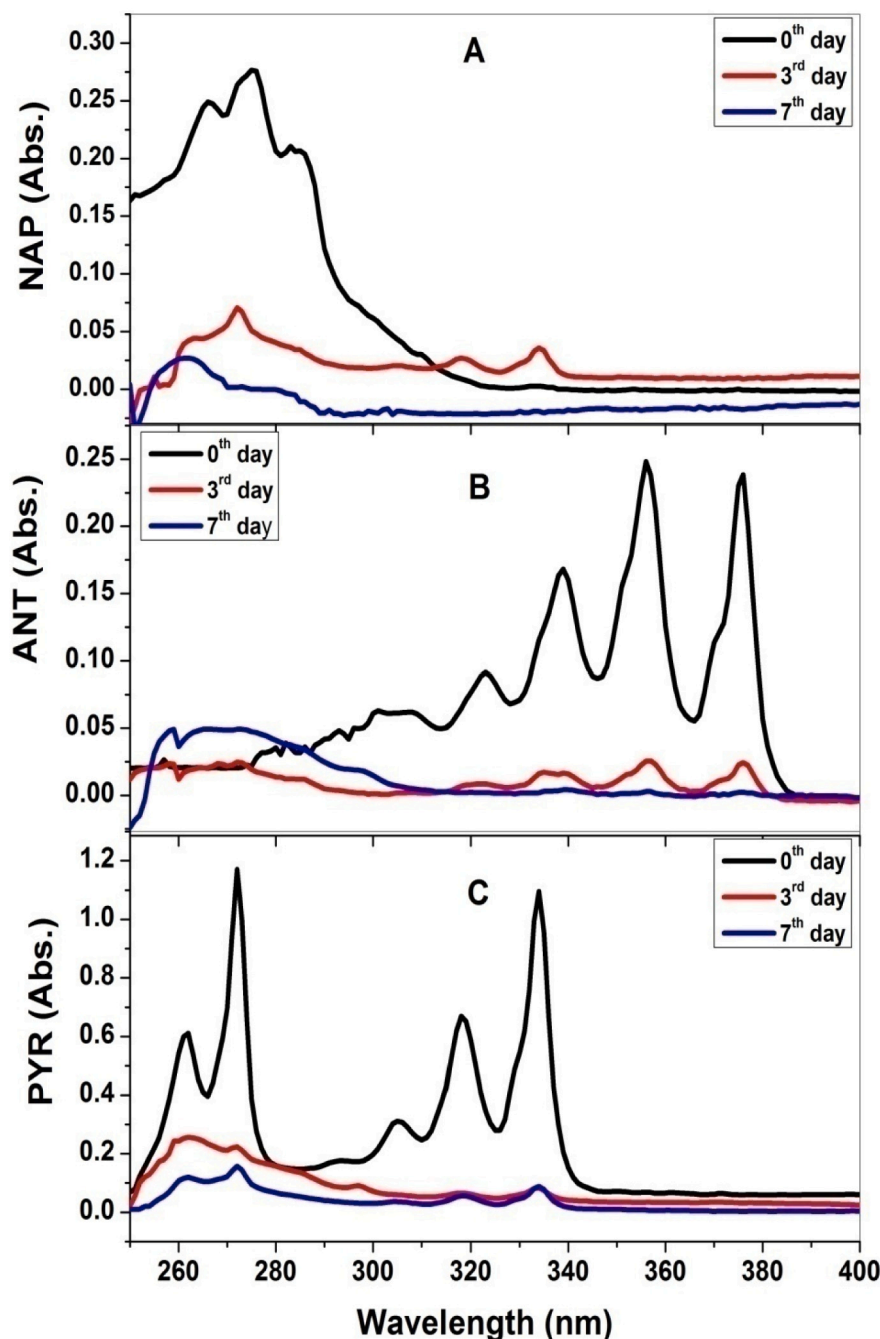
Fig. 4. Spectrophotometric analysis of Naphthalene (NAP) (A), Anthracene (ANT) (B) and Pyrene (PYR) (C) extraction form culture media with *C. vulgaris* cells after 0th day, 3rd day and 7th day of cultivation.

Table 3
Dehydrogenase activity (μg of TF (triphenylformazane) mL^{-1} h^{-1}) in Naphthalene (NAP), Anthracene (ANT) and Pyrene (PYR) exposed *C. vulgaris* cells . *** ($p < 0.001$), ** ($p < 0.01$) and * ($p < 0.05$) represent significant differences between the control and treatments ($\pm$SD, $n = 3$). Different alphabets indicate significant difference among treatments.

Treatments	Dehydrogenase activity (3rd day)	Dehydrogenase activity (7th day)
Control	0.106 ± 0.01[c]	0.280 ± 0.03[a]
NAP	0.135 ± 0.01**,[b]	0.216 ± 0.02*,[b]
ANT	0.165 ± 0.02***,[a]	0.194 ± 0.02***,[b]
PYR	0.052 ± 0.01***,[d]	0.060 ± 0.01***,[c]

for PAHs indicates that this species has the capability to remove low as well as high molecular weight organic pollutants, so *C. vulgaris* can be used as bioremediation of PAHs from contaminated environment. Further, high molecular weight PAH may inhibit metabolic and photosynthetic processes, leading to reduced cell growth and biomass production. *C. vulgaris* was found to be most sensitive to 4 ring PYR in comparison to other PAHs tested (2 ring NAP and 3 ring ANT) suggesting that characteristics of PAHs such as structure and molecular weight affects their impact on algal cells. The difference in toxicity level could be because their molecular weight and benzene ring arrangement.

CRediT authorship contribution statement

Rupal Singh Tomar-Conceptualization, designed and performed the
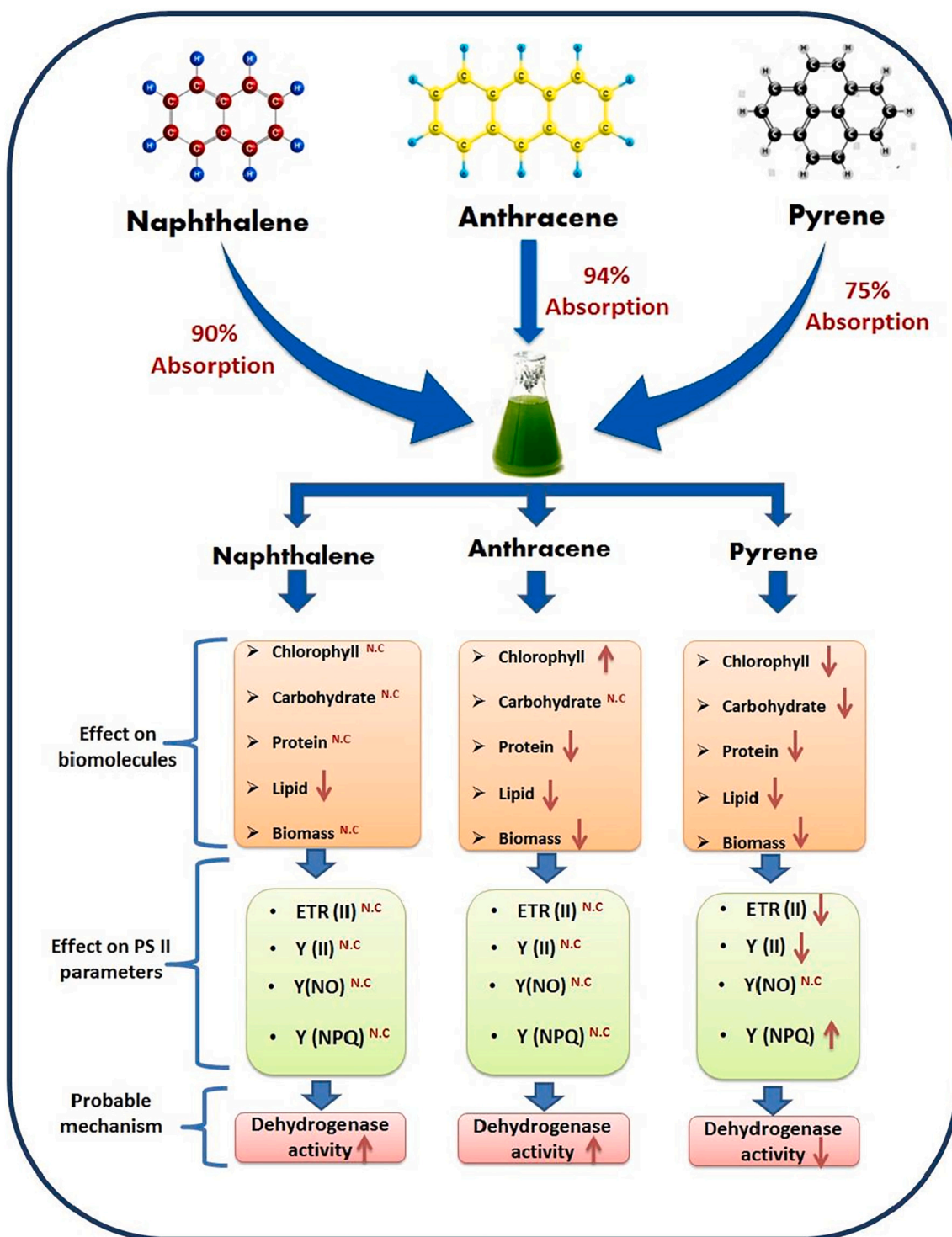
Fig. 5. A schematic representation of the summary of the results. (NC, not change significantly).

experiments, Data curation, Writing – Original draft preparation. **Prabha Rai-Kalal**-Investigation, and performed lab work. **Anjana Jajoo**-Conceptualization, designed the experiments, Supervision, Writing – Reviewing and Editing.

Declaration of competing interest

The authors declare that they have no known competing financial interests or personal relationships that could have appeared to influence the work reported in this paper.

References

[1] M. Diaz, V. Mora, F. Pedrozo, D. Nichela, G. Baffico, Evaluation of native acidophilic algae species as potential indicators of polycyclic aromatic hydrocarbon (PAH) soil contamination, J. Appl. Phycol. 27 (2015) 321–325.

[2] E.S.E. Aldaby, A.M.M. Mawad, Pyrene biodegradation capability of two different microalgal strains, Glob. NEST J. 21 (2019) 291–296.

[3] A. Aksmann, Z. Tukaj, Intact anthracene inhibits photosynthesis in algal cells: a fluorescence induction study on *Chlamydomonas reinhardtii* cw92 strain, Chemosphere 74 (2008) 26–32.

[4] R.S. Tomar, A. Jajoo, Enzymatic pathway involved in the degradation of fluoranthene by microalgae *Chlorella vulgaris*, Ecotoxicology 30 (2021) 268–276.

[5] S. Asghari, F. Rajabi, R. Tarrahi, S.Y. Salehi-Lisar, S. Asnaashari, Y. Omidi, A. Movafeghi, Potential of the green microalga *Chlorella vulgaris* to fight against fluorene contamination: evaluation of antioxidant systems and identification of intermediate biodegradation compounds, J. Appl. Phycol. 32 (2020) 411–419.

[6] A. Bennett, T.S. Bianchi, J.C. Means, The effects of PAH contamination and grazing on the abundance and composition of micro phytobenthos in salt marsh sediments (Pass Fourchon, LA, USA) II. The use of plant pigments as biomarkers, Estuar. Coast. Shelf Sci. 50 (2000) 425–439.

[7] A. Lei, Z. Hu, Y. Wong, N.F. Tam, Antioxidant responses of microalgal species to pyrene, J. Appl. Phycol. 18 (2006) 67–78.

[8] M. Megharaj, I. Singleton, N.C. McClure, R. Naidu, Influence of petroleum hydrocarbon contamination on microalgae and microbial activities in a long term contaminated soil, Arch. Environ. Contam. Toxicol. 38 (2000) 439–445.

[9] A. Jajoo, N.R. Mekala, R.S. Tomar, M. Grieco, M. Tikkanen, E.M. Aro, Inhibitory effects of polycyclic aromatic hydrocarbons (PAHs) on photosynthetic performance are not related to their aromaticity, J. Photochem. Photobiol. B Biol. 137 (2014) 151–155.

[10] R.S. Tomar, A. Jajoo, Photosynthetic response in wheat plants caused by the phototoxicity of fluoranthene, Funct. Plant Biol. 46 (2019) 725–731.

[11] L. Jain, A. Jajoo, Protection of PSI and PSII complexes of wheat from toxic effect of anthracene by *Bacillus subtilis* (NCIM 5594), Photosynth. Res. 146 (2020) 197–211.

[12] H. Cao, C. Wang, H. Liu, W. Jia, H. Sun, Enzyme activities during benzo[a]pyrene degradation by the fungus *Lasiodiplodia theobromae* isolated from a polluted soil, Sci. Rep. 10 (2020) 865.

[13] A.E.-L. Hesham, A.M. Mawad, Y.M. Mostafa, A. Shoreit, Study of enhancement and inhibition phenomena and genes relating to degradation of petroleum polycyclic aromatic hydrocarbons in isolated bacteria, Microbiology 83 (2014) 599–607.

[14] Z. Yan, H. Jiang, X. Li, Y. Shi, Accelerated removal of pyrene and benzo [a] pyrene in freshwater sediments with amendment of cyanobacteria-derived organic matter, J. Hazard. Mater. 272 (2014) 66–74.

[15] L.C. Pessòa, K.M. Deamici, L.A.M. Pontes, J.I. Druzian, Assis D. de Jesus, Technological prospection of microalgae-based biorefinery approach for effluent treatment, Algal Res. 60 (2021), 102504.

[16] M. Zabochnicka-Świątek, M. Krzywonos, H.M. Kalaji, N.I. El-Sheery, J.B. Bień, Influence of clinoptilolite on the efficiency of heavy metal removal from wastewater by *Chlorella vulgaris*, Desalin. Water Treat. 117 (2018) 49–57.

[17] S.R. Subashchandrabose, P. Logeshwaran, K. Venkateswarlu, R. Naidu, M. Megharaj, Pyrene degradation by Chlorella sp. MM3 in liquid medium and soil slurry: possible role of dihydrolipoamide acetyltransferase in pyrene biodegradation, Algal Res. 23 (2017) 223–232.

[18] S.R. Subashchandrabose, L. Wang, K. Venkateswarlu, R. Naidu, M. Megharaj, Interactive effects of PAHs and heavy metal mixtures on oxidative stress in Chlorella sp. MM3 as determined by artificial neural network and genetic algorithm, Algal Res. 21 (2017) 203–212.

[19] A.-P. Lei, Z.-L. Hu, Y.-S. Wong, N.F.-Y. Tam, Removal of fluoranthene and pyrene by different microalgal species, Bioresour. Technol. 98 (2007) 273–280.

[20] S.M.N. Chan, T. Luan, M.H. Wong, N.F.Y. Tam, Removal and biodegradation of polycyclic aromatic hydrocarbons by *Selenastrum capricornutum*, Environ. Toxicol. Chem. 25 (2006) 1772–1779.

[21] H.I. Abdel-Shafy, M.S.M. Mansour, A review on polycyclic aromatic hydrocarbons: source environmental impact, effect on human health and remediation, Egypt. J. Pet. 25 (2016) 107–123.

[22] E.B. Nilsen, R.J. Rosenbauer, C.C. Fuller, B.J. Jaffe, Sedimentary organic biomarkers suggest detrimental effects of PAHs on estuarine microbial biomass during the 20th century in San Francisco Bay, CA, USA, Chemosphere 119 (2015) 961–970.

[23] N.R. Couling, M.G. Towell, K.T. Semple, Biodegradation of PAHs in soil: influence of chemical structure, concentration and multiple amendment, Environ. Pollut. 158 (2010), 3411e3420.

[24] E. Puglisi, F. Cappa, G. Fragolis, A. Trevisan, A.A.M. Del Re, Bioavailability and degradation of phenanthrene in compost amended soils, Chemosphere 67 (2007), 548e556.

[25] J.L. Stroud, A.H. Rhodes, G.I. Paton, K.T. Semple, Using supercritical fluid extraction to measure the desorption and bioaccessibility of phenanthrene in soils, Environ. Pollut. 156 (2008), 664e670.

[26] S.K. Mishra, W.I. Suh, W. Farooq, M. Moon, A. Shrivastav, M.S. Park, J.-W. Yang, Rapid quantification of microalgal lipids in aqueous medium by a simple colorimetric method, Bioresour. Technol. 155 (2014) 330–333.

[27] L.M.L. Laurens, T.A. Dempster, H.D.T. Jones, E.J. Wolfrum, S. Van Wychen, J.S. P. McAllister, M. Rencenberger, K.J. Parchert, L.M. Gloe, Algal biomass constituent analysis: method uncertainties and investigation of the underlying measuring chemistries, Anal. Chem. 84 (2012) 1879–1887.

[28] S.P. Slocombe, M. Ross, N. Thomas, S. McNeill, M.S. Stanley, A rapid and general method for measurement of protein in microalgal biomass, Bioresour. Technol. 129 (2013) 51–57.

[29] S. Dere, T. Gunes, R. Sivaci, Spectrophotometric determination of chlorophyll-*a, b* and total carotenoid contents of some algae species using different solvents, Turk. J. Bot. 22 (1998) 13–17.

[30] S. Lundstedt, P. Haglund, L. Oberg, Degradation and formation of polycyclic aromatic compounds during bioslurry treatment of an aged gasworks soil, Environ. Toxicol. Chem. 22 (2003) 1413–1420.

[31] A. Aksmanna, T. Shutovab, G. Samuelssonb, Z. Tukaja, The mechanism of anthracene interaction with photosynthetic apparatus: a study using intact cells, thylakoid membranes and PS II complexes isolated from *Chlamydomonas reinhardtii*, Aquat. Toxicol. 104 (2011) 205–210.

[32] G.E. Bragin, T.F. Parkerton, A.D. Redman, D.J. Letinksi, J.D. Butler, M.L. Paumen, C.A. Sutherland, T.M. Knarr, M. Comber, K. den Haan, Chronic toxicity of selected polycyclic aromatic hydrocarbons to algae and crustaceans using passive dosing, Environ. Toxicol. Chem. 35 (2016) 2948–2957.

[33] W. Khpalwak, M.S. Abdel-dayem, H. Sakugawa, Individual and combined effects of fluoranthene, phenanthrene, mannitol and sulfuric acid on marigold (*Calendula officinalis*), Ecotoxicol. Environ. Saf. 148 (2018) 834–841.

[34] R.S. Tomar, A. Jajoo, Photomodified fluoranthene exerts more harmful effects as compared to intact fluoranthene by inhibiting growth and photosynthetic processes, Ecotoxicol. Environ. Saf. 122 (2015) 31–36.

[35] E. Dinç, M.G. Ceppi, S.Z. Tóth, M. Bottka, G. Schansker, The Chl*a* fluorescence intensity is remarkably insensitive to changes in the chlorophyll content of the leaf as long as the chl*a/b* ratio remains unaffected, Biochim. Biophys. Acta Bioenerg. 1817 (2012) 770–779.

[36] X. Wang, X. Zhu, X. Chen, B. Lv, X. Wang, D. Wang, Phenanthrene and pyrene disturbed the growth of *Microcystis aeruginosa* as co-cultured with *Chlorella pyrenoidosa*, Environ. Sci. Pollut. Res. 27 (2020) 45957–45964.

[37] S. Mathur, R.S. Tomar, A. Jajoo, Arbuscular mycorrhizal fungi (AMF) protects photosynthetic apparatus of wheat under drought stress, Photosynth. Res. 139 (2019) 227–238.

[38] R. Zhang, T.D. Sharkey, Photosynthetic electron transport and proton flux under moderate heat stress, Photosynth. Res. 100 (2009) 29–43.

[39] N.R. Baker, Chlorophyll fluorescence: a probe of photosynthesis in vivo, Annu. Rev. Plant Biol. 59 (2008) 89–113.

[40] N.I. Elsheery, V.S.J. Sunoj, Y. Wen, J.J. Zhu, G. Muralidharan, K.F. Cao, Foliar application of nanoparticles mitigates the chilling effect on photosynthesis and photoprotectionin sugarcane, Plant Physiol. Biochem. 149 (2020) 50–56.

[41] N.I. Elsheery, B. Wilske, J.L. Zhang, K.F. Cao, Cheek seasonal variations in gas exchange and chlorophyll fluorescence in the leaves of five mango cultivars in southern Yunnan, China, J. Hortic. Sci. Biotechnol. 82 (2007) 855–862.

[42] W. Vredenberg, M. Durchan, O. Prášil, Photochemical and photoelectrochemical quenching of chlorophyll fluorescence in photosystem II, Biochim. Biophys. Acta 1787 (2009) 1468–1478.

[43] C. Paliwal, M. Mitra, K. Bhayani, S.V. Bharadwaj, T. Ghosh, S. Dubey, S. Mishra, Abiotic stresses as tools for metabolites in microalgae, Bioresour. Technol. 244 (2017) 1216–1226.

[44] D. Tang, W. Han, P. Li, X. Miao, J. Zhong, CO2biofixation and fatty acid composition of *Scenedesmus obliquus* and *Chlorella pyrenoidosa* in response to different CO2 levels, Bioresour. Technol. 102 (2011) 3071–3076.

[45] S. Li, R. Chu, D. Hua, Z. Yin, F. Mo, T. Hu, C. Liu, L. Zhu, Combined effects of 17β-estradiol and copper on growth, biochemical characteristics and pollutant removals of freshwater microalgae *Scenedesmus dimorphus*, Sci. Total Environ. 730 (2020), 138597.

[46] A.N. Croxton, G.H. Wikfors, R.D. Schulterbrandt-Gragg, The use of flow cytometric applications to measure the effects of PAHs on growth, membrane integrity, and relative lipid content of the benthic diatom, *Nitzschia brevirostris*, Mar. Pollut. Bull. 91 (2015) 160–165.

[47] F. Sami, M. Yusuf, M. Faizan, A. Faraz, S. Hayat, Role of sugars under abiotic stress, Plant Physiol. Biochem. 109 (2016) 54–61.

| Frontiers in Plant Science

Improving photosynthesis through multidisciplinary efforts: The next frontier of photosynthesis research

Xin-Guang Zhu[1]*, Mirza Hasanuzzaman[2], Anjana Jajoo[3], Tracy Lawson[4], Rongcheng Lin[5], Chun-Ming Liu[6], Lu-Ning Liu[7], Zhenfeng Liu[8], Congming Lu[9], Michael Moustakas[10], Thomas Roach[11], Qingfeng Song[12], Xinyou Yin[13] and Wangfeng Zhang[14]

[1]Center of Excellence for Molecular Plant Sciences, Chinese Academy of Sciences, Shanghai, China, [2]Department of Agronomy, Faculty of Agriculture, Sher-e-Bangla Agricultural University, Dhaka, Bangladesh, [3]School of Biotechnology, Devi Ahilya University, Indore, India, [4]School of Life Science, University of Essex, Colchester, United Kingdom, [5]Key Laboratory of Photobiology, Institute of Botany, Chinese Academy of Sciences, Beijing, China, [6]School of Advanced Agricultural Sciences, Peking University, Beijing, China, [7]Institute of Systems, Molecular and Integrative Biology, University of Liverpool, Liverpool, United Kingdom, [8]National Laboratory of Biomacromolecules, Institute of Biophysics, Chinese Academy of Sciences, Beijing, China, [9]School of Life Sciences, Shandong Agricultural University, Taian, China, [10]Department of Botany, School of Biology, Aristotle University of Thessaloniki, Thessaloniki, Greece, [11]Department of Botany, University of Innsbruck, Innsbruck, Austria, [12]Center of Excellence for Molecular Plant Sciences, Chinese Academy of Sciences, Shanghai, China, [13]Department of Plant Sciences, Centre for Crop Systems Analysis, Wageningen University & Research, Wageningen, Netherlands, [14]Department of Agronomy, Shihezi University, Shihezi, China

The light-dependent release of oxygen from plants was first discovered in the 1770s by Joseph Priestley and Jan Ingenhousz. More recently, the enzyme-catalyzed pathway of carbon assimilation was characterized by Melvin Calvin, James Bassham, and Andrew Benson in 1950, and since then, photosynthesis has been intensively studied by hundreds and thousands of other pioneers. So far, the major components of photosynthesis in different systems and the regulations over these components have been gradually revealed. Now, photosynthesis research is entering a new era, with the ambitious goal of providing new green solutions for overcoming the challenges facing our society, such as ensuring the sustainable supply of food, fiber, and fuel, as well as improving the ecological stability of our planet. We can also conceive that one day we may also leave our planet to live on others, but certainly not without photoautotrophs! Developing photosynthetic systems, both natural and artificial, with greater efficiency in using resources, such as light, nitrogen, CO_2, and water, to benefit human society and our planet, is becoming a new frontier of research and a hallmark of this exciting era of photosynthesis research.

Why is there large scope to improve photosynthesis?

There are great variations in the photosynthetic energy conversion efficiency in extant plants, which are nonetheless usually less than 1/3 of the theoretical optimal photosynthetic light use efficiency (Zhu et al., 2008; Slattery and Ort, 2015; Yin and Struik, 2015). The increased production of biomass and yield in major crops under Free Air CO_2 Enrichment experiments shows that increasing photosynthesis can indeed increase crop yield (Long et al., 2006). Many arguments can be used to explain why evolution has not resulted in optimal photosynthesis. First, evolution selects for survival over productivity. Usually, one particular anatomical, physiological or developmental feature, which confers better tolerance to a particular stress, can offer plants higher fitness in their growth habitat regardless of whether the plant by chance has a high photosynthetic rate or not. As an extreme example, having mechanisms to maintain a high water use efficiency, e.g., the Crassulacean acid metabolism, will be a preferred option for survival in an extremely dry environment while maintaining a superior photosynthetic rate becomes less critical under this condition. Second, since photosynthesis first evolved, there have been dramatic changes in climate, such as CO_2 levels, temperature, precipitation, etc., all historically leading to specialized adaptations that can now be considered "outdated." Just in the past 200 years, atmospheric CO_2 levels increased from about 200 ppm to 410 ppm, average global temperatures have soared by $1.5°C$ and precipitation has become increasingly erratic (IPCC Climate Change, 2021). Such rapid changes open up possibilities to optimize photosynthesis toward current and future climate scenarios. Furthermore, the climate is changing at a speed faster than the speed of plant adaptation. This has been demonstrated earlier, for example, by the kinetic properties of Rubisco, for which kinetic properties fit better to the CO_2 level of 400,000 years ago (Zhu et al., 2004). The changes in the global temperature also have a major impact on photosynthetic performance (Sage and Kubien, 2007). Thus, sub-optimality of photosynthesis can be related to the legacy of evolution. Rubisco evolved 2.4 billion years ago, which was a hypoxic and CO_2-rich environment, under which the inefficiency of Rubisco carboxylation activity was not relevant (Banda et al., 2020).

In contrast to these reasons why evolution has not selected the optimal photosynthesis, there are also other parallel arguments on the current photosynthetic properties that may already represent an "optimal" choice for plants. The balance between plant growth and stress resistance in a highly variable and potentially stressful environment may also prevent the maximization of photosynthesis and hence growth potential (Zhang et al., 2020), i.e., the diverse photosynthetic properties in nature represent different evolutionary choices for plants to survive and thrive in their habitats without human

intervention. Along this vein, it is interesting to note that, green plants, purple bacteria, and green sulfur bacteria have drastically different absorption spectra, however, their current light absorption spectrum may be an "optimal" design for the light conditions they commonly experience (Arp and Kistner-Morris, 2020). Similarly, Rubisco, being able to catalyze both ribulose bisphosphate (RuBP) carboxylation and also RuBP oxygenation, may also well represent an evolutionary preferred choice compared to a hypothetically perfect Rubisco, which can only catalyze RuBP carboxylation. This is again because, under stress conditions, this RuBP oxygenation capacity can not only help dissipate excess light energy but also help maintain a metabolite pool which can, when needed, be used to rapidly provide intermediates for the Calvin-Benson cycle (Stitt and Borghi, 2021).

A few factors underlie huge opportunities to improve photosynthesis. First, the rapid global climate change outpaced the speed of plant evolution, as discussed earlier. Second, during crop domestication, crops have drastically different growth habitats compared to those of their ancestors. For example, modern crops usually are grown in monoculture as a dense canopy, as compared to their ancestors which often have access to plenty of sunlight. Thirdly, compared to the situation of plants growing in the wild, which can only rely on their repertoire of weapons and solutions to cope with stresses, crops in agriculture can be protected through human intervention (irrigation, fertilizer application, disease control, etc). As a result, plants can take a competitive growth strategy, rather than a stress tolerant or ruderal strategy (Grime, 1977).

Though it is desirable for plants to have a high demand for improving photosynthetic efficiency, it is worth noting here that, under certain conditions, such as under high light, the photosynthetic efficiency becomes less important, while effective photoprotective mechanisms and ensuring total photosynthetic yield becomes more relevant for plants. Indeed, sophisticated mechanisms have evolved to ensure high photosynthetic yield under high light, especially under concurrent high light and stress combinations, while at the same time confer higher quantum yield when the light becomes a scarce resource (Ort, 2001). This scenario again implies opportunities to utilize the excess energy which is otherwise largely wasted in photoprotection, as shown in the recent success of engineering a faster recovery from photoprotection for greater biomass production (Kromdijk et al., 2016).

Here, we emphasize that the rapid development of synthetic biology tools now offers new opportunities to create completely new designs of improved photosynthetic systems and tailoring photosynthesis to the increasing demands in the context of our changing climate (Zhu et al., 2020). In the following sections, we briefly discuss the available opportunities, the tools used to support studying photosynthesis, and the associated research areas.

An incomplete list of options to improve photosynthesis

First, we provide an incomplete list of opportunities to improve photosynthetic efficiency:

(1) Creating more efficient light harvesting systems, which could utilize the expanded solar spectrum for the generation of proton motive force for generation of ATP and NADPH (Ort et al., 2015) and/or smaller chlorophyll antenna size and lower chlorophyll content reducing the excess absorption of sunlight and improving photosynthetic efficiency (Ort et al., 2011; Moustakas et al., 2022).

(2) Creating more efficient photo-protection systems to minimize heat dissipation when unnecessary and to maximize photochemistry;

(3) Creating more efficient state transition and electron transferring between PSII and PSI under changing environment to maximize light-use efficiency;

(4) Generating a Rubisco with a greater catalytic rate and higher specificity for CO_2;

(5) Repurposing efficient CO_2-concentrating mechanisms, either these are Kranz type CO_2-concentrating mechanisms, or carboxysome- or pyrenoid-based systems to decrease the Rubisco oxygenation flux;

(6) Creating a novel pathway to cope with photorespiratory CO_2 and ammonia loss to minimize the energy associated with refixation of CO_2 and ammonia;

(7) Developing an effective combination of biological CO_2 fixation with solar energy capture to further increase the efficiency of harvesting light energy through capitalizing on the high light conversion efficiency of photovoltaic systems;

(8) Developing nanomaterials to enable better capturing and delivery of CO_2 to Rubisco to decrease the Rubisco oxygenation;

(9) Enhancing antioxidant defense under natural changing conditions to decrease the photodamage;

(10) Development of artificial systems that cope better with high light different conditions through channeling the excess light for production of renewable chemical energy;

(11) Overcoming sink limitations of photosynthesis;

(12) Developing improved stomatal dynamics to increase water and light use efficiency.

(13) Develop photosynthetic systems that can better utilize fluctuating light conditions;

(14) Creation of novel photosynthetic systems which may enable human space exploration.

These are all basic elements required to build a repertoire of highly efficient systems. When these modules for higher efficiency are individually developed, or achieved in combination, we could gain increased plant yield potential either for biomass or grain or storage tissues, as well as greener energy sources.

Technologies and tools to support a new era of photosynthesis research

The rapid progress in many new technologies and tools provides sufficient toolsets for us to overcome these grand challenges and goals (Table 1). These major technological advances that will revolutionize photosynthesis research in the future include:

- **Techniques to scan photosynthetic systems.** The advances in the fluorescence imaging techniques for *in vivo* scanning of natural photosynthetic systems will enable *in situ* characterization of photosynthetic pigment-protein complexes and their distribution/dynamics under different conditions (Casella et al., 2017; Mullineaux and Liu, 2020). This information and elucidation of their physiological significance will provide basic information which is needed for the future de novo design of artificial photosynthetic systems.

- **Techniques for studying the molecular and supramolecular basis of photosynthesis.** The recent development of cryo-electron microscopy (cryo-EM) technology enables rapid progress in solving the structures of major proteins, protein complexes and supercomplexes involved in photosynthesis at near-atomic resolutions through the single-particle analysis method (Wei et al., 2016; Su et al., 2017; Zhang et al., 2017; Malone et al., 2019; Pi et al., 2019; Pan et al., 2020). Atomic force microscopy (AFM) technology provides the opportunity to delineate the lateral arrangement, protein interactions and dynamics of photosynthetic complexes in the context of photosynthetic membranes (Liu and Scheuring, 2013; Wood et al., 2018; Zhao et al., 2020). In addition, the cryo-electron tomography (cryo-ET) method allows researchers to visualize the *in situ* arrangement of photosynthetic complexes in chloroplasts and CO_2-fixing organelles (Engel et al., 2015; Freeman Rosenzweig et al., 2017; Wietrzynski et al., 2020; Gupta et al., 2021; Ni et al., 2022). The structural information combined with the variation of genomic sequences and corresponding changes in biophysical or biochemical properties of the proteins/protein complexes will enable the determination of the molecular and supramolecular basis underlying photosynthetic processes and regulation. The detailed physical mechanisms can then be revealed through a combination of such biological or genetic manipulation,

TABLE 1   Methods used to study photosynthesis at different scales.

	Protein, pigment protein complexes and thylakoid membrane scale	Chloroplast, cellular and leaf scales	Cellular and leaf scales
Tools for structure and morphological characterization	Cryo-EM, cryo-ET, AFM, transmission EM, freeze-fracture EM, fluorescence imaging	Cryo-ET, Scanning EM, light microscope	Image based phenomics
Signals used for functional characterization	Fluorescence emission, absorption spectrum, gas exchange signal, oxygen evolution, isotope discrimination, metabolomics, fluxomics	Gas exchange signal, fluorescence emission signal, reflectance signal	Gas exchange signal, fluorescence emission signal, reflectance signal
Theoretical models used to describe photosynthesis (or a component of photosynthesis) at different scales	Molecular dynamics models, quantum mechanics models, molecular mechanics models, reaction diffusion models	Reaction diffusion models, dynamic systems models, steady state models	Steady state models, dynamic systems models, reaction diffusion models

e.g., base editing, experiments with molecular dynamics simulations, especially those that combine quantum mechanics and molecular mechanics (MoD QM/MM) (Liguori et al., 2020) and artificial intelligence-based protein structure prediction (Jumper et al., 2021). It is worth pointing out here that the combination of multiple approaches will not only enable studies on the structure-function relationship of proteins or protein complexes, but also may stimulate *ab initio* design of new protein/protein complexes with desired properties (Hsia et al., 2021).

- **Techniques to mine superiority within the natural variation of photosynthesis.** Though in current plants, a photosynthetic system with all components in an optimal state is not yet available, there are great natural variations of photosynthetic machinery across diverse photosynthetic organisms. High-throughput plant phenotyping techniques combined with genome-wide association techniques and genetic tools can allow the identification of novel genes controlling photosynthetic efficiency and characterize those genetic variations conferring superior traits for some components of photosynthesis.

- **Multi-scale systems modeling of photosynthesis.** The modeling will allow not only the dissection of biological, biophysical, and biochemical mechanisms controlling the efficiency of a particular photosynthetic protein or complex, but also the rational design of optimal photosynthetic systems for greater efficiency under different environments (Xiao et al., 2017). Novel photosynthetic models enable accurate prediction of the photosynthesis process and its regulation at different scales still needs to be developed.
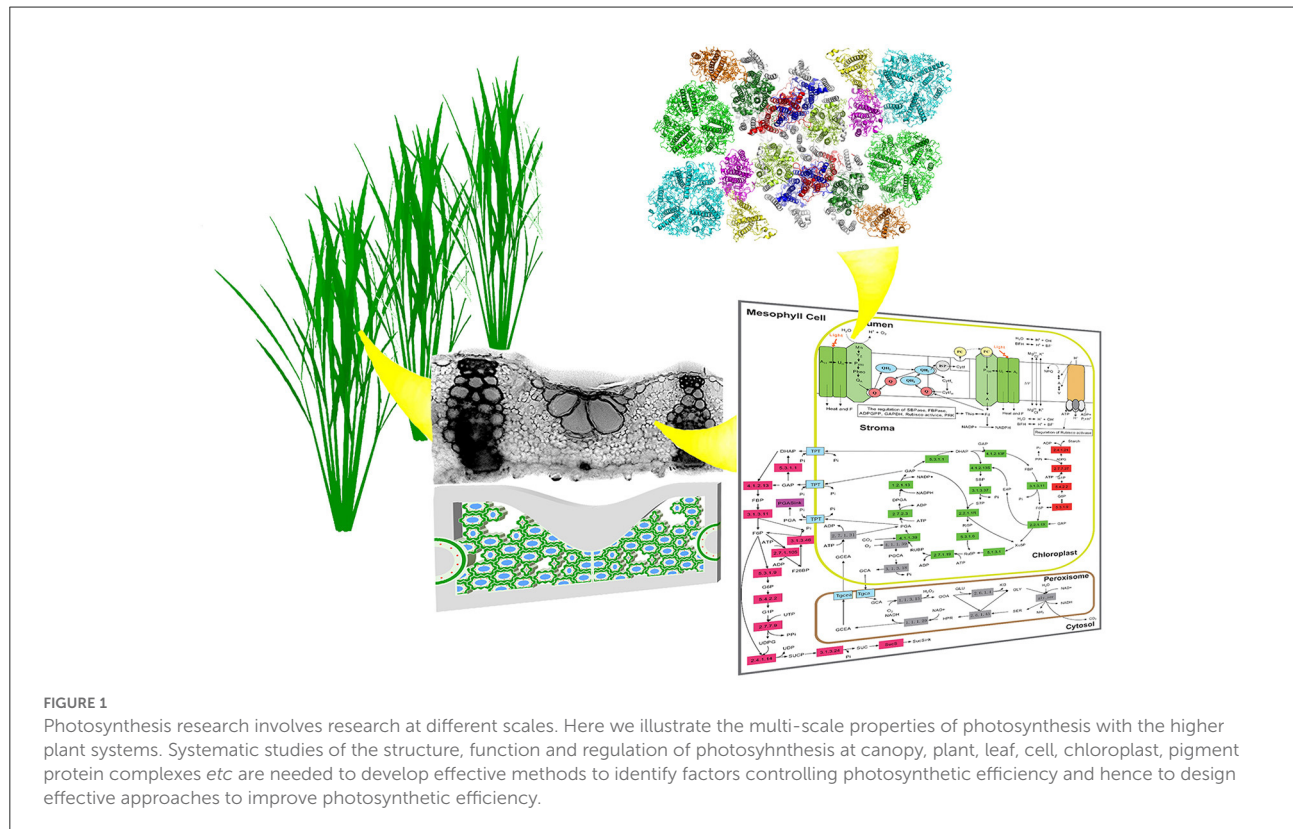
- **Availability of versatile synthetic biology tools allowing targeted manipulation of photosynthesis.** A highly efficient photosystem requires a strongly coordinated expression of genes that encode the photosystem components. Many promoters that confer precise temporal, spatial, or tissue-specific expression of target genes are available (Kummari et al., 2020); furthermore, with rapid advances in single-cell transcriptomics and stereomics data, new promoters conferring either temporal or spatial or development, or environment specificity will be rapidly identified (Xia et al., 2022). CRISPR-CAS9 tools enable fine-tuning expression levels and translation efficiency have been developed (Jiang and Doudna, 2017). All these will enable an unprecedented opportunity to design and implement new photosynthetic systems.

- **Guided evolution techniques.** Though during evolution, photosynthetic efficiency might not be a target that selection acts on, we can now implement guided evolution where optimal photosynthetic efficiency or enhanced properties of specific photosynthetic proteins can be a target for the experiment, as shown in the development of new CO_2 fixation pathway in *Escherichia coli* (Antonovsky et al., 2016). Guided evolution tools combined with artificial intelligence can be used to support the optimization of photosynthetic proteins, such as Rubisco or new photosynthetic pathways, or even the creation of new options for improved photosynthetic efficiency, taking advantage of the power of random mutation and selection.

Research areas on photosynthesis to support development of new strategies for improved photosynthetic efficiency

As the basic process ultimately responsible for the generation of food, fiber, and fuel for our society, and also a crucial component of the global carbon cycle and the water cycle, photosynthesis is arguably one of the most important biological processes on this planet. Understanding how photosynthesis works, and how to further optimize it, will be a never-ending pursuit of humanity. Photosynthesis not only supplies materials and energy supporting our living organisms on Earth, but also holds the promise to provide the basic needs for humans in the forthcoming era of space life. The Photosynthesis and Photobiology section of Frontiers in Plant Sciences provides a unique arena for scientists working in this field to publish their recent advances in these fields; it will also be a window for industrial partners and stakeholders to present their recent development. Advances in photosynthesis research will be a showcase of the triumph of multi-disciplinary research across the diversity of photosynthetic organisms. This Photosynthesis and Photobiology section will welcome high-quality fundamental and applied research across all areas of photosynthesis and photobiology, which include but are not limited to:

- Architecture, assembly, biogenesis, and functional regulation of pigment-protein complexes, supercomplexes, and megacomplexes involved in the light reactions.
- Structure and mechanism of enzymes and transporters associated with photosynthesis and their regulation
- Structure and function of thylakoid membrane systems
- Mechanisms of light energy absorption, transfer, and conversion processes under different light regimes
- Structure, function, genetics, and reconstruction of different CO_2-concentrating mechanisms (CCM)
- Structure and variation of gene regulatory networks controlling photosynthesis
- Factors controlling stomatal conductance and mesophyll conductance
- Factors controlling leaf and canopy photosynthesis
- Structure, function and genetic regulation of crassulacean acid metabolism
- Photosynthesis under changing climate conditions or stress conditions
- Photosynthesis under different supplies of either macromineral or microelement
- Multiscale models of photosynthesis

FIGURE 1

Photosynthesis research involves research at different scales. Here we illustrate the multi-scale properties of photosynthesis with the higher plant systems. Systematic studies of the structure, function and regulation of photosyhnthesis at canopy, plant, leaf, cell, chloroplast, pigment protein complexes *etc* are needed to develop effective methods to identify factors controlling photosynthetic efficiency and hence to design effective approaches to improve photosynthetic efficiency.

- Evolution of photosynthesis
- Photosynthesis on planets other than earth
- Natural variation of photosynthesis and their genetic basis
- Synthetic biology of photosynthesis for better enzymes, systems, or pathways
- Crop improvement for higher photosynthetic efficiency under a changing climate
- Light-induced signal transduction and photomorphogenesis
- Artificial photosynthesis and clean energy generation
- Creation of new hybrid photosynthetic systems for greater light use efficiency.

Photosynthesis research is entering a new era, where more and more work targets at enhancing its efficiency, in addition to the characterization of natural photosynthetic systems. Given that efficiency is inherently a system's property, i.e., it is a result of all the interacting components, rather than any single component. As a result, studying photosynthetic efficiency and identifying new options to improve efficiency will inevitably require the examination of photosynthesis at a range of spatial and temporal scales (Figure 1). Therefore, in this new era of photosynthesis research, we will witness the final success of capitalizing on the power of photosynthesis tailored to gain optimal efficiency for different environments, which will rely on accurate *in silico* prediction of photosynthesis in action from the first principle based on the spatial arrangement of photosynthetic pigment-protein complexes, and sequence and structure of individual proteins involved. After centuries of research on photosynthesis, the twenty-first century will witness how photosynthesis research will help advance our agricultural and energy development, and sustainably maintain or even improve our environment. The Photosynthesis and Photobiology section of Frontiers in Plant Sciences will serve as an arena for the whole photosynthesis research community to team up and work together to welcome this new era of photosynthesis research.

Author contributions

X-GZ drafted the article. All authors contributed to the article and approved the submitted version.

Conflict of interest

The authors declare that the research was conducted in the absence of any commercial or financial relationships that could be construed as a potential conflict of interest.

Publisher's note

All claims expressed in this article are solely those of the authors and do not necessarily represent those of their affiliated organizations, or those of the publisher, the editors and the reviewers. Any product that may be evaluated in this article, or claim that may be made by its manufacturer, is not guaranteed or endorsed by the publisher.

References

Antonovsky, N., Gleizer, S., Noor, E., Zohar, Y., Herz, E., Barenholz, U., et al. (2016). Sugar synthesis from CO_2 in *Escherichia coli*. *Cell* 166, 115–125. doi: 10.1016/j.cell.2016.05.064

Arp, T. B., and Kistner-Morris, J. (2020). Quieting a noisy antenna reproduces photosynthetic light-harvesting spectra. *Science* 368, 1490–1495. doi: 10.1126/science.aba6630

Banda, D. M., Pereira, J. H., Liu, A. K., Orr, D. J., Hammel, M., He, C., et al. (2020). Novel bacterial clade reveals origin of form I Rubisco. *Nat. Plants* 6, 1158–1166. doi: 10.1038/s41477-020-0 0762-4

Casella, S., Huang, F., Mason, D., Zhao, G. Y., Johnson, G. N., Mullineaux, C. W., et al. (2017). Dissecting the native architecture and dynamics of cyanobacterial photosynthetic machinery. *Mol. Plant* 10, 1434–1448. doi: 10.1016/j.molp.2017.09.019

Engel, B. D., Schaffer, M., Kuhn Cuellar, L., Villa, E., Plitzko, J. M., Baumeister, W., et al. (2015). Native architecture of the *Chlamydomonas* chloroplast revealed by in situ cryo-electron tomography. *Elife* 4, e04889. doi: 10.7554/eLife.04889

Freeman Rosenzweig, E. S., Xu, B., Kuhn Cuellar, L., Martinez-Sanchez, A., Schaffer, M., Strauss, M., et al. (2017). The eukaryotic CO_2-concentrating organelle is liquid-like and exhibits dynamic reorganization. *Cell* 171, 148–162. e119. doi: 10.1016/j.cell.2017.08.008

Grime, J. P. (1977). Evidence for the existence of three primary strategies in plants and its relevance to ecological and evolutionary theory. *Am. Nat.* 111, 1169–1194. doi: 10.1086/283244

Gupta, T. K., Klumpe, S., Gries, K., Heinz, S., Wietrzynski, W., Ohnishi, N., et al. (2021). (2021). Structural basis for VIPP1 oligomerization and maintenance of thylakoid membrane integrity. *Cell* 184, 3643.e3623–3659.e3623. doi: 10.1016/j.cell.2021.05.011

Hsia, Y., Mout, R., Sheffler, W., Edman, N. I., Vulovic, I., Park, Y. J., et al. (2021). Design of multi-scale protein complexes by hierarchical building block fusion. *Nat. Commun* 12, 2294. doi: 10.1038/s41467-021-22276-z

IPCC Climate Change (2021). *The Physical Science Basis. Working Group I Contribution to the Sixth Assessment Report of the International Panel on Climate Change*. Cambridge, UK; New York, NY: Cambridge University Press 2021.

Jiang, F., and Doudna, J. A. (2017). CRISPR–Cas9 structures and mechanisms. *Ann. Rev. Biophys.* 46, 505–529. doi: 10.1146/annurev-biophys-062215-010822

Jumper, J., Evans, R., Pritzel, A., Green, T., Figurnov, M., Ronneberger, O., et al. (2021). Highly accurate protein structure prediction with AlphaFold. *Nature* 596, 583–589. doi: 10.1038/s41586-021-03819-2

Kromdijk, J., Głowacka, K., Leonelli, L., Gabilly, S. T., Iwai, M., Niyogi, K. K., et al. (2016). Improving photosynthesis and crop productivity by accelerating recovery from photoprotection. *Science* 354, 857. doi: 10.1126/science.aai8878

Kummari, D., Palakolanu, S. R., Kishor, P. B. K., Bhatnagar-Mathur, P., Singam, P., Vadez, V., et al. (2020). An update and perspectives on the use of promoters in plant genetic engineering. *J. Biosci.* 45,119. doi: 10.1007/s12038-020-00087-6

Liguori, N., Croce, R., Marrink, S. J., and Thallmair, S. (2020). Molecular dynamics simulations in photosynthesis. *Photosynth Res.* 144, 273–295. doi: 10.1007/s11120-020-00741-y

Liu, L. N., and Scheuring, S. (2013). Investigation of photosynthetic membrane structure using atomic force microscopy. *Trends Plant Sci.* 18, 277–286. doi: 10.1016/j.tplants.2013.03.001

Long, S. P., Ainsworth, E. A., Leakey, A. D. B., Nosberger, J., and Ort, D. R. (2006). Food for thought: Lower-than-expected crop yield stimulation with rising CO_2 concentrations. *Science* 312, 1918–1921. doi: 10.1126/science.1114722

Malone, L. A., Qian, P., Mayneord, G. E., Hitchcock, A., Farmer, D. A., Thompson, R. F., et al. (2019). Cryo-EM structure of the spinach cytochrome b_6f complex at 3, 6. Å resolution. *Nature* 575:535–539. doi: 10.1038/s41586-019-1746-6

Moustakas, M., Sperdouli, I., Adamakis, I.-., D. S., Moustaka, J., Işgören, S., et al. (2022). Harnessing the role of foliar applied salicylic acid in decreasing chlorophyll content to reassess photosystem II photoprotection in crop plants. *Int. J. Mol. Sci.* 23, 7038. doi: 10.3390/ijms23137038

Mullineaux, C. W., and Liu, L.-N. (2020). Membrane dynamics in phototrophic bacteria. *Ann. Rev. Microbiol.* 74, 633–654. doi: 10.1146/annurev-micro-020518-120134

Ni, T., Sun, Y., Burn, W., Al-Hazeem, M. M. J., Zhu, Y., Yu, X., et al. (2022). Structure and assembly of cargo Rubisco in two native α-carboxysomes. *Nat. Commun.* 13, 4299. doi: 10.1038/s41467-022-32004-w

Ort, D. R. (2001). When there is too much light. *Plant Physiol.* 125, 29–32. doi: 10.1104/pp.125.1.29

Ort, D. R., Merchant, S. S., Alric, J., Barkan, A., Blankenship, R. E., Bock, R., et al. (2015). Redesigning photosynthesis to sustainably meet global food and bioenergy demand. *Proc. Natl. Acad. Sci. U.S.A.* 112, 8529–8536. doi: 10.1073/pnas.1424031112

Ort, D. R., Zhu, X. G., and Melis, A. (2011). Optimizing antenna size to maximize photosynthetic efficiency. *Plant Physiol.* 155, 79–85. doi: 10.1104/pp.110.165886

Pan, X., Cao, D., Xie, F., Xu, F., Su, X., Mi, H., et al. (2020). Structural basis for electron transport mechanism of complex I-like photosynthetic NAD(P)H dehydrogenase. *Nat. Commun.* 11, 610–610. doi: 10.1038/s41467-020-14456-0

Pi, X., Zhao, S., Wang, W., Liu, D., Xu, C., Han, G., et al. (2019). The pigment-protein network of a diatom photosystem II-light-harvesting antenna supercomplex. *Science* 365, aax4406. doi: 10.1126/science.aax4406

Sage, R. F., and Kubien, D. S. (2007). The temperature response of C3 and C4 photosynthesis. *Plant, Cell Environ.* 30, 1086–1106. doi: 10.1111/j.1365-3040.2007.01682.x

Slattery, R. A., and Ort, D. R. (2015). Photosynthetic energy conversion efficiency: setting a baseline for gauging future improvements in important food and biofuel crops. *Plant Physiol.* 168, 383–392. doi: 10.1104/pp.15.00066

Stitt, M., and Borghi, G. L. (2021). Targeted metabolite profiling as a top down approach to uncover inter species diversity and identify key conserved operational features in the Calvin-Benson cycle. *J. Exp. Bot.* 72, 5961–5986. doi: 10.1093/jxb/erab291

Su, X., Ma, J., Wei, X., Cao, P., Zhu, D., Chang, W., et al. (2017). Structure and assembly mechanism of plant $C_2S_2M_2$-type PSII-LHCII supercomplex. *Science* 357, 815–820. doi: 10.1126/science.aan0327

Wei, X., Su, X., Cao, P., Liu, X., Chang, W., Li, M., et al. (2016). Structure of spinach photosystem II-LHCII supercomplex at 3, 2. Å resolution. *Nature* 534, 69–74. doi: 10.1038/nature18020

Wietrzynski, W., Schaffer, M., Tegunov, D., Albert, S., Kanazawa, A., Plitzko, J. M., et al. (2020). Charting the native architecture of Chlamydomonas thylakoid membranes with single-molecule precision. *Elife* 9, e53740. doi: 10.7554/eLife.53740

Wood, W. H. J., MacGregor-Chatwin, C., Barnett, S. F. H., Mayneord, G. E., Huang, X., Hobbs, J. K., et al. (2018). Dynamic thylakoid stacking regulates the balance between linear and cyclic photosynthetic electron transfer. *Nat. Plants* 4, 116–127. doi: 10.1038/s41477-017-0092-7

Xia, K., Sun, H. X., Li, J., Li, J., Zhao, Y., Chen, L., et al. (2022). The single-cell stereo-seq reveals region-specific cell subtypes and transcriptome profiling in Arabidopsis leaves. *Dev Cell* 57, 1299.e1294–1310.e1294. doi: 10.1016/j.devcel.2022.04.011

Xiao, Y., Chang, T. G., Song, Q.-F., Wang, S., Tholen, D., Wang, Y., et al. (2017). ePlant for quantitative and predictive plant science research in the big data era – Lay the foundation for the future model guided crop breeding, engineering and agronomy. *Quant. Biol.* 5, 260–271. doi: 10.1007/s40484-017-0110-9

Yin, X., and Struik, P. C. (2015). Constraints to the potential efficiency of converting solar radiation into phytoenergy in annual crops: from leaf biochemistry to canopy physiology and crop ecology. *J. Exp. Bot.* 66, 6535–6549. doi: 10.1093/jxb/erv371

Zhang, H., Zhao, Y., and Zhu, J.-K. (2020). Thriving under stress: how plants balance growth and the stress response. *Dev. Cell* 55, 529–543. doi: 10.1016/j.devcel.2020.10.012

Zhang, J., Ma, J., Liu, D., Qin, S., Sun, S., Zhao, J., et al. (2017). Structure of phycobilisome from the red alga *Griffithsia pacifica*. *Nature* 551, 57–63. doi: 10.1038/nature24278

Zhao, L.-S., Huokko, T., Wilson, S., Simpson, D. M., Wang, Q., Ruban, A. V., et al. (2020). Structural variability, coordination and adaptation of a native photosynthetic machinery. *Nat. Plants* 6, 869–882. doi: 10.1038/s41477-020-0694-3

Zhu, X.-G., Portis Jr, A. R., and Long, S. P. (2004). Would transformation of C3 crop plants with foreign Rubisco increase productivity? A computational analysis extrapolating from kinetic properties to canopy photosynthesis. *Plant Cell Environ.* 27, 155–165. doi: 10.1046/j.1365-3040.2004.01142.x

Zhu, X. G., Long, S. P., and Ort, D. R. (2008). What is the maximum efficiency with which photosynthesis can convert solar energy into biomass? *Curr. Opin. Biotechnol.* 19, 153–159. doi: 10.1016/j.copbio.2008.02.004

Zhu, X. G., Ort, D. R., Parry, M., and von Caemmerer, S. (2020). A wish list for synthetic biology in photosynthesis research. *J. Exp. Bot.* 71, 2219–2225. doi: 10.1093/jxb/eraa075

Special issue on Recent advances in photomodulation in higher plants, algae, and bryophytes

Light intensity affects tolerance of pyrene in *Chlorella vulgaris* and *Scenedesmus acutus*

R.S. TOMAR[*], R. ATRE[*], D. SHARMA[*], P. RAI-KALAL[*], and A. JAJOO[*,**,+] iD

School of Life Science, Devi Ahilya University, 452017 Indore, India[*]
School of Biotechnology, Devi Ahilya University, 452017 Indore, India[**]

Abstract

The impact of light intensity on the toxicity of pyrene, a 4-ring polycyclic aromatic hydrocarbon (PAH), was studied in *Chlorella vulgaris* and *Scenedesmus acutus*. Both species were cultured under low light, LL [50–60 μmol(photon) $m^{-2} s^{-1}$], and high light, HL [100–110 μmol(photon) $m^{-2} s^{-1}$] conditions to study the effects of pyrene (PYR) toxicity on growth parameters, the content of biomolecules, chlorophyll content, and photosynthetic efficiency. In the presence of PYR, *S. acutus* could grow well in LL and HL intensity. On the other hand, *C. vulgaris* showed a drastic decrease in growth and photosynthesis during HL conditions due to PYR toxicity. Regulation of nonphotochemical and photochemical quenching was responsible for the survival of *S. acutus* under PYR toxicity in LL and HL conditions. Thus, *S. acutus* seems to be a more promising candidate for pyrene degradation under varying light conditions.

Keywords: *Chlorella vulgaris*; light intensity; photosynthesis; pyrene; *Scenedesmus acutus*.

Introduction

Microalgae play a crucial role as primary producers in aquatic habitats by providing food and bioenergy sources for all organisms as well as by powering food webs and biogeochemical cycles (Baidya *et al.* 2021). Algae are small with a comparably large surface area, due to which their exposure to toxic water-borne contaminants increases. The concentration of polycyclic aromatic hydrocarbons (PAHs), one of the persistent organic contaminants in environmental systems, such as rivers, marine sediments, drinking water supplies, groundwater, and coastal estuaries, is at an alarming level (Olayinka *et al.* 2018). Toxic effects of PAHs on freshwater algae concerning growth, photosynthesis, and respiration were reported (Aksmann *et al.* 2011, Tomar and Jajoo 2021). However, inhibition of photosynthesis is more important as it results in reduced growth resulting in lesser biomass

Highlights

- *Chlorella vulgaris* is more sensitive to PYR in high light than in low light intensity
- *Scenedesmus acutus* regulates $Y_{(NPQ)}$ and $Y_{(NO)}$ to protect PSII from pyrene toxicity
- *Scenedesmus acutus* is more suitable for the removal of pyrene under varying light conditions

yield. Moreover, light intensity plays an important role in algal photosynthesis, therefore, tolerance of algae to toxic substances is also expected to change with varying light intensities.

Light is a key parameter in microalgae cultivation. Light intensity has been reported to influence microalgae productivity and nutrient removal efficiency (Abu-Ghosh *et al*. 2016, Binnal and Babu 2017, González-Camejo *et al.* 2019). The growth of microalgae is proportional to the activity of PSI and PSII; they are both sensitive to light conditions (Nama *et al.* 2015). If the light intensity value is below or exceeds the optimum, performance of PSI and PSII is altered (Nama *et al.* 2015). The effects of light intensity, photoperiods, and light wavelength on algal growth have been extensively reported (Yan *et al.* 2013, Gris *et al.* 2014, González-Camejo *et al*. 2019). However, the effect of light intensity on the removal of organic pollutants by microalgae cultivation has not been studied in detail.

The Chlorophyta microalgae, *Chlorella vulgaris* (*C. vulgaris*) and *Scenedesmus acutus* (*S. acutus*), are unicellular photosynthetic eukaryotes found in many aquatic habitats. Both are sensitive to physicochemical changes and pollution in the surrounding environment, therefore, they are frequently used as model organisms for phytotoxicological studies. Despite large numbers of toxicity studies of pollutants such as metals and herbicides, the impact of PAHs on algal growth with different environmental factors remains poorly understood. Previous results suggest that different light intensities have a significant influence on regulating growth and photosynthesis in algae (Kim *et al.* 2013, Xu *et al.* 2016).

In the present study, pyrene (PYR) was chosen as a representative PAH since it is one of the most toxic PAHs and is listed as a priority pollutant by USEPA. Pyrene is a high-molecular-mass 4-ring PAH with higher water solubility (Juhasz and Naidu 2000). PYR harms the natural development of phytoplankton communities and algal growth (Petersen *et al.* 2008). It is thought to be a potent photosensitizer that causes intracellular oxidative stress and obstruction of the photosynthetic electron transport chain (Häder *et al.* 2015). This study compares the ecotoxicological effects of PYR on growth, pigment content, and photosynthesis of two algal species, *C. vulgaris* and *S. acutus*. The overall goal of the present work is to find a more suitable algal species that can tolerate PYR toxicity under varying light (low and high) conditions.

Materials and methods

Algal species and culture conditions: Freshwater micro-algal species *C. vulgaris* was procured from Phycospectrum Environmental Research Centre, Chennai, India, and *S. acutus* from National Chemical Laboratory (NCL), Pune, India. Cells were grown in BG11 media (*M1958*, *Himedia*, India). Mother cultures were illuminated with white light having the intensity of 60 µmol(photon) m^{-2} s^{-1} at 25°C and a diurnal cycle of 16 h light and 8 h dark in the algal culture room. After 7–10 d when the exponential growth phase arrived, cells were centrifuged at 2,500 × *g* for 5 min and harvested for further experiments.

Experimental setup: For each treatment, three conical flasks (250 mL, Erlenmeyer flasks), containing 150 mL of culture medium were used. Algal mass was inoculated to each conical flask so that an initial optical density of 0.1 at 680 nm was observed. Optical density was measured by UV–VIS spectrophotometer (*Evolution 201*, *Thermo Scientific*, USA). After inoculation, 75 µL of stock solution (PYR in acetone) was added to 150 mL of media to obtain the effective concentration of 5 mg L^{-1}. The flasks without any addition of PYR were used as control. The growing conditions involved two different light intensities, low light (LL) [50–60 µmol(photon) m^{-2} s^{-1}] and high light (HL) [100–110 µmol(photon) m^{-2} s^{-1}] for both species. After 7 d of incubation, algal samples of all treatments were retrieved for various experiments.

Algal growth and biomass: Microalgal growth was monitored regularly at an interval of 24 h by measuring optical density (OD) at 680 nm using a UV–VIS spectrophotometer. Dry biomass was estimated after drying 100 mL of culture in a hot air oven at 80°C for 4–6 h. The growth rate [d^{-1}] was calculated using the following equation: GR [d^{-1}] = (lnN$_2$ – lnN$_0$)/(t$_2$ – t$_0$), where N$_2$ is the OD at time t$_2$ and N$_0$ is the OD at time t$_0$ (day 0).

Lipid, carbohydrate, and protein content: Lipid content was estimated by sulpho-phospho-vanillin (SPV) colorimetric method as described in Mishra *et al*. (2014). In brief, phospho-vanillin reagent was prepared by initially dissolving 0.6 g of vanillin in 10 mL of absolute ethanol: 90 mL of deionized water and stirred continuously. Subsequently, 400 mL of concentrated phosphoric acid was added to the mixture, and the resulting reagent was stored in the dark until use. Around 40 mL of algal cell culture was centrifuged at 5,000 × *g* and the pellet was suspended in 100 µL of water. Then, 2 mL of concentrated (98%) sulfuric acid was added to the sample and heated for 10 min at 100°C, and then cooled for 5 min in ice bath. Then, 5 mL of freshly prepared phospho-vanillin reagent was added, and the sample was incubated for 15 min at 37°C incubator shaker at 200 rpm. Absorbance reading at 530 nm was taken in order to quantify the lipid within the sample.

Carbohydrate content was estimated by phenol–sulfuric acid method as described in Laurens *et al*. (2012). Protein estimation was done according to Slocombe *et al*. (2013) with some changes. In brief, protein extraction was done by 6% TCA (trichloroacetic acid) and kept at room temperature overnight. Protein content in each sample was estimated with Folin–Ciocalteu phenol reagent and absorbance of each sample was read at 600 nm (*Evolution 201*, *Thermo Scientific*, USA).

Chlorophyll (Chl) content: Pigment content was determined using the following method: from all treatments, 5 mL of culture was taken and centrifuged at 2,500 × *g* for 5 min. The supernatant was discarded and 5 mL of 99.9% methanol was added to the pellet, mixed

properly, and incubated at 90°C for 5 min. The culture was centrifuged at 9,000 × g for 5 min and the supernatant was used for pigment estimation (*Evolution 201*, *Thermo Scientific*, USA). Calculations were done as mentioned in Dere *et al.* (1998).

Chl *a* fluorescence: Measurements of the quantum yields of energy conversion in PSII were carried out through saturation pulse technique, using a pulse amplitude modulator (*Dual PAM-100*, *Heinz Walz*, Effeltrich, Germany) system in intact algal cell culture. The algal sample was dark adapted for 30 min at 23 ± 2°C before measurements, and then 3 mL of cell culture was taken in a cuvette for recording the induction curve. A weak modulated light [12 µmol(photon) m^{-2} s^{-1}] was given to get minimal fluorescence (F_0), followed by actinic light [53 µmol(photon) m^{-2} s^{-1}], and saturating pulse (SP) [6,000 µmol(photon) m^{-2} s^{-1}] to achieve maximum fluorescence (F_m). After the determination of F_0 and F_m, the induction curve was analyzed using *Dual PAM-100* software. The induction curve was recorded with SP for 5 min to achieve the steady state of the photosynthetic apparatus, and then the actinic light was turned off.

Proline content: Proline was extracted using 3% sulphosalicylic acid and estimated using L-proline as a standard as described in Bates *et al.* (1973). Briefly, harvested fresh algal biomass was homogenized in 3 mL of 3% sulphosalicylic acid and then centrifuged at 6,000 rpm for 10 min. The supernatant (1 mL) was heated with 1 mL of ninhydrin and 1 mL of glacial acetic acid at 100°C for 1 h. Proline was quantified spectrophotometrically at 440 nm by use of a standard curve of L-proline.

Total polyphenol content: Total phenolics were colorimetrically determined using Folin–Ciocalteu reagent as described by Cajnko *et al.* (2019) with slight modifications.

Statistical analysis: Data were analyzed by using *Graphpad Prism 5.01* software (La Jolla, CA, USA). Results were analyzed using a one-way analysis of variance (*ANOVA*) followed by the *Newman–Keuls* multiple comparison test. Significance was determined at $p < 0.001$(* $p < 0.05$, ** $p < 0.01$, *** $p < 0.001$), and results were expressed as mean values ± SD. All the experiments were done five times in replicates of three.

Results

Algal cell growth: The carrier solvent acetone had no adverse effects on cellular growth, physiological function, or photosynthetic efficiency of both algal species. Growth is a critical endpoint measure that indicates an overall vitality of a population under the examined conditions. When PYR was added to the culture medium, specific growth rates of both species were inhibited although the impact depended upon individual species and light conditions. In HL with PYR, the final biomass and growth of *C. vulgaris* were substantially lower than that of *S. acutus* (Fig. 1). In *C. vulgaris* cells during PYR in HL conditions, biomass was 0.125 mg mL^{-1}, which was the lowest of all treatments.

Biomolecules of algal cells: In the present study, the impact on cell protein, lipid, and carbohydrate content in response to LL and HL was measured in the presence of PYR (Fig. 2). In *S. acutus* cells, protein content was 248 µg mg^{-1}(DM) in control (C) and LL and 183 µg mg^{-1}(DM) in PYR and LL conditions while it was 432 µg mg^{-1}(DM) in C and HL and 434 µg mg^{-1}(DM) in PYR-exposed cells after 7 d of cultivation (Fig. 2A). In case of *C. vulgaris*, protein content was 294 µg mg^{-1}(DM) in C and LL and 246 µg mg^{-1}(DM) in PYR and LL treatment. It was seen that the maximum amount of protein was obtained from *C. vulgaris* from C and HL conditions, while it decreased significantly in PYR and HL (Fig. 2B).
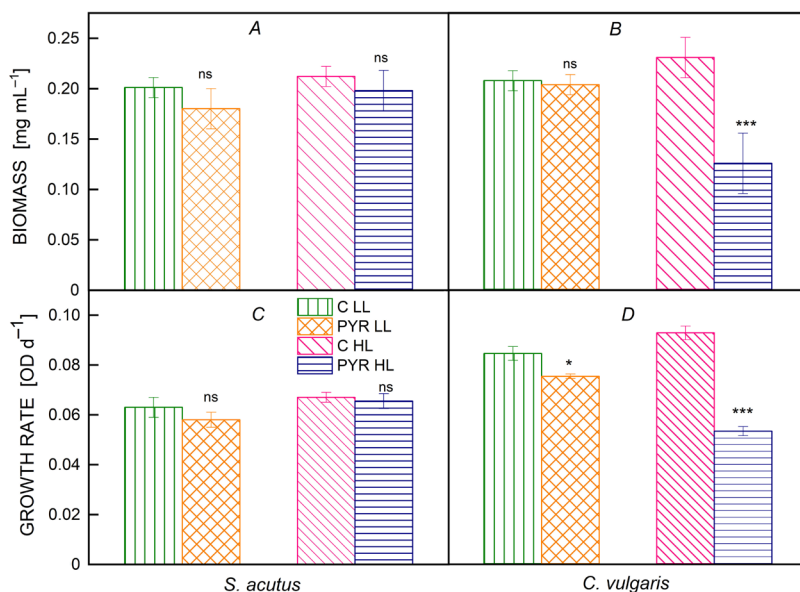

Fig. 1. Biomass (*A,B*) and growth rate (*C,D*) of *Scenedesmus acutus* and *Chlorella vulgaris* under LL and HL conditions with PYR exposure. Error bars represent standard deviation (*n* = 3). *** ($p < 0.001$), ** ($p < 0.01$), and * ($p < 0.05$) represent significant differences between the control and respective treatment, ns = nonsignificant. C – control; HL – high light; LL – low light; PYR – pyrene.
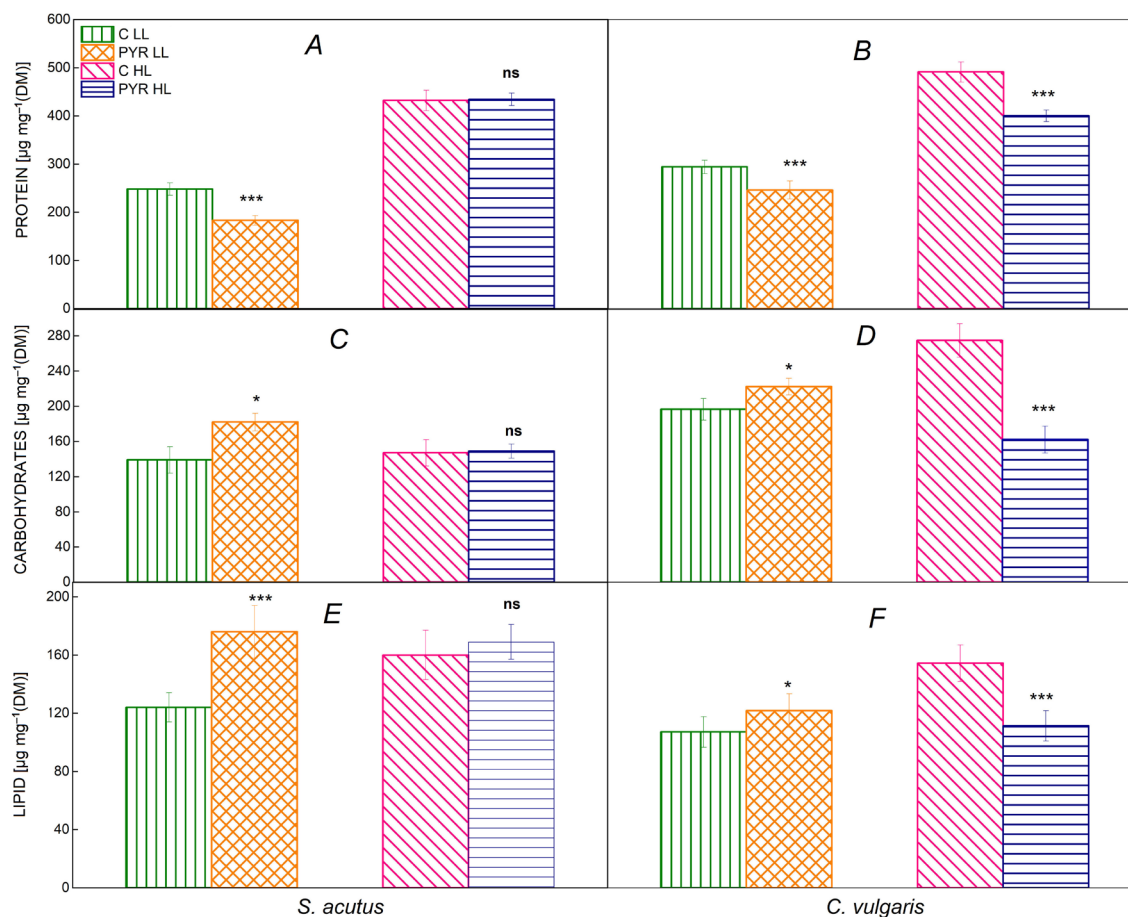
33

Fig. 2. Effects of different light intensities on the protein content (*A,B*), carbohydrate content (*C,D*), and lipid content (*E,F*) in *Scenedesmus acutus* and *Chlorella vulgaris* with PYR exposure. Error bars represent standard deviation (*n* = 3). *** (*p*<0.001), ** (*p*<0.01), and * (*p*<0.05) represent significant differences between the control and treatments, ns = nonsignificant. C – control; HL – high light; LL – low light; PYR – pyrene.

Carbohydrates and lipids also play important role in carbon partitioning, osmotic homeostasis, and metabolism of algal cells (Li *et al.* 2020). In the present study, carbohydrate content increased from 139 µg mg^{-1}(DM) (C and LL) to 182 µg mg^{-1}(DM) in PYR and LL while it was not affected by PYR and HL as compared to C and HL in *S. acutus* (Fig. 2C). Similarly, lipid content increased in PYR and LL conditions in both cells, while it was unaffected in PYR and HL in *S. acutus* (Fig. 2E,F). Interestingly, carbohydrate and lipid contents were extremely reduced in *C. vulgaris* in the PYR and HL conditions (Fig. 2D,F).

Proline and polyphenol content: The change in anti-oxidant molecules varied under different light conditions in both algal species. PYR LL and PYR HL treatments induced a considerable increase in proline concentration in *S. acutus* cells when compared with C LL and C HL as seen in Fig. 3. PYR LL treatment raised proline content by 75% as compared to C LL in *C. vulgaris* cells, but PYR HL treatment decreased proline content by 20% in comparison to C HL treatment. Additionally, in *S. acutus*,
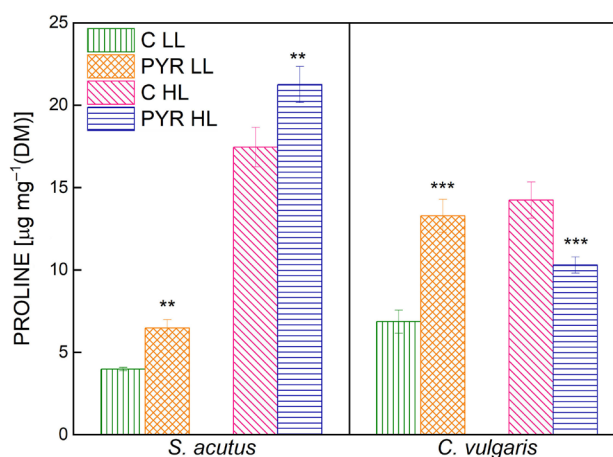

Fig. 3. Effects of different light intensities on the proline content of *Scenedesmus acutus* and *Chlorella vulgaris* with PYR exposure. Error bars represent standard deviation (*n* = 3). *** (*p*<0.001), ** (*p*<0.01), and * (*p*<0.05) represent significant differences between the control and treatments, ns = nonsignificant. C – control; HL – high light; LL – low light; PYR – pyrene.

PYR LL treatment resulted in a 9% drop in polyphenol content compared to C LL, but an increase was observed in PYR HL-treated cells compared to C HL (Fig. 4). On the other hand, in *C. vulgaris* cells, PYR LL caused a large rise in polyphenol content compared to C LL, whereas PYR HL caused a considerable drop (22%) in polyphenol content compared to C HL treatment (Fig. 4).

Photosynthetic pigments: To determine the effect of light intensity under PYR toxicity on photosynthesis, photosynthetic pigments (Chl *a*, Chl *b*, total Chl, and carotenoids) of *S. acutus* and *C. vulgaris* were measured (Table 1). Under LL and HL intensity along with PYR, the concentrations of Chl *a*, Chl *b*, and total Chl were reduced significantly in both species. However, this was lower in *S. acutus* in HL with PYR treatment (only 11%
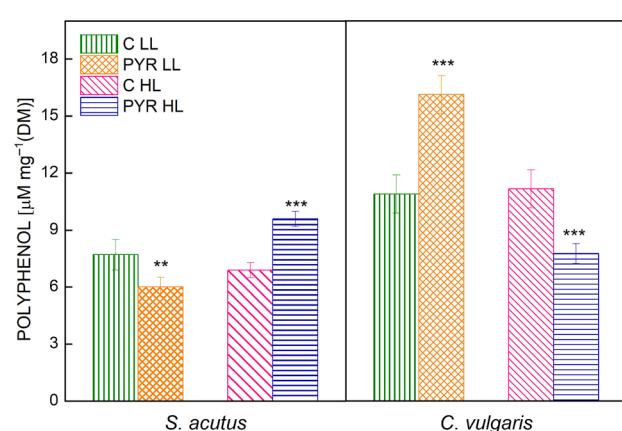

Fig. 4. Effects of different light intensities on the polyphenol content of *Scenedesmus acutus* and *Chlorella vulgaris* with PYR exposure. Error bars represent standard deviation ($n = 3$). *** ($p<0.001$), ** ($p<0.01$), and * ($p<0.05$) represent significant differences between the control and treatments, ns = nonsignificant. C – control; HL – high light; LL – low light; PYR – pyrene.

decrease as compared to C HL in *S. acutus*), compared to in *C. vulgaris* in PYR HL conditions (55% decrease as compared to C HL in *C. vulgaris*). Similarly, with PYR exposure, carotenoid concentration showed the same pattern in both species with both LL and HL (Table 1).

Efficiency of photosystem II in algal cells: The influence of light on PYR toxicity in both algal species was also evaluated using Chl *a* fluorescence kinetics. Table 2 shows the Chl *a* fluorescence parameters obtained with various treatments. In *S. acutus* in LL conditions, PYR exposure induced a significant increase in initial fluorescence (F_0), although it was unchanged in PYR HL treatment compared to C HL. It was also observed that F_0 was unaffected by PYR in *C. vulgaris* cells during the LL conditions but was reduced dramatically during the HL conditions (Table 2). Furthermore, maximal Chl *a* intensity (F_m) in *S. acutus* cells did not change in any of the conditions, whereas it declined severely in *C. vulgaris* cells during PYR HL and remained only 8% of C HL. In *S. acutus*, the quantum yield of PSII (F_v/F_m) decreased in the PYR LL treatment compared to the C LL treatment (Table 2). However, F_v/F_m was found to be the lowest with PYR HL treatment in *C. vulgaris*, as shown in Table 2. During both LL and HL, the value of F_v/F_0, which represents the efficiency of the oxygen-evolving complex, dropped considerably with PYR treatment in both algal species, however, the decline was deeper in *C. vulgaris*.

To evaluate the light energy-utilization efficiency of PSII, we compared the quantum yields of energy conversion within PSII in *S. acutus* and *C. vulgaris* cells in LL and HL with PYR exposure. The addition of PYR did not cause any significant change in $Y_{(II)}$ (quantum yield of PSII) in *S. acutus* during HL (Fig. 5) while, it was slightly reduced in PYR LL treatment (15% of C LL) (Fig. 5). In case of *C. vulgaris*, PYR caused a decrease in $Y_{(II)}$ and $Y_{(NO)}$ but not significantly in LL conditions, although the value of nonphotochemical quenching [$Y_{(NPQ)}$] increased (Fig. 6). However, a huge decrease was

Table 1. Effects on photosynthetic pigments content (Chl *a*, Chl *b*, total Chl, and carotenoids) in [µg mg^{-1}(DM)] in *Scenedesmus acutus* and *Chlorella vulgaris* under PYR exposure. Data are presented as the mean value of three replicates ± standard deviation. Significant differences were calculated according to *Newman–Keuls* multiple comparison test (ns = nonsignificant,*$p<0.05$, *$p<0.01$, and ***$p<0.001$). C – control; HL – high light; LL – low light; PYR – pyrene.

Treatment	Chl *a*	Chl *b*	Total Chl	Car (X+C)
Scenedesmus acutus				
C LL	19.4 ± 1.0	12.3 ± 1.6	31.7 ± 2.3	2.6 ± 0.4
PYR LL	14.2 ± 1.1*	9.1 ± 1.1*	23.3 ± 2.1*	2.2 ± 0.5[ns]
C HL	19.5 ± 2.1	17.6 ± 1.41	37.1 ± 2.4	2.7 ± 0.1
PYR HL	17.2 ± 1.6*	10.4 ± 1.1***	27.6 ± 2.1***	2.7 ± 0.3[ns]
Chlorella vulgaris				
C LL	25.5 ± 1.3	21.8 ± 2.1	47.4 ± 2.9	2.4 ± 0.2
PYR LL	17.1 ± 1.0*	14.3 ± 1.8**	31.4 ± 2.3***	1.5 ± 0.3***
C HL	28.3 ± 1.9	19.2 ± 1.5	47.5 ± 2.7	2.8 ± 0.1
PYR HL	12.6 ± 1.0***	10.9 ± 1.3***	23.5 ± 2.1***	0.6 ± 0.0***

Table 2. Effects of different light intensities on Chl *a* fluorescence parameters in *Scenedesmus acutus* and *Chlorella vulgaris* under PYR exposure. Data are presented as the mean value of three replicates ± standard deviation. Significant differences were calculated according to *Newman–Keuls* multiple comparison test (ns = nonsignificant, $*p<0.05$, $*p<0.01$, and $***p<0.001$). C – control; HL – high light; LL – low light; PYR – pyrene.

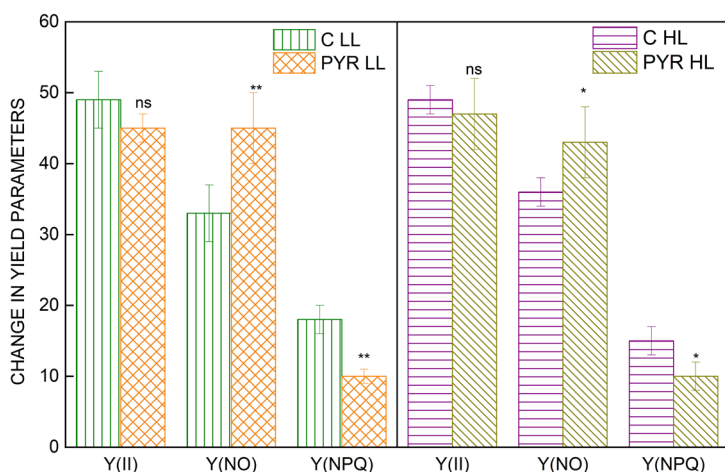| Treatment	F_0	F_m	F_v/F_m	F_v/F_0
Scenedesmus acutus				
C LL	0.06 ± 0.00	0.25 ± 0.01	0.76 ± 0.02	3.1 ± 0.5
PYR LL	$0.07 \pm 0.00^{**}$	0.25 ± 0.02^{ns}	$0.71 \pm 0.01^{*}$	$2.4 \pm 0.4^{**}$
C HL	0.07 ± 0.00	0.30 ± 0.01	0.76 ± 0.01	3.2 ± 0.4
PYR HL	0.08 ± 0.02^{ns}	0.31 ± 0.01^{ns}	$0.73 \pm 0.02^{*}$	$2.7 \pm 0.1^{***}$
Chlorella vulgaris				
C LL	0.10 ± 0.00	0.30 ± 0.01	0.66 ± 0.04	1.97 ± 0.32
PYR LL	0.10 ± 0.00^{ns}	$0.27 \pm 0.01^{*}$	$0.64 \pm 0.11^{*}$	$1.72 \pm 0.61^{*}$
C HL	0.09 ± 0.00	0.32 ± 0.02	0.73 ± 0.05	2.69 ± 0.41
PYR HL	$0.01 \pm 0.00^{***}$	$0.03 \pm 0.21^{***}$	$0.56 \pm 0.05^{***}$	$1.27 \pm 0.22^{***}$

Fig. 5. Comparative analysis of quantum yields of *Scenedesmus acutus* with LL and HL under PYR exposure. Data are presented as the mean value of three replicates ± standard deviation. Significant differences were calculated according to *Newman–Keuls* multiple comparison test (ns = nonsignificant, $*p<0.05$, $*p<0.01$, and $***p<0.001$). C – control; HL – high light; LL – low light; PYR – pyrene.
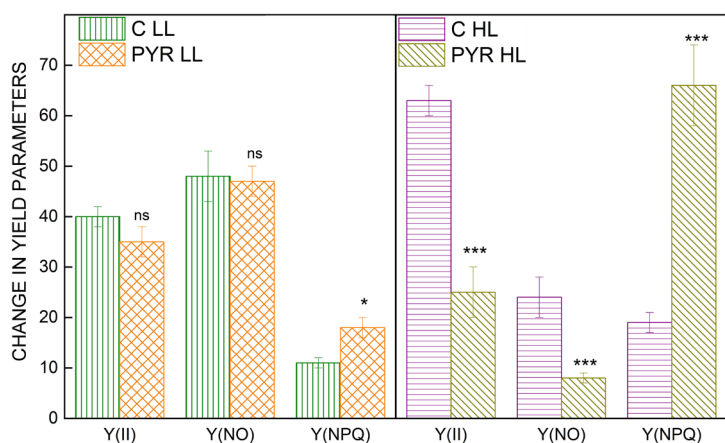

Fig. 6. Comparative analysis of quantum yields of *Chlorella vulgaris* with LL and HL under PYR exposure. Data are presented as the mean value of three replicates ± standard deviation. Significant differences were calculated according to *Newman–Keuls* multiple comparison test (ns = nonsignificant, $*p<0.05$, $*p<0.01$, and $***p<0.001$). C – control; HL – high light; LL – low light; PYR – pyrene.

observed in $Y_{(II)}$ and $Y_{(NO)}$ with PYR HL treatment which was related to a higher degree of PSII inhibition (Fig. 6). Compared with the C HL, PYR HL-exposed cells showed 3.5 times higher value of $Y_{(NPQ)}$ in *C. vulgaris* cells.

Discussion

This paper presents for the first time comparative data on the photosynthetic efficiency of two algal species grown

under PYR toxicity in response to low and high light intensities. Most of the toxicity data available are related to the effects of PYR on freshwater microalgae and are based on growth inhibition, while here we explained the light regulation of photosynthetic parameters as well. The level of growth and biomass suppression caused by PYR exposure in *C. vulgaris* was higher than that of *S. acutus* in both light intensities (LL and HL). Moreover, the extent of growth inhibition varied depending on the light intensity of individual tested species (Fig. 1). The growth rate and biomass were almost stable with LL but a drastic growth inhibition was observed when *C. vulgaris* cells were grown with HL. An accumulation of PAH in the lipid component of cells (Tomar and Jajoo 2021) and consequent alteration in membrane properties (Kottuparambil and Park 2019) may be responsible for the reduction in growth. The growth of *S. acutus* cells was better than that of *C. vulgaris* in PYR HL treatment. This result indicates that the *S. acutus* cells could tolerate PYR more in HL conditions.

PAHs have a significant influence on biomolecules of algae which change to adapt to different environmental conditions. Because PYR is hydrophobic, its harmful effects on green algae could be due to interference with cell biomolecules (Tomar and Jajoo 2021). The biochemical composition of algae is also influenced by variations in light intensity, for example, changes in the content of lipids, carbohydrates, and pigments, as well as the growth of microalgae (Tang *et al.* 2011, Paliwal *et al.* 2017). It is speculated that PYR could disrupt the functioning of algal cells as it rapidly interacts with proteins and lipids *in vivo* (Croxton *et al.* 2015). The obtained data revealed that PYR LL treatments altered biomolecules in *S. acutus*, but during HL, the number of biomolecules did not change significantly. In this investigation, exposure to PYR resulted in a much lower lipid and carbohydrate content in *C. vulgaris* in PYR HL conditions compared to PYR LL. Reduced carbohydrates and lipid content with PYR HL could be attributed to osmotic imbalance and cell division suppression (Cheng and He 2014). These findings suggest that PYR under HL has a greater impact on the synthesis of various biomolecules in *C. vulgaris* cells and it is unable to safeguard its metabolic functions. It is suggested that under different light intensities, microalgae may have various processes for carbon partitioning, which could change biomolecule levels (Nzayisenga *et al.* 2020).

To cope with oxidative stress, various antioxidant molecules contribute to survival and tolerance mechanisms in algae. Proline and polyphenol are two important osmolytes and antioxidants produced during stress in algae. Higher production of proline in *S. acutus* cells shows that it has a protective role through scavenging free radicals, stabilizing subcellular structure, and maintaining redox imbalance and homeostasis of the cell (Meena *et al.* 2019). Similar to proline, polyphenols are also regarded as strong antioxidants (Lee *et al.* 2015). Polyphenols suppress the generation of free radicals and act as direct radical scavengers of the lipid peroxidation chain reactions (chain breakers) (Tsao 2010). In *S. acutus* PYR LL and HL treatment caused the increase in proline content, which indicates its better ability to scavenge ROS.

Similarly, an increase in proline and polyphenol content in *C. vulgaris* under PYR LL was observed, however, PYR HL showed lower proline and polyphenol content. It might be due to the activation of polyphenol oxidase enzyme by PYR during HL which oxidizes polyphenols by removing electrons and leaving them unstable.

In this study, Chl *a*, Chl *b*, and carotenoid contents were significantly affected by PYR under LL and HL conditions in both algal species (Table 2). It is well documented that exposure of green algae and plants to different toxicants leads to alteration in photosynthetic pigment contents and photosynthetic efficiency (Aksmann *et al.* 2011, Jajoo *et al.* 2014, Tomar and Jajoo 2014, 2021). Moreover, light is important for Chl and other pigment syntheses that absorb light of different wavelengths (Zarmi *et al.* 2020). It was found that light intensity significantly influenced the pigment content of *S. acutus* (Table 2). However, the lowest values of Chl and carotenoids were observed in *C. vulgaris* under PYR HL condition as compared to other treatments. In *C. vulgaris*, under PYR HL condition, PYR was probably more absorbed by the algal cells and inhibited the synthesis of photosynthetic pigments or resulted in pigment degradation.

Apart from changes in the growth of algal cells and photosynthetic pigment contents, the light intensity also affected the photosynthetic efficiency, specially PSII activity. Chl *a* fluorescence measurements were performed to examine the impact of light intensity with PYR toxicity on PSII in both algal species. F_0 is minimal fluorescence level when all antenna pigment complexes associated with the photosystem are assumed to be open (dark-adapted) and F_m is maximal fluorescence level when a high-intensity flash has been applied and all antenna sites are assumed to be closed. A drop in these fluorescence parameters (F_0 and F_m) in *C. vulgaris* during PYR HL treatment might be a result of many combined processes, such as enhancement in the capacity of light-harvesting complex II (LHCII) or an increase in the number of inactive RCs of PSII, which indicated a reduction in cells photosynthetic performance due to downregulation of photochemical efficiency (Elsheery and Cao 2008, Elsheery *et al.* 2008). In this study, F_m decreased drastically in response to PYR HL stress, probably due to disorganization of Chl structure (Hazrati *et al.* 2016). In contrast, *S. acutus* maintained F_0 and F_m values in PYR HL treatment, however, an increase was observed in F_0 during PYR LL treatment. The efficiency of the oxygen-evolving complex (F_v/F_0) decreased in both algal cells with all treatments, implying that PYR at low and high light intensity affected negatively the donor side of PSII. The F_v/F_m value is the ratio of variable fluorescence to maximal fluorescence and calculated as $F_m − F_0/F_m$. It measures the maximum efficiency of PSII when all PSII centers are open (Mathur *et al.* 2019, Jain and Jajoo 2020). This value can be used to estimate the potential efficiency of PSII by taking dark-adapted measurements. We found that *S. acutus* can maintain maximum efficiency of PSII (F_v/F_m) in both light treatments while it decreased drastically in *C. vulgaris* during the PYR HL condition. This indicates that PYR toxicity is exerted also by inhibition of cytochrome b_6/f complex as well as photooxidative damage to PSII during high light intensity. Our results suggest that

S. acutus has a more efficient protective mechanism for PSII which enables it to tolerate PYR even at HL intensity.

We further measured the photochemical quantum yield of PSII, which gives information about the response of PSII photochemistry, to PYR toxicity with low and high light intensities (Fig. 6). $Y_{(II)}$ represents the fraction of excitation energy used for photochemistry at PSII. The remaining fraction, $1 - Y_{(II)}$, tells about the dissipation of remaining energy. It is the sum of the yields of regulated dissipation [$Y_{(NPQ)}$], and unregulated dissipation, [$Y_{(NO)}$] (Mathur *et al.* 2019, Jain and Jajoo 2020). As evident from the results, PYR HL reduced the F_v/F_m ratio in *C. vulgaris* and the energy requirements for the reduction of quinone decreased largely. This accounts for the reduction in $Y_{(II)}$ and a corresponding increase in $Y_{(NPQ)}$ with PYR HL. Higher $Y_{(NPQ)}$ suggests inhibition of electron transport exerted by PYR HL. These PSII quantum yield parameters collectively indicated the reduced efficiency of photochemical energy regulation imposed by PYR exposure in *C. vulgaris* during HL. We noted that during low light intensity, PYR did not show major photosynthetic toxicity in *C. vulgaris* at the PSII level. The drop in $Y_{(NO)}$ and high rise in $Y_{(NPQ)}$ in PYR HL-exposed cells reflect damage to PSII but still with a protective mechanism through NPQ to protect itself against photochemical damage. A decrease in $Y_{(II)}$ also reflects a reduction in the number of active PSII centers and it may also be associated with a decrease in Chl *a* content in PYR HL-treated cells (Khpalwak *et al.* 2018, Tomar and Jajoo 2015, 2019). Moreover, a significant increase in Chl *a/b* ratio was reported, which indicated that antenna size was affected (Dinç *et al.* 2012). This change may be partially attributed to the augmentation of the NPQ values. During PYR exposure, an increase in $Y_{(NPQ)}$ is often reflected by a decrease of $Y_{(NO)}$ which can compensate for a decrease in PSII activity. Surprisingly, under PYR LL and HL, a higher $Y_{(NO)}$ and lower $Y_{(NPQ)}$ were observed in *S. acutus*, while the $Y_{(II)}$ was not significantly changed. Thus, a balance exists between $Y_{(NPQ)}$ and $Y_{(NO)}$ to maintain $Y_{(II)}$. Some other mechanisms, such as cyclic electron transport and the water–water cycle, might be involved in the protection and regulation of photosynthetic efficiency in *S. acutus* cells (Sun *et al.* 2020). However, the mechanisms underlying the interaction between $Y_{(NPQ)}$ and $Y_{(NO)}$ remain elusive.

It is concluded that light intensity of 50–60 and 100–110 μmol(photon) m^{-2} s^{-1}, are both suitable for the growth of *S. acutus* under PYR toxicity. Further, *S. acutus* was able to maintain its biomolecule composition when cultured under HL exposure. In this study, the biomolecule content of *C. vulgaris* was comparatively lower in PYR HL treatment than that of PYR LL culture condition. In *C. vulgaris* with PYR exposure, significantly low cell density, growth, and biomass values were observed in high light intensity, which is also supported by the negatively modulated photosynthetic process. It can be suggested that during HL, PYR may be absorbed rapidly and accumulated in cell membranes and organelles. PYR accumulation in membranes probably results in increased proton permeability, as well as an expansion of the membrane surface area, inhibiting primary ion pumps

and causing the electrical potential and pH gradient to dissipate, inhibiting cellular growth (Petersen and Dahllöf 2007, Croxton *et al.* 2015). More important, because these are strongly connected processes, each being a result of the usage of energy from light and nutrients, a reduction in photosynthesis can lead to reduced growth. It was reported that some of the metabolites of PYR are quinones (Alegbeleye *et al.* 2017, Bukowska and Duchnowicz 2022) which can cause modifications in the photosynthetic machinery and can result in a significant decrease in energy output within chloroplasts. In this study, *S. acutus* exhibited higher pigment content and quantum yield of PSII as compared to *C. vulgaris* during PYR HL conditions. However, *S. acutus* shows better performance of all measured parameters in both high and low light intensities. Another interesting finding, which warrants further mechanistic and physiological attention, is the fine regulation of $Y_{(NO)}$ and $Y_{(NPQ)}$ in *S. acutus* for the protection of PSII. Therefore, *S. acutus* seems to be a more promising candidate for the removal of pyrene from the environment under varying light conditions.

References

Abu-Ghosh S., Fixler D., Dubinsky Z., Iluz D.: Flashing light in microalgae biotechnology. – Bioresource Technol. **203**: 357-363, 2016.

Aksmann A., Shutova T., Samuelsson G., Tukaj Z.: The mechanism of anthracene interaction with photosynthetic apparatus: A study using intact cells, thylakoid membranes and PSII complexes isolated from *Chlamydomonas reinhardtii*. – Aquat. Toxicol. **104**: 205-210, 2011.

Alegbeleye O.O., Opeolu B.O., Jackson V.A.: Polycyclic aromatic hydrocarbons: A critical review of environmental occurrence and bioremediation. – Environ. Manage. **60**: 758-783, 2017.

Baidya A., Akter T., Islam M.R. *et al.*: Effect of different wavelengths of LED light on the growth, chlorophyll, β-carotene content and proximate composition of *Chlorella ellipsoidea*. – Heliyon **7**: e08525, 2021.

Bates L.S., Waldren R.P., Teare I.D.: Rapid determination of free proline for water-stress studies. – Plant Soil **39**: 205-207, 1973.

Binnal P., Babu P.N.: Optimization of environmental factors affecting tertiary treatment of municipal wastewater by *Chlorella protothecoides* in a lab scale photobioreactor. – J. Water Process Eng. **17**: 290-298, 2017.

Bukowska B., Duchnowicz P.: Molecular mechanisms of action of selected substances involved in the reduction of benzo[*a*] pyrene-induced oxidative stress. – Molecules **27**: 1379, 2022.

Cajnko M.M., Novak U., Likozar B.: Cascade valorization process of brown alga seaweed *Laminaria hyperborea* by isolation of polyphenols and alginate. – J. Appl. Phycol. **31**: 3915-3924, 2019.

Cheng D., He Q.: Assessment of environmental stresses for enhanced microalgal biofuel production – an overview. – Front. Energy Res. **2**: 26, 2014.

Croxton A.N., Wikfors G.H., Schulterbrandt-Gragg III R.D.: The use of flow cytometric applications to measure the effects of PAHs on growth, membrane integrity, and relative lipid content of the benthic diatom, *Nitzschia brevirostris*. – Mar. Pollut. Bull. **91**: 160-165, 2015.

Dere S., Güneş T., Sivaci R.: Spectrophotometric determination of chlorophyll-*a*, *b* and total carotenoid contents of some

algae species using different solvents. – Turk. J. Bot. **22**: 13-17, 1998.

Dinç E., Ceppi M.G., Tóth S.Z. *et al.*: The Chl *a* fluorescence intensity is remarkably insensitive to changes in the chlorophyll content of the leaf as long as the Chl *a/b* ratio remains unaffected. – BBA-Bioenergetics **1817**: 770-779, 2012.

Elsheery N.I., Cao K.F.: Gas exchange, chlorophyll fluorescence, and osmotic adjustment in two mango cultivars under drought stress. – Acta Physiol. Plant. **30**: 769-777, 2008.

Elsheery N.I., Wilske B., Cao K.F.: The effect of night chilling on gas exchange and chlorophyll fluorescence of two mango cultivars growing under two irradiances. – Acta Bot. Yunnan. **30**: 447-456, 2008.

González-Camejo J., Viruela A., Ruano M.V. *et al.*: Effect of light intensity, light duration and photoperiods in the performance of an outdoor photobioreactor for urban wastewater treatment. – Algal Res. **40**: 101511, 2019.

Gris B., Morosinotto T., Giacometti G.M. *et al.*: Cultivation of *Scenedesmus obliquus* in photobioreactors: effects of light intensities and light–dark cycles on growth, productivity, and biochemical composition. – Appl. Biochem. Biotech. **172**: 2377-2389, 2014.

Hazrati S., Tahmasebi-Sarvestani Z., Modarres-Sanavy S.A.M. *et al.*: Effects of water stress and light intensity on chlorophyll fluorescence parameters and pigments of *Aloe vera* L. – Plant Physiol. Bioch. **106**: 141-148, 2016.

Häder D.P., Williamson C.E., Wängberg S.A. *et al.*: Effects of UV radiation on aquatic ecosystems and interactions with other environmental factors. – Photoch. Photobio. Sci. **14**: 108-126, 2015.

Jain L., Jajoo A.: Protection of PSI and PSII complexes of wheat from toxic effect of anthracene by *Bacillus subtilis* (NCIM 5594). – Photosynth. Res. **146**: 197-211, 2020.

Jajoo A., Mekala N.R., Tomar R.S. *et al.*: Inhibitory effects of polycyclic aromatic hydrocarbons (PAHs) on photosynthetic performance are not related to their aromaticity. – J. Photoch. Photobio. B **137**: 151-155, 2014.

Juhasz A.L., Naidu R.: Bioremediation of high molecular weight polycyclic aromatic hydrocarbons: a review of the microbial degradation of benzo[*a*]pyrene. – Int. Biodeterior. Biodegradation **45**: 57-88, 2000.

Khpalwak W., Abdel-dayem S.M., Sakugawa H.: Individual and combined effects of fluoranthene, phenanthrene, mannitol and sulfuric acid on marigold (*Calendula officinalis*). – Ecotox. Environ. Safe. **148**: 834-841, 2018.

Kim S.-H., Liu K.-H., Lee S.-Y. *et al.*: Effects of light intensity and nitrogen starvation on glycerolipid, glycerophospholipid, and carotenoid composition in *Dunaliella tertiolecta* culture. – PLoS ONE **8**: e72415, 2013.

Kottuparambil S., Park J.: Anthracene phytotoxicity in the freshwater flagellate alga *Euglena agilis* Carter. – Sci. Rep.-UK **9**: 15323, 2019.

Laurens L.M.L., Dempster T.A., Jones H.D.T. *et al.*: Algal biomass constituent analysis: method uncertainties and investigation of the underlying measuring chemistries. – Anal. Chem. **84**: 1879-1887, 2012.

Lee C.Y., Nanah C.N., Held R.A. *et al.*: Effect of electron donating groups on polyphenol-based antioxidant dendrimers. – Biochimie **111**: 125-134, 2015.

Li S., Chu R., Hua D. *et al.*: Combined effects of 17β-estradiol and copper on growth, biochemical characteristics and pollutant removals of freshwater microalgae *Scenedesmus dimorphus*. – Sci. Total Environ. **730**: 138597, 2020.

Mathur S., Tomar R.S., Jajoo A.: Arbuscular mycorrhizal fungi (AMF) protects photosynthetic apparatus of wheat under drought stress. – Photosynth. Res. **139**: 227-238, 2019.

Meena M., Divyanshu K., Kumar S. *et al.*: Regulation of L-proline biosynthesis, signal transduction, transport, accumulation and its vital role in plants during variable environmental conditions. – Heliyon **5**: e02952, 2019.

Mishra S.K., Suh W.I., Farooq W. *et al.*: Rapid quantification of microalgal lipids in aqueous medium by a simple colorimetric method. – Bioresource Technol. **155**: 330-333, 2014.

Nama S., Madireddi S.K., Devadasu E.R., Subramanyam R.: High light induced changes in organization, protein profile and function of photosynthetic machinery in *Chlamydomonas reinhardtii*. – J. Photoch. Photobio. B **152**: 367-376, 2015.

Nzayisenga J.C., Farge X., Groll S.L., Sellstedt A.: Effects of light intensity on growth and lipid production in microalgae grown in wastewater. – Biotechnol. Biofuels **13**: 4, 2020.

Olayinka O.O., Adewusi A.A., Olarenwaju O.O., Aladesida A.A.: Concentration of polycyclic aromatic hydrocarbons and estimated human health risk of water samples around Atlas Cove, Lagos, Nigeria. – J. Health Pollut. **6**: 181210, 2018.

Paliwal C., Mitra M., Bhayani K. *et al.*: Abiotic stresses as tools for metabolites in microalgae. – Bioresource Technol. **244**: 1216-1226, 2017.

Petersen D.G., Dahllöf I.: Combined effects of pyrene and UV-light on algae and bacteria in an arctic sediment. – Ecotoxicology **16**: 371-377, 2007.

Petersen D.G., Reichenberg F., Dahllöf I.: Phototoxicity of pyrene affects benthic algae and bacteria from the Arctic. – Environ. Sci. Technol. **42**: 1371-1376, 2008.

Slocombe S.P., Ross M., Thomas N. *et al.*: A rapid and general method for measurement of protein in micro-algal biomass. – Bioresource Technol. **129**: 51-57, 2013.

Sun H., Yang Y.J., Huang W.: The water-water cycle is more effective in regulating redox state of photosystem I under fluctuating light than cyclic electron transport. – BBA-Bioenergetics **1861**: 148235, 2020.

Tang D., Han W., Li P. *et al.*: CO_2 biofixation and fatty acid composition of *Scenedesmus obliquus* and *Chlorella pyrenoidosa* in response to different CO_2 levels. – Bioresource Technol. **102**: 3071-3076, 2011.

Tomar R.S., Jajoo A.: Fluoranthene, a polycyclic aromatic hydrocarbon, inhibits light as well as dark reactions of photosynthesis in wheat (*Triticum aestivum*). – Ecotox. Environ. Safe. **109**: 110-115, 2014.

Tomar R.S., Jajoo A.: Photomodified fluoranthene exerts more harmful effects as compared to intact fluoranthene by inhibiting growth and photosynthetic processes in wheat. – Ecotox. Environ. Safe. **122**: 31-36, 2015.

Tomar R.S., Jajoo A.: Photosynthetic response in wheat plants caused by the phototoxicity of fluoranthene. – Funct. Plant Biol. **46**: 725-731, 2019.

Tomar R.S., Jajoo A.: Enzymatic pathway involved in the degradation of fluoranthene by microalgae *Chlorella vulgaris*. – Ecotoxicology **30**: 268-276, 2021.

Tsao R.: Chemistry and biochemistry of dietary polyphenols. – Nutrients **2**: 1231-1246, 2010.

Xu Y., Ibrahim I.M., Harvey P.J.: The influence of photoperiod and light intensity on the growth and photosynthesis of *Dunaliella salina* (Chlorophyta) CCAP 19/30. – Plant Physiol. Bioch. **106**: 305-315, 2016.

Yan C., Zhang L., Luo X., Zheng Z.: Effects of various LED light wavelengths and intensities on the performance of purifying synthetic domestic sewage by microalgae at different influent C/N ratios. – Ecol. Eng. **51**: 24-32, 2013.

Zarmi Y., Gordon J.M., Mahulkar A. *et al.*: Enhanced algal photosynthetic photon efficiency by pulsed light. – iScience **23**: 101115, 2020.

Isolation, purification and characterization of a protease from the seeds of Artocarpus heterophyllus

Monika Pandey
School of Life Sciences, Devi Ahilya Vishwavidyalaya, Indore-452 001, Madhya Pradesh, India

Krishnan Hajela
School of Life Sciences, Devi Ahilya Vishwavidyalaya, Indore-452 001, Madhya Pradesh, India

Abstract

Proteases are being widely used in various industries like detergent, leather, food and pharmaceuticals.Protease was purified to homogeneity from the seeds of *Artocarpus heterophyllus*. The enzyme was found to be a tetramer having molecular mass of 74 kDa. Gelatin zymography showed a clear band of proteolysis. The enzyme isolated and purified was a serine protease, as indicated by its inhibition with PMSF. The enzyme was stable at broad pH and temperature ranges with pH and temperature optima at 8.5 and 50°C, respectively. The presence of some divalent ions enhanced the activity. With the addition of calcium, change in absorption and emission spectra was observed in spectrofluorometric analysis. The Km and V_{max} for the enzyme was found to be 0.229 µM and 0.014 µM min^{-1}, respectively, using BAPNA as a substrate. The enzyme consisted 4.44% alpha helix and 44.17% beta sheets when measured by CD spectra. Dynamic light scattering of the protease for particle size distribution revealed the mono-dispersity of the sample. Easy purification and paramount stability of protease makes it a good candidate for industrial and pharmaceutical applications.

Evaluation of C4b as an adjunct marker in symptomatic RT-PCR negative Covid-19 cases

Bandana Kumari,[1] Krishnan Hajela,[2] Asgar Ali,[1] Abhay Kumar Sharma,[1] Rajesh Kumar Yadav,[1] Alok Ranjan,[3] Rathish Nair,[4] Shreekant Bharti,[5] Satish Dipankar,[6] Prabhat Kumar Singh,[7] and Sadhana Sharma[✉1,8]

Abstract

Introduction

Detecting low viral load has been a challenge in this pandemic, which has led to its escalated transmission. Complement activation has been implicated in pathogenesis of Covid-19 infection. Thus, evaluation of complement activation in suspected Covid-19 infection may help to detect infection and limit false negative cases thus limiting transmission of infection. We speculate that measuring C4b, produced from an activated complement system due to the presence of Covid-19 may help in its detection, even when the viral titers are low.

Methods

Plasma C4b levels of symptomatic RT-PCR positive patients (cases, n = 40); symptomatic RT-PCR negative patients (n = 35) and asymptomatic RT-PCR negative controls (n = 40) were evaluated. Plasma C5b-9, IL-6, D-dimer and C1-Inhibitor (C1-INH) were also measured in cases and controls. ELISA kits were used for all measurements. Statistical analyses were carried out using Stata, version 12 (Stata Corp., Texas, USA).

Results

C4b levels were found to be significantly increased in RT-PCR positive patients as compared to asymptomatic RT-PCR negative controls. RT-PCR negative but symptomatic patients still showed increased C4b levels. The significantly higher levels of C4b in cases with a cut-off value of ≥ 116 ng/ml with optimum sensitivity and specificity of 80% and 52% respectively is indicative of its

Feedback

Mannose-binding lectin gene 2 variant DD (rs 5030737) is associated with susceptibility to COVID-19 infection in the urban population of Patna City (India)

Sadhana Sharma [1], Bandana Kumari [2], Asgar Ali [2], Pankaj Kumar Patel [3], Abhay Kumar Sharma [2], Rathish Nair [4], Prabhat Kumar Singh [5], Krishnan Hajela [6]

Affiliations
PMID: 37204457   PMCID: PMC10196310   DOI: 10.1007/s00438-023-02030-4
Free PMC article

Abstract

The study aimed to measure plasma levels of Mannose-Binding Lectin (MBL) and MBL-associated serine protease-2 (MASP-2) and their polymorphisms in COVID-19 patients and controls to detect association. As MBL is a protein of immunological importance, it may contribute to the first-line host defence against SARS-CoV-2. MBL initiates the lectin pathway of complement activation with help of MASP-1 and MASP-2. Hence, appropriate serum levels of MBL and MASPs are crucial in getting protection from the disease. The polymorphisms of MBL and MASP genes affect their plasma levels, impacting their protective function and thus may manifest susceptibility, extreme variability in the clinical symptoms and progression of COVID-19 disease. The present study was conducted to find plasma levels and genetic variations in MBL and MASP-2 in COVID-19 patients and controls using PCR-RFLP and ELISA, respectively.The present study was conducted to find plasma levels and genetic variations in MBL and MASP-2 in COVID-19 patients and controls using PCR-RFLP and ELISA, respectively. Our results indicate that median serum levels of MBL and MASP-2 were significantly low in diseased cases but attained normal levels on recovery. Only genotype DD was found to be associated with COVID-19 cases in the urban population of Patna city.

Keywords: COVID-19; MASP-2; MBL genotyping; SARS-COV-2.

PubMed Disclaimer

Figures

Fig. 1 A Serum levels for MBL...

Fig. 2 A Serum levels of MASP-2...
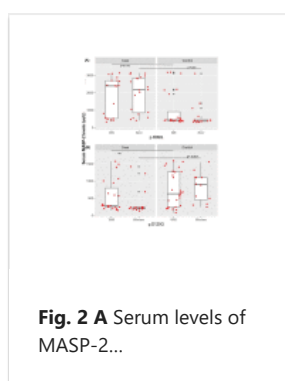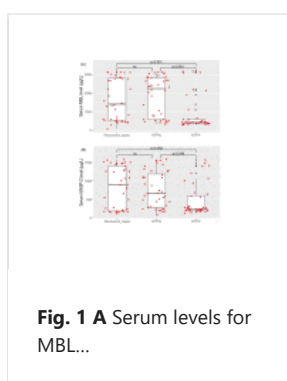
Structural and accessibility studies highlight the differential Binding of Clemizole to TRPC5 and TRPC6

Uzma Saqib[1], Isaac S. Demaree[2], Alexander G. Obukhov[2,3], Mirza S. Baig[4], Mohd Shahnawaz Khan[5], Nojood Altwaijry[5], Mochammad Arfin Fardiansyah Nasution[6,7], Kenji Mizuguchi[6,7], **Krishnan Hajela[1]***

*Corresponding Author: hajelak@gmail.com

Abstract

Background: Transient Receptor Potential Canonical 5 (TRPC5) and TRPC6 channels play critical physiological roles in various cell types. Their involvement in numerous disease progression mechanisms has led to extensive search for their inhibitors. Although several potent TRPC inhibitors have been developed and the structure of their binding sites were mapped using cryo electron microscopy, a comprehensive understanding of the molecular interactions within the inhibitor binding site of TRPCs remains elusive.

Objective: This study aims to decipher the structural determinants and molecular mechanisms contributing to the differential binding of clemizole to TRPC5 and TRPC6, with a particular focus on the accessibility of binding site residues. This information will help us understand what molecular features allow for selective binding, which is a key characteristic of clinically effective pharmacological agents.

Methods: Using computational methodologies, we conducted an in-depth molecular docking analysis of clemizole with TRPC5 and TRPC6 channels. The protein structures were retrieved from publicly accessible protein databases. Discovery Studio 2020 Client Visualizer and Chimera software facilitated our *in-silico* mutation experiments and enabled us to identify the critical structural elements influencing clemizole binding.

Results: Our study reveals key molecular determinants at the clemizole binding site, specifically outlining the role of residues' Accessible Surface Area (ASA) and Relative Accessible Surface Area (RASA) in differential binding. We found that lower accessibility of TRPC6 binding site residues, compared to those in TRPC5, could account for the lower affinity binding of clemizole to TRPC6.

Conclusion: This work illuminates the pivotal role of binding site residue accessibility in determining the affinity of clemizole to TRPC5 and TRPC6. A nuanced understanding of the distinct binding properties between these homologous proteins may pave the way for the development of more selective inhibitors, promising improved therapeutic efficacy and fewer off-target effects. By demystifying the structural and molecular subtleties of TRPC inhibitors, this research could significantly accelerate the drug discovery process, offering hope to patients afflicted with TRPC-related diseases.

Keywords: Transient Receptor Potential Canonical (TRPC); clemizole; Molecular docking; Inhibitor binding site; In silico mutation; Drug discovery; Selective inhibitors; Protein-ligand interaction; MD simulation

Fibrinogen Cleavage by Lectin Pathway Proteases: Roles and Implications

Madhuri M[1]; Kumari P[1]; Ali A[1]; Roy D[1]; Hajela S[2]; Kumari B[1]; Hajela K[3*]; Sharma S[1*]

[1]All India Institute of Medical Sciences, Patna, India
[2]Mahakaushal University, Jabalpur, Madhya Pradesh, India
[3]School of Life Sciences, DAVV, Indore, India

*Corresponding author: Sadhana Sharma

Department of Biochemistry, All India Institute of Medical Sciences, Patna - 801507, Bihar, India
Tel: 9631280481
E-mail: drsadhanas@aiimspatna.org, sharmasadhana.7@gmail.com

Abstract

The lectin pathway proteases (MASPs) are diverse in regard to their substrate selectivity and also have substrates outside the complement pathway. These proteases have been reported to cleave proteins of the coagulation cascade. MASP-1 has thrombin-like activity and therefore cleaves fibrinogen, fibrin and prothrombin. MASP-2 also participates in coagulation by cleaving prothrombin. Thus, these proteases are key players in the process of thrombosis and thrombolysis, therefore have implications in thrombotic vascular diseases. The cleaved fragments of fibrinogen and fibrin, consequently produced during coagulation and fibrinolysis, are important in the repair process and hence may have involvement in inflammatory and fibro-proliferative diseases. Also, altered levels of MBL and its associated serine proteases reported to be involved in different diseases such as cardiovascular diseases, diabetes, cancer, sepsis, stroke, COVID-19 etc. may have a role in thrombosis and thrombolysis. Upregulated lectin pathway-associated proteins predispose towards autoimmune disease susceptibility and may also exhibit off-target activities resulting in clot formation. Thus, the lectin pathway and its associated proteases are of great importance in normal circumstances where it plays a role in the maintenance of hemostasis and homeostasis, playing a preventive role in infections. Modulation in the level of MASPs proteases could be developed as a promising approach to treat a variety of infections and diseases.

Keywords: Fibrinogen; MBL; MASPs; Thrombin; Coagulation; Fibrinolysis

Abbreviations: MASPs: MBL Associated Serine Protease; rMASP-Recombinant MASP; FPA and FPB: Fibrinopeptide A and B, Respectively; TAFI: Thrombin-Activated Fibrinolysis Inhibitor; DIC: Disseminated Intravascular Coagulation; CVD: Cardiovascular Diseases; LP: Lectin Pathway.

Introduction

Fibrinogen is a serum glycoprotein which is synthesized by the liver. It is a large molecular weight (340kDa) protein with three pairs of non-identical polypeptide chains (Hexameric homodimer) [1]. Such a structure of fibrinogen supports its complex roles in hemostasis and homeostasis [2]. During an inflammatory response, this protein is upregulated and expressed more. Different variants of fibrinogen are also formed as a result of alternative splicing. These have unique properties to contribute to the coagulation process following any vascular injury [3]. During coagulation, fibrinogen conversion to fibrin occurs via thrombin-mediated proteolytic cleavage. It produces intermediate protofibrils followed by mature fibers which eventually provide stable hemostatic clots and prevent blood loss at sites of tissue damage [4]. The processes of hemostasis and thrombosis involve interactions between fibrinogen and/or fibrin and plasma proteins and receptors on platelets, leukocytes, endothelial cells, and other cells [4]. Disorders in fibrinogen concentration and/or function increase the risk of bleeding, thrombosis, and infection [5]. Also, recent studies suggest that abnormal thrombin generation patterns produce abnormally structured clots that are associated with an increased risk of bleeding or thrombosis [6,4].

Further, a network of circulating blood cells and soluble proteins constitutes the host's immune system which not only provides protection from various diseases but maintains homeostasis too. The complement system is one component of the immune system, which is a set of soluble proteins, which get

Chemical or enzymatic deglycosylation and germination abrogates the inhibitory activity of *Cyamopsis tetragonoloba* trypsin inhibitor

Preeti Patidar[1] · Mamta Bhayal[1] · Sumati Hajela[2] · Krishnan Hajela[1]

Abstract

A glycosylated heat stable trypsin chymotrypsin inhibitor was isolated from *Cyamopsis tetragonoloba* seeds. It is being reported for the first time that deglycosylation of the inhibitor chemically by Trifluoro methane sulfonic acid or enzymatically by salivary amylase or fungal diastase abrogates the inhibitory activity indicating that glycosylation was important for inhibitory activity of the protein. Treatment with salivary amylase decreases the inhibition in *in vitro* digestion experiment also. Germination of *Cyamopsis tetragonoloba* seeds results in reduction in inhibitory activity with concomitant increase in amylase activity. It is speculated that increase in amylase during germination decreases the protease inhibitory activity by deglycosylating the inhibitor.

Keywords *Cyamopsis tetragonoloba* · Glycosylation · Deglycosylation · Germination

Abbreviations

CTTI	*Cyamopsis tetragonoloba* trypsin inhibitor
TFMS	Trifluoro methane sulfonic acid
BAPNA	Nα-Benzyl-L-arginine 4-nitroanilide
SDS-PAGE	Sodium dodecyl sulphate polyacrylamide gel electrophoresis
DEAE	Diethylaminoethyl

Legume seeds normally contain large quantities of proteinases inhibitors which inhibit proteases like trypsin, chymotrypsin elastase etc. (Laskowski and Laskowski 1954). *Cyamopsis tetragonoloba* seeds of Sarit Soumya-700 variety, (Rajasthan) India were obtained from local vendor. The *Cyamopsis tetragonoloba* inhibitor was isolated by ammonium sulphate precipitation, ion exchange and gel filtration method essentially as described earlier (Hajela et al. 1999). Carbohydrate content of the purified inhibitor before and after treatment with salivary amylase was checked by the method of Dubois et al. (Dubois et al. 1980). The inhibition of trypsin and chymotrypsin by purified inhibitor was determined using chromogenic substrates (1 mM) BAPNA for trypsin and (5 mM) N-Succinyl-L-phenylalanine-p-nitroanilide for chymotrypsin (Norioka et al. 1988). The deglycosylation of *Cyamopsis tetragonoloba* inhibitor was done using TFMS (Edge 2003) and also by salivary amylase and a fungal diastase. The effect of salivary amylase concentration on *Cyamopsis tetragonoloba* inhibitor's inhibitory activity was determined by addition of different concentrations of salivary amylase/ fungal diastase (10 µg, 20 µg, 30 µg, 40 µg, 50 and 60 µg) prepared in phosphate buffer saline pH 7.2 to 15 µg of inhibitor. After incubation for 1 h at 37^0 C, the protease inhibitory activity was assayed under optimal conditions. Inhibitor without salivary amylase/fungal diastase treatment is represented as + ve control.

To study the effect of time of incubation, *Cyamopsis tetragonoloba* inhibitor(15 µg) was preincubated with salivary amylase or (30 µg) at 37^0 C for different time intervals (1 h, 2 h, 3 h, 4 h, 5 h, 6 and 12 h) and inhibitory activity was checked by using standard assay method. For deglycosylation of inhibitor diastase from *Aspergillus oryzae* (Sigma, lot number BCBW175) was also used in a similar manner.

To check the inhibitor digestibility by pepsin, 1 ml of purified *Cyamopsis tetragonoloba* inhibitor (100 µg/ml) was adjusted to pH 2.0 by dilute HCl and was added to 100 µl of pepsin (20 µg) (from porcine gastric mucosa,

✉ Krishnan Hajela
hajelak@gmail.com

[1] School of Life Sciences, Devi Ahilya University, Khandwa Road Campus, 452001 Indore, India

[2] Department of Biotechnology IPS Academy, Rajendra Nagar, Indore, India

Identification of substrates of MBL Associated Serine Protease-1 (MASP-1) from human plasma using N-terminomics strategy

Sonali R. Bhagwat [a] [b] , Komal Choudhary [b], Nirali Pandya [a], Sadhana Sharma [c], Sanjeeva Srivastava [d], Amit Kumar [a], Krishnan Hajela [b]

Show more ∨

∝ Share   🟵 Cite

Abstract

MBL Associated Serine Protease-1 (MASP-1) is an abundant enzyme of the lectin complement pathway. MASP-1 cleaves numerous substrates like MASP-2, MASP-3, C2, C3i, fibrinogen, FXIII and prothrombin. It has thrombin-like specificity and can cleave thrombin substrates. Owing to its high concentration and relaxed substrate specificity, MASP-1 has substrates outside the complement system and can influence other proteolytic cascades and physiological processes. The unidentified substrates may assist us to ascertain the role(s) of MASP-1. In this study, we used a high-throughput N-terminomics method to identify substrates of MASP-1 from human plasma. We have identified 35 putative substrates of MASP-1. Among the identified proteins, alpha 2-antiplasmin, alpha-1-acid glycoprotein, antithrombin III, and siglec-6 were demonstrated to be cleaved by MASP-1. We have discussed the physiological relevance of cleavage of these substrates by MASP-1. The expression of Siglec-6 and MASP-1 has been reported in the B cells. Alpha-1-acid glycoprotein cleavage by MASP-1 may occur in the acute phase as it is known to be an inhibitor of platelet aggregation, whereas MASP-1 triggers platelet aggregation. The cleavage alpha2 antiplasmin by MASP-1 implies that MASP-1 may be promoting plasmin-mediated fibrinolysis. Our study supports that MASP-1 may be implicated in thrombosis as well as thrombolysis.

Introduction

The intrusion of pathogens in the biological system is resisted by the immune system by responding through the activation of various complement pathways. The lectin complement pathway is activated when the molecules that recognize the pattern of sugar moieties on the surface of the pathogen [mannan-binding lectin (MBL), collectin 11 (CLK11), and ficolins] form complexes with MBL-associated serine proteases (MASP 1, 2 and 3), and mannose-binding lectin associated proteins (MAp19 and MAp44). MASP-1 is the most abundant protease in the lectin pathway and is known to have a relaxed substrate specificity. The physiological role of MASP-1 is therefore arguable. Also, MASP-1 can cleave C3 but with very low efficiency (Dobó et al., 2009; Matsushita et al., 2000), and the physiological relevance of this cleavage are also not fully understood. Furthermore, MASP-1 is reported to cleave fibrinogen and factor XIII, but with less efficiency as compared with thrombin (Hess et al., 2012; Hajela et al., 2002; Gulla et al., 2010). Although it has been demonstrated that ascidian MASP-1 cleaves ascidian C3 directly(Fujita, 2002) but for human MASP-1 the kinetic data of this reaction is lacking (Beltrame et al., 2015). Therefore, clarifying the role and physiological significance of MASP-1 is important. The reported substrates of MASP-1 are MASP-1 (auto-activation), MASP-2, C2 from complement proteins leading to the activation of the lectin pathway of complement activation and other protein like fibrinogen (Dobó et al., 2009), factorXIII (Dobó et al., 2009), kininogen (Dobó et al., 2011), PAR-4 (Megyeri et al., 2009), and prothrombin (Jenny et al., 2015a). MASP-1 has a wide substrate-binding cavity, as well as a broad substrate specificity (Dobó et al., 2009) and recognizes substrates of complement pathway as well as that of the coagulation cascade. As the in vivo natural substrates of MASP-1 are not yet well characterized, there is a strong possibility that the diversity of its physiological functions is not understood in its entirety.

In this paper, we contemplate the possibility of the occurrence of many substrates of MASP-1 that have not yet been identified. Also, the method of identifying the substrates of MASP-1 using a high throughput proteomics-based method -the N-terminomics strategy- has not been performed earlier. In this study, we have attempted to identify putative substrates of MASP-1 in plasma that may be contributing to the effective functioning of the complement pathway or other biological processes. Briefly, the method involves blocking the α-NH$_2$ group of peptides or proteins using chemical methods like metal ion catalyzed transamination, allowing the ε-NH$_2$ group of lysine residue to be intact. Proteolytic cleavage by test serine protease was performed followed by blocking of the ε-NH$_2$ group of lysine residues by guanidination, in reaction conditions where the neo-N termini remain unmodified. The α-NH$_2$ groups of neo-peptides were biotinylated

Isolation, purification and characterization of a protease from the seeds of *Artocarpus heterophyllus*

Monika Pandey & Krishnan Hajela*

School of Life Sciences, Devi Ahilya Vishwavidyalaya, Indore-452 001, Madhya Pradesh, India

Proteases are being widely used in various industries like detergent, leather, food and pharmaceuticals.Protease was purified to homogeneity from the seeds of *Artocarpus heterophyllus*. The enzyme was found to be a tetramer having molecular mass of 74 kDa. Gelatin zymography showed a clear band of proteolysis. The enzyme isolated and purified was a serine protease, as indicated by its inhibition with PMSF. The enzyme was stable at broad pH and temperature ranges with pH and temperature optima at 8.5 and 50°C, respectively. The presence of some divalent ions enhanced the activity. With the addition of calcium, change in absorption and emission spectra was observed in spectrofluorometric analysis. The Km and V_{max} for the enzyme was found to be 0.229 µM and 0.014 µM min^{-1}, respectively, using BAPNA as a substrate. The enzyme consisted 4.44% alpha helix and 44.17% beta sheets when measured by CD spectra. Dynamic light scattering of the protease for particle size distribution revealed the mono-dispersity of the sample. Easy purification and paramount stability of protease makes it a good candidate for industrial and pharmaceutical applications.

Keywords: *Artocarpus heterophyllus*, BAPNA, CD spectra, Dynamic light scattering, Proteases, Serine endopeptidase

Proteolytic enzymes are intricately involved in many biological processes of plant life cycle like they play a central role in plant growth and development[1]. These proteases help in plant defence by producing hypersensitive response upon attack of any pathogens[2], by involving in the processes of plant's innate immunity[3] they generate an immune response[4]. Plant proteolytic enzymes also play indispensable role in plant germination by helping in proteolysis of the proteins accumulated in seeds[5]. Some proteases that are present in chloroplast play a key role in the maintenance of photosystem eventually helping in photosynthesis[6]. These proteases have a major function in programmed cell death and senescence signalling cascades[7]. Proteases are the proteins encoded by plant genome which are highly stable and can work in wide pH ranges and temperatures[8]. Plant proteases can be obtained from various plant sources, for instance seeds, roots, flowers, leaves, latex, *etc*. It has been used from ancient times as a folk medicine as anthelmintic, antitumor, antimicrobial, analgesic, antioxidant, anti-inflammatory, to clear skin infections, to enhance wound healing[9]. Hence, plant proteases has a vital role in therapeutics and this make them potential target for research in unexplored medicinal values[10]. Artocarpus tree is a member of Moraceae family, also named as mulberry family. Many different species of this genus are known and found in India and other continents of Southeast Asia. These are: *Artocarpus heterophyllus*, commonly known as jackfruit; *A. integer*, also known as cempedak; *A. camans*, known as bread nut and *A. altilis*, also known as breadfruit[11]. Although, no evidences have been found about industrial applications of Artocarpus proteases yet. Some studies have concluded that some plant proteolytic enzymes are very specific to their target or substrate. Purification and characterization of a protease from *Artocarpus heterophyllus* and delineation of its specific substrates is hereby being reported.

Materials and Methods

Materials

Artocarpus heterophyllus seeds were procured from the local market in Indore (India). Ammonium sulfate, sodium dodecyl sulphate (SDS), was purchased from SRL, N-α-Benzoyl-DL-arginine þ-nitroanilide

---

Purification and biochemical characterization of protease from the seeds of *Cyamopsis tetragonoloba*

Rajesh Kumar Rawaliya[1], Preeti Patidar[1], Sadhana Sharma[2], Krishnan Hajela[1]*

[1]School of Life Sciences, Devi Ahilya University Indore, India.
[2]Department of Biochemistry, All India Institute of Medical Sciences, Patna, India.

ABSTRACT

The present study was carried out to isolate, purify, and characterize protease from the seeds of *Cyamopsis tetragonoloba*. The protease was precipitated by a 60% ammonium sulfate cut and further purified by elution from ion-exchange chromatography at 0.3 M NaCl. The sodium dodecyl sulfate-polyacrylamide gel electrophoresis result showed that protease was monomeric having 69.9 kDa molecular weight. Gelatin zymography was carried out to confirm the proteolytic activity of the protease. The protease has a wide range of substrate specificity and could cleave natural substrates like casein, gelatin, bovine serum albumin (BSA), hemoglobin (Hb), and synthetic substrate like N-αBenzoyl-DL-arginine þ-nitroanilide (BAPNA). The V_{max} value of the protease was 102.04 μM/minute with casein as the substrate and K_m value was 56.56 μM/minute. The purified protease was completely inhibited by serine proteases inhibitors like Phenyl Methyl Sulfonyl Fluoride, soybean trypsin inhibitor, and aprotinin, and not inhibited by other protease inhibitors. This concluded that the purified protease was serine protease. The protease was highly stable at a wide range of temperatures from 20°C to 70°C. Gelatin showed the highest proteolytic activity when compared to the casein, Hb, and BSA. BAPNA showed 1.5101 U/mg specific activity. The sugar content of protease was estimated by the method of DuBois. The protease was highly glycosylated and contained 35 μg of sugar in 0.2 mg of protease.

1. INTRODUCTION

Cyamopsis tetragonoloba is an edible crop of annual legume plants belonging to the family of Fabaceae. It is cultivated in different regions of India like Rajasthan, MP, Haryana, and Punjab. It is an excellent source of guar gum and has high protein content [1,2]. It is used in cosmetics, textiles, paper industry, drilling, exploration mining, petroleum industry, and beverages [3]. It is known for its drought and high-temperature tolerance ability due to its deep roots [4].

Proteases of the tropical plants show high stability toward high temperature compared with proteases from many other plants since they tend to adapt and cope with differences in environmental temperature that is pivotal for survival of plants [5,6]. Higher temperature tends to denature enzymes by breaking hydrogen bonds [7].

Plants represent an excellent source of enzymes due to various characteristics. The leguminous plant seeds contain a high amount of protein. Legumes accumulate a high level of protease and protease inhibitors that regulate the overburden of protein [8]. Proteases are involved in the physiological process of plants including germination, plant growth, development, chloroplast synthesis, ubiquitination of misfolded protein, and programmed cell death [9–12].

Protease contributes 65% of the world enzyme market to the annual sale of enzymes [13]. Plant proteases are also currently used as therapeutic enzymes in wound healing, treatment of cancer, digestion disorder, infection, and food industry [14,15]. Plant proteases are also used in feather processing, bioremediation, and biotransformation.

---

*Corresponding Author
Krishnan Hajela, School of Life Sciences, Devi Ahilya University Indore,
India. E-mail: hajelak @ gmail.com

Mobile technology: A tool for healthcare and a boon in pandemic

Sadhana Sharma[1], Bandana Kumari[1], Asgar Ali[1], Rajesh K. Yadav[1], Abhay K. Sharma[1], Krishan K. Sharma[2], Krishnan Hajela[3], Girish K. Singh[4]

Departments of [1]Biochemistry and [2]Neurosurgery, (Trauma and Emergency), All India Institute of Medical Sciences, Patna, Bihar, [3]Department of Biochemistry, School of Life Sciences, Devi Ahilya Vishwavidyalaya, Indore, Madhya Pradesh, [4]Department of Orthopedics, Era Medical College, Lucknow, Uttar Pradesh, India

Abstract

Healthcare systems deal with disease prevention, early detection, diagnosis, investigation, and timely, affordable, and safe treatment. For the delivery of services in the health sector, communication is the key to linking the service provider and the patients. Mobile technology in the recent past has rendered various platforms of communications for the healthcare system. Thus, in health, mobile technology has greatly contributed to time management and cost reduction for healthcare at every level including hospital visits to individual appointments with doctors, hence the convenience. With advancements in mobile technologies and the growing number of mobile users, newer opportunities have opened up for the use of mobiles for patient care. Emerging information and communication technologies with the help of the Internet of Things (IoT) have been instrumental in integrating different domains of the health sector with mobile technology. Thus, the technology may have the potential to become powerful medical tools to support the health sector at all levels of care. In this review, the concept, applications, and advantages of mobile technology for health and the present pandemic have been discussed. It also discusses mobile health technology, as a support system for convenient and safer healthcare for public health, and the opportunities to improve its applications for unseen future health crises.

Keywords: Healthcare, medical tool, mHealth, mobile technology, pandemic, telemedicine

Introduction

"Crisis breeds the strength to cope with it. The Corona crisis of 2020 has highlighted the need to be able to help patients without getting exposed to the infection. We do not know how many such crises, how soon, will be faced in future, but we definitely know how to fight better next time".

Health care systems work on communication to provide all health-related services in any setting. It is the most essential requirement to establish a link between the health care provider and the patient. In earlier times, physical visits of patients to a hospital or a health care facility were the prime requirement to communicate about the ailments to seek health services.

Once considered a luxury of the rich, mobile phones are now an everyday communication necessity for people across the globe. There are over 7 billion wireless subscribers worldwide, and about 3.9 billion (51.2%) have access to the Internet.[1] It is predicted that the global distribution of smartphone users will be more than 4.78 billion in 2021.[2]

Mobile phones have proved to be a useful tool to provide an instant channel for communication for transmitting demographic, clinical, and investigational and progress data to health care providers and timely, credible advice to health

Access this article online

Quick Response Code:

Website:
www.jfmpc.com

DOI:
10.4103/jfmpc.jfmpc_1114_21

How to cite this article: Sharma S, Kumari B, Ali A, Yadav RK, Sharma AK, Sharma KK, *et al*. Mobile technology: A tool for healthcare and a boon in pandemic. J Family Med Prim Care 2022;11:37-43.

ORIGINAL ARTICLE

Medium optimization for submerged fermentative production of β-cyclodextrin glucosyltransferase by isolated novel alkalihalophilic *Bacillus* sp. NCIM 5799 using statistical approach

P. Solanki [iD] and T. Banerjee

Applied Microbiology Laboratory, School of Life Sciences, Devi Ahilya Vishwavidhaylaya, Indore, Madhya-Pradesh, India

Significance and Impact of the Study: The novel isolated alkalihalophilic *Bacillus* sp. NCIM 5799 is a predominant producer of β-cyclodextrin glucosyltransferase (β-CGTase). This was the first report that the production of β-CGTase was enhanced by applying two statistical approaches that are PBD and CCD-RSM. The novel isolated *Bacillus* sp. NCIM 5799 could be utilized for industrial production of β-CGTase.

Abstract

β-cyclodextrin glucosyltransferase (β-CGTase) is an essential enzyme to catalyse the biotransformation of starch into β-cyclodextrins (β-CD). β-CD has widespread applications in the biomedical, pharmaceutical and food industries. The present study focused on β-CGTase production using an efficient natural microbial strain and statistical production optimization for enhanced production. The isolated organism *Bacillus* sp. NCIM 5799 was found to be 5 μm short bacilli under FE-SEM and alkalihalophilic in nature. The β-CGTase production was optimized using a combination of Plackett–Burman design (PBD) and Central Composite Design—Response Surface Methodology (CCD-RSM). On PBD screening Na_2CO_3, peptone and $MgSO_4.7H_2O$ were found to be significant for optimal β-CGTase production, whereas the soluble starch and K_2HPO_4 concentrations were found to be nonsignificant for β-CGTase production. The significant factors obtained after PBD were further optimized using CCD-RSM design. Peptone was found to have a significant interaction effect with Na_2CO_3, and $MgSO_4 \cdot 7H_2O$ and Na_2CO_3 exhibited a significant effect on the production of CGTase. The production of β-CGTase was enhanced in the presence of peptone (3%) and Na_2CO_3 (0·8%). CGTase production obtained was 156·76 U/ml when optimized using CCD-RSM. The final optimized medium (RSM) shows 7·7- and 5·4-fold high productions as compared to un-optimized and one factor at a time production media.

Introduction

Starch is a vital storage material synthesized by plants during photosynthesis as a carbon and energy source. Numerous alkaliphilic micro-organisms degrade starch by producing extracellular amylases and utilizing it as a carbon source. Cyclodextrin glucosyltransferase (EC 2·4·1·19) is an important member of the starch degrading alpha-amylase family. Cyclodextrin glucosyltransferase (CGTase) is widely utilized to produce cyclic nonreducing, homogenous malto-

oligosaccharide called cyclodextrins (CDs) (Kelly *et al.* 2009). It is assumed that the production of CDs by CGTase is to monopolize starch substrates and thus cannot be utilized by other micro-organisms deficient in CGTase (Hashimoto *et al.* 2001). In addition, CDs are internalized via a unique ABC transport protein present in the membrane of the CGTase producer and utilized as a substrate (Qi and Zimmermann 2005).

CGTase catalyses four reactions, viz., cyclization (production of CD), coupling (breakdown of CD), disproportion

(shift the linear oligosaccharide to another oligosaccharide) and hydrolysis (use of water molecule to degrade longer polysaccharides into shorter fragments). Native CGTase produces different amounts of α, β and γ-CD, having 6, 7 and 8 glucose units joined by α-1,4-glycosidic bond. According to the different CDs produced; CGTase is typically divided into three subcategories α, β and γ-CGTase (Arce-Vázquez et al. 2016).

CDs are biocompatible, truncated cone-shaped molecules, having a hydrophobic internal surface and hydrophilic outer surface (Van der Veen et al. 2000). This arrangement forms a cavity of different internal diameters (depending on the type of CD), capable of forming a host-guest complex with a wide range of hydrophobic compounds. Instead of α, and ϒ-CD, β-CD has a noteworthy industrial value for its cavity size, low aqueous solubility and low toxicity (Ibrahim et al. 2012). In addition, the β-CD inclusion complex is rapidly prepared, and thus commands superior industrial demand for native and as well as various derivative forms (viz., methyl-βCD, hydroxy propyl-βCD and randomy methylated-βCD) (Junior et al. 2019).

The industrial utilization of β-CD includes pharmaceutical, agrochemical, biochemical, food, textile and cosmetics applications (Szejtli 2004) owing to its ability to form a water-dissolving complex and restructuring the host physicochemical properties (Alves-Prado et al. 2007). Other recently developed important application of β-CD in the biomedical field includes bioseparation, enzymatic catalysis, biochemical sensing, biomedical diagnosis and therapy (Xu et al. 2021).

CGTase that produces one kind of CD is industrially demanding because it decreases the purification cost (Gawande et al. 1998). The production of CGTase has been reported to be influenced by nutritional parameters. Moreover, designing the appropriate production medium increases productivity and lowers the overall cost of the product and thus the cost of manufacturing (Abdella et al. 2020; Singh et al. 2017).

Screening of important nutritional factors and their parameter optimization is imperative for production optimization (Bezerra et al. 2008). The parameter optimization can be strategized in two ways, the univariate (one factor at a time) way and multivariate (Response Surface Methodologies) techniques. The univariate method for production optimization is traditional, laborious and expensive. Also, the interaction between the significant variables is neglected in the classical univariate approach. Several types of statistical experimental designs have been utilized to evaluate production optimization. The Plackett–Burman design (PBD), is highly useful in screening studies for identifying the significant factors from a large number of variables. PBD helps to identify important components from a large number of variables in a smaller number of trials. This reduction creates additional opportunities to allow for replicates, improving the overall fidelity of the results as compared to the multivariable DOE approach.

The significant variables selected using PBD were further optimized using statistical and mathematical optimization tools such as response surface methodology (RSM) for enhanced production which includes central composite design (CCD). These approaches combine to provide the ideal concentration of the specific key medium components. Various researchers have used this method of determining the best medium composition in a variety of fermentation processes (Ramesh and Ramachandra Murty 2014; Singh et al. 2017; Aboyeji et al. 2020).

The work presented in this paper aims to utilize the novel isolate Bacillus sp. NCIM 5799, which produces solely β-CD (Solanki et al. 2022). The growth parameters of isolated bacteria Bacillus sp. at different pH and NaCl concentrations were evaluated. Furthermore, the β-cyclodextrin glucosyltransferase (β-CGTase) production optimization was conducted by two approaches. First, screening of the significant medium components using PBD, and second, the significant medium constituents identified in PBD were evaluated using RSM that included CCD to identify the interaction effect between significant variables. Both methods were employed to increase the overall β-CGTase production.

Results and discussion

Evaluation of morphological and alkalihalophilic nature of isolate

Figure 1 shows the morphology of isolated Bacillus sp. NCIM 5799 (a and b) using FE-SEM under magnification of 10 000–16 000×. Micrographs revealed that the organism was 5 μm short rod-shaped bacilli with an average diameter of 405·4 nm. The bacterial cells in the micrograph appeared as single cells, paired, and in short chains.

The growth of isolated Bacillus sp. under various pH and different concentrations of NaCl was determined in terms of OD_{600nm} which is depicted in Fig. 1c,d respectively. For measuring the growth under different pH, the optical density (OD) of the sample was withdrawn at 2–24 h of incubation. In addition, the growth under various NaCl concentrations was measured from 2 to 48 h. Among all the pH tested, no growth was found at any time of incubation in pH 6·5 and 7. With a subsequent increment in the pH range of the medium from 7·5 to 12, enhancements in growth were observed. Moderate growth was observed in pH 7·5 as compared to the neutral (pH 7) or slightly acidic (pH 6·5) medium.
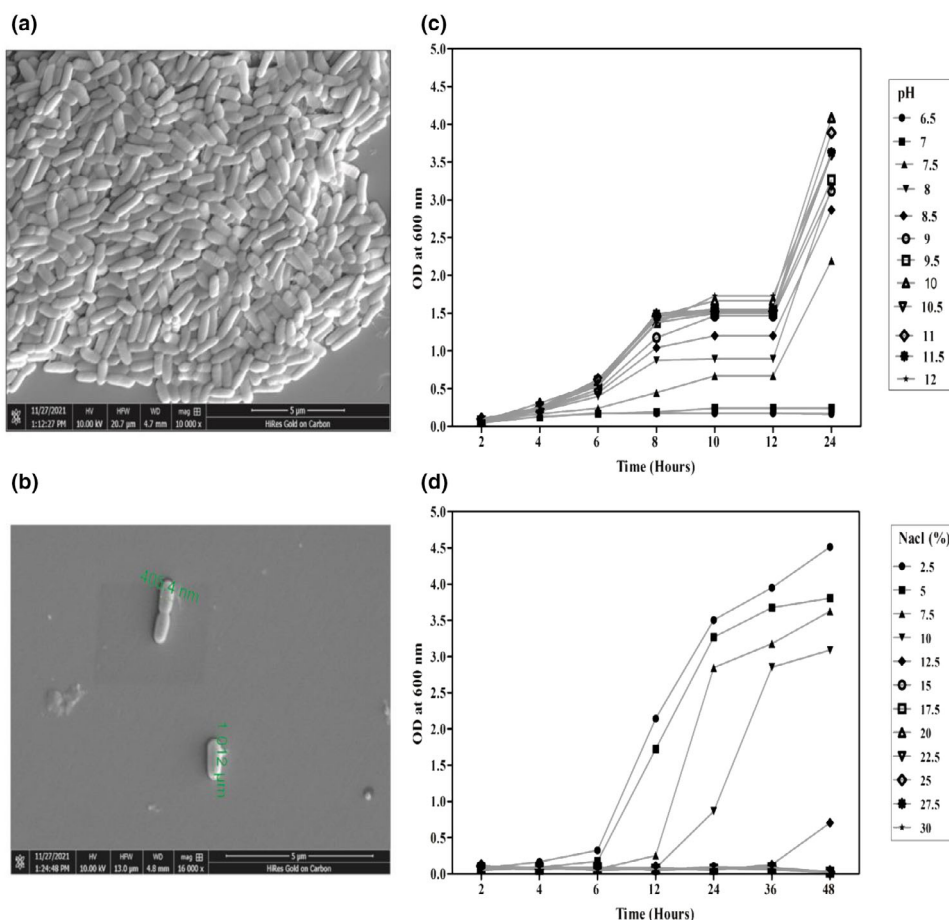
Figure 1 (a and b) Micrograph showing the rod-shaped morphology of isolated novel *Bacillus* sp. NCIM 5799 after the overnight growth and c and d showing growth of isolated novel *Bacillus* sp. NCIM 5799 under the influence of c various pH and d different concentrations of NaCl. Different lines in the graphs represent various pH and NaCl concentrations.

A subsequent increase in pH till 9 led to a clear incremental growth pattern starting from 6 h incubation. Further, an increase in pH to 12 did not improve the growth any further; however, the growth pattern of all the curves from pH 9·5 to 12 remained tightly clustered throughout the incubation period. There was no negative effect of increasing the pH on the organism growth up to pH 12.

At 24-h incubation, pH 10 was found to support the highest growth and pH values beyond 10 also supported growth to an almost equivalent extent. It is clear from the figure that the organism grows better in strongly alkaline conditions.

To test the halophilic nature of the isolated organism, the growth curve was studied in presence of NaCl in the range of 2·5–30% NaCl concentration. In the initial 6 h of incubation, negligible growth could be observed, however, on further incubation cultures with 2·5, 5, 7·5 and 10% concentrations of NaCl showed promising growth. Further increase in the salt concentration beyond 10% up

to 48 h of incubation, led to a sharp decline in growth. This confirms that the organism is moderately halotolerant and thus can be termed as halophilic (Bowers *et al.* 2009).

A comparative investigation of different alkaliphilic and halophilic CGTase producer strains led to a preferentially β-CD production (Abelyan *et al.* 2004). A similar study was conducted by Ibrahim *et al.* (2013), on *Amphibacillus* sp. NPST−10 which grew better at up to 6% of NaCl concentration and pH 9. Further decline in growth was observed above pH 9·5 and 15% NaCl concentration.

Optimization of production medium for β-CGTase using statistical tools

The important medium constituents were 4% soluble starch, 2% peptone, 0·1% K_2HPO_4, 0·04% $MgSO_4 \cdot 7H_2O$ and 1% Na_2CO_3 (Ibrahim *et al.* 2005) were used for β-CGTase production in submerged fermentation (shake

flask) for novel isolated *Bacillus* sp. NCIM 5799. These medium ingredients were selected based on initial conventional optimization studies (Solanki *et al.* 2022), and the selected medium constituents were evaluated by PBD and CCD-RSM. Overnight culture of *Bacillus* sp. NCIM 5799 raised in the nutrient broth of pH 10 at 30°C was used to inoculate the production media. The inoculated media was incubated at 30°C for 96 h and the culture supernatant was used as the enzyme solution. The β-CGTase assay was carried out utilizing the ability of β-CD to complex phenolphthalein indicator dye. The percentage reduction in absorbance at 550 nm was interpolated in the calibration curve to calculate the amount of CGTase in the fermentation broth. The literature survey reveals that this is the first study to optimize the medium ingredient using two statistical optimization strategies for β-CGTase production. In this study, isolated *Bacillus* sp. NCIM 5799 was used for β-CGTase production by applying PBD and CCD-RSM.

Screening of key medium components by Placket–Burman design

To evaluate the most significant variables for β-CGTase production PBD design was construed for *Bacillus* sp. (Plackett and Burman 1946). Five different independent variables were used for PBD analysis viz., soluble starch, peptone, dipotassium hydrogen phosphate, magnesium sulphate heptahydrate and sodium carbonate. A total of 26 experiment trials were conducted in triplicates at 30°C and 130 rev min^{-1}. Each medium variable was screened at three levels and the result was interpreted in terms of β-CGTase production as a dependent variable (Table 1). The PBD model adequacy for β-CGTase production by *Bacillus* sp. was calculated using the Student's *t*-test and ANOVA (Table 2). Those variables having a *P*-value <0·05 were considered to be having a significant effect on β-CGTase production and were selected for further statistical optimization studies.

Na$_2$CO$_3$ which is used as a pH adjuster of the medium has a *P*-value of 0·00018 was considered the most significant factor followed by peptone as a nitrogen source (0·00024), and MgSO$_4$·7H$_2$O as a mineral salt (0·04462) respectively. Among all significant variables, soluble starch (0·56372) and K$_2$HPO$_4$ (0·45662) exerted a negative effect, whereas the other medium constituents showed a positive effect on β-CGTase production. The same concept was graphically illustrated using Pareto chart of variables. The *t*-value of 2·101 for 95% confidence interval is plotted as a vertical line. Figure 2 shows the horizontal bars extending beyond the value of 2101 as having a significant effect (cut-off value of the model). Hence, factors Na$_2$CO$_3$, MgSO$_4$·7H$_2$O and peptone were considered as

Table 1 The Plackett–Burman design for screening the significant medium components for β-CGTase production using *Bacillus* sp. PBS1 NCIM 5799

Trials no	Block	A	B	C	D	E	β-CGTase production
1	1	−	−	+	+	+	2·69928
2	1	+	+	−	+	+	20·8917
3	1	−	+	+	+	−	62·7466
4	1	−	−	−	−	−	14·2240
5	1	−	+	+	−	+	14·8705
6	1	−	+	−	−	−	41·1998
7	1	+	−	−	−	+	4·21679
8	1	+	+	−	+	+	71·3147
9	1	0	0	0	0	0	4·87155
10	1	+	−	+	+	−	8·24424
11	1	+	−	+	−	−	9·35579
12	1	−	−	−	+	+	4·92511
13	1	+	+	+	−	+	20·2876
14	2	−	−	−	+	+	27·4256
15	2	+	−	+	+	−	50·9593
16	2	−	−	−	−	−	59·5367
17	2	+	+	+	−	+	59·3716
18	2	−	+	+	+	−	101·972
19	2	−	−	+	+	+	34·1830
20	2	−	+	+	−	+	51·0263
21	2	+	+	−	+	+	63·1094
22	2	+	−	−	−	+	44·8359
23	2	−	+	−	−	−	52·1429
24	2	+	−	+	−	−	43·4995
25	2	+	+	−	+	−	130·585
26	2	0	0	0	0	0	89·7627

In the table, different alphabet denotes medium ingredient, e.g. A = soluble starch, B = peptone, C = K$_2$HPO$_4$, D = MgSO$_4$·7H$_2$O and E = Na$_2$CO$_3$.

Table 2 ANOVA of Placket–Burman design

| Source	df	Adj SS	Adj MS	*F*-value	*P*-value
Model	7	25 476·6	3639·5	10·87	0·000
Blocks	1	11 956·7	11 956·7	35·72	0·000
Linear	5	13 478·9	2695·8	8·05	0·000
A	1	115·8	115·8	0·35	0·564
B	1	7155·8	7155·8	21·38	0·000
C	1	193·8	193·8	0·58	0·457
D	1	1559·9	1559·9	4·66	0·045
E	1	4453·7	4453·7	13·30	0·002
Curvature	1	40·9	40·9	0·12	0·731
Error	18	6025·5	334·8		
Total	25	31 502·1			

In the table, different alphabet denotes medium ingredient, e.g. A = soluble starch, B = peptone, C = K$_2$HPO$_4$, D = MgSO$_4$·7H$_2$O and E = Na$_2$CO$_3$.

significant variables and their effects on β-CGTase production were further optimized using CCD (RSM). The remaining insignificant variables were used at a fixed concentration in all the further experiments (soluble starch 8 and 0·1% K$_2$HPO$_4$).
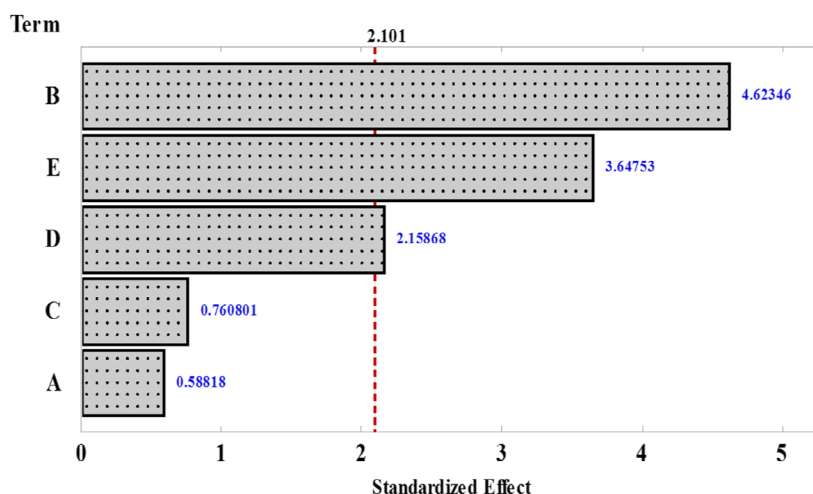
A = soluble starch, B = peptone, C = dipotassium hydrogen phosphate, D = magnesium sulfate and E = sodium carbonate

Figure 2 Pareto chart of standardized effect represents the order of significant factors taken for PBD affecting the β-CGTase production by isolated Bacillus sp. NCIM 5799. In the graph A = soluble starch, B = peptone, C = K_2HPO_4, D = $MgSO_4 \cdot 7H_2O$ and E = Na_2CO_3. The 2·101 value represents the standardized effect of the model. The different bar represents the various medium components taken from one factor at a time. The standardized effect ranges from 0·588 to 4·623.

The improved production of CGTase depends on the organism, as well as optimum culture media (Upadhyay et al. 2020). Statistical optimization of the production medium is a very useful tool for enhanced production using natural isolate. The most significant variables in the PBD screening experiment were peptone, Na_2CO_3 and $MgSO_4$ ($P < 0.01$). In addition to that soluble starch and K_2HPO_4 ($P > 0.01$) were found to be insignificant medium constituents (Fig. 2). The screening of key medium components by PBD for β-CGTase production was previously reported by Ahmed and El-Refai (2010), Sivaramareddy et al. (2014) and Rajput et al. (2016). Similar observations were reported by Sivaramareddy et al. (2014) where peptone was found to be significant, whereas Ahmed and El-Refai (2010) found starch to be insignificant in β-CGTase production. In addition, Mahat et al. (2004) found K_2HPO_4 to be insignificant for CGTase production. Contradictory results were observed by Rajput et al. (2016) where soluble starch and K_2HPO_4 were found to be significant, whereas $MgSO_4$ and peptone were insignificant for β-CGTase production. Few works of literature reported starch and K_2HPO_4 to be insignificant for CGTase production. This could be explained by the fact that the utilization of medium constituents is an organism-dependent phenomenon.

Optimization of significant variables using response surface methodology

We have succeeded in optimizing the media constituents using RSM for improved production of CGTase. The effect of selected significant variables, peptone (X_1), Na_2CO_3 (X_2) and $MgSO_4 \cdot 7H_2O$ (X_3), on β-CGTase production was studied and the results are presented in Table 3. The result of the CCD experiment revealed that the maximum β-CGTase production was observed in experimental runs number 1 and 9, which were 145·28 and 147·58 U ml^{-1} respectively. Based on the full quadratic regression model application, it appeared that the peptone × Na_2CO_3 (P-value = 0·000), and peptone × $MgSO_4 \cdot 7H_2O$ (P-value = 0·010) have a significant effect; whereas, Na_2CO_3 × $MgSO_4 \cdot 7H_2O$ interaction was found insignificant for β-CGTase production. In the quadratic effect, only Na_2CO_3 showed a significant effect on production (P-value = 0·0032). After analysing the CCD model the regression equation or polynomial equation was generated as shown in the following equation:

$$Y = 26.1 + 71.8X_1 - 37.4 X_2 - 440 X_3 - 3.27 X_1 \times X_1$$
$$+ 10.55 X_2 + 5308 X_3 \times X_3 - 18.29 X_1$$
$$\times X_2 - 252 X_1 \times X_3 + 175 X_2 \times X_3 \quad (1)$$

where Y is the β-CGTase production (U ml^{-1}), X_1 is peptone, X_2 Na_2CO_3 and X_3 is $MgSO_4 \cdot 7H_2O$.

RSM results implicated that interaction between peptone and Na_2CO_3 (0·00) was the most significant followed by peptone and $MgSO_4$ (0·010), whereas the interaction between Na_2CO_3 and $MgSO_4$ (0·156) was not significant for β-CGTase production (Table 4).

The response surface plot is a graphical presentation of the regression equation (Blanco et al. 2012). It is plotted

Table 3 Experimental CCD-RSM for 2^3 full factorial design and response β-CGTase production

Trial	Blocks	Coded value			CGTase pro-duction U ml^{-1}
		Peptone (X₁)	Na₂CO₃ (X₂)	MgSO₄·7H₂O (X₃)	
1	1	1	−1	−1	145·2805539
2	1	0	0	0	47·11907901
3	1	−1	−1	−1	32·73969938
4	1	1	1	−1	45·00434957
5	1	1	−1	1	109·9785524
6	1	−1	−1	−1	35·66113332
7	1	0	0	0	47·14057038
8	1	0	0	0	48·90842471
9	1	1	−1	−1	147·5843513
10	1	0	0	0	46·92324596
11	1	1	1	1	36·06215138
12	1	−1	1	1	24·24766281
13	1	−1	1	−1	10·34227147
14	1	0	0	0	45·3022233
15	1	−1	1	−1	10·93164811
16	1	1	1	1	34·81238151
17	1	0	0	0	49·14114636
18	1	1	−1	1	109·2146817
19	1	−1	−1	1	44·60092016
20	1	0	0	0	39·57818529
21	1	−1	−1	1	43·87815635
22	1	1	1	−1	36·67609692
23	1	−1	1	1	25·51170213
24	1	0	0	0	39·22130564
25	2	0	1·633	0	26·68651261
26	2	0	−1·633	0	87·27391899
27	2	0	0	−1·633	55·35032026
28	2	0	1·633	0	24·70703784
29	2	−1·633	0	0	16·97519604
30	2	0	0	0	39·27049138
31	2	0	0	1·633	44·52729289
32	2	0	0	−1·633	56·48878259
33	2	−1·633	0	0	19·57911614
34	2	0	0	0	31·42652928
35	2	0	0	1·633	40·52174256
36	2	0	−1·633	0	88·598719
37	2	1·633	0	0	33·45205221
38	2	0	0	0	43·05917462
39	2	1·633	0	0	33·70255917
40	2	0	0	0	47·54214227

to understand the interaction of components and the optimum concentration of each component (peptone, sodium carbonate and magnesium sulphate) required for β-CGTase production by isolated *Bacillus* sp. NCIM 5799 (Fig. 3). These results indicate that the most important factors which influence β-CGTase production were Na₂CO₃ > peptone > MgSO₄·7H₂O. The highest β-CGTase production (~147·25 U ml^{-1}) was attained in a medium containing peptone (X₁) 3%, Na₂CO₃ (X₂) 0·8

and MgSO₄·7H₂O (X₃) 0·02% at 96 h of incubation (Table 3).

Various researchers have found that the production of CGTase by alkaliphilic organisms requires Na₂CO₃ (Bernardi *et al.* 2015). In addition, CGTase production in the alkaline pH range is valuable because it reduces the propensity of starch gelatinization, which decreases the tackiness of starch at an elevated concentration in the fermentation medium (Peixoto *et al.* 2020). Also, Na₂CO₃ provides an alkaline medium for an alkaliphilic organism to accelerate CGTase production. Peptone was found to be the second significant medium nutrient for CGTase production; it contains a high concentration of amino acids and peptides which serve to provide the necessary nitrogen requirement of the organism. A similar finding was observed by Blanco *et al.* (2009), where nitrogen and sodium carbonate were found to be the most influencing factors and their interaction was also essential for CGTase production by alkaliphilic *Bacillus* sp. gives 96·07 U ml^{-1}. Likewise, Ibrahim *et al.* (2005) found 54·9 U ml^{-1} β-CGTase production using *Bacillus* G1 with peptone and sodium carbonate at 2 and 1% concentrations.

The isolated *Bacillus* sp. NCIM 5799 yielded 156·76 U ml^{-1} β-CGTase production under optimized conditions (PBD and CCD-RSM). Likewise, the highest CGTase production was observed using *B. lehensis* was 134·05 U ml^{-1} achieved in 72 h of incubation (Blanco *et al.* 2012). Comparative analysis with previously reported literature on natural CGTase producers and their statistical optimizations studies were categorized into two categories with reference to *Bacillus* sp. NCIM 5799 CGTase activity, as lower and higher CGTase producers. Lower CGTase production was observed from 0·45 to 80·12 U ml^{-1} (Mahat *et al.* 2004; Upadhyay *et al.* 2020; Mostafa *et al.* 2021), whereas the only a few research groups found higher CGTase production using natural isolates between 284 and 1087 U ml^{-1} (Atanasova *et al.* 2008; Coelho *et al.* 2016; Peixoto *et al.* 2020). Thus the isolated *Bacillus* sp. NCIM 5799 appears to be one of the most prolific natural isolates for the production of β-CGTase.

The regression equation obtained from ANOVA with the R^2 value of 0·8881 revealed that the model could explain 88·81% variation in the response. The adjusted R^2 and predicted R^2 values were 0·8495 and 0·7474 respectively. The R^2 value was near 1·0 and the two factors were positive and close to each other, indicating a good statistical model. A very low P-value and high F value of the model show good significance of the model. Other workers like Ai-Noi *et al.* (2008), Dalmotra *et al.* (2016) and Ibrahim *et al.* (2005) reported the use of statistical optimization for CGTase production and obtained R^2 of 84·9, 89·7 and

Table 4 Analysis of variance of the regression model of the culture medium of β-CGTase production of *Bacillus* sp. PBS1 NCIM 5799

Source	df	SS	MS	F	Pr > F	Significance
Model	10	34 445·0	3444·5	23·01	0·0000	***
Linear effect						
Peptone (X_1)	1	8881·8	8881·8	59·33	0·0000	***
Na_2CO_3 (X_2)	1	15776·7	15776·7	105·39	0·0000	***
$MgSO_4 \cdot 7H_2O$ (X_3)	1	238·0	238·0	1·59	0·2174	NS
Squared effect						
$X_1 \times X_1$	1	413·8	413·8	2·76	0·1071	NS
$X_2 \times X_2$	1	1535·8	1535·8	10·26	0·0032	**
$X_3 \times X_3$	1	602·9	602·9	4·03	0·0541	NS
Two-way interaction						
$X_1 \times X_2$	1	4680·5	4680·5	31·27	0·0000	***
$X_1 \times X_3$	1	1106·2	1106·2	7·39	0·0109	***
$X_2 \times X_3$	1	317·5	317·5	2·12	0·1560	NS

In the table, df = degree of freedom, SS = sum of square, MS = mean square. **$P < 0.01$; ***$P < 0.001$.
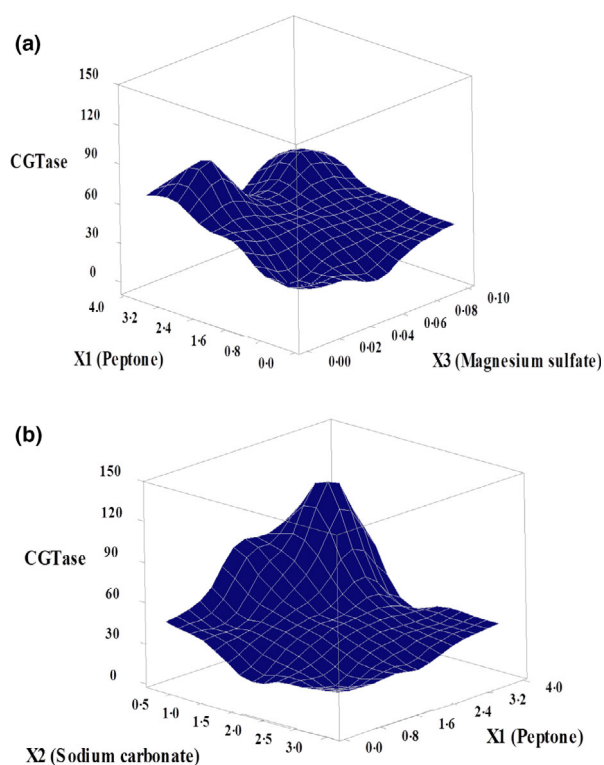
Figure 3 Response surface graph showing the β-CGTase production in the presence of important medium constituents (a) peptone (X1) and magnesium sulphate (X3), (b) peptone (X1) and sodium carbonate (X2).

98·9 respectively. Our value of 88·81 is comparable and in line with the previous reports.

Validation of the statistical model

Validation of the statistical model was confirmed by production under conditions of maximum β-CGTase

production obtained by CCD. Further CGTase production was analysed using comparative analysis of three media, viz. un-optimized medium (Ibrahim *et al.* 2005), OFAT medium (Solanki *et al.* 2022), and RSM-optimized medium at different time intervals from 24 to 120 h. On the comparative investigation and validation of the statistical model, it was found that RSM-optimized medium yielded maximum β-CGTase production as compared to the un-optimized and OFAT medium. 77 and 54% improvement was observed in RSM-optimized medium as compared to the un-optimized medium and OFAT medium (Fig. 4). For all the media tested highest production was observed at 96 h of incubation. Under optimized conditions, the predicted β-CGTase production was calculated at 157·23 U ml^{-1}, while 156·76 U ml^{-1} was observed. The obtained experimental values were determined to be quite close to the predicted values thereby confirming the validity of the statistical model.

Ibrahim *et al.* (2005) found a 53% improvement in β-CGTase production in RSM-optimized medium as compared to the basal medium. Similarly, Elsayed and Abdelwahed (2020) found a 45% improvement in cholesterol oxidase production as compared to an un-optimized medium.

This denotes the importance of successive production optimization strategy and their importance to upscale the production of β-CGTase. The model generated was successful in increasing β-CGTase production using isolated *Bacillus* sp. NCIM 5799 and the highest production was achieved using RSM-optimized medium.

Materials and methods

Micro-organism and culture conditions

The β-CGTase producing organism was previously isolated from rhizospheric soil of potatoes from Indore,
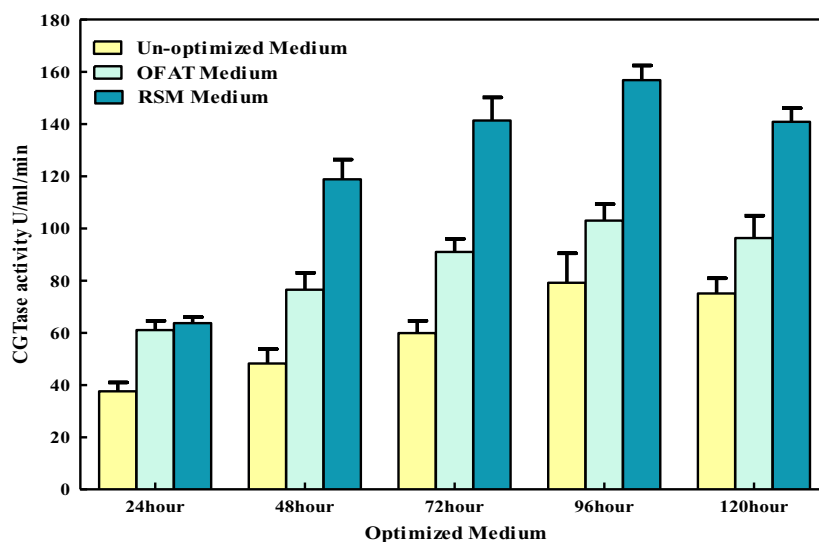
Figure 4 Validation of statistical optimization medium (RSM medium) concerning one factor at a time medium (OFAT medium) and un-optimized medium using isolated novel alkaliphilic *Bacillus* sp. NCIM 5799 at different time intervals.

Madhya-Pradesh, India (22·7196°N 75·8577°E). The new isolate produced only β-CD as the sole product and is deposited in NCIM culture collection under the accession number *Bacillus* sp. NCIM 5799 (National Collection of Industrial Microorganism, Pune India). The 16 s rRNA gene sequence was deposited to NCBI with accession numbers MN938303.

Morphological observation of β-CGTase soil isolate

The morphological characterization was done using field-emission scanning electron microscope (450 FE-SEM), Bruker, U.S. To obtain a stationary phase of growth, the single colonies were inoculated in NB broth (pH 10) and incubated at 30°C overnight. The smear was dehydrated serially with an alcohol (ethanol) gradient from 30 to 100%, each for 10mins (Singh *et al.* 2019).

Evaluation of alkalihalophilic nature of isolate

Evaluation of the alkalihalophilic nature of isolated *Bacillus* sp. in terms of growth was carried out spectrophotometrically by measuring OD_{600nm} on Shimadzu-UV2401 PC double beam spectrophotometer in triplicate and the mean was calculated. A 2 ml aliquot of bacterial culture was withdrawn at regular time intervals. The pH of the nutrient broth was in the range of 6·5–12 with an increment of 0·5 and the pH of the medium was adjusted using 0·1 N HCl and NaOH. Also, the effect of NaCl concentration was checked in the range of 2·5–30% with an increment of 2·5% and was added to the nutrient broth at selected optimal pH.

Culture condition and β-CGTase production

CGTase production was carried out in 150 ml Erlenmeyer flasks with 30 ml of sterilized medium containing (w/v) 4% soluble starch, 2% peptone, 0·1% K_2HPO_4, 0·04% $MgSO_4 \cdot 7H_2O$ and 1% Na_2CO_3 (Ibrahim *et al.* 2005) added separately after autoclaving. A 10% inoculum was added to the production media and incubated at 30°C, 130 rev min^{-1} on a gyratory shaker. Samples were withdrawn at 96 h of incubation.

Determination of β-CGTase production in crude enzyme

To detect CGTase production, samples were harvested at a single point at 96 h. The 96-h enzyme sample was withdrawn, centrifuged and obtained supernatant was 1 : 15 diluted using phosphate buffer (50 mmol l^{-1}). The assay was carried out using the 0·1 ml of diluted CGTase, 1% soluble starch in 50 mmol l^{-1} phosphate buffer pH 7 at 60°C for 15 min. The reaction was stopped by increasing the temperature to 100°C for 5 min (Goel and Nene 1995). The control mixture was prepared similarly without adding enzyme. The amount of β-CD present in the fermentation broth (basal β-CD) was also estimated and deducted from the final readings. One unit of enzyme activity was defined as the amount of enzyme required for the production of 1 μmole β-CD per minute under standard assay conditions.

Screening of significant nutritional variables by Plackett–Burman design

PBD with a three-level factorial design was used (Plackett and Burman 1946). For creating a PBD screening design

five variables were included; starch, peptone, K_2HPO_4, $MgSO_4 \cdot 7H_2O$ and Na_2CO_3. All the experiments were performed according to the design matrix generated by MINITAB 18·1 displayed in Table S1. To identify the significant effects of the selected five variables, the experiment was conducted in 25 randomized experimental runs with two blocks. In the design table, all the variables are designed as numerical values plus (+) indicating higher concentration, minus (−) indicating lower concentration and zero (0) indicating the middle concentration. The β-CGTase production was set as the response variable.

Optimization of β-CGTase production by response surface methodology followed by CCD

The significant factors selected from PBD using a high confidence level (>95%) were further evaluated using RSM. The combined effect of these significant factors as well as the interaction between those factors on β-CGTase production of *Bacillus* sp. NCIM 5799 was carried by CCD. 2^3 full factorial design with three factors namely peptone (X_1), Na_2CO_3 (X_2) and $MgSO_4 \cdot 7H_2O$ (X_3) was used to construct the design matrix in two blocks, and two replicates with $\alpha = 1 \cdot 633$ (Table S2). The relationship between response and the independent variable was analysed by fitting into the second-order polynomial equation in Eqn 1.

$$Y = b_0 + \Sigma b_i x_i + \Sigma b_{ii} x_i^2 + \Sigma b_{ij} x_i x_j \qquad (2)$$

where $Y =$ is response variable (β-CGTase production), $b_0 =$ regression coefficient, $b_i =$ linear coefficient, $b_{ii} =$ quadratic coefficient, $b_{ij} =$ interaction coefficient, $x_i x_j =$ input variable. A predicted response was generated using the second-order polynomial equation generated by MINITAB 18.

Validation of the statistical model

Validation and comparative evaluation of CGTase production of RSM medium with un-medium and OFAT (one factor at a time) was also carried out. The samples were withdrawn at 24- to 120-h time intervals and checked for β-CGTase.

Statistical analysis

All the data are graphically presented as mean ± SD of triplicates (? = 3). P values <0·05 were considered significant with a confidence limit of 95%. The statistical experiments were designed using MINITAB 18.

Authors' contribution

Authors Solanki, P. and Banerjee, T. contributed to the design of the experiment and the data analysis. Solanki,

P. performed the experimental work. Both authors edited the paper.

Conflicts of Interest

The authors declare no conflict of interest regarding the paper's publication.

Data availability statement

The data that support the findings of this study are available from the corresponding author upon reasonable request.

References

Abdella, M.A., El-Sherbiny, G.M., El-Shamy, A.R., Atalla, S.M. and Ahmed, S.A. (2020) Statistical optimization of chemical modification of chitosan-magnetic nano-particles beads to promote *Bacillus subtilis* MK1 α-amylase immobilization and its application. *Bull Natl Res Centre* **44**, 1–13. https://doi.org/10.1186/s42269-020-00301-3.

Abelyan, V.A., Balayan, A.M., Ghochikyan, V.T. and Markosyan, A.A. (2004) Transglycosylation of stevioside by cyclodextrin glucanotransferases of various groups of microorganisms. *Appl Biochem Microbiol* **40**, 129–134. https://doi.org/10.1023/b:abim.0000018914.08571.50.

Aboyeji, O.O., Oloke, J.K., Arinkoola, A.O., Oke, M.A. and Ishola, M.M. (2020) Optimization of media components and fermentation conditions for citric acid production from sweet potato peel starch hydrolysate by *Aspergillus niger*. *Scientific African* **10**, e00554. https://doi.org/10.1016/j.sciaf.2020.e00554.

Ahmed, E.M. and El-Refai, H.A. (2010) Cyclodextrin glucosyltransferase production by *Bacillus megaterium* NCR: evaluation and optimization of culture conditions using factorial design. *Indian J Microbiol* **50**, 303–308. https://doi.org/10.1007/s12088-010-0009-x.

Ai-Noi, S., Abd-Aziz, S., Alitheen, N., Hassan, O. and Karim, M.A. (2008) Optimization of cyclodextrin glycosyltransferase production by response surface methodology approach. *Biotechnology* **7**, 10–18. https://doi.org/10.3923/biotech.2008.10.18.

Alves-Prado, H.F., Carneiro, A.A.J., Pavezzi, F.C., Gomes, E., Boscolo, M., Franco, C.M.L. and Silva, R.D. (2007) Production of cyclodextrins by CGTase from *Bacillus*

clausii using different starches as substrates. In *Biotechnology for Fuels and Chemicals*. pp. 123–133. Humana Press. https://doi.org/10.1007/s12010-007-8093-z.

Arce-Vázquez, M.B., Ponce-Alquicira, E., Delgado-Fornué, E., Pedroza-Islas, R., Díaz-Godínez, G. and Soriano-Santos, J.O.R.G.E. (2016) Integral use of Amaranth starch to obtain cyclodextrin glycosyltransferase, by *Bacillus megaterium*, to produce β-cyclodextrin. *Front Microbiol* **7**, 1513. https://doi.org/10.3389/fmicb.2016.01513.

Atanasova, N., Petrova, P., Ivanova, V., Yankov, D., Vassileva, A. and Tonkova, A. (2008) Isolation of novel alkaliphilic *Bacillus* strains for cyclodextrin glucanotransferase production. *Appl Biochem Biotechnol* **149**, 155–167. https://doi.org/10.1007/s12010-007-8128-5.

Bernardi, N.Z., Blanco, K.C., Monti, R. and Contiero, J. (2015) Optimization of cyclodextrin glycosyltransferase production from sorghum. *J Food Ind Microbiol* **1**, 2. https://doi.org/10.4172/2572-4134.1000102.

Bezerra, M.A., Santelli, R.E., Oliveira, E.P., Villar, L.S. and Escaleira, L.A. (2008) Response surface methodology (RSM) as a tool for optimization in analytical chemistry. *Talanta* **76**, 965–977. https://doi.org/10.1016/j.talanta.2008.05.019.

Blanco, K.C., de Lima, C.J., Monti, R., Martins, J., Bernardi, N.S. and Contiero, J. (2012) *Bacillus lehensis*—an alkali-tolerant bacterium isolated from cassava starch wastewater: optimization of parameters for cyclodextrin glycosyltransferase production. *Ann Microbiol* **62**, 329–337. https://doi.org/10.1007/s13213-011-0266-x.

Blanco, K.C., De Lima, C.J.B., De Oliveir, P.A.P.L.V., Piao, A.C.S. and Contiero, J. (2009) Cyclodextrin glycosyltransferase production by the *Bacillus* sp., subgroup alcalophilus using a central composite design. *Res J Microbiol* **4**, 450–459. https://doi.org/10.3923/jm.2009.450.459.

Bowers, K.J., Mesbah, N.M. and Wiegel, J. (2009) Biodiversity of poly-extremophilic bacteria: does combining the extremes of high salt, alkaline pH and elevated temperature approach a physico-chemical boundary for life? *Saline Systems* **5**, 1–8. https://doi.org/10.1186/1746-1448-5-9.

Coelho, S.L.D.A., Magalhães, V.C., Marbach, P.A.S. and Cazetta, M.L. (2016) A new alkalophilic isolate of bacillus as a producer of cyclodextrin glycosyltransferase using cassava flour. *Braz J Microbiol* **47**, 120–128. https://doi.org/10.1016/j.bjm.2015.11.01.

Dalmotra, N., Tripathi, A.D., Srivastava, S.K., Arya, S.K. and Naik, B. (2016) Statistical optimization of cyclodextrin glycosyltransferase (CGTase) production from *Bacillus macerans* in batch cultivation and its purification. *Int J Food Ferment Technol* **6**, 261 0.5958/2277-9396.2016.00049.0.

Elsayed, E.A. and Abdelwahed, N.A. (2020) Medium optimization by response surface methodology for improved cholesterol oxidase production by a newly

isolated *Streptomyces rochei* NAM-19 strain. *BioMed Res Int* **6**, 1870807. https://doi.org/10.1155/2020/1870807.

Gawande, B.N., Singh, R.K., Chauhan, A.K., Goel, A. and Patkar, A.Y. (1998) Optimization of cyclomaltodextrin glucanotransferase production from *Bacillus firmus*. *Enzyme Microb Technol* **22**, 288–291. https://doi.org/10.1016/s0141-0229(97)00184-1.

Goel, A. and Nene, S.N. (1995) Modifications in the phenolphthalein method for spectrophotometric estimation of beta cyclodextrin. *Starch-Stärke* **47**, 399–400.

Hashimoto, Y., Yamamoto, T., Fujiwara, S., Takagi, M. and Imanaka, T. (2001) Extracellular synthesis, specific recognition, and intracellular degradation of cyclomaltodextrins by the hyperthermophilic archaeon *Thermococcus* sp. strain B1001. *J Bacteriol* **183**, 5050–5057. https://doi.org/10.1128/JB.183.17.5050-5057.2001.

Ibrahim, A.S., Al-Salamah, A.A., El-Tayeb, M.A. and El-Badawi, Y.B. (2013) Enhancement of Amphibacillus sp NPST-10 cyclodextrin glucanotransferase production by optimizing physio-environmental factors. *J Pure Appl Microbiol* **7**, 2597–2606. https://doi.org/10.3390/ijms130810505.

Ibrahim, A.S., Al-Salamah, A.A., El-Tayeb, M.A., El-Badawi, Y.B. and Antranikian, G. (2012) A novel cyclodextrin glycosyltransferase from alkaliphilic *Amphibacillus* sp. NPST−10: purification and properties. *Int J Mol Sci* **13**, 10505–10522. https://doi.org/10.3390/ijms130810505.

Ibrahim, H.M., Yusoff, W.M.W., Hamid, A.A., Illias, R.M., Hassan, O. and Omar, O. (2005) Optimization of medium for the production of β-cyclodextrin glucanotransferase using central composite design (CCD). *Process Biochem* **40**, 753–758. https://doi.org/10.1016/j.procbio.2004.01.042.

Junior, O.V., Barão, C.E., Matioli, G., Zanoelo, E.F., Cardozo-Filho, L. and Faria-Filho, F. (2019) Complexation and physicochemical analysis of hydrophobic molecules of methyl jasmonate with hydroxypropyl-β–cyclodextrin. *Acta Sci Technol* **41**, 39611. https://doi.org/10.4025/actascitechnol.v41i1.39611.

Kelly, R.M., Dijkhuizen, L. and Leemhuis, H. (2009) The evolution of cyclodextrin glucanotransferase product specificity. *Appl Microbiol Biotechnol* **84**, 119–133. https://doi.org/10.1007/s00253-009-1988-6.

Mahat, M.K., Illias, R.M., Rahman, R.A., Abd Rashid, N.A., Mahmood, N.A.N., Hassan, O., Aziz, S.A. and Kamaruddin, K. (2004) Production of cyclodextrin glucanotransferase (CGTase) from alkalophilic *Bacillus* sp. TS1−1: media optimization using experimental design. *Enzyme Microb Technol* **35**, 467–473. https://doi.org/10.1016/j.enzmictec.2004.07.008.

Mostafa, Y.S., Alamri, S.A., Alrumman, S.A., Taha, T.H., Hashem, M., Moustafa, M. and Fahmy, L.I. (2021) Biosynthesis of raw starch degrading β-cyclodextrin glycosyltransferase by immobilized cells of *Bacillus licheniformis* using potato wastewater. *Biocell* **45**, 1661–1672. https://doi.org/10.32604/biocell.2021.016193

Peixoto, C.M., de Araújo Coelho, S.L. and Cazetta, M.L. (2020) Byproducts from cassava industry: alternative substrates for cyclodextrin glycosyltransferase production by alkalophilic *Bacillus trypoxylicola* SM-02. In *Anales de Biología*, Vol. **42**, pp. 37–46. Murcia: Servicio de Publicaciones de la Universidad de Murcia.

Plackett, R.L. and Burman, J.P. (1946) The design of optimum multifactorial experiments. *Biometrika* **33**, 305–325. https://doi.org/10.1093/biomet/33.4.305.

Qi, Q. and Zimmermann, W. (2005) Cyclodextrin glucanotransferase: from gene to applications. *Appl Microbiol Biotechnol* **66**, 475–485. https://doi.org/10.1007/s00253-004-1781-5.

Rajput, K.N., Patel, K.C. and Trivedi, U.B. (2016) (2016) screening and selection of medium components for cyclodextrin glucanotransferase production by new alkaliphile *Microbacterium terrae* KNR 9 using plackett-burman design. *Biotechnol Res Int.* https://doi.org/10.1155/2016/3584807.

Ramesh, V. and Ramachandra Murty, V. (2014) Sequential statistical optimization of media components for the production of glucoamylase by thermophilic fungus *Humicola grisea* MTCC 352. *Enzyme Res* **2014**, 1–9. https://doi.org/10.1155/2014/317940

Singh, D., Thakur, S., Thayil, S.M. and Kesavan, A.K. (2019) Characterization of a cold-active, detergent-stable metallopeptidase purified from *Bacillus* sp. S1DI 10 using response surface methodology. *PloS one* **14**, e0216990. https://doi.org/10.1371/journal.pone.0216990.

Singh, V., Haque, S., Niwas, R., Srivastava, A., Pasupuleti, M. and Tripathi, C. (2017) Strategies for fermentation medium optimization: an in-depth review. *Front Microbiol* **7**, 2087. 10.3389%2Ffmicb.2016.02087.

Sivaramareddy, A., Srihari, P. and Kezia, D. (2014) Cyclodextrin glucosyltransferase produced by *Bacillus amyloliquefaciens* KST5: a Plackett-Burman design approach. *J Pharm Res* **8**, 1191–1197.

Solanki, P., Awadhiya, P. and Banerjee, T. (2022) Conventional production optimization of cyclodextrin glucosyl transferase by a novel isolate of *Bacillus* sp. PBS1 from potato rhizosphere. *J Microbiol Biotechnol Food Sci* **2014**, 5130–5130. https://doi.org/10.55251/jmbfs.5130.

Szejtli, J. (2004) Past, present, and future of cyclodextrin research. *Pure Appl Chem* **76**, 1825–1845. https://doi.org/10.1351/pac200476101825

Upadhyay, D., Shrivastava, D., Chauhan, A., Singh, N.K. and Kulshreshtha, N.M. (2020) Production and optimization of cyclodextrin glucanotranferase from *Bacillus* sp. SS2. *J Microbiol Biotechnol Food Sci* **10**, 159–165. https://doi.org/10.15414/jmbfs.2020.10.2.159-165.

Van der Veen, B.A., Uitdehaag, J.C., Dijkstra, B.W. and Dijkhuizen, L. (2000) Engineering of cyclodextrin glycosyltransferase reaction and product specificity. *Biochim et Biophys Acta* **1543**, 336–360. https://doi.org/10.1016/s0167-4838(00)00233-8.

Xu, W., Li, X., Wang, L., Li, S., Chu, S., Wang, J., and Liu, J. (2021) Design of cyclodextrin-based functional systems for biomedical applications. Front Chem 22. https://doi.org/10.3389/fchem.2021.635507

Supporting Information

Additional Supporting Information may be found in the online version of this article:

Table S1. Production medium components and their concentrations used in Plackett Burman Screening Design.

Table S2. Independent factor and coded values of CCD for β-CGTase production

Graphical Abstract

The contents of this page will be used as part of the graphical abstract
of html only. It will not be published as part of main article.

Significance and Impact of the Study: The novel isolated alkalihalophilic *Bacillus* sp. NCIM 5799 is a predominant producer of β-cyclodextrin glucosyltransferase (β-CGTase). This was the first report that the production of β-CGTase was enhanced by applying two statistical approaches that are PBD and CCD-RSM. The novel isolated *Bacillus* sp. NCIM 5799 could be utilized for industrial production of β-CGTase.

CONVENTIONAL PRODUCTION OPTIMIZATION OF CYCLODEXTRIN GLUCOSYL TRANSFERASE BY A NOVEL ISOLATE OF *BACILLUS* SP. PBS1 FROM POTATO RHIZOSPHERE

Preetibala Solanki[1], Pushpendra Awadhiya[1] and Tushar Banerjee[1]*

Address(es): Preetibala Solanki
[1] School of Life Sciences, Devi Ahilya Vishwavidhaylaya Indore, India.

*Corresponding author: preetisolanki2604@gmail.com

ABSTRACT

The cyclodextrin glucosyltransferase enzyme (CGTase) is an industrially crucial enzyme for the production of β-cyclodextrin (β-CD). CGTase has a high propensity to produce a mixture of cyclodextrins (CDs). From the industrial perspective, a CGTase that produces only one type of CD is of critical importance. *Bacillus* sp. PBS1 produced CGTase that converts starch solely into β-CD. The isolated strain PBS1 was found to close similarity with alkaliphilic *Bacillus* sp. based on biochemical, morphological, and phylogenetic analysis of its 16s rRNA gene sequencing. The selection and optimization of media ingredients are warranted for the best possible production of β-CD. These steps were carried out by conventional optimization strategies. The presence of glucose, maltose, lactose, sucrose, galactose, mannitol, nitrates, urea, metal salts, and K_2HPO_4 led to the suppression of CGTase production. The improved enzyme production was observed in peptone, soluble starch, magnesium sulfate, and Na_2CO_3. The organism produces maximum CGTase (93.42 ± 2.4 U/ml) at 96-hour incubation in the optimized production medium containing 8% starch, 2% peptone, 0.06% $MgSO_4.7H_2O$, 0.5% Na_2CO_3, and having pH of 9.3. The optimization of the medium led to ~16% improvement in CGTase production by *Bacillus* sp. PBS1.

Keywords: CGTase, *Bacillus* sp. PBS1, β-cyclodextrin, Production optimization

INTRODUCTION

Cyclodextrins are known for their torus-shaped structure having a hydrophilic surface and hydrophobic cavity. As the name suggests, cyclodextrins have a cyclic arrangement of α-(1,4) linked glucose units. The diameter of the hydrophobic cavity of β-CD (7.8 Å) enables it to form water-soluble inclusion complexes with many hydrophobic compounds. This unique property of cyclodextrins makes them potentially valuable for pharmaceutical, medical, cosmetic, agricultural, environmental, textile and food industries (**Sun *et al*., 2011; Zhang *et al.,* 2019; Buschmann *et al*., 2002; Fenyvesi E., 2011; Bezerra *et al*., 2020; Maskooki *et al*., 2013**). Cyclodextrins are natural, non-reducing, cyclic malto-oligosaccharides (**Sabioni *et al.,* 1992**). Depending on glucose residues, cyclodextrins are categorized into three major types; α-CD having six glucose units, β-CD having seven glucose units, and γ-CD having eight glucose units (**Van der Veen *et al.,* 2000**). Cyclodextrins are produced by the cyclodextrin glucosyltransferase enzyme (CGTase, EC 2.4.1.19). To produce CD, partial degradation of starch and cyclization of the oligomer is catalyzed by the CGTase. CGTase is a member of the amylolytic glucosylase family that catalyzes intramolecular transglycosylation, cyclization as well as reversible intermolecular transglycosylation including coupling, and disproportionation of malto-oligosaccharides, at the same time has a weak starch hydrolyzing activity (**Tonocovo *et al*., 1998**). The CGTase enzyme is thought to be evolved from the α-amylase family by specific mutations in the substrate-binding site (**Kelly *et al.,* 2009**). CGTase enzyme is produced by several genera of bacteria such as *B. licheniformis, B. firmus, B. circulans, B. clausii, Brevibacillus brevis, B. stearothermophilus, Klebsiella pnemoniae*, *and Microbacterium terrae* (**Boniha *et al*., 2006; Gawande and Patkar 2001; Rosso *et al*., 2002; Kim *et al*., 1997; Alves Prado *et al*., 2008; Chung *et al*., 1998 Burhan *et al*., 2005; Rajput *et al*., 2016**). The most prominent CGTase producers are alkalophilic *Bacillus* sp. (**Tonocova *et al*., 2000**) [Table1]. The majority of CGTase produces β-CD as the core product with a low concentration of α and γ-CD. Conventionally, depending on the significant product of CGTase, the enzyme is named α, β, and γ-CGTase, respectively (**Vazquez *et al.,* 2016**). If the same organism produces them, it would be necessary to separate all the three cyclodextrins from the reaction mixture which might be tedious and costly. To avoid expensive separation and purification steps, a strain that produces a single type of CD (**Thatai *et al*., 1999**).
Microbial enzyme production is influenced by several factors, such as; medium ingredients, pH, presence of inducers and metal ions, etc. Screening and incorporation of appropriate carbon, nitrogen, and other nutrient sources is warranted for designing an efficient and cost-effective production medium (**Wang *et al.,* 2018**).

The presented work describes the screening and isolation of a CGTase producing organism that produces only β-CD. Biochemical identification of isolated organisms was followed by attesting by an automated VITECK 2 compact system and molecular identification by 16s-rRNA sequencing. To assess the effect of various ingredients and optimize the production of CGTase, classical, one factor at a time approach was adopted. Which the authors believe is a pre-requisite for any optimization effort for a novel isolate.

Table 1 Some of the important natural key CGTase producer organisms and their enzyme activity

CGTase producer strain	CGTase activity (U/ml)	References
Bacillus firmus	0.77	**Silva *et al*. (2021)**
Bacillus macerans	3.53	**Dalmotra *et al*. (2016)**
Bacillus megaterium	57.75	**Vazquez *et al*. (2016)**
Bacillus lehensis	0.45	**Elbaz *et al*. (2015)**
Bacillus firmus strain 37	0.22	**Santos *et al*. (2013)**
Bacillus lehensis	18.9	**Yap *et al*. (2010)**
Bacillus sp. TS1	78.05	**Zain *et al*. (2006)**
Bacillus G1	54.9	**Ibrahim *et al*. (2005)**
Bacillus circulans DF 9R	5.8	**Rosso *et al*. (2002)**

MATERIAL AND METHODS

Chemicals

All the chemicals used in the experiments were of analytical grade. β-CD was purchased from SD Fine-Chem Limited, Mumbai, India. Phenolphthalein (PHP) and soluble starch were from Merck Ltd. Mumbai, India. Media components were procured from Himedia Laboratories, Mumbai, India. Substrates like tapioca, wheat, and rice starch were procured from Urban Platter, Mumbai, India. Potato starch and maize starch were sourced from Loba Chemie Pvt Ltd, Mumbai, India.

Isolation and screening of CGTase producer strain

The screening was preceded by an enrichment process. One gram of soil was added in 10 ml. normal saline (0.85% NaCl), and then 0.1 ml. was transferred into two 150 ml. Erlenmeyer flask containing 30ml of enrichment medium (soluble starch 1%, peptone 0.5%, yeast extract 0.5%, K_2HPO_4 0.1%, $MgSO_4$ 0.02%, and Na_2CO_3 1% (separately autoclaved). Flasks were incubated at 28^0C, 130 rpm on a gyratory

shaker for 24 hours. 0.1ml. sample from these enrichment flasks was inoculated in modified Horikoshi screening medium plates containing 0.94 mM phenolphthalein (**Geetha *et al*., 2010**). The plates were incubated at 28^0C for 48 hours. After the incubation, clear zones were developed due to the complexation of phenolphthalein inside the hydrophobic core of β-CD, due to its equivalent size with the hydrophobic core. To avoid false positives due to acid production, the plates were covered with 1N NaOH before zone size measurement. The colonies with the largest clear zone were selected for CGTase production. This clear zone was compared with known CGTase producer *Cytobacillus firmus* NCIM 5119.

Screening of α and γ-CGTase producer on the agar plate

The detection of α and γ-CGTase production by the isolated β -CD producer strain on Horikoshi screening medium containing methyl orange (0.035mM) for α-CD and bromocresol green (5mM) for γ-CD was used (**Menocci *et al*., 2008**). Methyl orange and bromocresol green have appropriate molecular sizes to fit in the hydrophobic cavity of α and γ-CGTase, respectively (**Makela *et al*., 1990**).

Characterization and identification of isolated microorganism

The isolate was characterized by following the steps of Bergey's manual **(1957)** of determinative bacteriology. Gram staining and biochemical identification were performed. Further identification by VITECK 2 compact system analysis (Biomerieux Diagnostics) and molecular 16s rRNA sequencing at National Chemical Laboratory (NCIM), Pune was done. The DNA sequences were deposited to NCBI GenBank through the BankIt procedure. The 16s rRNA sequence was matched with NCBI data base trough BLASTn program. The alignment of nucleotide sequence of similar sequence was done by ClustalW. The evolutionary history was inferred by the neighbor-joining method. Phylogenetic tree was constructed using MEGAX software (10.0.5). The bootstrap analysis was based on 1000 resembling.

Maintenance of Microorganism

Isolated organisms were grown on nutrient agar (NA) slants of pH 10.5 and incubated at 28^0C for 24 hours. After incubation and confluent growth, nutrient agar slants were maintained at 4^0C. Sub-culturing was done every 15 days on the same medium.

CGTase Assay

To assay CGTase, 2 ml. samples were centrifuged (10000 rpm for 20min) to obtain cell-free supernatant. The assay mixture consisted of 1% soluble starch in 50mM phosphate buffer having pH 7. The diluted (based on initial activity) enzyme (0.1ml) was added to the assay mixture and incubated at room temperature for 5 minutes. Final incubation was carried out in a water bath for 15min at 60^0C. The reaction was stopped by increasing the temperature to 100^0C for 5 minutes (**Goel and Nene, 1995**). Control was prepared similarly without enzyme.
The amount of β-CD present in the fermentation broth (basal β-CD) was also estimated and deducted from the final readings. One unit of enzyme activity was defined as the amount of enzyme required for the production of 1 μmol β-CD per minute under standard assay conditions.
The standard curve for β-CD was plotted in the range from 20 to 240μg. β-cyclodextrin stock was prepared in 50mM Tris-HCl buffer (2mg/ml), and PHP stock (4mM) was prepared in ethanol. The working solution was prepared by diluting 0.5ml of stock in 4.5ml of Tris-HCl buffer. PHP working solution was prepared by adding 1ml of 4mM stock solution in 4ml of ethanol (95%) for 100ml of 125mM carbonate buffer (pH 10.8). Colour reduction of PHP stock may cause false detection of β-CD; thus calibration curve was drawn in every experiment.

Selection of suitable production medium for CGTase

Seven different media compositions described by **Zain *et al*. (2007); Horikoshi *et al*. (1982); Blanco *et al*. (2009); Thombre *et al*. (2013); Mahat *et al*. (2004); Ibrahim *et al*. (2004); and Ravinder *et al*. (2012)** were selected for the study [Table 2]. To prepare inoculum, a loop full of isolated organism was inoculated in nutrient broth having pH 10.5 and incubated at 30^0C at 130 rpm on a gyratory shaker for 24 hours. 10% inoculum was added to the production media and incubated for 24 hours at 30^0C, 130 rpm. Samples were drawn aseptically at 96 hours. Further parameter optimization studies were carried out only to the selected production medium.

Table 2 Production medium used for CGTase production

S.N	Contains	Medium concentrations (%)						
		A	B	C	D	E	F	G
1	Soluble Starch	2	1	0.75	2	2	4	3
2	Peptone	-	0.50	0.50	1	5	2	0.50
3	Trptone	-	-	0.50	-	-	-	-
4	Yeast extract	1	0.50	-	0.50	5	-	0.50
5	K_2HPO_4	0.10	0.10	0.10	-	0.10	0.10	-
6	$MgSO_4$	0.02	0.02	0.01	-	0.02	0.04	0.02
7	Na_2HPO_4	-	-	-	-	-	-	0.10
8	Na_2CO_3	1	1	1	1	1	1	-

Media optimization for CGTase production by isolated *Bacillus* sp.

Once the production medium was selected, the effect of different starch sources, sugars, a sugar alcohol (mannitol), organic and inorganic nitrogen sources, and different metal ions was studied. For these studies, single-point sampling at 96 h was done.
Starch sources included in the study were soluble starch, rice starch, tapioca starch, wheat starch, potato starch, maize starch at 4% concentration. The effect of sugars (glucose, sucrose, maltose, lactose) and mannitol were studied at 0.1M concentration.
Organic nitrogen sources (peptone, yeast extract, malt extract, tryptone, casein, and corn steep liquor) were studied at a 2% concentration. Inorganic sources (potassium nitrate, sodium nitrate, ammonium nitrate, ammonium sulfate, ammonium chloride, and urea) was added in the medium at the same nitrogen content as peptone.
The presence of metal ions has been reported to improve enzyme production (**Wang *et al*., 2018**). The effect of various metal ions viz., $MnSO_4$, $MgSO_4.7H_2O$, KCl, $FeSO_4$, $CaCl_2$, $CoCl_2$, $CuSO_4$. were studied at 5mM concentration.
Other important medium components like K_2HPO_4, Na_2CO_3 and their concentration variations were studied.

Statistical analysis

All the studies were conducted in triplicate, and the data were analyzed using one-way analysis of variance (ANOVA) followed by Bonferroni multiple comparison tests using Graphpad Prism version 5.00 for windows. The data is graphically presented as mean ± SD of triplicates ($n = 3$).

RESULTS AND DISCUSSION

Screening of CGTase producer

Soil samples were collected from potato cultivation fields of the Malwa region of Madhya Pradesh. The highest zone was observed in soil sample IV (rhizosphere soil of spoiled potato) after 24 hours of incubation. This culture was purified by the standard microbiological protocol using Horikoshi (PHP) screening medium [Figure 1]. The isolated bacterium was found to be Gram-positive, rod-shaped, motile, and capsulated. The discerning biochemical tests were performed [Table 3]. The isolated organism has creamy circular colonies with an entire margin and smooth surface on nutrient agar pH 10.
The organism was inspected by a preliminary screening of α and γ-CD production as described by **Menocci *et al*. (2008).** No clear zone was observed in both screening mediums. This result concluded that the organism was unable to form an inclusion complex with methyl orange and bromocresol green to produce α and γ-CD [Figure 1]. A similar observation was noted for *Bacillus* sp. BACAR produces only β-CD (**Menocci *et al*., 2008**). This result confirms the findings of **Gawande and Patkar (2001)** that α and γ-CD producer strains are rare.
The formation of CDs appear to be dependent on a variety of factors such as amino acid composition of the enzyme, their orientation and sequence, further the type of CD formed is also found to be dependent on the incubation conditions and time of incubation. It has been found that initially the enzyme based on the substrate concentration produces a wide variety of CDs while after incubation of sufficient duration the larger CDs are rapidly reused via intermolecular transglycosylation reactions to produce a preferred / typical mix of CDs (**Terada *et al*., 1997** and **Qi *et al*., 2005**). The exact sequence or conditions required for the production of one type of CDs, still remains elusive despite some limited success.
Our study has consisted with previous reports that the enzyme from the alkaliphilic bacterial strain produces preferentially β-CD (**Abelyan *et al*., 2002**). The isolated organism was found to predominantly produce β-CD; hence it was classified as a β-CGTase producer.
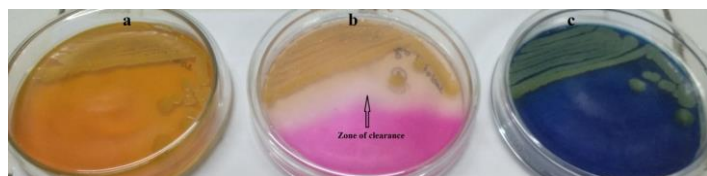
Figure 1 Isolation and screening for CGTase activities **a.** Methyl orange (0.035mM) agar plate for α-CGTase showing no reduction of orange colour by the isolated organism, **b.** PHP (0.94mM) agar plate for β-CGTase showing a reduction in pink colour around the colonies due to inclusion complex formation between PHP and β-CD and **c.** Bromocresol green (0.02mM) plate for γ-CGTase showing no reduction in green colour.

Table 3 Biochemical characterization of CGTase producer isolated from potato rhizosphere

Tests	Results[a]
Motility	Motile
Nitrate Reductase	-
Indole Synthesis	+
Urease	+
Catalase	+
Gelatine hydrolysis	-
Casein hydrolysis	-
Starch hydrolysis	+
Growth in 6.5% Nacl	+

[a] – negative; + positive

VITECK 2 compact analysis and 16s rRNA phylogenetic analysis of isolated strain

VITECK 2 system is utilized for fast, reliable microbial identification and to detect antibiotic sensitivity of desired microorganisms. In Gram's staining organism was found to be Gram-positive bacilli, so for VITECK 2 biochemical characterization, a Bacillus identification card (BCL) was used. That included 46 biochemical tests, e.g. carbon source utilization, enzymatic degradation, and antibiotic resistance [Table 4]. However, the VITECK 2 compact analysis did not show a biochemical pattern similar to other known *Bacillus sp.* present in the BCL card. Thus advanced characterization was done using the molecular approach. The 16s rRNA gene sequence used for identification was 1373 bp long. On BLASTn analysis of *Bacillus* sp. PBS1 on NCBI showing ~98.91 to 98.69% similarity with *Alkalihalobacillus lehensis* and *Alkalihalobacillus hunanensis*. The *Bacillus* sp. PBS1 found to more closely to *Alkalihalobacillus lehensis* strain JO-26 with 98.91% similarity (GeneBank accession No. MF321817). The most similar sequence was retrieved from NCBI for the identification of evolutionary history between our isolated and known organisms. The 16S rRNA phylogenetic tree of alkaliphilic *Bacillus* sp. PBS1 showed significant similarity with *Alkalihalobacillus lehensis* by sharing the same clad in phylogenetic tree [Figure 2]. Based on morphological, biochemical, and phylogenetic analysis, the isolated organism was identified as *Bacillus sp.* and the isolated organism was designated as *Bacillus sp.* PBS1. The gene sequence of the 16s rRNA gene was submitted to the NCBI Gene bank database with accession number MN938303. In addition, culture was deposited NCIM (CSIR NCL Pune).

Figure 2 Neighbor-joining phylogenetic tree showing evolutionary relationship between *Bacillus* sp. PBS1 and closely related *Bacillus* species with 1000 bootstraps replicate. Numbers at nodes represent bootstrap values (%). Scale bar indicates the genetic distance of 0.001.

Table 4 VITECK 2 Compact biochemical characteristics of CGTase producer

Carbon Utilization	Result[a]	Enzyme activities	Result[a]
Cyclodextrin	-	Beta-xylosidase	+
D-galactose	-	L-lysine arylamidase	-
Glycogen	+	L-aspartate arylamidase	+
Myo-inositol	+	Leucine- arylamidase	+
Ellman	-	Phenylalanine arylamidase	+
Methyl-d-xyloside	-	L-proline arylamidase	-
Maltotriose	+	Beta-galactosidase	-
D-mannitol	+	L-pyrrolidinyl arylamidase	+
D-mannose	+	Alpha-galactosidase	+
D-melezitose	-	Alanine arylamidase	+
N-acetyl-d-glucosamine	+	Tyrosine arylamidase	+
Palatinose	+	Beta-n-acetyl-glucosaminidase	+
L-rhamnose	-	Ala-phe-pro arylamidase	+
Pyruvate	+	Methyl-A-D-glucopyranosidase acidification	-
D-tagatose	-	Alpha-mannosidase	-
D-trehalose	+	Glycine acylamidase	+
Inulin	+	Beta-glucosidase	+
D-glucose	+	Beta-mannosidase	-
D-ribose	+	Phosphoryl choline	+

Putresicin assimilation	-	Alpha-glucosidase	-
Esculin hydrolysis	+		
Antibiotic Resistance			
Kanamycin resistance	-		
Oleandomycin resistance	+		
Polymixin B resistance	+		

[a] – negative; + positive

Selection of production medium

The selection of an appropriate production medium is a must for optimal enzyme production. After the literature survey, different medium compositions were selected for the study of CGTase production by *Bacillus* sp. PBS1. The compositions of the different mediums have been described in the materials and method section. Among the seven tested medium compositions, medium F supported maximum CGTase production being 77.13 ± 0.14 U/ml [Figure 3]. Medium F contained the highest amount of substrate (4% soluble starch), organic nitrogen (2% peptone), and magnesium sulfate (0.04%) as compared to other media included in the study. Next to medium F, medium D and B have also supported CGTase production being 60.71 ± 0.62 and 55.6 5 ± 074 U/ml. Deficient CGTase production was observed in medium G, which could be attributed to a neutral pH of the medium. The effect of different medium compositions on CGTase was in the order of F>D>B>E>A>C>G. Medium F was previously optimized by **Ibrahim *et al*. (2004)** for *Bacillus* G1 and reported 54.9 U/ml CGTase production. Medium F was selected for further optimization studies.
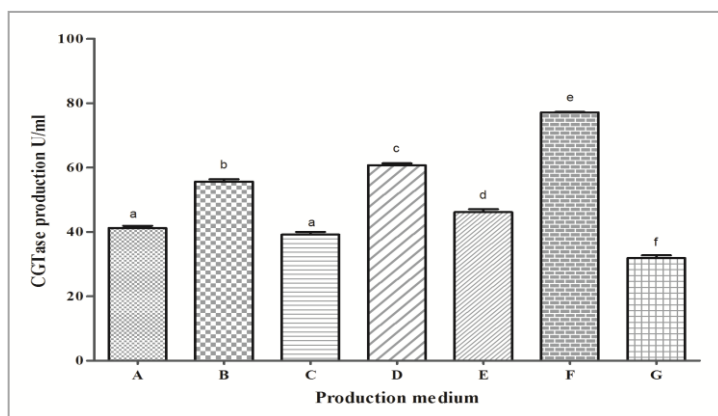
Figure 3 Effect of different fermentation mediums for CGTase production by isolated *Bacillus sp.* PBS1. Symbols having the same alphabets are not significantly different from each other P < 0.05. Standard deviation (Mean ± SD, n = 3) is represented by the bars.

Comparison with a known CGTase producer

The isolated strain was compared for CGTase production with a known CGTase producer, *Cytobacillus firmus* NCIM 5119 (**Gawande *et al.*, 1998**). Medium F was used for the comparison. *Bacillus sp.* PBS1 produced a maximum of 81.69 ± 2.26 U/ml CGTase [Figure 4] whereas the *Cytobacillus firmus* NCIM 5119 yielded 60.49 ± 2.17 U/ml CGTase. In our studies *Bacillus* sp. PBS1 exhibited higher CGTase production as compared with the known producer, being 21 % more.
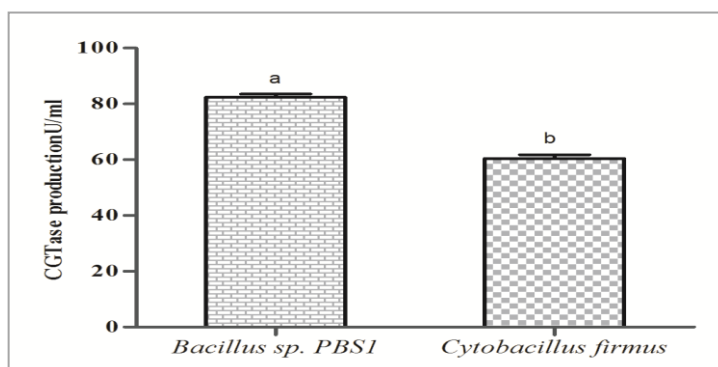
Figure 4 Comparison of CGTase production between *Cytobacillus firmus* NCIM 5119 and *Bacillus* sp. PBS1 in F medium P < 0.05. Standard deviation (Mean ± SD, n = 3) is represented by the bars.

Screening of Medium Components for CGTase Production

Effect of sugars

Carbon source is considered to be one of the most important constituents for enzyme production. Some carbon sources (glucose, sucrose, maltose, mannitol, and lactose) were supplemented to the medium F to evaluate their effect on CGTase production. All of them resulted in suppression of CGTase production [Figure 5]. Maltose and glucose were found to exert the highest suppressive effect (~70-80% decline) when used along with starch. The enzyme production was recorded to be 9.53 ± 1.05 and 18.54 ± 1.59 U/ml in the presence of maltose and glucose, respectively. This observation is supported by the findings of **Letsididi *et al.* (2011); Gawande *et al.* (1998); Higuti *et al.,* (2004); Elbaz *et al.* (2015) and Ramli *et al.* (2010)** reported that the production of CGTase was suppressed when simple sugars were present in the medium. Probably, the presence of an easily utilizable carbon source suppresses the ability of an organism to catabolize starch. **Tonocova (1998)** and **Wang *et al.* (2006)** assumed that glucose and maltose might possess a catabolic repression effect. Contrary to that, **Jamuna *et al.* (1993)** reported maximum CGTase production by *B. cereus* in a medium supplemented with glucose and xylose. The effect of simpler sugars on CGTase production appears to be an organism-dependent phenomenon.
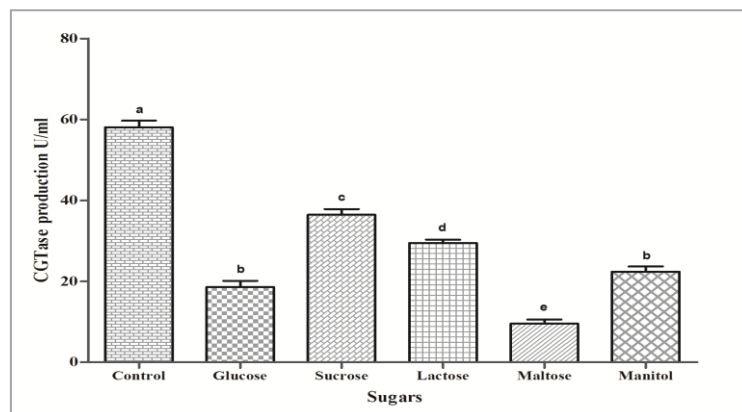

Figure 5 Effect of supplementation of different sugars on CGTase production by *Bacillus* sp. PBS1 in medium F. Symbols having the same alphabets are not significantly different from each other P < 0.05. Standard deviation (Mean ± SD, n = 3) is represented by the bars.

Effect of starch sources

The effect of starch sources viz. rice starch, tapioca starch, wheat starch, potato starch, maize starch, and soluble starch were compared for the CGTase production. Starches were supplemented (4%) one at a time in medium F. Soluble starch was found to be most effective for CGTase production (61.56 ± 0.67 U/ml) [Figure 6]. Soluble starch has been reported for CGTase production by *Microbacterium terra* KNR9 (**Rajput *et al.,* 2016**), *Bacillus lehensis* S8 (**Vidya *et al.,* 2012**), and *Bacillus* G1 (**Ibrahim *et al.,* 2005**). Next to soluble starch, tapioca starch and rice starch were found to support 51.71 ± 5.4 U/ml and 50.20 ± 5.5 U/ml enzyme production, respectively. Maize and wheat starch were least supportive for CGTase production (33.29 ± 0.32 U/ml and 33.79 ± 4.1 U/ml). **Gawade *et al.* (1998)** found corn starch to be the best substrate for CGTase production by *Bacillus firmus* at 2.1%. The difference in enzyme production in different starches could be attributed to the difference in the physical nature of starches (**Ibrahim *et al.,* 2005**). The utilizability of starch for CGTase production appears to depend on its physical and chemical structure.
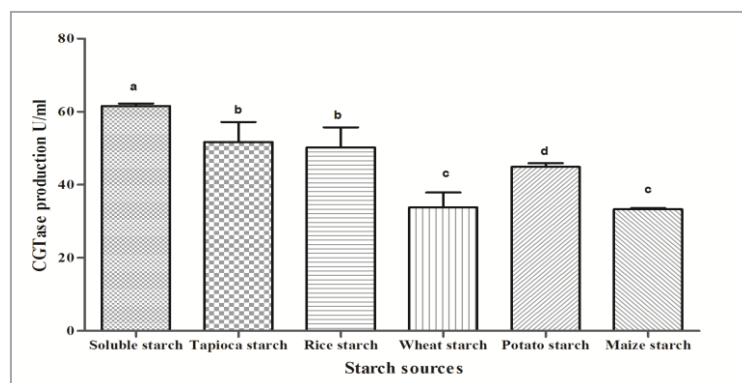

Figure 6 Effect of various starches on CGTase production by isolated *Bacillus* sp. PBS1 in medium F. Symbols having the same alphabets are not significantly different from each other P < 0.05. Standard deviation (Mean ± SD, n = 3) is represented by the bars.

Effect of nitrogen source (inorganic)

To evaluate the effect of inorganic nitrogen sources on CGTase production, peptone was replaced with various inorganic nitrogen sources (potassium nitrate, sodium nitrate, ammonium nitrate, ammonium sulfate, ammonium chloride, and urea) in medium F. All the inorganic nitrogen sources suppressed the CGTase production. 49-60% reduction in CGTase production was observed when peptone was replaced by an inorganic nitrogen source. Control having the organic nitrogen source (peptone) showed maximum CGTase production 89.61 ± 2.9 U/ml [Figure 7]. Among all the tested inorganic nitrogen sources, the best CGTase production was observed in the presence of sodium nitrate (40.85 ± 2.35 U/ml).
Yang *et al.* (2017) have also reported that NH_4^+, NO_3^-, and urea have an inhibitory effect on CGTase production. In contrast, **Rasso *et al.* (2002)** reported ammonium sulphate (0.5%) to be the optimum nitrogen source for CGTase production (3.06 U/ml) by *B. circulans* DF 9R compared to organic nitrogen sources.
The organism *Bacillus* sp. PBS1 is urease positive but probably due to the alkaline pH of the medium organism might not utilize urea. There is a possibility of the breakdown of urea in the form of ammonia at alkaline pH. The organism is nitrate negative; thus nitrates cannot be utilized efficiently.

Our study confirms the finding of previous studies that inorganic nitrogen sources are not suitable for CGTase production (**Yang et al., 2017, Rajput et al., 2016 and Yap et al., 2010**). It can be concluded that CGTase production would be higher when the production medium is supplemented with peptone as a nitrogen source.
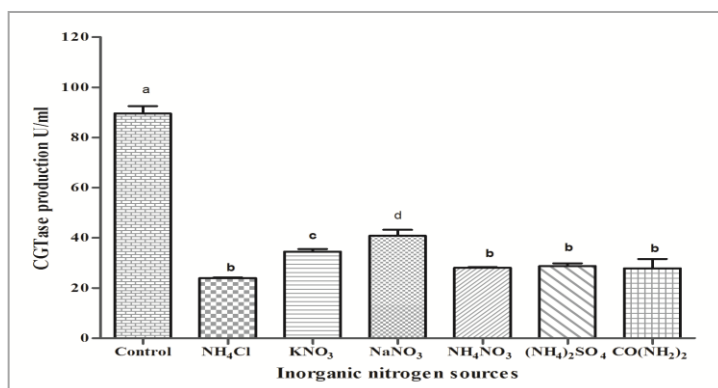

Figure 7 Effect of different inorganic nitrogen sources on CGTase production by *Bacillus* sp. PBS1 in medium F, peptone considered as control. Symbols having the same alphabets are not significantly different from each other P < 0.05. Standard deviation (Mean ± SD, n = 3) is represented by the bars.

Effect of organic nitrogen source

Organic nitrogen has been reported to be essential for growth and CGTase production (**Wang et al., 2018**). Six different organic nitrogen sources were compared to find out the best for CGTase production. Peptone, yeast extract, malt extract, tryptone, casein, and corn steep liquor were supplemented one at a time in medium F. The concentration of various organic nitrogen sources was adjusted so as to equate the nitrogen content available in 2% peptone. 2% w/v peptone was found to be the best nitrogen source for CGTase production. It supported 92.37 ± 6.16 U/ml CGTase enzyme production [Figure 8]. Next to peptone, tryptone (68.21 $\pm$ 7.73 U/ml) and corn steep liquor (52.53 $\pm$ 2.84 U/ml) were found to be good for CGTase production. The use of malt extract as a nitrogen source resulted in very low enzyme production (18.28 $\pm$ 1.41 U/ml). **Ibrahim et al. (2005)** reported that peptone significantly enhanced the CGTase production amongst yeast extract, soybean, and glutamate tested. However, the maximum production was only 17.05 U/ml. While on the contrary, **Yang et al. (2017)** found tryptone as the best organic nitrogen source (3.13 U/ml). **Gawande et al. (1998)** reported that when peptone was used in combination with corn steep liquor it gave the highest CGTase production (24.51 U/ml).
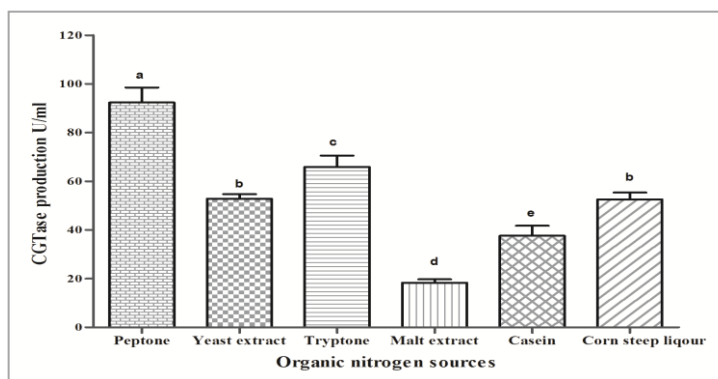

Figure 8 Effect of various organic nitrogen sources on CGTase production by *Bacillus* sp. PBS1 in medium F. Symbols having the same alphabets are not significantly different from each other P < 0.05. Standard deviation (Mean ± SD, n = 3) is represented by the bars.

Effect of metal salts

To observe the effect of metal ions 5mM concentration, $MnSO_4$, $FeSO_4$, $CuSO_4$, $CoCl_2$, $CaCl_2$, and KCl were added in medium F. 1.62 mM $MgSO_4$ being an ingredient in medium F was treated as control. In the presence of $MgSO_4$ (control), 88.03±4.38 U/ml enzyme was produced [Figure 9]. All the other tested metal ions had shown a deleterious effect on CGTase production. The enzyme production in the presence of other metal ions was in decreasing order as follows $MnSO_4$< KCl< $FeSO_4$ < $CaCl_2$ < $CoCl_2$ < $CuSO_4$. However, no significant difference between $MnSO_4$, KCl, $FeSO_4$ was found. Several studies revealed that Mg^{2+} is essential for accelerating the CGTase production, being a cofactor of CGTase (**Blanco et al., 2009; Mora et al., 2012; Yang et al., 2017**). Various studies showed that Ca^{2+} is helpful for active enzyme conformation and stabilizing thermal stability. However, in our study, Ca^{2+} was found to inhibit enzyme production slightly. **Rosso et al.**

(2002); Yang et al. (2017) also reported that Ca^{2+} has no positive effect on CGTase production.
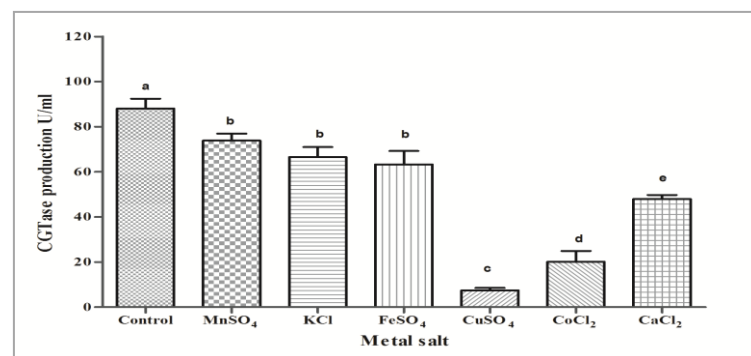

Figure 9 Effect of various metal salts on CGTase production by *Bacillus* sp. PBS1 in medium F. Symbols having the same alphabets are not significantly different from each other P < 0.05. Standard deviation (Mean ± SD, n = 3) is represented by the bars.

Concentration Variation of Selected Production Medium Ingredients

Effect of starch concentration variation

The concentration variation of medium ingredients found to enhance CGTase production was studied further. Substrate concentration affects enzyme production. CGTase is an inducible enzyme (**Gawade et al., 1998**); thus, changing starch concentration is expected to affect enzyme production. In this case, soluble starch was found the best amongst all the tested starch sources. To evaluate the effect on CGTase production, different concentrations of soluble starch (2%, 4%, 6%, 8%, 10%, 12%, and 14%) were added to medium F. Maximum CGTase production was recorded at 8% (91.63 ± 2.48 U/ml) concentration. Further increase in soluble starch concentration led to a decrease in CGTase production [Figure 10]. Similar results were also observed by **Rakmai and Cheirsilp (2015)** that increasing starch concentration beyond 10% led to a decline in CGTase production.

The possible causes of inhibition of enzyme production at high substrate concentrations can be attributed to the increased viscosity resulting in the reduced mass transfer of nutrients and metabolites (**Yap et al., 2010**). **Zain et al. (2007); Elbaz et al. (2015)** reported that the presence of higher starch concentration leads to high glucose accumulation, which in turn causes suppression of CGTase production.
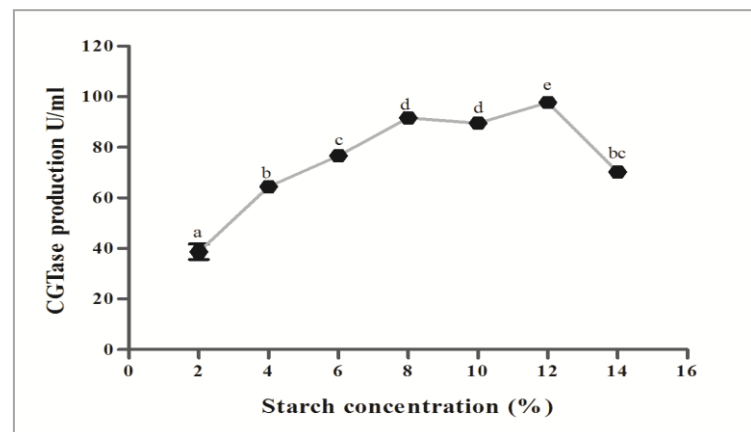

Figure 10 Effect of various concentrations of soluble starch on CGTase production. Symbols having the same alphabets are not significantly different from each other P < 0.05. Standard deviation (Mean ± SD, n = 3) is represented by the bars.

Effect of peptone concentration variation

Organic nitrogen (peptone) was found to increase CGTase production. A 2% concentration of peptone led to the highest CGTase production (93.42 ± 2.4 U/ml) [Figure 11]. Increasing the peptone concentration from 0.5 to 2% led to the concomitant increase in CGTase production (53.86 $\pm$ 2.6 to 93.42 $\pm$ 2.4 U/ml). Further increase in peptone concentration led to a dose-dependent decrease in CGTase production (30.11 ± 0.07 U/ml). **Ibrahim et al. (2005)** reported 55.3 U/ml CGTase productions at 2% peptone. Other authors have also found that higher concentrations of organic nitrogen sources inhibit CGTase production (**Ibrahim et al., 2005 and Elbaz et al., 2015**). The presence of a higher amount of complex

nitrogen source might trigger the secretion of proteases, which could degrade CGTase (**Yang *et al.*, 2017**).
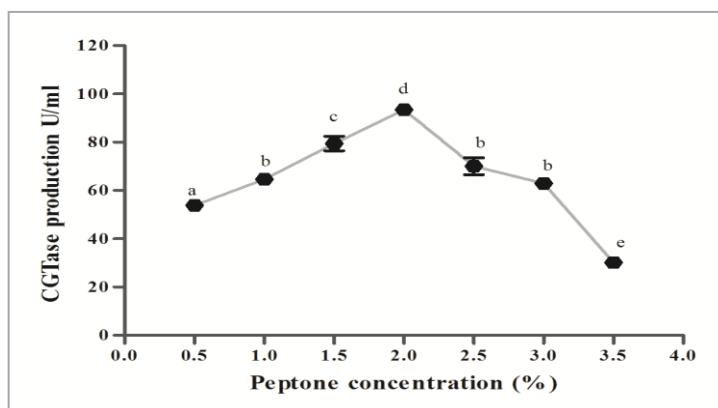

Figure 11 Effect of various concentrations of peptone on CGTase production. Symbols having the same alphabets are not significantly different from each other P < 0.05. Standard deviation (Mean ± SD, n = 3) is represented by the bars.

Effect of dipotassium hydrogen phosphate concentration variation

No positive effect of K_2HPO_4 addition on CGTase production could be detected at any of the tested concentrations (0.5, 1.0, 1.5, 2.0, and 2.5). Furthermore, an increase in K_2HPO_4 concentration led to a dose-dependent decline in CGTase production [Figure 12]. At 2.5% concentration of K_2HPO_4, 62% reduction was observed as compared to control. Control which was devoid of K_2HPO_4 showed maximum CGTase production (82.17 ± 2.34 U/ml). **Mahat *et al.* (2004)** also reported that K_2HPO_4 had no significant effect on CGTase production.
These results differ from **Wang *et al.* (2018)**, where increased production (3230 U/ml mutant strain of β-CGTase H163C) was observed when K_2HPO_4 was used. Likewise, K_2HPO_4 was reported as a crucial factor for influencing CGTase production by *Bacillus megaterium* NCR; the pH of the medium was 7(**Ahmed and Refai 2010**). The pH of the medium might affect the role of phosphate metabolism in the bacteria.
To verify the negative effect of the K_2HPO_4 experiment was repeated several times. It was found that the *Bacillus sp.* PBS1 produces CGTase in the limited environment of potassium and phosphate. The absence of K_2HPO_4 favours good CGTase production.
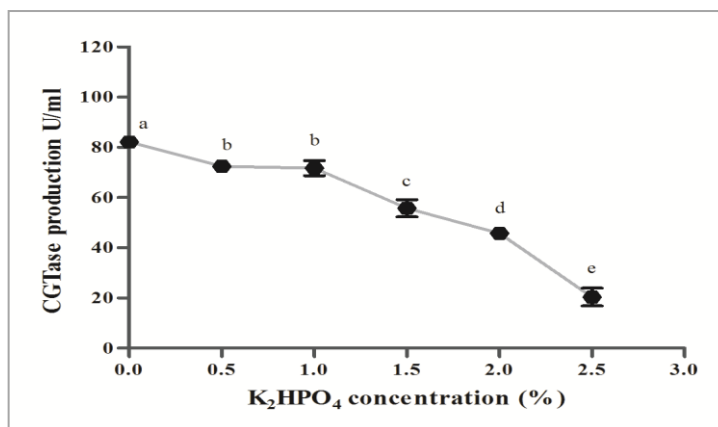

Figure 12 Effect of different concentrations of dipotassium hydrogen phosphate on CGTase production. Symbols having the same alphabets are not significantly different from each other P < 0.05. Standard deviation (Mean ± SD, n = 3) is represented by the bars.

Effect of magnesium sulfate concentration

The different concentrations tested ranged from 0.02 to 0.08% (with an increment of 0.02%) added to the production medium F. As shown in figure 13, 0.06% concentration was found to enhance the CGTase production significantly. At the same time, no significant difference was observed in 0.02 to 0.04% concentrations. At 0.08% concentration, production was declined slightly.
For *Bacillus* G1, 0.04% $MgSO_4$ was found to be suitable leading to17.48 U/ml enzyme production (**Ibrahim *et al.*, 2005**). **Wang *et al.*, (2018)** observed that 0.02% magnesium sulfate (3.05 U/ml) was significant in promoting CGTase production. *Bacillus* sp. PBS1 required a slightly higher concentration of $MgSO_4$ as compared to known CGTase producers.
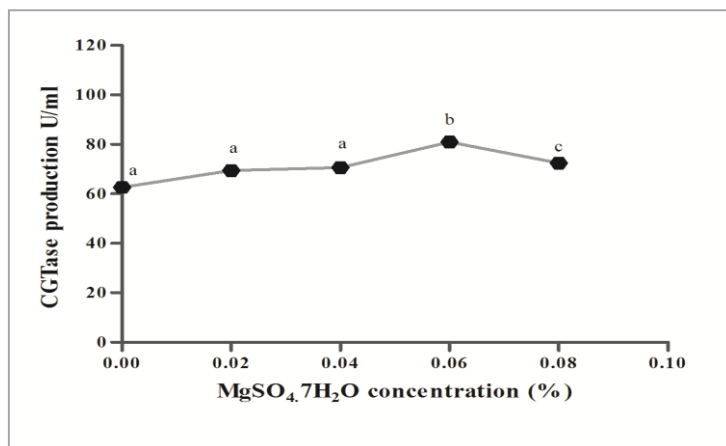

Figure 13 Effect of magnesium sulfate heptahydrate concentration on CGTase production. Symbols having the same alphabets are not significantly different from each other P < 0.05. Standard deviation (Mean ± SD, n = 3) is represented by the bars.

Effect of sodium carbonate concentration

Na_2CO_3 is used to adjust pH and as a source of Na^+. The effect of initial pH was evaluated by varying the concentration of Na_2CO_3. Na_2CO_3 was added in medium F after sterilization (separately autoclaved). At varying concentrations as, 0%, 0.5, 1% (Control), 1.5%, 2%, 2.5% and their respective pH were 6.95, 9.83, 10.68, 11, 11.30 and 11.46. The 0.5% concentration having a pH of 9.3 ± 0.1 showed the highest production of 82.32U/ml [Figure 14]. Comparatively low enzyme production (zero concentration) was observed without Na_2CO_3, possibly due to the neutral pH of the medium. Further increase in Na_2CO_3 concentration from 1% to 2.5% led to a 53% reduction CGTase production.
Higher pH might lead to cell lysis, which results in reduced enzyme production. *B. firmus* (**Gawande *et al.*, 1998**), *Bacillus* G1 (**Ibrahim *et al.*, 2005**), and *Bacillus lehensis* S8 (**Yap *et al.*, 2010**) were reported to produce maximum CGTase production at 1% Na_2CO_3 concentration.
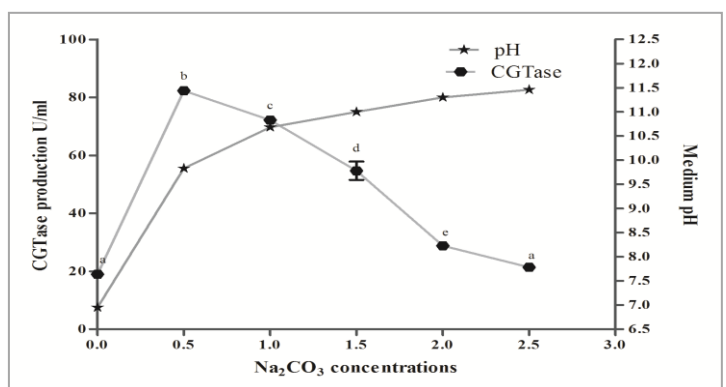

Figure 14 Effect of various concentrations of sodium carbonate and respective pH on CGTase production. Symbols having the same alphabets are not significantly different from each other P < 0.05. Standard deviation (Mean ± SD, n = 3) is represented by the bars.

CONCLUSION

Isolated organism, *Bacillus sp.* PBS1 deposited to NCIM and assigned culture accession number NCIM 5799. Phylogenetic and molecular characterization of *Bacillus sp.* PBS1 (NCIM 5799) revealed it to be a novel CGTase producer strain. Moreover it has capability to produce 21% higher CGTase as compared to *Cytobacillus firmus* NCIM 5119.
The medium optimized for CGTase production contains 8% soluble starch, 2% peptone, 0.06% magnesium sulfate, and 0.5% sodium carbonate, having final pH of 9.3. This modified medium F was found to be optimal for the production of CGTase enzyme using *Bacillus sp.* PBS1. The medium optimization process led to an overall 16% improvement (from 77.29 to 93.42 U/mL) in enzyme production.

REFERENCES

Abelyan, V. A., Balayan, A. M., Ghochikyan, V. T., & Markosyan, A. A. (2004). Transglycosylation of Stevioside by Cyclodextrin Glucanotransferases of Various Groups of Microorganisms. *Applied Biochemistry and Microbiology*, 40(2), 129–134. https://doi:10.1023/b:abim.0000018914.08571.50

Ahmed, E. M., & El-Refai, H. A. (2010). Cyclodextrin glucosyltransferase production by Bacillus megaterium NCR: evaluation and optimization of culture conditions using factorial design. I*ndian Journal of Microbiology*, 50(3), 303–308. https://doi:10.1007/s12088-010-0009-x

Alves-Prado, H. F., Carneiro, A. A., Pavezzi, F. C., Gomes, E., Boscolo, M., Franco, C. M., & da Silva, R. (2008). Production of cyclodextrins by CGTase from Bacillus clausii using different starches as substrates. *Applied biochemistry and biotechnology*, *146* (1-3), 3–13. https://doi.org/10.1007/s12010-007-8093-z

Arce-Vázquez, M. B., Ponce-Alquicira, E., Delgado-Fornué, E., Pedroza-Islas, R., Díaz-Godínez, G., & Soriano-Santos, J. (2016). Integral Use of Amaranth Starch to Obtain Cyclodextrin Glycosyltransferase, by *Bacillus megaterium*, to Produce β-Cyclodextrin. *Frontiers in microbiology*, *7*, 1513. https://doi.org/10.3389/fmicb.2016.01513

Bergey, D.H., Robert, S.B., (1957). Bergey's Manual of Determinative Bacteriology. *Williams & Wilkins Co: Baltimore*. https://doi.org/10.5962/bhl.title.10728

Bezerra, F. M., Lis, M. J., Firmino, H. B., Dias da Silva, J. G., Curto Valle, R. de C. S., Borges Valle, J. A., & Tessaro, A. L. (2020). The Role of β-Cyclodextrin in the Textile Industry. *Review Molecules*, 25(16), 3624. https://doi:10.3390/molecules25163624

Blanco, K. C., De Lima, C. J. B., De Oliveir, P. A. P. L. V., Piao, A. C. S., & Contiero, J. (2009). Cyclodextrin Glycosyltransferase Production by the Bacillus sp., Subgroup alcalophilus using a Central Composite Design. *Research Journal of Microbiology*, 4(11), 450–459. https://doi:10.3923/jm.2009.450.459

Bonilha, P. R. M., Menocci, V., Goulart, A. J., Polizeli, M. de L. T. de M., & Monti, R. (2006). Cyclodextrin glycosyltransferase from Bacillus licheniformis: optimization of production and its properties. *Brazilian Journal of Microbiology*, 37(3), 317–323. https://doi:10.1590/s1517-83822006000300022

Burhan, N., Sapundzhiev, T. and Beschkov, V. (2005) Mathematical Modelling of Cyclodextrin-Glucanotransferase Production by Batch Cultivation. *Biochemical Engineering Journal*, 24, 73-77. https://doi.org/10.1016/j.bej.2005.02.007

Buschmann, H. J., & Schollmeyer, E. (2002). Application of cyclodextrins in cosmetic products: A review. *Journal of cosmetic science*, 53(3), 185–191. https://pubmed.ncbi.nlm.nih.gov/12053209/

Chung, H.J., Yoon, S.H., Lee, M.J., Kim, M.J., Kweon, K.S., Lee, W., Wan Kim J.W, Oh, B.A, Lee H.S., Spiridonova V.A., & Park K.H. (1998). Characterization of a Thermostable Cyclodextrin Glucanotransferase Isolated from Bacillus stearothermophilus ET1. *Journal of Agricultural and Food Chemistry* 46 (3), 952−95 https://doi.org/10.1021/jf970707d

Dalmotra, N., Tripathi, A. D., Srivastava, S. K., Arya, S. K., & Naik, B. (2016). Statistical optimization of cyclodextrin glycosyltransferase (CGTase) production from Bacillus macerans in batch cultivation and its purification. *International Journal of Food and Fermentation Technology*, 6(2), 261. https://doi:10.5958/2277-9396.2016.00049.0

Elbaz, A. F., Sobhi, A., & ElMekawy, A. (2014). Purification and characterization of cyclodextrin β-glucanotransferase from novel alkalophilic bacilli. *Bioprocess and Biosystems Engineering*, 38(4), 767–776. https://doi.org/10.1007/s00449-014-1318-y

Fenyvesi, Eva. (2011) 25: 1-7. *CycloLab R&D Laboratory Ltd*., Hungary.

Gawande, B. N., & Patkar, A. Y. (2001). Purification and properties of a novel raw starch degrading-cyclodextrin glycosyltransferase from Klebsiella pneumoniae AS- 22. *Enzyme and Microbial Technology*, 28(9-10), 735–743. https://doi:10.1016/s0141-0229(01)00347-7

Gawande, B. N., & Patkar, A. Y. (1999). Application of factorial designs for optimization of cyclodextrin glycosyltransferase production from Klebsiella pneumoniae pneumoniae AS-22. *Biotechnology and bioengineering*, *64*(2), 168–173. https://doi.org/10.1002/(SICI)1097-0290(19990720)64:2%3C168::AID-BIT5%3E3.0.CO;2-5

Gawande, B. N., Singh, R. K., Chauhan, A. K., Goel, A., & Patkar, A. Y. (1998). Optimization of cyclomaltodextrin glucanotransferase production from Bacillus firmus. Enzyme and Microbial Technology, 22(4), 288–291. https://doi:10.1016/s0141-0229(97)00184-1

Geetha, R., & More, S. (2010). Isolation and Characterization of Cyclodextrin Glucanotransferase from Soil Bacterium. *Research Journal of Biological Sciences*, 5(10), 699–707. https://doi:10.3923/rjbsci.2010.699.707

Goel, A., & Nene, S. N. (1995). Modifications in the Phenolphthalein Method for Spectrophotometric Estimation of Beta Cyclodextrin. *Starch - Stärke*, 47(10), 399–400. https://doi:10.1002/star.19950471006

Higuti, H.I., Silva, P.A., Papp J., Okiyama, V.M., Andrade, E. A., Marcondes, A.A., & Nascimento A.J. (2004). Colorimetric Determination of α and β-cyclodextrins and studies on Optimization of CGTase Production from *B. firmus* Using Factorial Designs. *Brazilian archives of biology and technology,* 47 (6), 837-841. https://doi.org/10.11590/S01516-89132004000600001

Horikoshi K., Nakamura N., Matsuzawa N., & Yamamoto M. (1982) Industrial Production of Cyclodextrins. In: Szejtli J. (eds) Proceedings of the First International Symposium on Cyclodextrins. *Advances in Inclusion Science*, vol 1. Springer, Dordrecht. https://doi.org/10.1007/978-94-009-7855-3_3

Ibrahim, H. M., Yusoff, W. M. W., Hamid, A. A., & Omar, O. (2010). Enhancement of Cyclodextrin Glucanotransferase Production by Bacillus G1 using Different Fermentation Modes. *Biotechnology* 9(4), 506–512. https://doi:10.3923/biotech.2010.506.512

Ibrahim, H. M., Yusoff, W. M. W., Hamid, A. A., Illias, R. M., Hassan, O., & Omar, O. (2005). Optimization of medium for the production of β-cyclodextrin glucanotransferase using Central Composite Design (CCD). *Process Biochemistry*, 40(2), 753–758. https://doi:10.1016/j.procbio.2004.01.042

Jamuna, R., Saswathi, N., Sheela, R., & Ramakrishna, S. V. (1993). Synthesis of Cyclodextrin Glucosyl Transferase by Bacillus cereus for the production of cyclodextrins. *Applied Biochemistry and Biotechnology*, 43(3), 163–176. https://doi:10.1007/bf02916450

Kamble, R., and Gupte, A. (2014). Cyclodextrin glycosyltransferase production by alkaliphilic *bacillus sp.* isolated from rice cultivated soil and media optimization using taguchi method. *International Journal of pharmaceutical sciences and Research,* 7 (5), 2754-2762. http://dx.doi.org/10.13040/

Kelly, R. M., Dijkhuizen, L., & Leemhuis, H. (2009). The evolution of cyclodextrin glucanotransferase product specificity. *Applied microbiology and biotechnology*, *84* (1), 119–133. https://doi.org/10.1007/s00253-009-1988-6

Kim, M.H., Sohn C.B., Lim, Y.H., Oh, T.K., (1997). Purification and characterization of cyclodextrin glycosyltransferase from *Bacillus brevis* CD162. *Agricultural Chemistry and Biotechnology*, 40 (6), 465-471.

Letsididi, R., Sun, T., Mu, W., Kessy, N. H., Djakpo, O., & Jiang, B. (2011). Production of a Thermoactive B-cyclodextrin Glycosyltransferase with a High Starch Hydrolytic Activity from an Alkalitolerant Bacillus Licheniformis Sk 13.002 Strain. *Asian Journal of Biotechnology*, 3 (3), 214–225. https://doi:10.3923/ajbkr.2011.214.225

Mahat, M. K., Illias, R. M., Rahman, R. A., Rashid, N. A. A., Mahmood, N. A. N., Hassan, O., & Kamaruddin, K. (2004). Production of cyclodextrin glucanotransferase (CGTase) from alkalophilic Bacillus sp. TS1-1: media optimization using experimental design. *Enzyme and Microbial Technology*, 35(5), 467–473. https://doi:10.1016/j.enzmictec.2004.07.008

Mäkelä, M. J., Paavilainen, S. K., & Korpela, T. K. (1990). Growth dynamics of cyclomaltodextrin glucanotransferase producing *Bacillus circulans* var. *alkalophilus. Canadian Journal of Microbiology* 36, 176–182. https://doi: 10.1139/m90-031

Maskooki, A. M., Beheshti, S. H. R., Valibeigi, S., & Feizi, J. (2013). Effect of Cholesterol Removal Processing Using β-Cyclodextrin on Main Components of Milk. *International Journal of Food Science*, 2013,1–6. https://doi:10.1155/2013/215305

Menocci, V., Goulart, A. J., Adalberto, P. R., Tavano, O. L., Marques, D. P., Contiero, J., & Monti, R. (2008). Cyclodextrin glycosyltransferase production by new Bacillus sp. strains isolated from brazilian soil. *Brazilian Journal of Microbiology*, 39 (4), 682–688. https://doi.org/10.1590/S1517-83822008000004000016

More, S.S., Niraja, R., Chris, E. C., Byadgi, A.M., Shwetha, V. & Mangaraj S.D. (2012). Isolation, Purification and Biochemical Characterization of CGTase from *Bacillus halodurans. Croatian Journal of Food Technology Biotechnology and Nutrition* 7, 90-97. https://hrcak.srce.hr/84932

Moriwaki, C., Costa, G. L., Pazzetto, R., Zanin, G. M., Moraes, F. F., Portilho, M., & Matioli, G. (2007). Production and characterization of a new cyclodextrin glycosyltransferase from Bacillus firmus isolated from Brazilian soil. *Process Biochemistry*, 42(10), 1384–1390. https://doi:10.1016/j.procbio.2007.07.007

Qi, Q., & Zimmermann, W. (2004). Cyclodextrin glucanotransferase: from gene to applications. *Applied Microbiology and Biotechnology*, 66(5), 475–485. https://doi:10.1007/s00253-004-1781-5

Rajput, K. N., Patel, K. C., & Trivedi, U. B. (2016). A novel cyclodextrin glucanotransferase from an alkaliphile Microbacterium terrae KNR 9: purification and properties. *3 Biotech*, *6*(2), 168. https://doi.org/10.1007/s13205-016-0495-6

Rajput, K. N., Patel, K. C., & Trivedi, U. B. (2016). Screening and Selection of Medium Components for Cyclodextrin Glucanotransferase Production by New Alkaliphile Microbacterium terrae KNR 9 Using Plackett-Burman Design. *Biotechnology Research International*, 2016, 1–7. https://doi:10.1155/2016/3584807

Rakmai, J., & Cheirsilp, B. (2016). Continuous production of β-cyclodextrin by cyclodextrin glycosyltransferase immobilized in mixed gel beads: Comparative study in continuous stirred tank reactor and packed bed reactor. *Biochemical Engineering Journal*, 105, 107–113. https://doi:10.1016/j.bej.2015.09.011

Ramli, N., Abd-Aziz, S., Hassan, M. A., Alitheen, N., & Kamaruddin, K. (2010). Potential cyclodextrin glycosyltransferase producer from locally isolated bacteria. *African Journal of Biotechnology*, *9* (43), 7317-7321. https://doi.org/10.5897/AJB10.081

Ravinder, K., Prabhakar, T., & Bhavanidevi, R. (2012). Optimization of process parameters for the production of cyclodextrin glycosyltransferase by newly

isolated bacillus sp. Tpr71h by conventional method. *International Journal of Advanced Biotechnology and Research,* 3 (2) 578-584.

Rosso, A. M., Ferrarotti, S. A., Krymkiewicz, N., & Nudel, B. C. (2002). Optimisation of batch culture conditions for cyclodextrin glucanotransferase production from Bacillus circulans DF 9R. *Microbial cell factories, 1*(1), 3. https://doi.org/10.1186/1475-2859-1-3

Sabioni, J.G., Park Y.K. (1992). Production and characterization of cyclodextrin glucanotrasferase from *Bacillus lentus*. *Starch* 44 (6) 225–229 https://doi.org/10.1002/star.19920440607

Silva, L., Matioli, G., Zanin, G. & Moraes, F. (2021). Batch CGTase Production with Free and Immobilized *Bacillus firmus* Strain 37 in Bovine Bone Charcoal. *Advances in Chemical Engineering and Science* 11 (1) 91-104. https://www.scirp.org/journal/aces

Sun, H., Seshadri, M., Lingard, S., Monaghan, W., Faoagali, J., Chan, E., McDonald, H., Houston, T., King, M., Peak, I., Wilson, J. C., Haywood, A., Spencer, B., Dunn, P. & Grant, G. D. (2011). Antibacterial Activity of β-Cyclodextrin and 2-Hydroxypropyl-β-Cyclodextrin Trimethoprim Complexes. *Current Research in Microbiology*, *2*(1), 1-8. https://doi.org/10.3844/ajmsp.2011.1.8

Terada, Y., Yanase, M., Takata H., Takaha, T., & Okada S. (1997) Cyclodextrins are not the major cyclic alpha-1,4-glucans produced by the initial action of cyclodextrin glucanotransferase on amylose. *Journal Biological Chemistry,* 272 (25) 15729–15733. https://doi.org/10.1074/jbc.272.25.15729

Thatai, A., Kumar, M., & Mukherjee, K. J. (1999). A single step purification process for cyclodextrin glucanotransferase from a Bacillus sp. isolated from soil. *Preparative biochemistry & biotechnology*, *29*(1), 35–47. https://doi.org/10.1080/10826069908544691

Thombre, R.S, Kanekar, P.P. & Rajwade, J.M. (2013) Synthesis of β-cyclodextrin by CGTase produced by Bacillus lichenoformis MCM-B-1010. *International Journal of Pharma and Bio Sciences* 4 (1) 515 – 523.

Tonkova, A. (1998). Bacterial cyclodextringlucotransferase. *Enzyme Microbia Technol* 22 (8) 678–86. https://doi.org/10.1016/S0141-0229(97)00263-9

Van der Veen BA, Uitdehaag, J. C., Dijkstra, B. W., & Dijkhuizen, L. (2000). Engineering of cyclodextrin glycosyltransferase reaction and product specificity. *Biochimica et biophysica acta*, *1543* (2), 336–360. https://doi.org/10.1016/s0167-4838(00)00233-8

Vidya, A.S., More, V.S. & More, S.S. (2012). Isolation, purification and characterization of a novel CGTase from alkalophilic Bacillus lehensis SV1. *BioTechnology,* 6 (7),226-234

Wang, H., Zhou, W., Li, H., & Bu, R. (2018). Optimization of the fermentation conditions for the mutant strain of β-cyclodextrin glycosyltransferase H167C to produce cyclodextrins. *3 Biotech*, *8* (3), 165. https://doi.org/10.1007/s13205-018-1182-6

Yang, Y. N., Shan, W. X., & Wang, P. W. (2017). Upscale production of a recombinant cyclodextrin glycosyltransferase from Paenibacillus macerans in Escherichia coli. *3 Biotech*, *7*(3): 207. https://doi.org/10.1007/s13205-017-0838-y

Yap, W.P., Ariff, B.A., Woo, K.K., & Hii, L.S., (2010). Production of Cyclodextrin Glycosyltransferase (CGTase) by *Bacillus lehensis* S8 using Sago Starch as Carbon Source. *Journal of Biological Sciences*,10:676-681. https://scialert.net/abstract/?doi=jbs.2010.676.68

Zain, W. S. W. M., Illias, R. M., Salleh, M. M., Hassan, O., Rahman, R. A., & Hamid, A. A. (2007). Production of cyclodextrin glucanotransferase from alkalophilic Bacillus sp. TS1-1: Optimization of carbon and nitrogen concentration in the feed medium using central composite design. *Biochemical Engineering Journal*, 33(1), 26–33. https://doi:10.1016/j.bej.2006.09.024

Zhang, Y. M., Xu, X., Yu, Q., Yu, H. J., & Liu, Y. (2019). Drug Displacement Strategy for Treatment of Acute Liver Injury with Cyclodextrin-Liposome Nanoassembly. *iScience*, *15*, 223–233. https://doi.org/10.1016/j.isci.2019.04.029
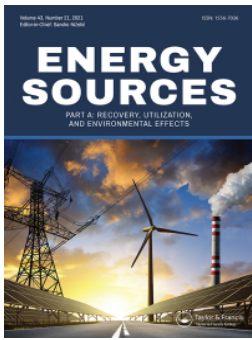
Effect of chemical, physical, and biological pre-treatment of food wastes on bio-hydrogen production by dark anaerobic fermentation under mesophilic conditions

Khushboo Swapnil Bhurat, Tushar Banerjee, Prakash Vasantrao Bobde & Swapnil Sureshchandra Bhurat

Published online: 09 Feb 2023.

Submit your article to this journal ↗

View related articles ↗

View Crossmark data ↗

Taylor & Francis
Taylor & Francis Group

Check for updates

Effect of chemical, physical, and biological pre-treatment of food wastes on bio-hydrogen production by dark anaerobic fermentation under mesophilic conditions

Khushboo Swapnil Bhurat[a,c], Tushar Banerjee[a], Prakash Vasantrao Bobde[b], and Swapnil Sureshchandra Bhurat [iD][b,c]

[a]School of life science, Devi Ahilya University, Indore, Madhya Pradesh, India; [b]School of Engineering, University of Petroleum and Energy Studies (UPES), Dehradun, India; [c]D Y Patil International University, Akurdi, Pune

ABSTRACT

With an overall aim of utilizing lignocellulosic food waste as feedstock for anaerobic fermentation and optimizing the reaction for improving energy output, a two-stage anaerobic dark fermentation reactor was set up. This study discusses the evaluation of different pre-treatment methods used to pre-treat the food waste before using it as a substrate for anaerobic fermentation. Five different techniques from physical, chemical, and biological pre-treatment methods, namely, autoclaving, acid pre-treatment, alkali pre-treatment, aeration, and fungal pre-treatment were used for pre-treatment of the substrate. The analysis was also evaluated by the multilevel categoric factorial design of the experiment model. The experiment found that all five pre-treatments improved the hydrogen and methane yield from the reaction. More precisely, fungal pre-treatment shows an almost 3.8-fold improvement in hydrogen yield compared to control conditions and a 1.7-fold increase in methane yield compared to control. The statistical analysis showed that the reaction time duration (day) has a more significant impact on the results than the pre-treatment technique. The model's F-Values of 24.14 for hydrogen yield and 44.34 for methane yield indicate substantially. However, the actual hydrogen and methane yields are in good accord with the DOE predicted results.

Introduction

The heavy food waste generation worldwide has become an alarming problem due to inadequate and inappropriate waste management techniques. Proper management of this food waste is needed to decrease the greenhouse gas (GHG) emissions, slow the devastation of nature through land conversion and emissions, and save money (Hamish Forbes and O'connor 2021). Researchers are developing the techniques to convert the food waste into a sustainable and cost-effective energy sources (Cappai et al. 2015; Hassan, Hemdan, and El-Gohary 2020). Since the Paris Agreement in 2015, many countries have focused on long-standing strategies and nationally determined contributions to reduce their GHG emissions and reach carbon neutrality. The researchers have been aimed toward generating hydrogen, a clean fuel that does not produce greenhouse gases when burned, while simultaneously dealing with a rising food waste problem (Lee and Chung 2010; Park et al. 2021). Therefore, it can be an efficient and sustainable option to use the food waste for renewable and sustainable fuels generation, like, hydrogen (Kuang et al. 2020). The production of hydrogen from waste will help us achieve emissions goals under the Paris Agreement and reduce dependency on fossil fuels.

CONTACT Swapnil Sureshchandra Bhurat ✉ swapnilsbhurat@gmail.com ⬛ School of Engineering, University of Petroleum and Energy Studies, Energy Acres, Bidholi Campus, Dehradun, Uttarakhand 248007, India

Certainly, hydrogen is the fuel of the future; however, it is vital to note that there are many challenges in producing hydrogen from waste biomass. It is reported by many researchers that the demand for H2 is growing exponentially, and it is expected the demand from steel and ammonia manufacturing industries would be around 4 EJ/year and 22 EJ/year in year 2050 (Hoang et al. 2021). The selection of a nonpolluting, sustainable, and economical hydrogen production process is critical to achieve hydrogen-based fuel production. The primary production technologies presently used for H_2 production include thermal, electrolytic, photolytic, and biological processes (Bhurat et al. 2020). Compared to the physical and chemical methods, biological techniques of hydrogen production are less energy demanding and nonpolluting as they utilize biological wastes as feedstock (Bhurat et al. 2020; Rai and Singh 2013). Hydrogen production using dark fermentation technology is a comparatively simpler and economical approach to convert biological wastes into fuel (Guo et al. 2010; Noblecourt et al. 2018). Moreover, intermediate stages of the anaerobic fermentation also produce valuable intermediates such as acetic acid, butyric acid, and lactic acid (Abubackar et al. 2019).

However, a major difficulty in dark fermentation is the multifaceted lignocellulosic material present in substrates like food waste. The intricate structural polysaccharide molecules present in the bio-waste-like food present a limitation for energy generation. The characteristics of such complex structural molecules in the feedstock restrict micro-organisms from digesting it and generating energy (Bhurat et al. 2020; Cheng and Liu 2012). Various researchers have reported improvements in hydrogen and biogas production after treatment of feedstock using different pre-treatment. Researchers credit the improvement in yield to the degradation of complex structural compounds present in bio-waste due to pre-treatment. Generally, different pretreatment methods have impact on different properties of the lignocellulosic waste to different degrees. Still, all methods have a significant effect on the breakdown of lignocellulosic biomass (Ravindran et al. 2018). Pre-treatment of the lignocellulosic waste improve the gas yield by reducing crystallinity of cellulose and decreasing lignin content (Mirahmadi et al. 2010; Salehian and Karimi 2013). Different physical (Hernández et al. 2019), chemical (Assawamongkholsiri, Reungsang, and Pattra 2013), and biological (Cheng et al. 2015) method individually or in combination have resulted in enhanced hydrogen and biogas yields. However, the selection of pre-treatment method considers several factors, like the type of lignocellu-losic biomass, downstream process, feasibility of the process, and the scale of the process (Hoang et al. 2021, 2021). Besides, the selection of appropriate bioreactor is also of equal importance (Alvarez and Liden 2008). Other than this, the co-digestion of food waste with different substrates like sludge, manure, etc., may be used to improve biogas or bio-hydrogen yields (Náthia-Neves et al. 2018; Rattanapan et al. 2019).

This study aims to evaluate effect of different pre-treatments on the food waste as feedstock for better hydrogen yield. Further, another object of this was to optimize the two-stage fermentation using the pre-treated raw material. With the stated object, the raw mixed food waste was selected as a starting material for producing hydrogen and biogas using two stage anaerobic fermentation process. The lignocellulosic food waste was treated with different pre-treatments, including acid treatment, alkali treatment, heat treatment by autoclavation, fungal treatment, and aeration. The pre-treated material was then inoculated with anaerobic sewage sludge for anaerobic fermentation. In order to understand the effects of pre-treatment, the hydrogen content obtained in stage one of fermentation and methane yield obtained in stage two of the fermentation process, at different hydraulic retention time (HRT) was compared with the control conditions. Further, the experiment was evaluated using multilevel categoric factorial design of the experiment model to estimate the performance of different pre-treatment methods used in this study. The findings of this study identified fungal pre-treatment as the most suitable pre-treatment among those tested, for treating lignocellulosic waste and also the most favorable temperature and pH for the same. This study is milestone in standardizing the hydrogen production from lignocellulosic waste on large scale.

Materials and methods

Microbial enrichment experiment pla

The inoculum selected was the mixed anaerobic microbial consortium from the sewage treatment plant in sludge. The inoculum was first filtered through course filter to eliminate unwanted materials like sand and stones. The filtrate thus obtained was used as inoculum. The microbial enrichment by acid shock was performed independently. For this, the parent inoculum was added with orthophosphoric acid to bring down the pH to 3 and was incubated under anaerobic conditions for 24 h. After incubation, the inoculum pH was adjusted to 6 with 1 N NaOH and was used as inoculum for bio-hydrogen production. Untreated parent inoculum was used as a control.

Characteristics of food waste

The food waste consisting of uncooked vegetable peels and leftovers was collected every 2–3 weeks from a canteen kitchen at Dehradun, Uttarakhand, India. Contaminating materials like paper and polythene were distant manually. The food waste was shredded using a blender to the size of 0.5 cm size. The chopped food waste was then stored in zip lock plastic bags carrying 250 g each. The bags were stored at around −18°C until the successive use. The food waste was checked for the different parameters, including moisture content, Chemical Oxygen Demand (COD), total solids (TS) and volatile solids (VS), etc according to Standard Methods 2540 G and 5220 B, respectively (Rice, B, and Eaton 1915). For total nitrogen determination, the Kjeldahl nitrogen determination method was used (Lang 1958). The total phosphorus and Biological oxygen demand (BOD) content was estimated using the technique followed by Lucas (2014) (Lucas 2014).

Table 1 summarizes the average composition of Total Solid, moisture content, Phosphorus, and *Kjeldahl* Nitrogen, and other vital factors of the substrate used. These findings may be used to derive a correlation for the waste composition and hydrogen and methane yield obtained.

Substrate pre-treatment

For the present study, experiments were designed to calculate the effect of various physical, chemical, and biological pre-treatment methods on food waste under the anaerobic condition to enhance hydrogen production efficiency.

Biological pre-treatment

Two biological pretreatment methods were tested here, including fungal pretreatment and aeration. They are used to break down the cross-linked structures in lignocellulosic material present in the food waste. For fungal pre-treatment, *Pleurotus djamor* spawn was collected from a local mushroom cultivation plant. The mushroom *Pleurotus djamor* is a white rot fungus. The mycelium of this fungus is known for its ability to secrete a range of enzymes including both saccharifying enzymes like cellulases, hemicellulases, and xylanases and oxidative enzymes including laccases (Dal Picolli et al.

Table 1. Characteristics of food waste.

Parameter (Unit)	Value
Total Solid (g.kg-1 wb)	187.78
Fixed Solids (g.kg-1 wb)	42.29
Moisture content (g.kg-1 wb)	812
Volatile solid (g.kg-1 wb)	145.49
Ash (%)	22.52
COD (mg O_2/L)	158
BOD (mg O_2/L)	15.1
Kjeldahl Nitrogen (g N/g)	0.044
Phosphorus (μg P/g)	2.97

2018; Jafari et al. 2007). The mycelia were allowed to grow in potato dextrose broth (PDB) composed of 20% potato and 2% glucose. The PDB inoculated with fungal spawn was incubated at 30°C on a rotary shaker (150 rpm) for 2 days. The liquid mycelial cultures were used as inoculum for the subsequent pre-treatment experiments. While using for pre-treatment experiments, the liquid mycelial cultures were homogenized by high-speed agitation in a blender at around 100 RPM.

For fungal pre-treatment 10 g food waste was diluted in 10 ml tap water to obtain 1 mg/ml concentration and was mixed with 20 mL nutrient solution composed with 1.5% $(NH_4)_2SO_4$, 0.6% $MgSO_4$ $7H2O$ and 0.3% KH_2PO_4 (pH-6) into a 250 mL Erlenmeyer flask. The mixture was autoclaved at 121°C for 25 min. 10 mL of homogenized liquid mycelial cultures were added into the experimental flask and mixed thoroughly with the substrates using a glass rod. All flasks were incubated in an incubator at 30°C. The fungus-treated substrates were collected for reducing sugar analysis using Dinitrosalicylic acid sodium hydroxide (DNSA) method after a specific cultivation time interval (2, 4, 6, and 8 days) (Venkata Mohan, Lalit Babu, and Sarma 2008). The pre-treatment duration showing maximum glucose production was selected for pre-treatment of substrate before two stage fermentation.

For pre-treatment by aeration the regulating air pump was used (*Micronvac Engineers Single Phase Laboratory Air Pump*) for 60 min. The airflow rate was maintained while feeding the waste material and was~400 l of O_2. Non-aerated food waste was used for the control operations to conclude the effect of aeration (Sarkar and Mohan 2017).

Chemical pre-treatment

For chemical pre-treatment, 10 g of food waste sample was mixed with different concentrations (1%, 2%, 4%, and 8% (w/v), respectively, of dilute HCl (or NaOH) and boiled for 30 min. The mixture was then neutralized to pH 7.0 (Cui et al. 2010). The samples were used to check the cellulose hydrolysis. The total reduced sugar contents in 1.0 g of the food waste before and after HCl and NaOH pre-treatment was noted using DNSA method.

Based on the difference observed in the sugar content after pre-treatment (results not disclosed here), the most favorable condition of pre-treatment was identified for the next experiment for pre-treating the substrate before two-stage fermentation.

Physical pre-treatment

For physical pre-treatment, the food waste was subjected to autoclaving at 120°C for 20 min (Abubackar et al. 2019). Negative control was also used, wherein the food waste was chopped and fed directly to dark fermentation without any further pre-treatment.

Two-stage anaerobic fermentation system

A continuous two-stage anaerobic fermentation system was used for the hydrogen and methane fermentation. The working volume of the first stage reactor, used for hydrogen production, was 4 L and that of the second stage reactor, used for methane production, was 6 L.

The first-stage and second-stage reactor were maintained at 40°C and room temperature, respectively (based on the optimum temperature condition observed in previous study) (Bhurat et al. 2021). The reactor temperature was controlled using a thermal plate with an accuracy of±0.1°C, and pH was checked using MARS auto Digital pH meter and was maintained using pump that added acid or alkali based on the pH difference sensed by pH meter. The first-stage reactor was a batch stirred tank reactor (STR), stirred at a speed of 50–90 rpm. The pre-treated samples after different pre-treatment test conditions were added in the first reactor to the volume of 2 L. 20-ml enriched mixed microbial consortium was used to inoculate the reactor. The reactors were sparged with 0.5 vvm N_2 to achieve the anaerobic condition. With the two reactors working together, the first reactor was operated for 8 days. After 8 days, the contents from the first reactor were pumped out in a closed container where the pH of the mix was brought to neutral by adding 0.1 N NaOH or 0.1 N HCl. The content was then transferred to the second reactor. This reactor was

continuously fed with the effluent from first reactor till it 4 L capacity. The volume was maintained by pumping out extra content through a manual pump. The second reactor was operated at HRTs of 8, 12, 15, 20, and 30 days (Algapani et al. 2018). The reactor was made with stainless steel (SS 304) and were enclosed with a light impermeable black sheet on lids and windows. To ensure an anaerobic environment, a leakage test was performed before the operation (Kossmann and Pönitz 2011). For every test condition, one untreated control was assayed.

Figure 1 demonstrates the details of each reactor used in Continuous two-stage anaerobic fermentation

Gas analyses

An important component of the research is a qualitative and quantitative analysis of the gases formed. The gases formed in both reactors were monitored for quantitative and qualitative analysis using the gas flow meter and gas chromatography. This study collected 2–5 ml of a gas sample using a gas-tight syringe from the test condition at every 24 h time interval. The qualitative analysis data were extracted using gas chromatography by injecting with those samples. The volume of total gas formed was monitored using the gas flow meters installed. For qualitative and quantitative analysis of the gases produced, NUCON make Gas chromatograph (GC) system equipped with a thermal conductivity detector (TCD) was used. The standard system component of GC was HayesepD 80/100 packed column and the carrier gas used was Argon, at a flow rate of 20 mL/min. During gas analysis, the injection port, oven, and detector were set for the operating temperature at 70°C, 50°C, and 70°C, respectively.

Statistical analysis by multilevel categoric factorial design of experiment (DOE)

Based on the differences in the levels of pre-treatment method and day evaluated for a statistical model of hydrogen and methane yield optimization in this work, a multilevel factorial (two-factor) DOE was deemed appropriate. As in the case of this study, the simplest forms of designs required only two elements. There were a* levels of Pre-treatment method and b* levels of Days in a factorial design. In general, n duplicates exist.

Experimental data from the Taber test was used as essential components for creating a 2-factor interaction (2FI) full factorial DOE model to examine the primary influence of the variables on the yield. In Design-Expert software, factor A was set to six levels and factor B to eight levels for flawless modeling and simulation of the trial runs. The DOE is shown in Table 2.
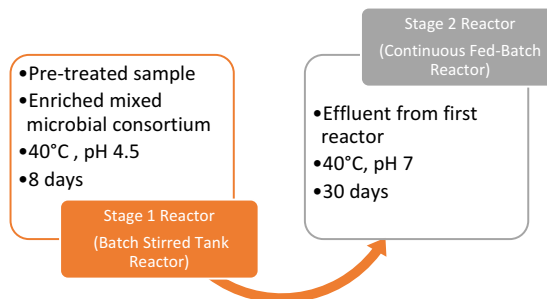

Figure 1. Flow of the processes followed in two stage anaerobic fermentation.

Table 2. DOE design factors with levels.

Factor	Name	Type	SubType	Levels
For hydrogen yield				
A	Pretreatment method	Categoric	Nominal	Control, fungal, autoclave, aeration, HCl, NaOH
B	Day	Categoric	Nominal	1, 2, 3, 4, 5, 6, 7, 8
For methane yield				
A	Pretreatment method	Categoric	Nominal	Control, fungal, autoclave, aeration, HCl, NaOH
B	Day	Categoric	Nominal	8, 12, 15, 20, 30

Result and discussion

Effect of pre-treatment on food waste

Five different pre-treatment methods falling under the chemical, physical and biological pre-treatment types were tested on food waste. The control condition, wherein the food waste was not pre-treated by any pre-treatment, was used for comparison to study the effect of pre-treatment. The pre-treatments showed positive effect on hydrogen yield as well as methane yield from the same substrate. In comparison to the control condition, all pre-treatments conditions showed a marked influence on the acidogenic metabolites, i.e., hydrogen and methane, as depicted in Figure 2.

Effect of biological pre-treatment

The effect of biological pre-treatment shows remarkable improvements in hydrogen yield. When the substrate was pre-treated using aeration pre-treatment, a 3.3-fold increase in hydrogen yield was observed compared to the control condition. Improved hydrogen yield by air sparging may be attributed to the suppression of the methanogens and their activity. Higher methane yield was also evident in stage two of the reaction compared to control. This may be because of the speedy hydrolysis of carbohydrates present in the waste.

The fungus-treated substrates that was collected for cellulase activity investigation after each specific time interval shown maximum free sugar composition after treatment for 6 days. Hence, when the substrate was being prepared for analyzing the effect of fungal pre-treatment on hydrogen yield, it was treated with the fungal pre-treatment method as discussed in section 2.2.1. for 6 days.

High activity of cellulase enzyme during the pre-treatment dissolved lignocelluloses more efficiently. Hydrolyzation of complex lignocellulosic compounds into simpler and soluble substances became more appropriate for hydrogen fermentation hence showed improvement in hydrogen yield. The hydrogen yield after treating the substrate with fungal pre-treatment was observed to be maximum. A close 3.8-fold improvement in hydrogen yield in comparison to control conditions was evident on 5th day. After that there was a decrease in the yield till 8th day. The boost in hydrogen production might be associated with more cellulase produced by *P. djamor* that improved hydrolysis of cellulosic components and produced easily digestible substances available to hydrogen-producing microorganisms.

Also, methane yield in two-stage anaerobic reaction of the fungal pre-treatment treated substrate shown 1.7-fold increase in comparison to control. Compared to physical or chemical pre-treatment, the fungal pre-treatment proved to be a more promising and environmental-friendly method for improving bioconversion efficacy of lignocellulosic waste. Similar results were obtained on pre-treatment of wheat straw by white rot fungi. 1.8-fold increase in hydrogen yield was obtained in this study compared to un-pre-treated group (Zhi and Wang 2014). Whereas a 2-fold increase in hydrogen yield was evidenced on pre-treating the cornstalk by *Trichoderma reesei* (Cheng and Liu 2012). Also, fungal pre-treatment process is easy to scale up requires less water, low energy input and cheap equipment. However, it may require a little more time compared to chemical and physical pre-treatment methods.
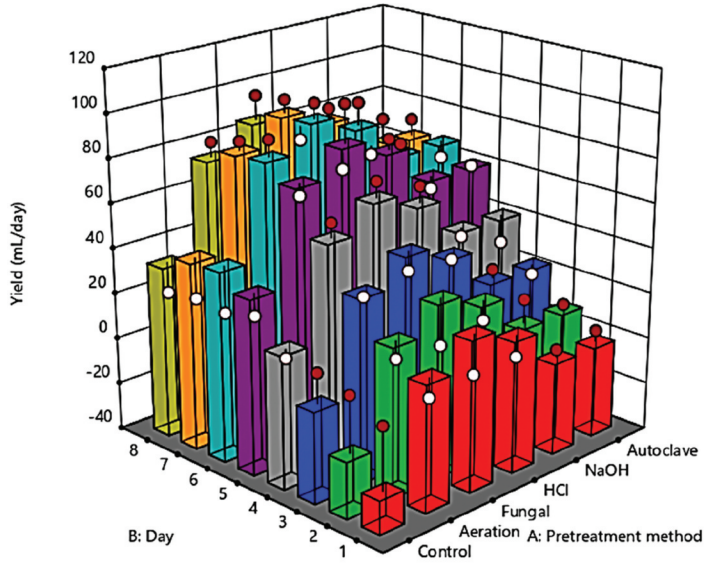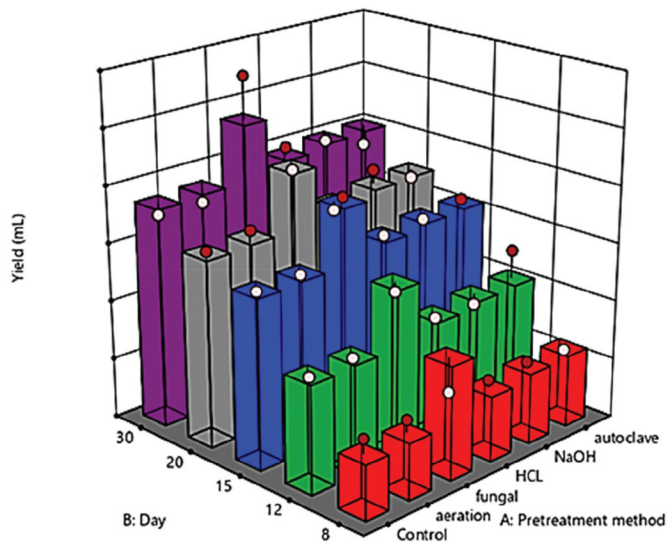
Figure 2. Effect of pre-treatment of food waste on (A) hydrogen and (B) methane yield in dark anaerobic fermentation.

Effect of chemical pre-treatment

Among the various pre-treatment methods studied, chemical pre-treatment of food waste evidenced relatively higher hydrogen yield than the control experiment but lower than that in biological pre-treatment. Acid pre-treatment with 8% HCl showed a 3.5-fold improvement in hydrogen yield and

a 1.2-fold improvement in methane yield compared to the control condition. Whereas pre-treatment by 8% NaOH showed a 2.7-fold increase in hydrogen yield and a 1.17-fold improvement in methane yield. The chemical pre-treatment procedure's improvements in hydrogen yield may be because of its selective inhibition capacity of methanogenic activity without disturbing the hydrogen production. Researchers have reported that a co-enzyme M reductase complex is a principal component for methanogenesis, inhibited by acid pre-treatment, thus suppressing methanogenic activity (Mu et al. 2006). Alkali pre-treatments increase cellulose digestibility by enhancing lignin solubilization and decreasing cellulose crystallinity (Yang et al. 2014). Chemical methods, although are faster compared to biological methods, are not environment-friendly and has the limitation of the production of inhibitors.

Effect of physical pre-treatment

In the two-stage fermentation experiment where the substrate was pre-treated by autoclaving, an improvement in hydrogen yield was evident. A maximum improvement in hydrogen yield of almost 2.78-fold was detected within 7 days and then the hydrogen yield decreased. Whereas methane yield in the second stage of fermentation seen only 1.06-fold improvement compared to the control condition. This high hydrogen yield during the first stage of anaerobic fermentation maybe because autoclaving of the substrate made the sugars readily available for degradation by microbes. While the decrease or not so significant effect in the second stage might be because of the non-availability of highly biodegradable organic matter.

Similarly, Abubakhar et al. observed a steep rise in hydrogen yield after autoclaving the solid food waste and experienced a sudden decrease in the rate. A 44% improvement in hydrogen percentage and 51% improvements in total hydrogen production compared with the non-autoclaved waste was witnessed in this study (Abubackar et al. 2019). Also, similar improvement in biogas yield was also observed on pre-treatment of food waste by autoclaving (Deepanraj, Sivasubramanian, and Jayaraj 2017). In addition, comparable treatments like liquid hot water pre-treatment have also shown remarkable improvement in fuel production form biomass (Chen et al. 2022). However, these physical pre-treatment methods are efficient yet very costly. Also, these processes face limitations of recalcitrance, heterogeneity, compositional, and diversity of biomass (Chen et al. 2022).

Statistical analysis

Figure 3 depicts the 2FI influences model derived from the Design of experiment (DOE) of 48 and 30 hydrogen and methane yield experiments, respectively. The results demonstrated that both variables in the designs are exceptional. The time duration of reaction (day) has a more significant impact on the results than the pre-treatment technique.

Table 3 displays the model's computational and numerical relevance. The findings in Table 3 demonstrated that the created model is adequate and reliable; hence, the equations may be utilized to predict response for given amounts of pre-treatment method and day. The model's F-values of 24.14 for hydrogen yield and 44.34 for methane yield indicate the importance of model. There is only a 0.01% chance that an F-value this large could occur due to noise. The P-values in the quantitative model for hydrogen and methane yield found to be below 0.0003. The model is significant if the P-value is less than 0.0500. Pre-treatment method and day are essential model components in this scenario. The predicted R^2 values of 0.7973 and 0.8926 conform to the adjusted R^2 values of 0.8553 and 0.9308 for hydrogen and methane yields, respectively; that is, the gap becomes less than 0.2. Adeq Precision measures the signal-to-noise (S/N) ratio. A ratio larger than 4 is preferred. As a result, the model may be utilized to explore the design space. Similar findings may be seen in the research done by Stojanovi et al., who investigated the tribological behavior of ABCs using factorial methods (Dimaki et al. 2016).
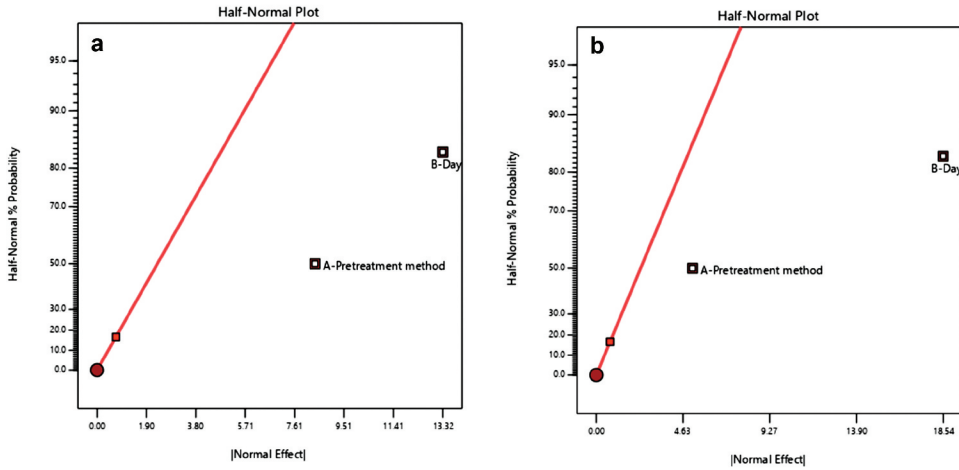
Figure 3. 2FI normal effect model plots for a) hydrogen yield and b) methane yield.

Table 3. Quantitative model of the 2FI model.

| For Hydrogen Yield						
Source	Sum of Squares	df	Mean Square	F-value	p-value	
Model	45323.26	12	3776.94	24.14	<0.0001	Significant
A-Pretreatment method	13452.53	5	2690.51	17.2	<0.0001	
B-Day	31870.73	7	4552.96	29.11	<0.0001	
Residual	5475	35	156.43			
Cor Total	50798.26	47				
Fit Statistics						
Std. Dev.	12.51		R^2		0.8922	
Mean	48.39		Adjusted R^2		0.8553	
C.V. %	25.85		Predicted R^2		0.7973	
			Adeq Precision		18.5878	
For Methane Yield						
Source	Sum of Squares	df	Mean Square	F-value	p-value	
Model	347500.00	9	38609.32	44.34	<0.0001	significant
A-Pretreatment method	33725.2	5	6745.04	7.75	0.0003	
B-Day	313800.00	4	78439.66	90.08	<0.0001	
Residual	17414.9	20	870.74			
Cor Total	364900.00	29				
Fit Statistics						
Std. Dev.	29.51		R^2		0.9523	
Mean	185.41		Adjusted R^2		0.9308	
C.V. %	15.91		Predicted R^2		0.8926	
			Adeq Precision		22.6619	

Figure 4 describes the optimum condition for getting a high yield concentration of hydrogen and methane with desirability. This implies that the pre-treatment of food waste with the fungal pre-treatment method is the most suitable pre-treatment, and the optimum hydrogen yield is obtained on 6th day of dark anaerobic fermentation. At the same time, optimum methane yield is expected on 30th day of fermentation.

Conclusion

The two-stage anaerobic dark fermentation experiment performed using food waste as feedstock demonstrated that pre-treatment of the feedstock was evident to improve the hydrogen and methane
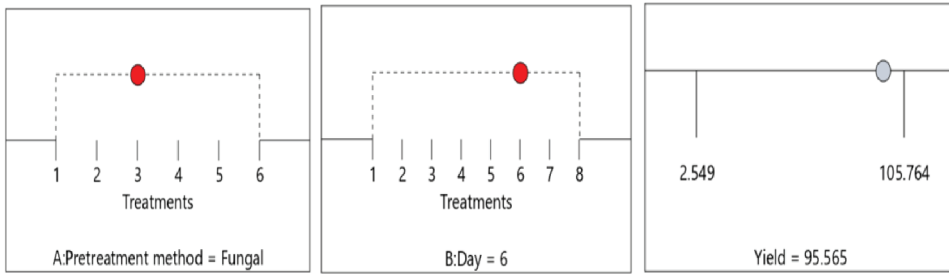
(a) Optimum condition for hydrogen yield and predicted optimum yield of hydrogen
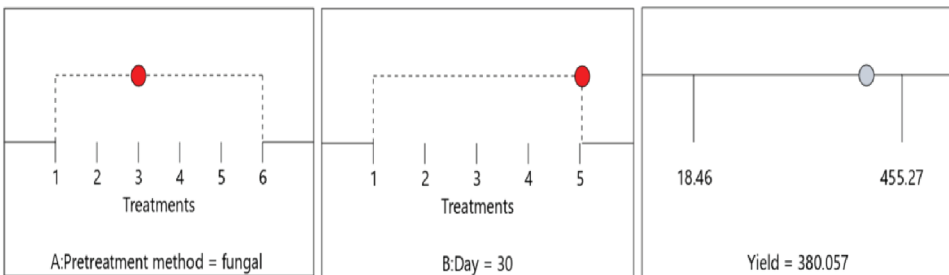
(b) Optimum condition for methane yield and predicted optimum yield of methane

Figure 4. Optimum condition for getting high yield concentration of hydrogen and methane with desirability one.

yield. All pre-treatment methods positively influenced the overall hydrogen and methane yield compared to the control experiments. This may be attributed to the capacity of the pre-treatment methods to uncomplicated the structural compounds and dissolving them into their monomers. This might have made it easier for digestion and conversion to hydrogen and methane easier by the microorganisms. Individually, fungal pre-treatment of food waste was found to be the most effective and this may be attributed to the exocrine enzymes being secreted by the *P. djamor*. This method is more straightforward and less energy demanding and releases nontoxic and nonpolluting by-products and end products. Fungal pre-treatment can also be combined with other pre-treatment methods for elevating the hydrogen output. Multilevel categoric factorial Design of experiment model was successfully used to evaluate the relative performance of different pretreatment methods used in this study. However, it is crucial to find and optimize the correct balance between increasing H_2 yield and lowering the limiting factors of the lignocellulosic bio-hydrogen production system. A multidisciplinary approach for improvement and optimization of this process can make milestone moves in the direction of waste management as well as sustainable energy research.

Abbreviations

Abbreviation	Full form
°C	Degree Celsius
AD	Anaerobic Digestion
AF	Anaerobic Fermentation
ANOVA	Analysis of Variance
BioH$_2$	Bio-hydrogen
BOD	Biological Oxygen Demand

C	Carbon
CH_4	Methane
CNG	Compressed Natural Gas
CO	Carbon mono-oxide
CO_2	Carbon di oxide
COD	Chemical Oxygen Demand
COD: N	COD to nitrogen ratio
CSTR	Continuous Stirred Tank Reactor
C/N	Carbon to Nitrogen ratio
g	Gram
g/L	Gram per Liter
GC	Gas Chromatograph
gCOD/L/day	Gram chemical oxygen demand per liter per day
h	Hour
H_2	Hydrogen
H-CNG	Compressed Natural Gas with Hydrogen blend
H_2O	Water
HRT	Hydraulic Retention Time
kg	Kilogram
kg/day	Kilogram per day
mg	Milligram
mL/g VS	Milligram per gram volatile solids
mL CH4/gVS added	Milliliter methane per gram volatile solids added
mL H2/gVS added	Milliliter hydrogen per gram volatile solids added
MSW	Municipal Solid Waste
OFMSW	Organic Fraction of Municipal Solid Waste
pH	Hydrogen ion concentration
TKN	Total Kjeldal Nitrogen
TS	Total Solid
TSS	Total suspended solids
TVFA	Total Volatile Fatty Acid
TVS	Total Volatile Solids
VS	Volatile Solid

Acknowledgements

Disclosure statement

No potential conflict of interest was reported by the authors.

ORCID

Swapnil Sureshchandra Bhurat (iD) http://orcid.org/0000-0002-1788-8494

References

Abubackar, H. N., T. Keskin, K. Arslan, C. Vural, D. Aksu, D. K. Yavuzyılmaz, G. Ozdemir, and N. Azbar. 2019. Effects of size and autoclavation of fruit and vegetable wastes on biohydrogen production by dark dry anaerobic fermentation under mesophilic condition. *International journal of hydrogen energy* 44 (33):17767–80. doi:10.1016/j.ijhydene. 2019.05.106.

Algapani, D. E., W. Qiao, F. di Pumpo, D. Bianchi, S. M. Wandera, F. Adani, and R. Dong. 2018. Long-term bio-H2 and bio-CH4 production from food waste in a continuous two-stage system: Energy efficiency and conversion pathways. *Bioresource Technology* 248:204–13. doi:10.1016/j.biortech.2017.05.164.

Alvarez, R., and G. Liden. 2008. Semi-continuous co-digestion of solid slaughterhouse waste, manure, and fruit and vegetable waste. *Renewable Energy* 33 (4):726–34. doi:10.1016/j.renene.2007.05.001.

Assawamongkholsiri, T., A. Reungsang, and S. Pattra. 2013. Effect of acid, heat and combined acid-heat pretreatments of anaerobic sludge on hydrogen production by anaerobic mixed cultures. *International Journal of Hydrogen Energy* 38 (14):6146–53. doi:10.1016/j.ijhydene.2012.12.138.

Bhurat, K. S., T. Banerjee, J. K. Pandey, and P. Belapurkar. 2020. Fermentative bio-hydrogen production using lignocellulosic waste biomass: A review. *Waste Disposal & Sustainable Energy* 2:249–64. doi:10.1007/s42768-020-00054-9.

Bhurat, K. S., T. Banerjee, J. K. Pandey, and S. S. Bhurat. 2021. A lab fermenter level study on anaerobic hydrogen fermentation using potato peel waste: Effect of pH, temperature, and substrate pre-treatment. *Journal of Material Cycles & Waste Management* 23:1–9. doi:10.1007/s10163-021-01242-3.

Cappai, G., G. De Gioannis, A. Muntoni, A. Polettini, R. Pomi, and D. Spiga 2015. Effect of inoculum to substrate ratio (ISR) on hydrogen production through dark fermentation of food waste. Proceedings of the Fifteenth International Waste Management and Landfill Symposium, S. Margherita di Pula, Cagliari, Italy, CISA Publisher, Italy.

Cheng, J., R. Lin, L. Ding, W. Song, Y. Li, J. Zhou, and K. Cen. 2015. Fermentative hydrogen and methane cogeneration from cassava residues: Effect of pretreatment on structural characterization and fermentation performance. *Bioresource Technology* 179:407–13. doi:10.1016/j.biortech.2014.12.050.

Cheng, X. -Y., and C. -Z. Liu. 2012. Fungal pretreatment enhances hydrogen production via thermophilic fermentation of cornstalk. *Applied Energy* 91 (1):1–6. doi:10.1016/j.apenergy.2011.09.014.

Chen, W. -H., S. Nižetić, R. Sirohi, Z. Huang, R. Luque, A. M. Papadopoulos, R. Sakthivel, X. P. Nguyen, and A. T. Hoang. 2022. Liquid hot water as sustainable biomass pretreatment technique for bioenergy production: A review. *Bioresource Technology* 344:126207. doi:10.1016/j.biortech.2021.126207.

Cui, M., Z. Yuan, X. Zhi, L. Wei, and J. Shen. 2010. Biohydrogen production from poplar leaves pretreated by different methods using anaerobic mixed bacteria. *International Journal of Hydrogen Energy* 35 (9):4041–47. doi:10.1016/j.ijhydene.2010.02.035.

Dal Picolli, T., K. Regalin Aver, R. Claudete Fontana, and M. Camassola. 2018. High-performance of Agaricus blazei fungus for the biological pretreatment of elephant grass. *Biotechnology Progress* 34 (1):42–50. doi:10.1002/btpr.2529.

Deepanraj, B., V. Sivasubramanian, and S. Jayaraj. 2017. Effect of substrate pretreatment on biogas production through anaerobic digestion of food waste. *International Journal of Hydrogen Energy* 42 (42):26522–28. doi:10.1016/j.ijhydene.2017.06.178.

Dimaki, A., A. I. Dmitriev, N. Menga, A. Papangelo, M. Ciavarella, and V. L. Popov. 2016. Fast high-resolution simulation of the gross slip wear of axially symmetric contacts. *Tribology Transactions* 59 (1):189–94. doi:10.1080/10402004.2015.1065529.

Guo, X. M., E. Trably, E. Latrille, H. Carrere, and J. -P. Steyer. 2010. Hydrogen production from agricultural waste by dark fermentation: A review. *International Journal of Hydrogen Energy* 35 (19):10660–73. doi:10.1016/j.ijhydene.2010.03.008.

Hamish Forbes, T. Q., and C. O'connor. 2021. Unep food waste index report 2021Unep food waste index report 2021. *United Nations Environment Programme* (2021). https://wedocs.unep.org/handle/20.500.11822/35280?show=full.

Hassan, G. K., B. A. Hemdan, and F. A. El-Gohary. 2020. Utilization of food waste for bio-hydrogen and bio-methane production: Influences of temperature, OLR, and in situ aeration. *Journal of Material Cycles & Waste Management* 2:1218–26. doi:10.1007/s10163-020-01014-5.

Hernández, C., Z. L. Alamilla-Ortiz, A. E. Escalante, M. Navarro-Díaz, J. Carrillo-Reyes, I. Moreno-Andrade, and I. Valdez-Vazquez. 2019. Heat-shock treatment applied to inocula for H2 production decreases microbial diversities, interspecific interactions and performance using cellulose as substrate. *International Journal of Hydrogen Energy* 44 (26):13126–34. doi:10.1016/j.ijhydene.2019.03.124.

Hoang, A. T., Z. Huang, S. Nižetić, A. Pandey, X. P. Nguyen, R. Luque, H. C. Ong, Z. Said, T. H. Le, and V. V. Pham. 2021. Characteristics of hydrogen production from steam gasification of plant-originated lignocellulosic biomass and its prospects in Vietnam. *International journal of hydrogen energy* 47:4394–425. doi:10.1016/j.ijhydene.2021.11.091.

Hoang, A. T., S. Nizetic, H. C. Ong, C. T. Chong, and A. Atabani. 2021. Acid-based lignocellulosic biomass biorefinery for bioenergy production: Advantages, application constraints, and perspectives. *Journal of Environmental Management* 296:113194. doi:10.1016/j.jenvman.2021.113194.

Jafari, M., A. Nikkhah, A. A. Sadeghi, and M. Chamani. 2007. The effect of Pleurotus spp. fungi on chemical composition and in vitro digestibility of rice straw. *Pakistan Journal of Biological Sciences* 10 (15):2460–64. doi:10.3923/pjbs.2007.2460.2464.

Kossmann, W., and U. Pönitz. 2011. Biogas digest: Volume I-biogas basics. *Information and Advisory Service on Appropriate Technology* 1:1–46.

Kuang, Y., J. Zhao, Y. Gao, C. Lu, S. Luo, Y. Sun, and D. Zhang. 2020. Enhanced hydrogen production from food waste dark fermentation by potassium ferrate pretreatment. *Environmental Science & Pollution Research* 27 (15). doi:10.1007/s11356-020-08207-3.

Lang, C. A. 1958. Simple microdetermination of Kjeldahl nitrogen in biological materials. *Analytical Chemistry* 30 (10):1692–94. doi:10.1021/ac60142a038.

Lee, Y. -W., and J. Chung. 2010. Bioproduction of hydrogen from food waste by pilot-scale combined hydrogen/ methane fermentation. *International Journal of Hydrogen Energy* 35 (21):11746–55. doi:10.1016/j.ijhydene.2010.08. 093.

Lucas, C. K. G. 2014. *Biogas production from potato peel waste*. Portugal: Faculdade de Ciências e Tecnologia.

Mirahmadi, K., M. M. Kabir, A. Jeihanipour, K. Karimi, and M. Taherzadeh. 2010. Alkaline pretreatment of spruce and birch to improve bioethanol and biogas production. *BioResources* 5 (2):928–38.

Mu, Y., X. -J. Zheng, H. -Q. Yu, and R. -F. Zhu. 2006. Biological hydrogen production by anaerobic sludge at various temperatures. *International Journal of Hydrogen Energy* 31 (6):780–85. doi:10.1016/j.ijhydene.2005.06.016.

Náthia-Neves, G., T. D. A. Neves, M. Berni, G. Dragone, S. I. Mussatto, and T. Forster-Carneiro. 2018. Start-up phase of a two-stage anaerobic co-digestion process: Hydrogen and methane production from food waste and vinasse from ethanol industry. *Biofuel Research Journal* 5 (2):813–20. doi:10.18331/BRJ2018.5.2.5.

Noblecourt, A., G. Christophe, C. Larroche, and P. Fontanille. 2018. Hydrogen production by dark fermentation from pre-fermented depackaging food wastes. *Bioresource Technology* 247:864–70. doi:10.1016/j.biortech.2017.09.199.

Park, C., N. Lee, J. Kim, and J. Lee. 2021. Co-pyrolysis of food waste and wood bark to produce hydrogen with minimizing pollutant emissions. *Environmental Pollution* 270:116045. doi:10.1016/j.envpol.2020.116045.

Rai, P., and S. Singh. 2013. Biological production of clean energy: Hydrogen. In *Recent Advances in Microbiology SP Tiwari*, ed. <. I. I. A. I. Sharma and <. I. I. A. I. Gaur, 55–84. New York, USA: Nova Science Publishers Inc.

Rattanapan, C., L. Sinchai, T. Tachapattaworakul Suksaroj, D. Kantachote, and W. Ounsaneha. 2019. Biogas production by co-digestion of canteen food waste and domestic wastewater under organic loading rate and temperature optimization. *Environments* 6 (2):16. doi:10.3390/environments6020016.

Ravindran, R., S. Jaiswal, N. Abu-Ghannam, and A. K. Jaiswal. 2018. A comparative analysis of pretreatment strategies on the properties and hydrolysis of brewers' spent grain. *Bioresource Technology* 248:272–79. doi:10.1016/j.biortech. 2017.06.039.

Rice, E. W., R. B. B, and A. D. Eaton. 1915. *Standard methods for the examination of water and wastewater*. America: American Public Health Association, American Water Works Association, Water Environment Federation.

Salehian, P., and K. Karimi. 2013. Alkali pretreatment for improvement of biogas and ethanol production from different waste parts of pine tree. *Industrial & Engineering Chemistry Research* 52 (2):972–78. doi:10.1021/ie302805c.

Sarkar, O., and S. V. Mohan. 2017. Pre-aeration of food waste to augment acidogenic process at higher organic load: Valorizing biohydrogen, volatile fatty acids and biohythane. *Bioresource Technology* 242:68–76. doi:10.1016/j.bior tech.2017.05.053.

Venkata Mohan, S., V. Lalit Babu, and P. N. Sarma. 2008. Effect of various pretreatment methods on anaerobic mixed microflora to enhance biohydrogen production utilizing dairy wastewater as substrate. *Bioresource Technology* 99 (1):59–67. doi:10.1016/j.biortech.2006.12.004.

Yang, T. C., J. Kumaran, S. Amartey, M. Maki, X. Li, F. Lu, and W. Qin. 2014. Biofuels and bioproducts produced through microbial conversion of biomass. *Bioenergy Research: Advances and Applications* 1: 71–93.

Zhi, Z., and H. Wang. 2014. White-rot fungal pretreatment of wheat straw with Phanerochaete chrysosporium for biohydrogen production: Simultaneous saccharification and fermentation. *Bioprocess and Biosystems Engineering* 37 (7):1447–58. doi:10.1007/s00449-013-1117-x.